

1994

Functional Dynamics of Primate Retinal Ganglion Cells

Ethan A. Benardete

Follow this and additional works at: http://digitalcommons.rockefeller.edu/student_theses_and_dissertations



Part of the [Life Sciences Commons](#)

Recommended Citation

Benardete, Ethan A., "Functional Dynamics of Primate Retinal Ganglion Cells" (1994). *Student Theses and Dissertations*. 341.
http://digitalcommons.rockefeller.edu/student_theses_and_dissertations/341

This Thesis is brought to you for free and open access by Digital Commons @ RU. It has been accepted for inclusion in Student Theses and Dissertations by an authorized administrator of Digital Commons @ RU. For more information, please contact mcsweej@mail.rockefeller.edu.



Functional Dynamics of Primate Retinal Ganglion Cells

A thesis submitted to the Faculty of The Rockefeller University in partial fulfillment of the requirements for the degree of Doctor of Philosophy

by

Ethan A. Benardete

March, 1994

The Rockefeller University

New York, New York

To my family

But above the gray land and the spasms of bleak dust which drift endlessly over it, you perceive, after a moment, the eyes of Doctor T. J. Eckleberg. The eyes of Doctor T. J. Eckleberg are blue and gigantic--their retinas are one yard high. They look out of no face, but instead, from a pair of enormous yellow spectacles which pass over a non-existent nose. Evidently, some wild wag of an oculist set them there to fatten his practice in the borough of Queens, and then sank himself down into eternal blindness, or forgot them and moved away. But his eyes, dimmed a little by many paintless days under sun and rain, brood on over the solemn dumping ground.

-- F. Scott Fitzgerald, The Great Gatsby

Acknowledgments

The last four and a half years in the Knight laboratory have been exciting and challenging. I am grateful to my advisor, Dr. Ehud Kaplan, and the head of the laboratory, Bruce W. Knight, for generously supporting this research. Dr. Kaplan has taught me most of what I know about practical electrophysiology and the vast expanse of visual physiology. Bruce Knight has been a constant source of advice and encouragement on things both mathematical and biological. I also owe a large debt of gratitude to Dr. Jonathan D. Victor whose work on cat retinal ganglion cells provided much inspiration for the present work. In addition, Dr. Victor was instrumental in designing the multiple m-sequence technique and teaching me some of the subtleties of nonlinear systems analysis. Furthermore, I would like to thank my fellow student, Pratik Mukherjee, for providing valuable assistance and camaraderie. In addition, Yvonne Holland has assisted me with her excellent histological skills and has helped me with the arduous task of editing. Norman Milkman, the designer of the laboratory's visual stimulator, was also generous with his time in the early phases of this project when much programming needed to be done. For sundry and all too frequent electronic repairs, I would like to thank Michelangelo Rossetto, the laboratory's talented electronics expert. Finally, for day-to-day assistance, I am grateful to both Renée Gilodo and Ellen Paley, the laboratory's secretaries.

Table of Contents

1. Introduction	3
1.1 The Visual System	4
1.2 Nonlinear Systems.....	5
1.3 Optimal Systems	6
1.4 Retinal Anatomy and Physiology	7
1.5 M and P Physiology	10
1.6 White-Noise Analysis.....	14
1.7 Summary of Chapters.....	16
2. Materials and Methods	17
2.1 Experimental Procedures.....	18
2.1.1 Surgical Preparation	18
2.1.2 Preparation for Recording	19
2.1.3 Recording.....	21
2.1.4 Termination of the Experiment	24
2.2 Visual Stimuli.....	24
2.2.1 Spatial Patterns	25
2.2.2 Silent Substitution Method	27
2.3 Data Collection and Analysis.....	30
2.3.1 Drifting Gratings	31
2.3.2 Contrast-Reversing Experiments.....	32
2.3.3 Sum-of-Sinusoids Experiments.....	33
2.3.4 Perturbation Experiments	36
2.3.5 Step Response Experiments.....	37
2.3.6 M-Sequence Experiments.....	37
2.4 Classification of cells.....	41
2.4.1 Linearity of Spatial Summation.....	44
2.4.2 Spatial Frequency Response	47
2.5 Model Fits.....	48
2.5.1 First-Order Kernels.....	48
2.5.2 Second-Order Kernels	49
3. The Multiple M-Sequence Method	56
3.1 Overview	57
3.2 Introduction	57
3.3 Preliminaries	58
3.4 Types of Kernels	60
3.5 M-Sequences	62
3.6 Standard Approach	64
3.7 Elimination of Anomalies	69

3.8 The Hybrid M-Sequence Method	72
3.9 Higher-Order Systems.....	75
3.10 Multi-Input Systems.....	79
3.11 Relationship to Wiener Kernels	82
3.12 Relationship to the Sum-of-Sinusoids Approach.....	86
3.13 Discussion.....	87
3.14 Appendix I.....	88
3.15 Appendix II.....	89
4. P Cells: Center and Surround.....	94
4.1 Introduction	95
4.2 Linearity of Center and Surround	97
4.3 Effect of Dynamic Contrast on the First-Order Responses	100
4.4 Model Fits.....	101
4.5 Nonlinear Responses	109
4.6 LNL Model Fits	113
4.7 Center-Surround Interaction Experiments	127
4.8 Surround Effect in M cells.....	141
4.9 Circuit Model of the Nonlinear Surround Effect	142
4.10 Mathematical Development of the Circuit Model.....	143
4.10.1 Zeroth-Order Kernel.....	145
4.10.2 First-Order Kernels.....	145
4.10.3 Second-Order Kernels	148
4.11 The Relationship of the Kernels to the Model Fits	149
4.12 Kernel Predictions.....	150
4.13 Summary.....	151
5. P Cell Responses to Chromatic and Achromatic Stimuli	153
5.1 Introduction	154
5.2 Responses to Chromatic and Achromatic Gratings	155
5.3 Frequency Responses.....	168
5.4 Comparison with M Cell Chromatic and Achromatic Responses	170
5.5 Model Fits.....	174
5.5.1 M vs. P Comparison	176
5.6 Prediction of P Cell Chromatic and Achromatic Responses.....	178
5.7 Nonlinear Responses.....	180
5.8 Spatiotemporal Coupling within the P Cell Receptive Field.....	184
5.9 Summary.....	189
6. M Cell Dynamics	191
6.1 Introduction	192
6.2 Frequency Responses	194
6.3 Spatiotemporal Coupling.....	196
6.4 Model Fits.....	199
6.5 Step Responses	206

6.6 M Cell Chromatic Responses.....	212
6.7 The Spatial Profile of the Contrast Gain Control.....	221
6.8 The Temporal Characteristics of the Contrast Gain Control.....	225
6.9 Nonlinear Responses	226
6.10 Summary.....	231
7. Discussion.....	232
7.1 Summary.....	233
7.2 The Multiple M-sequence Technique.....	233
7.3 P cell Results.....	234
7.3.1 Linearity of the P cell Center and Surround	234
7.3.2 Nonlinear Responses of P cells	235
7.3.3 P Cell Chromatic Responses	237
7.3.4 M and P Differences	239
7.3.5 P Cell Anatomy	240
7.4 M cell results.....	241
7.4.1 The Contrast Gain Control	241
7.4.2 M Cell Relationship to Cat Retinal Ganglion Cells	242
7.4.3 M Cell Responses to Chromatic Stimuli.....	243
7.5 Conclusion	244
8. References.....	245

List of Tables

<i>Table 1-1. M and P cell comparison (From Kaplan et al., 1990).....</i>	<i>10</i>
<i>Table 2-1. Gun Intensity Values for Different Grating Types.....</i>	<i>30</i>
<i>Table 2-2. Luminance of the Red, Green, and Blue Guns of the CRT.....</i>	<i>30</i>
<i>Table 2-3. Low Frequency Sum-of-Sinusoids Set (Victor and Shapley, 1980).....</i>	<i>34</i>
<i>Table 2-4. High Frequency Sum-of-Sinusoids Set (Victor and Shapley, 1980).....</i>	<i>34</i>
<i>Table 2-5. Generating Polynomials for M-Sequences.....</i>	<i>40</i>
<i>Table 4-1. P Cell Center Parameters.....</i>	<i>106</i>
<i>Table 4-2. P Cell Surround Parameters.....</i>	<i>107</i>
<i>Table 4-3. The Mean Rate and Eccentricity of the P Cell Sample.....</i>	<i>107</i>
<i>Table 4-4. The Parameters of the LNL Model for the Second-Order Center Response of P cells.....</i>	<i>124</i>
<i>Table 4-5. The Parameters of the LLNL Model for the Second-Order Center-Surround Kernel</i>	<i>126</i>
<i>Table 4-6. Parameters Fit for 8 P ON Cells to Eq. (4-1) and a Regression Line for τ_L.....</i>	<i>141</i>
<i>Table 5-1. P Cell Chromatic Center Parameters</i>	<i>175</i>
<i>Table 5-2. P Cell Chromatic Surround Parameters</i>	<i>176</i>
<i>Table 5-3. P Cell Optimal Spatial Frequency Parameters</i>	<i>176</i>
<i>Table 5-4. M vs. P Center Parameters.....</i>	<i>177</i>
<i>Table 5-5. Parameters from the Fit of the modDOG Model to P Cell Spatial Frequency Responses</i>	<i>189</i>
<i>Table 6-1. The Fitted Parameters of the Linear Model to M cell Responses (at 0.0625 contrast)</i>	<i>206</i>
<i>Table 6-2. The Parameters of the LNL Model Fit to Second-Order M Cell Response.....</i>	<i>230</i>

Abbreviations

(RG)	red-green
(YB)	yellow-blue
A	anterior
C.V.	coefficient of variation (standard deviation/mean)
c/d	cycles per visual degree
CRF	contrast response function
Di	Diopter
FMT	fast m-transform
IM	intramuscular
IPL	inner plexiform layer
IR	inverse repeat
IV	intravenous
L	lateral
LGN	lateral geniculate nucleus
LNL	linear-nonlinear-linear
LLNL	linear-linear-nonlinear-linear
modDOG	modified Difference-of-Gaussians
OPL	outer plexiform layer
RMS	root-mean-square
S.D.	standard deviation
u.c.	unit contrast

Abstract

Contrast forms the substrate for human pattern vision. The retina is the first stage in the processing of complex spatial and temporal contrast signals. The responses of retinal ganglion cells to such signals provide the means to explore such processing in the retina. Most primate retinal ganglion cells fall into two broad classes, M and P, which have many anatomical and physiological differences. The responses of M and P cells to luminance and chromatic signals were studied using nonlinear systems analysis to determine the dynamics and the functional organization of the cells' receptive fields. Previously tried methods as well as a new method described here were used to study the interactions of contrast signals within the receptive fields of M and P cells.

The first-order responses of P cells to spots and annuli isolated the dynamics of the center and surround. The new multiple m-sequence method also allowed analysis of the second-order responses. Although traditionally viewed as "linear" cells, P cells display characteristic second-order kernels from their center and surround regions as well as a mixed center-surround cross-kernel. This nontrivial nonlinearity was explored further using spots and steady annuli which were set at several levels of illumination. These experiments demonstrated that the level of ambient illumination in the surround could affect the gain and dynamics of the P cell center.

The responses of P cells to chromatic and achromatic gratings were used to assess the interactions of different cone-driven inputs to P cells. While P cells appear to be

driven by opponent color mechanisms, responses to luminance contrast demonstrate a nonlinearity in the summation of cone signals.

The responses of M cells to chromatic and achromatic contrast signals differ substantially from those of P cells. The first-order responses of M cells show the contrast gain control phenomenon found in cat retinal ganglion cells (Shapley and Victor, 1978), a nonlinear contrast-response relationship. This phenomenon is recognized as an increasing amount of low frequency attenuation in response to increasing contrast stimulation. Most M cells have second-order responses similar to those from cat retinal ganglion cells. These nonlinearities in M and P cell responses lead to several conjectures about the anatomical organization and the functional roles of M and P cells.

The nonlinearity found in P cells can lead to dynamic regulation of contrast sensitivity and an enhanced selectivity to fine patterns. M cells, on the other hand, perform like an adaptive filter that is optimized to extract temporal information. The data suggest that the anatomical substrates of these M and P cell nonlinearities must be different.

Introduction

The Visual System

Nonlinear Systems

Optimal Systems

Retinal Anatomy and Physiology

M and P Physiology

White-Noise Analysis

Summary of Chapters

1. Introduction

1.1 *The Visual System*

The visual environment contains many complex variations in the patterns of light that fall on the eye. These patterns are typically quantified in terms of the spatial, temporal and spectral variations in the scene (Wyszecki and Stiles, 1982). The visual system must extract useful information about the environment using these signals. The retina is the first part of the visual system where these complex variations are transformed into neuronal signals. The retina is a neural network that begins the information-processing tasks that are undertaken by the visual system as a whole. From the study of retinal processing, one can hope to learn some of the general principles used by the visual system as well as the entire central nervous system in processing information. Much is already known about the retinae of many animals. Previous work, primarily on cold-blooded vertebrates has probed in some detail the neurophysiology of individual parts of this network: photoreceptor, bipolar, horizontal, amacrine, and ganglion cells. However, there are many differences between the retinae of these animals and those of humans, presumably because of the evolutionary pressure to optimize the visual system for different environments. Some primates, however, share a visual system remarkably similar to that of man (DeValois *et al.*, 1974a,b; DeValois and Morgan, 1974). The retinae of these primates, while having been investigated anatomically in some detail, have yet to be explored physiologically at the level of recording from each cell type, although some progress has been made (Dacheux and Raviola, 1990). However, the spike discharges and synaptic potentials from retinal ganglion cells of the primate can be recorded, and these

provide a window on the processing performed by the retinal network. If nothing else, one can say that the only information that the rest of the visual system receives about the visual scene is contained in the temporal pattern of spikes that travel down the axons of retinal ganglion cells which form the optic nerve. One can investigate how the retina processes visual information by presenting specific patterns of light to the eye and recording the responses of retinal ganglion cells. Thus, the retina becomes a black box wherein we can hope to describe its operation by mathematical relationships between the input and the output. Some of these relationships are already known and can be described as retinal processing principles, for instance, lateral inhibition (Ratliff, 1965). But we do not have to be satisfied with the black box approach, for much is currently known about the anatomy and the presumed role of different types of retinal ganglion cells so that the mathematical description can be related to the biology.

1.2 Nonlinear Systems

Mathematical descriptions of the visual system can be useful in organizing functional and anatomical information if they can relate how different kinds of visual information interact. If two signals affect the retina in a way that depends nontrivially on their interaction, this relationship implies both a physical substrate for their convergence and a functional significance to this relationship. This thesis describes experiments on how contrast signals, both achromatic and chromatic, interact in the retina. The study of these interactions implies a certain technical need to use methods beyond ordinary linear systems analysis. Linear systems themselves obey the principle of superposition which states that the response of a linear system to a sum of two signals, for example A and B, is the sum of

the response to A and the response to B (Schetzen, 1980). Signals therefore, in linear systems, do not interact. Furthermore, if a linear system has a series of stages, the exact order of those stages is indistinguishable given the input-output relation of the system (Oppenheim *et al.*, 1983). On the other hand, the techniques of nonlinear systems analysis described in Chapter 3, while they embrace linear systems as a subset of nonlinear systems, can also describe the interactions of signals within a system. In general, the ordering of stages in a nonlinear model is not completely arbitrary as for a linear system (Barrett, 1963; Rugh, 1981). In general, the overall response of a nonlinear system depends upon the ordering of its stages; conversely, its characterization will yield information regarding not only the nature of its stages but also their sequence, and this information can help to develop models of retinal processing and relate them to known anatomy and physiology.

1.3 Optimal Systems

Much recent theoretical effort has centered on the analysis of natural scenes and determination of optimal ways to transmit this information (Srinivasan *et al.*, 1982; Field, 1987). The optimal filter for this transmission often has a recognizable similarity to the receptive fields of the retina (Atick and Redlich, 1992). Clearly, millions of years of evolution may have optimized the retina for certain kinds of spatial and temporal analysis. In this same view, however, over short times, the visual scene presents a varying stimulus whose values fall somewhere within the range of possibilities for which the retina is optimized. Light and dark adaptation are two ways in which the retina readjusts to optimize itself to the environment (Shapley and Enroth-Cugell, 1984). These readjustments generally express themselves as nonlinearities, since adding or subtracting

signal brings about a change in the response of the system that is not simply a superposition of responses. Nonlinear interactions effect changes in the system characteristics as the input signals change. These changes may tell us what are the characteristics of the stimulus for which the system is optimized. The nonlinearities in retinal ganglion cells described herein can be viewed in this way.

This thesis investigates the interactions of contrast signals in the retina both spatially and temporally. These ideas are explored by recording the responses of two broad classes of retinal ganglion cells, M and P cells, to specially designed stimuli. The rest of this chapter will describe some of the background anatomy and visual physiology in relation to these two classes of cells, and will conclude with an overview of the rest of the thesis.

1.4 Retinal Anatomy and Physiology

Retinal ganglion cells form the output stage of the retina; their axons carry the signals from the retina to higher visual centers. This output reflects the processing of an enormous network preceding the retinal ganglion cells. A diagram of the primate retina shows the various cell types and some of the interconnections involved in transforming light impinging on the retina into a neuronal message (Fig. 1-1). An important concept for retinal physiology is that of the receptive field introduced by Hartline (1942). The receptive field of a retinal ganglion cell is defined as the region of retina in which light modulates the ganglion cell's response. In discussing retinal ganglion cell receptive fields, therefore, evidently, it is necessary to understand something of the preceding stages.

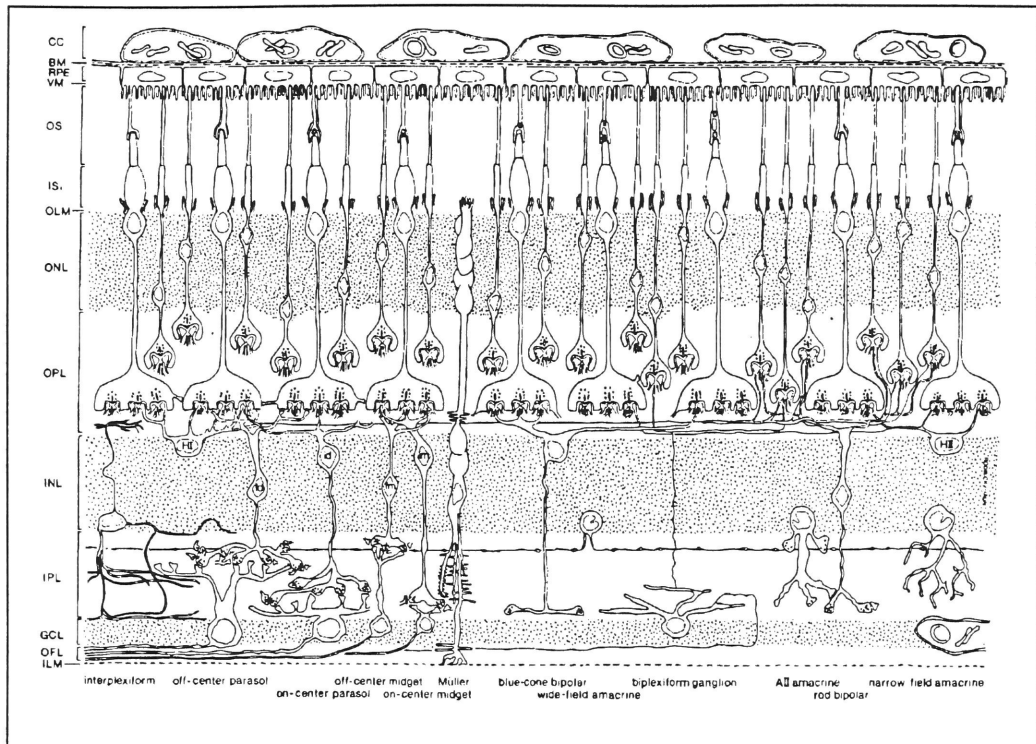


Figure 1-1. Schematic diagram of the primate retina showing many of the major cell types (Reproduced with permission from Rodieck, 1988).

Photons are captured by the photopigment molecules of photoreceptors, rods and cones, and by a complex series of chemical and ionic transductions, the arrival of a photon causes a decrease in neurotransmitter release from the photoreceptor (Baylor, 1987). The highly sensitive rods form the substrate for night (scotopic) vision, while at higher ambient light levels, the cones are the primary photoreceptors (Shapley and Enroth-Cugell, 1984). The cones, from a functional standpoint, fall into three classes based on their spectral sensitivity to light of long, middle, and short wavelengths (L, M and S) (Schnapf *et al.*, 1987). (At a molecular level, the three pigments may show slight variations within a class (Nathans *et al.*, 1986a,b)).

Photoreceptors form synapses with two types of cells, namely horizontal cells and bipolar cells (Rodieck, 1988; Wässle and Boycott, 1991). Each of these types falls into a number of classes. The two types of horizontal cells, H1 and H2, make lateral connections in the outer plexiform layer (OPL) contacting up to 15 cones (Boycott *et al.*, 1987). The bipolar cells that contact cones, on the other hand, come in four broad categories (Boycott and Wässle, 1991). One division is based on whether the bipolar makes a flat or invaginating synapse with cones. The axons of these bipolars terminate in different regions of the inner plexiform layer (IPL). Based on analogy with other vertebrates, the flat and invaginating division probably represents the functional ON and OFF classes (Famiglietti *et al.*, 1977; Nelson *et al.*, 1978). A second categorization of bipolar cells divides them into midget and diffuse types. The dendritic arborizations of midget bipolars make contact with a single cone (Rodieck, 1988). The diffuse type, on the other hand, typically contacts up to 7 cones of mixed type (L and M) (Boycott and Wässle, 1991).

The signals from bipolar cells are delivered by their axons to ganglion cells in the IPL. In the IPL, another type, the amacrine cell, makes extensive lateral contacts with ganglion cells. There are numerous amacrine cell types identified by cytochemical techniques based on various neuronal markers (Vaney, 1990). The physiological role of amacrine cells is largely unknown (except for the AII class (Kolb and Famiglietti, 1974)) although in lower vertebrates they demonstrate, in some cases, transient ON-OFF responses (Sakai and Naka, 1988a).

In the IPL, a midget bipolar contacts a midget ganglion cell (Dacey, 1993). The thalamic targets of these midget ganglion cells are in the parvocellular layers of the lateral geniculate nucleus (LGN) (Rodieck *et al.*, 1985). Consequently, the cells of this anatomical class are called P cells. Diffuse bipolars, on the other hand, contact ganglion cells that project to the magnocellular layers, which are called M or parasol cells (Boycott and Wässle, 1991). The dendritic fields of M cells have roughly 5 times the area of P cell dendritic fields near the fovea (Rodieck *et al.*, 1985).

Table 1-1. M and P cell comparison (From Kaplan et al., 1990).

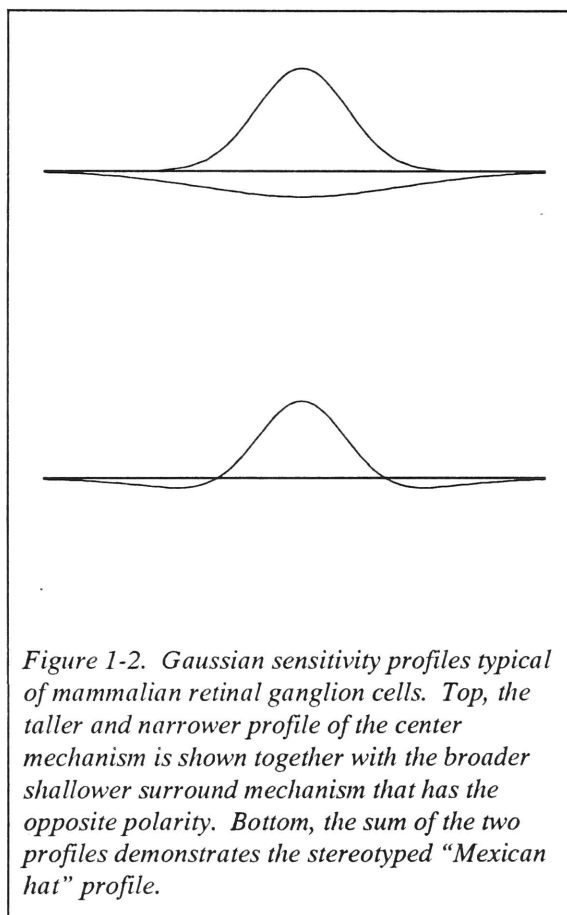
Property	P cells	M cells
Spectral selectivity	Yes	No
Luminance contrast gain	Lower	Higher
Receptive field size	Smaller	Larger
Spatial Resolution	Similar	Similar
LGN projection target	Parvocellular	Magnocellular
Conduction velocity	Lower	Higher
Cell size	Smaller	Larger
Response to light steps	Tonic	Phasic
Linearity of spatial summation	Linear ("X")	75% "X" 25% "Y"
Pattern vision at scotopic levels	No	Yes
Number of cells (in millions)	1.2	0.15

1.5 M and P Physiology

The M and P classes may be recorded from their LGN targets or directly in the retina and demonstrate different physiological properties. The segregation of M and P

afferents in the LGN further suggests that the two populations serve different roles. The main physiological differences are summarized in Table 1-1.

The spectral sensitivity of M and P cells was investigated first by DeValois *et al.* (1966) and by Wiesel and Hubel (1966), who recorded from parvocellular units in the LGN and Gouras (1968), who recorded in the retina. Distinct dynamical properties of M and P cells were first recognized by Gouras (1968) as he divided them into phasic and



tonic types, respectively. Later studies showed that this distinction also reflected differences in the temporal frequency response of M and P cells (Derrington and Lennie, 1984; Lee *et al.*, 1989a,b,c). The spatial structure of M and P cell receptive fields was first investigated by Wiesel and Hubel (1966) who recognized that, to a first approximation, the majority of primate LGN cells have circularly symmetric receptive fields with center and surround subregions. Early work on the receptive fields of cat retinal ganglion cells showed

that the center and surround subregions can be well modeled by Gaussian sensitivity profiles (Rodieck, 1965; Linsenmeier *et al.*, 1982) (Figure 1-2).

For P cells, the center and surround regions have different spectral sensitivities corresponding to the wavelengths that give opponent responses (Wiesel and Hubel, 1966). For example, consider a P ON cell (that is one that increases its steady discharge to diffuse white light), for which illumination of the central region by a long wavelength (red) light increases its spike rate while middle wavelength (green) illumination of the surrounding regions decreases the rate. Early categorization of P cells thus lead to the R+G-, R-G+, Y+B-, and Y-B+ (R = red, G = green, Y = yellow, and B = blue) segregation. Since then, some preference has been shown for designating these same cells by their presumed cone inputs (L+M-, L-M+, (L+M)+S-, and (L+M)-S+ (DeValois and DeValois, 1993). However, this designation suggests that the exact cone input to a specific type of P cell is known. Although physiological evidence has been provided by Derrington *et al.* (1984), Lee *et al.* (1987), and most recently by Reid and Shapley (1992) that the cone inputs to the P cell center and surround may be of a single cone type, I will adhere to the older classification scheme for the purpose of continuity and objectivity. The major objection to the older classification is that red, green, yellow, and blue are perceptual entities not likely to arise from individual ganglion cell classes; however, having pointed out that this discrepancy, it should not cause any confusion.

M cells, on the other hand, have broad spectral sensitivity in most studies (Wiesel and Hubel, 1966; Gouras, 1968; Lee *et al.*, 1987, 1988), although at least one study suggested that they may all be color-opponent (Derrington *et al.*, 1984). The properties of M and P receptive fields naturally suggest that P cells are devoted to some form of fine form and color processing (Schiller and Logothetis, 1990; Schiller *et al.*, 1990a,b) while

M cells with their broad spectral and high temporal resolution may form the substrate for a perceptual motion channel (Merigan *et al.*, 1991). To serve these roles, the dynamics and interactions of the M and P cell center and surround must be critical. Herein, they are explored.

A further critical distinction between the M and P classes was recognized by Kaplan and Shapley (1986). M cells are approximately 8-10 times more sensitive to luminance contrast than are P cells. This increased sensitivity was an incentive to explore the contrast processing of M cells further. This investigation (Benardete *et al.*, 1991, 1992a) led to the recognition of a nonlinearity in contrast processing similar to that found in the cat (Shapley and Victor, 1978, 1979a,b; Victor and Shapley, 1981). This nonlinearity, called the contrast gain control, found in M cells and not in P cells, is discussed in Chapter 6.

Finally, nonlinearities in spatial processing form the basis for a fundamental distinction among the ganglion cells in the cat retina (Enroth-Cugell and Robson, 1966; Hochstein and Shapley, 1976a,b). The X-Y distinction for cat retinal ganglion cells corresponds to linear and nonlinear spatial summation, respectively. In the monkey, only M cells have a similar dichotomy (Kaplan and Shapley, 1982); all P cells are X-like. When studied with nonlinear systems techniques, the Y cells of the cat show pronounced nonlinear responses. Analogously, some of these techniques were applied to M cells (Chapter 6), which demonstrate similar nonlinearities.

1.6 White-Noise Analysis

There have been very few studies of primate retinal ganglion cells using nonlinear systems techniques. Gielen *et al.* (1982) applied white-noise analysis to the study of LGN neuronal responses. They were able to calculate the first-order responses of LGN neurons to stimuli that excited only a single cone class (L, M, or S) with diffuse monochromatic light. Similar results using different techniques form part of Chapter 4. The technical limitations of their method may have prevented their analysis from uncovering some of the phenomena that I investigated. In general, it is important to note the strength of white-noise methods in studying nonlinear systems in general and the retina in particular.

One of the attractions of white noise as a test signal is that in a rigorous sense, real white noise approximates all other signals likely to be interesting (Wiener, 1958). Indeed, given sufficient time, white noise will approximate a given signal to an arbitrary degree (Schetzen, 1980). But white noise is a theoretical concept since it has infinite power. Even Gaussian white noise poses insurmountable barriers to implementation in the laboratory (Victor, 1992). Nevertheless, for the analysis of biological systems, signals that retain some of the features of white noise are worth considering both from a strictly biological point of view and from a theoretical one. First, for the retinal ganglion cell, the temporal pattern of light falling on its receptive field must be a fairly complex waveform. Indeed, eye movements introduce jitter into what the eye sees. The temporal variation in the retinal input is known to be essential for vision; stabilized images fade and quickly become invisible (Riggs *et al.*, 1953). Thus, the study of retinal ganglion cells with random or pseudorandom signals makes reasonable biological sense.

From the theoretical viewpoint, the Wiener-type methods provide a general basis for model-building, and there is a broad, mathematical and engineering literature on its use (Rugh, 1981). The use of such methods in cold-blooded vertebrates and lower mammals has also provided a good deal of insight into retinal function (Sakai *et al.*, 1988; Victor, 1988).

The principal reason for developing a modification of the m-sequence method pioneered by Sutter (1992) was to develop a Wiener-type method that was easily implemented for the purpose of studying *multi-input* nonlinear systems. Retinal ganglion cells fall into this class since their receptive fields are sensibly broken down into two or more sub-regions or mechanisms. For example, the receptive field of a primate P cell has a center and a surround, each of which might be studied independently. But the goal here was to elucidate the responses of each mechanism simultaneously (as they must perform in nature) in the presence of a single ambient stimulus. In addition, not only the first-order responses but also second-order terms were desired so that nonlinear interactions between and within subregions could be studied. With the P cell, the same center-surround paradigm could be extended to study the interaction of chromatically opponent mechanisms. The primate M cell could be studied in a similar way although existing methods (sum-of-sinusoids) already provided a strong technical basis. Chapter 3 addresses the theoretical background and construction of the multiple m-sequence method. Much of that material has appeared in Benardete and Victor (1994).

1.7 Summary of Chapters

In this thesis, I describe experiments which explore the function of primate retinal ganglion cells, with particular emphasis on those properties that can be described as nonlinear. Nonlinear systems analysis, previously applied to the retinal ganglion cells of other species, has provided valuable insight into the functional relationships of the vertebrate retina (Shapley and Victor, 1981; Sakai and Naka, 1988a,b,c). Therefore, I have used two proven methods (drifting gratings, sum-of-sinusoids) and enhanced previous techniques (m-sequences) in order to address several aspects of primate retinal function. Chapter 2 summarizes the experimental methods that were applied. Chapter 3 discusses nonlinear systems analysis in a general framework as it relates to the present work. Chapter 4 describes the dynamics of the P cell center and surround and investigates a dynamic nonlinearity in the receptive fields of P cells. Chapter 5 describes experiments that explored the chromatic properties of P cells.

In Chapter 6, the focus is on M cell dynamics. The principal result is the identification of the contrast gain control, previously demonstrated in cat retinal ganglion cells (Shapley and Victor, 1978), as a nonlinearity found in M cells and not in P cells. Chapter 6 also addresses the spatial and temporal properties of the M cell contrast gain control. Finally, Chapter 7 summarizes both P and M cell dynamics and relates the present findings to previous experimental and theoretical work.

Materials and Methods

Experimental Procedures

- Surgical Preparation

- Preparation for Recording

- Recording

- Termination of the Experiment

Visual Stimuli

- Spatial Patterns

- Silent Substitution Method

Data Collection and Analysis

- Drifting Gratings

- Contrast-Reversing Experiments

- Sum-of-Sinusoids Experiments

- Perturbation Experiments

- Step Response Experiments

- M-Sequence Experiments

Classification of cells

- Linearity of Spatial Summation

- Spatial Frequency Response

Model Fits

- First-Order Kernels

- Second-Order Kernels

2. Materials and Methods

2.1 Experimental Procedures

2.1.1 Surgical Preparation

These experiments were carried out on 38 primates of the species *Macaca fascicularis* and on two of the species *Macaca nemestrina*. These species are known to be similar to humans in many aspects of spatial and chromatic vision (DeValois *et al.*, 1974a,b). The same procedures were used for both species. All animals were male (2.5-4.5 kg). The experimental protocol was approved by the Rockefeller University Animal Care and Use Committee and steps were taken at all stages of the experiment to ensure that the animal experienced no pain or distress. The standard experimental method has been described elsewhere (Kaplan and Shapley, 1982), and will be summarized here. The monkey was initially anesthetized with an intermuscular (IM) injection of xylazine (Rompun, 2 mg/kg) followed by ketamine hydrochloride (Ketaset, 10 mg/kg). During surgery, the initial dose of ketamine was supplemented with either thiamylal (Surital, 2.5%) or pentothal (thiopental sodium, 2%) to maintain deep anesthesia. Under additional local anesthesia (lidocaine, 40 mg/ml), three cannulae, two venous and one arterial, were inserted into the femoral vessels for monitoring blood pressure and delivery of drugs and fluids. A tracheal tube was placed to enable artificial ventilation and to monitor the expired CO₂ and the respiratory rate. Anesthesia was maintained for the duration of the experiment by one of two methods. In more than half of the experiments (experiments 1-26), after an initial loading dose (400 mg), a steady infusion of urethane (ethyl carbamate,

20%) was delivered IV (3-15 mg/kg-h). In later experiments, pentothal was used IV as the sole anesthetic agent (3 mg/kg-h). Penicillin (750,000 units) and gentamicin sulfate (4 mg) were administered IM to provide antibacterial coverage. Dexamethasone phosphate (Decadron, 6 mg) was also given IV to prevent brain edema. Phenylephrine hydrochloride (10%) and atropine sulfate (1%) were applied to dilate the pupils and relax accommodation. The corneas were protected with hard gas-permeable contact lenses. In addition, in later experiments, an ophthalmic NSAID (Ocufen: flurbiprofen sodium, 0.03%) was applied to the corneas to reduce inflammation. During the course of the experiment, physiological saline (0.9%) was applied periodically to the eyes to further protect the corneas from dehydration. A continuous IV flow (approximately 3 ml/kg-h) of Ringer's solution with 5% dextrose was maintained throughout the experiment. A urinary catheter allowed for overall fluid monitoring.

2.1.2 Preparation for Recording

The animal was placed in a stereotaxic apparatus, and the head rigidly held by ear bars in the external meatus. A clamp on a lumbar vertebral spinous process suspended the animal and improved recording stability. The signal from a temperature probe inserted beneath the scapula controlled a heating pad to maintain normal core body temperature (37.5° C). Artificial pupils (3 mm in diameter) were placed in front of the contact lenses during the experiment. Paralysis was necessary in order to prevent eye movements and was maintained by continuous infusion of either gallamine triethiodide (Flaxedil, 5-10 mg/kg-h) or, in later experiments (36-38) vecuronium bromide (Norcuron, 0.25 mg/kg-h).

Retinoscopy with a streak retinoscope (Welch-Allen) gave an initial indication of the refractive error of the eyes which was typically in the range of 0-7 Di.

Continuous monitoring of the animal's vegetative physiology (expired CO₂, ECG, arterial blood pressure, and excreted fluid) provided a means for keeping the animal in good health. The blood pressure was usually within physiological limits (80-120 mm Hg). In case of a sudden drop in arterial pressure, extra fluid and occasionally a dose of metaraminol bitartate (Aramine, 1 mg) were administered. If the blood pressure exceeded the normal range, additional anesthesia was administered. During paralysis, the expired CO₂ was maintained at 3.5-4.0% by adjusting the rate and tidal volume of the artificial respirator. The ECG, blood pressure, respiration rate, and expired CO₂ were monitored by a Hewlett-Packard patient monitor (Model 78354A). Approximately every hour, the moistened room air delivered by the respirator was supplemented with pure O₂.

The eyes were routinely examined during the experiment to ensure that the physiological optics remained excellent. A requirement for continuing the experiment was the ability to observe small vessels on the retinal surface and optic disk as judged by ophthalmoscopic examination. In addition, every six hours the contact lenses were removed briefly and thoroughly cleaned with gas-permeable contact lens cleaning solution (Allergan) or plain saline. A modified fundus camera (Carl Zeiss, Opton) was used to map the position of the optic disk and fovea on a tangent screen located at a distance of 114 cm from the animal. At this distance, each degree of visual angle is equivalent to 0.5 cm, and thus this distance provides a convenient gauge of retinal eccentricity relative to the fovea.

The skin overlying the skull was retracted, and a stimulating electrode made from a twisted pair of Teflon-coated stainless steel wires (Medwire, 5 mils) with 0.5 mm of their tips exposed was stereotaxically guided into the optic chiasm at a nominal depth of 25 mm (Horsley-Clarke coordinates: 19 A, 0.5 L). Correct positioning of this electrode was verified by recording mass potentials while a bright, flashing spot was presented in each eye. This electrode allowed the measurement of cell latencies when an electrical stimulus (10 mA, 150 μ s) was applied. The location of the lateral geniculate nucleus (LGN) was marked on the surface of the skull using Horsley-Clarke coordinates (7 A, 11 L). The bone over this area was removed with a hand-held trephine (\sim 1 cm in diameter). Typically, a small chamber was constructed out of dental acrylic around the area.

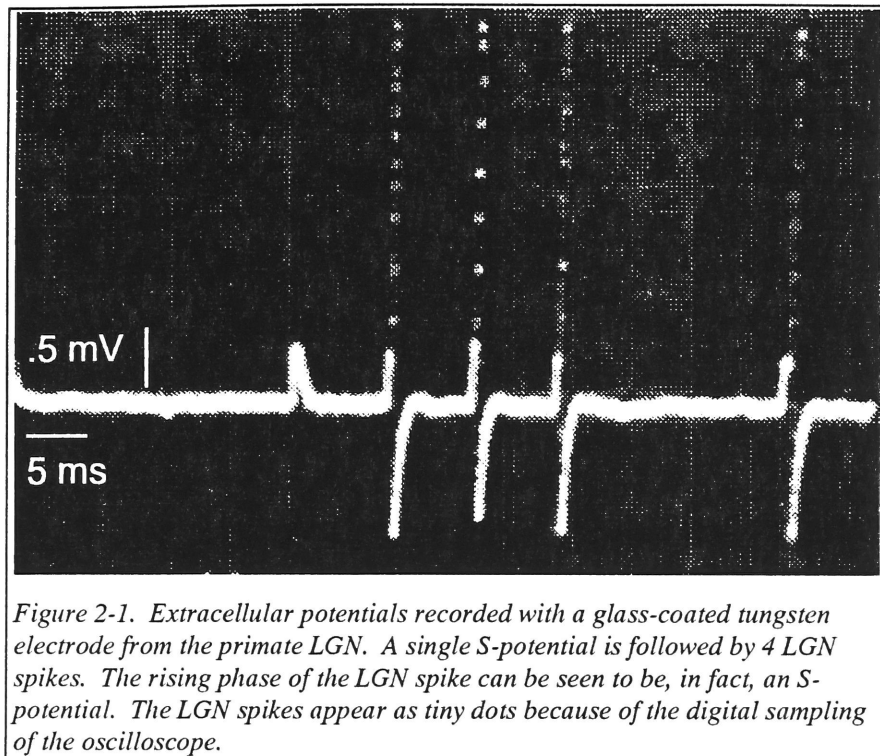
2.1.3 Recording

A motorized manipulator advanced a microelectrode down to the top of the LGN which is typically 23 mm beneath the surface of the cortex. The microelectrodes were of two types. In early experiments (experiments 1-18), saline-filled glass microelectrodes with an impedance of 7-19 M Ω at 500 Hz (shaft diameter: 1.5 mm) were used. In later experiments, commercial glass-coated tungsten electrodes (shaft diameter \cong 0.13 mm; exposed tip: 5-10 μ m) were used (Merrill and Ainsworth, 1972). These latter electrodes had the advantage, because of their fine diameter, of doing less injury to the recording site. These electrodes also improved recording stability.

The extracellular voltage was differentially amplified, displayed on an oscilloscope, and sent to an audio monitor. The electrode was advanced until the electrical activity

from the LGN could be reliably observed on the oscilloscope and heard on the audio monitor in response to a flashing light in either eye. The position of the electrode was secured by applying warm agar to the surface of the cortex around the electrode. The agar cools rapidly, forms a seal around the electrode, and covers the exposed cortex. The electrode was then advanced until the synaptic potentials (S-potentials) and LGN spikes of a single unit were detected above the background noise. The signal could be shaped by a bank of bandpass filters. A discriminator was set to send a pulse when an S-potential crossed the trigger. A separate channel was set to discriminate only the LGN spikes. The times of arrival of these pulses were recorded by a PDP 11/73 computer (Digital Equipment Corporation) to the nearest 0.1 ms. The S-potential rate (in units of impulses/second) provided the output variable for most of the subsequent analysis. Fig. 2-1 shows the typical appearance of S-potentials and LGN cell spikes on a digital oscilloscope during an experiment.

S-potentials provide an excellent means to monitor the activity of single retinal ganglion cells. Because the site of recording is in the LGN, only those retinal ganglion cells projecting to higher visual areas are monitored (as opposed to a retinal recording where ganglion cells projecting to the superior colliculus and other areas are part of the population). The retina is the sole origin of LGN S-potentials (Kaplan and Shapley, 1984), even though they are post-synaptic, and previous work has shown that the S-potential reflects the activity of a single retinal ganglion cell (Levick *et al.*, 1972).



In several experiments in which a tungsten recording electrode was used, at the end of the recording, current (10 μ A, 10 s) was passed through the electrode to mark the tissue around the cell. At the end of the experiment, the LGN of the animal was processed for histology (see below), and the exact position of the electrode was determined (see Figure 2-7).

The position of a cell's receptive field was determined by projecting a flashing spot on the tangent screen and finding the area of maximal response. Once the eccentricity of the cell's receptive field was marked, a mirror was placed in front of the animal in order to project the image of the CRT onto the cell's receptive field. The cell's receptive field was carefully aligned so that it was as near as possible to the center of the screen.

2.1.4 Termination of the Experiment

With proper care, the physiological state of the animal was stable for 4-7 days. At the end of an experiment, the animal was euthanized with an overdose of barbiturate (Nembutal, 70 mg/kg). If the LGN was to be processed for histology, the animal was deeply anesthetized with pentothal and brought into a specially built perfusion hood. A canula was inserted into the left ventricle of the heart after a small incision was made in the right atrium. A hemostat was placed around the descending aorta and the animal was perfused with at least 3 liters of physiological saline. The animal was then fixed with a solution of 10% formalin; the brain was removed from the skull, and the LGN blocked and extensively fixed. After fixation, the LGN was cut into 100 μm coronal sections on a freezing microtome and stained with cresyl violet.

2.2 Visual Stimuli

Stimuli were generated by a special-purpose computer (Milkman *et al.*, 1980) on a color CRT display (Conrac, model 7351) with a mean photopic luminance of 60 cd/m^2 . The display covered 7 deg x 7 deg at a distance of 228 cm from the animal. With this instrument, the red, green, and blue guns of the monitor could be independently modulated to produce various spatial and temporal patterns. The linearity of the output of the three guns was controlled via a lookup table generated by reading the output of a photocell before the experiment. Two different programs running on a PDP 11/73 computer were used to control the instrument. One program, UD73C, was written by Norman Milkman at the Laboratory of Biophysics, The Rockefeller University, and the other, MDX6RT, was written by Dr. Jonathan Victor at Cornell University Medical College and the

Laboratory of Biophysics. This section will present the spatial control over the stimulus that was common to both programs. The data collection and analysis section will indicate which program of the two was used for different types of experiments.

2.2.1 Spatial Patterns

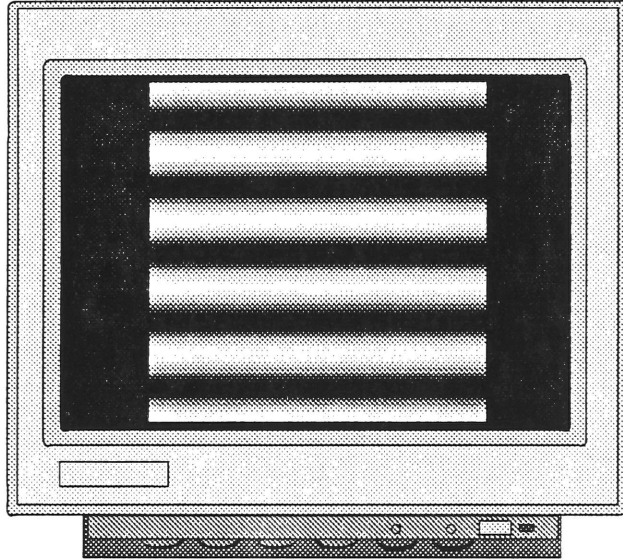


Figure 2-2. A black-white sine grating displayed on a CRT.

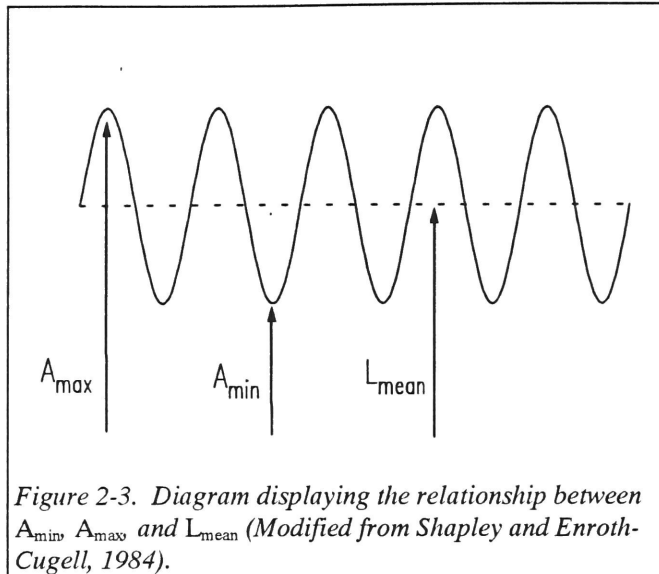
On the display, a sine grating could be produced that resembles Fig. 2-2.

The sinusoidal pattern could consist of either luminance or chromatic changes. For a sinusoidal variation, $P(x)$, around a mean luminance, L_{mean} , the mathematical representation is:

$$P(x) = L_{mean} + A \cos(2\pi kx) \quad (2-1)$$

where A is the amplitude of the modulation, x is the spatial position of the grating in visual degrees with center of the screen at $x = 0$, and k is the spatial frequency in cycles per

visual degree (c/d). A is referred to as the contrast and has a value of $\frac{A_{max} - A_{min}}{A_{max} + A_{min}}$ as can

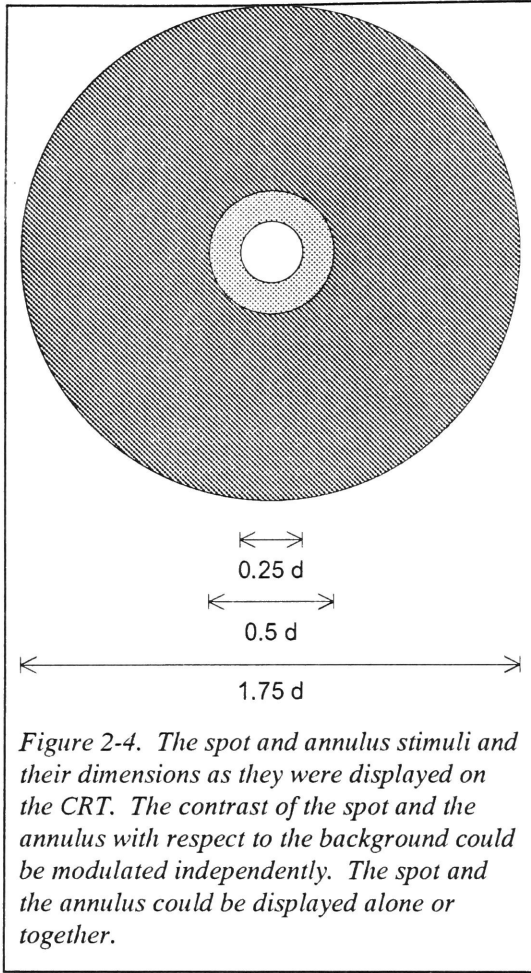


be verified from Fig. 2-3.

On a color monitor, A represents a triplet of values for a given sine grating. This triplet specifies the amplitude of modulation of each of the three guns: red, green, and blue. One way to represent A is $\{r, g, b\}$. L_{mean}

represents a constant triplet of red, green, and blue gun output that was set at 0.5 maximum output of each gun for all experiments.

A word of explanation is necessary about these stimuli. When the values r , g , and b are equal, each of the guns is being modulated at the same ratio as the mean level. Thus, variation in the grating is only a change in intensity above and below the mean. This grating thus modulates purely along a luminance axis. If r , g , and b are unequal, however, the grating is modulated in some other direction of color space. With such gratings, one can stimulate either luminance- or chromatically-sensitive neurons. This idea forms the basis for the experiments described below. The values of the red, green, and blue modulation were often chosen to specifically excite a single cone class or a specified combination of cone classes. The method of determining the proper values of $\{r, g, b\}$ is described in the next section.



Besides a sine grating stimulus, in other experiments, a small spot (0.25 deg in diameter) and/or an annulus (typical values 0.25 or 0.5 deg inner diameter (ID), 1.75 deg outer diameter (OD)) were produced on the CRT (Fig. 2-4). When presented simultaneously, the spot and the annulus could be modulated independently. In some experiments, a sine grating was produced inside the annular region.

2.2.2 Silent Substitution Method

A portion of the present work is devoted to understanding the cone inputs to

both P and M cells. The silent substitution method (Estévez and Spekreijse, 1974, 1982) provides a method for producing a stimulus that activates only a single cone class.

For example, a drifting sine grating that activates only L cones around the mean luminance, L_{mean} , is described by:

$$P(x, t) = L_{mean} + cA_L \cos(2\pi(kx - ft)) \quad (2-2)$$

where A_L is a triplet of red, green, and blue CRT gun intensity values that only activates L cones and c is a constant that specifies the relative magnitude of the stimulus, i.e. 1 for maximal stimulation and 0 for absence of modulation. For modulation of a single cone

class or any linear combination of cone classes within the physical limits of the CRT, A was chosen as follows. The spectral radiance of each of the guns of the CRT was measured with a photometer (PhotoResearch Pritchard-1980B) at 10 nm intervals in the range of 400 to 700 nm. The spectral sensitivity of each cone class in the macaque was assumed to be very similar to that calculated psychophysically by Smith and Pokorny (1972). According to the principle of univariance (Rushton *et al.*, 1973), each cone class was stimulated by an amount proportional to the spectral sensitivity at a particular wavelength and the energy emitted by a particular gun at that wavelength. Thus, each cone class received a certain amount of activation from each gun. For example, for the L cone type, the amount of stimulation due to the red gun is equal to:

$$L_R = \int_{\lambda_2}^{\lambda_1} S_L(\lambda) R(\lambda) d\lambda \quad (2-3)$$

where $S_L(\lambda)$ is the sensitivity of the L cone at wavelength λ and $R(\lambda)$ is the spectral radiance of the red gun at λ . Since the spectral radiance of each gun was measured at a discrete set of values, the integral, L_R , is replaced by the sum:

$$L_R \equiv \sum_{\lambda_1}^{\lambda_2} S(\lambda) R(\lambda) \Delta\lambda \quad (2-4)$$

The relative stimulation of the L cone class by each of the three guns was then calculated as the ratio of the cone excitation produced by a given gun to the total excitation:

$$\tilde{L}_R = \frac{L_R}{L_R + L_G + L_B} \quad (2-5)$$

Finally, for a desired set of relative values of stimulation of the L, M, and S cones, $\{l, m, s\}$, the following set of simultaneous equations were solved:

$$\begin{bmatrix} \tilde{L}_R & \tilde{L}_G & \tilde{L}_B \\ \tilde{M}_R & \tilde{M}_G & \tilde{M}_B \\ \tilde{S}_R & \tilde{S}_G & \tilde{S}_B \end{bmatrix} \begin{bmatrix} r \\ g \\ b \end{bmatrix} = \begin{bmatrix} l \\ m \\ s \end{bmatrix} \quad (2-6)$$

where $\begin{bmatrix} r \\ g \\ b \end{bmatrix}$ is the amplitude of modulation of each gun. With the Conrac monitor, because

of the physical limitations of the phosphors, maximum stimulation for L or M cones produced approximately 0.16 of the maximum cone excitation possible with a pure luminance stimulus. For S cones, the maximum was approximately 0.8.

In several types of experiments, different kinds of chromatic gratings were chosen. For experiments on (RG) P cells and M cells, an L cone-isolating grating and an M-cone isolating grating were used. For (YB) P cells, gratings that stimulated only S-cones and a grating that stimulated a combination of L and M cones in equal proportions (Y) was used. For (RG) P cells and M cells, a grating that stimulated a chosen L and M combination (L+M) was also used along with an isoluminant combination (L-M) of L and M cone stimulation. Analogously, a grating that stimulates L and M cones in synchrony with S cones (Y+S) and antagonistically with S cones (Y-S) was used for (YB) P cells.

To calculate the isoluminant grating, each gun of the Conrac monitor was also measured photometrically to determine its photopic luminance output (evaluated with the photopic luminous efficacy function $V(\lambda)$). The luminance of each cone-isolating grating

was calculated. A combination of L and M cone-isolating gratings was found that gave a total luminance modulation of 0. Typical values for the relative weightings of the red, green, and blue guns for each type of grating are given in Table 2-1. Table 2-2 gives the luminance of the three guns of the Conrac. The experiment-to-experiment and year-to-year variation of these values was small, so that the relative intensities of the guns in Table 2-1 were kept the same throughout the course of these experiments.

Table 2-1. Gun Intensity Values for Different Grating Types

Type of Grating	CRT Gun Values			Fraction of Maximal Cone Excitation			Relative Luminance
	Red	Green	Blue	L	M	S	
Black and White	1.0	1.0	1.0	1	1	1	1
L cone-isolating	0.98699	-0.13934	0.00106	0.1600	0	0	0.10316
M cone-isolating	-0.86770	0.33687	-0.02740	0	0.1600	0	0.05680
L+M cone stimulus	-0.99865	0.84410	-0.08753	0.2937	0.5224	0	0.39572
Isoluminant (L-M)	0.97300	-0.28542	0.01925	0.06180	-0.1100	0	0.00002
Yellow (Y)	0.63114	0.98762	-0.13174	0.8000	0.8000	0	0.80552
S cone-isolating	0.16887	-0.18762	0.93174	0	0	0.8000	-0.00551
Y + S stimulus	0.46440	0.30620	0.86540	0.4000	0.4000	0.8000	0.393136
Y - S stimulus	-0.14671	-0.68143	0.99767	-0.4000	-0.4000	0.8000	-0.40820

Table 2-2. Luminance of the Red, Green, and Blue Guns of the CRT

Photopic Luminance of the Guns (cd/m^2)		
Red	Green	Blue
11.62	39.99	5.608

2.3 Data Collection and Analysis

This section discusses each type of experiment that was performed and the principal methods of data analysis.

2.3.1 Drifting Gratings

A drifting sine grating was translated at a steady rate either up or down relative to the center of the CRT display (Eq. (2-2)). A drifting grating experiment followed one of two paradigms.

In the first paradigm, a black-white grating was drifted at a steady frequency, 4.23 Hz or 8.46 Hz, while the impulse arrival times of a unit responding to the stimulus were recorded by the PDP 11/73 computer. Each episode lasted 15.1552 s or 30.3104 s. A series of contrast values consisted of 0.01625, 0.03125, 0.0625, 0.125, 0.25, and 0.50. After each episode, the UD73C program which handled all the stimulus generation and data collection for these experiments would print a summary of the cell's responses that allowed ongoing monitoring of the cell during the experiment.

To analyze the cell's response to the stimulus, the impulse rate, $r(t)$, of the cell was calculated from the spike arrival times collected during the period of stimulation; the spikes were placed in 3.7 ms bins and the rate was calculated by dividing the number of spikes in the bin by the size of the bin. After the experiment, the data were ported to a personal computer for further analysis. Typically, the amplitude and phase of the response, $R(f)$, of the cell at the stimulation frequency, f , and at the second harmonic, $2f$, along with the mean rate $R(0)$ were calculated via a Fourier transform of the impulse rate:

$$R(f) = \langle r(t) \cdot e^{-2\pi i f t} \rangle \quad (2-7)$$

where $\langle \rangle$ denotes the average over complete cycles of the stimulus. This calculation was carried out using the Fast Fourier Transform (FFT) (Press *et al.*, 1989) in a custom-

written program. The variation of the cell's response with contrast formed the basis for the contrast response function (CRF) used in cell characterization (see below).

The cell's response, $R(f)$, was also measured at several spatial frequencies. The spatial frequency response of a cell allows one to estimate the size of its receptive field, i.e. the visual area over which it receives input. This method is used to estimate the spatial parameters of different parts of the P and M cell receptive field by fitting the spatial frequency response to a modified Difference-of-Gaussians (modDOG) model described in Chapter 5. A series of spatial frequencies and contrasts were chosen and interleaved in successive episodes of stimulation. More than one drift frequency was also used in order to get a more complete spatiotemporal description of the cell's responses. The spatial frequency values chosen were 0, 0.143, 0.429, 0.715, 1.00, 1.57, 2.15, 3.29, 4.43, 6.72, 9.01, and 18.16 c/d. Five types of gratings were chosen based on the type of cell. For (RG) P cells or M cells, a typical selection of gratings was: black-white, L cone-isolating, an M cone-isolating, L-M (isoluminance), and L+M (Table 2-1). For a (YB) P cell, the series consisted of black-white, yellow (Y), Y-S, and Y+S gratings. The overall scale, c (Eq. 2-2), was chosen to give qualitatively the best response for a particular cell without saturation. For ON cells, c was 0.2 for black-white gratings and 0.8 for colored gratings. For OFF cells, the values of c above were halved. Typical drift frequencies were 2.17, -2.17, 8.46, -8.46, 16.92, and -16.92 Hz. A negative drift frequency specifies that the grating drifts upward rather than downward.

2.3.2 Contrast-Reversing Experiments

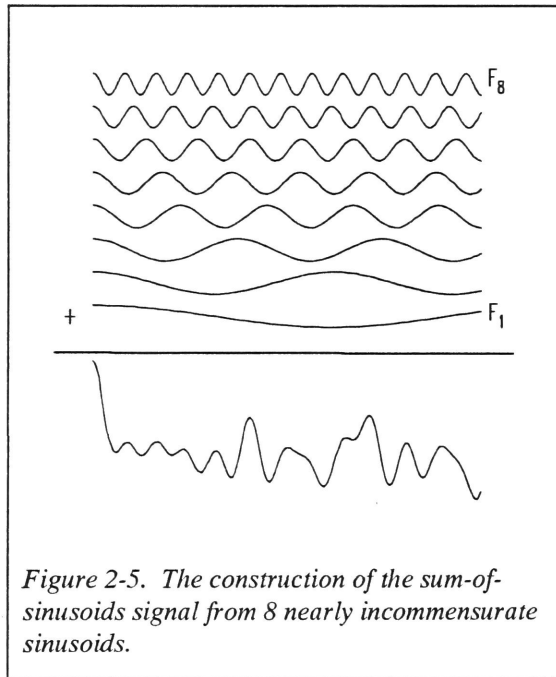
The contrast of a stationary sinusoidal grating can be modulated by a signal, $M(t)$:

$$L(x, t) = L_{mean} + A \cos(2\pi kx) \cdot M(t) \quad (2-8)$$

If $M(t) = \cos(2\pi ft + \phi)$ where ϕ is the temporal phase and f is the temporal frequency as before, the stimulus is a sinusoidal grating modulated temporally by a single sinusoid. The analysis proceeds as above (Eq. 2-7). Typically, the spatial phase of the grating was changed during each episode. This experiment provided the basis for determining whether a cell was X-like or Y-like (Hochstein and Shapley, 1976a,b).

2.3.3 Sum-of-Sinusoids Experiments

The sum-of-sinusoids method of Victor and Shapley (1980) was used to study the temporal frequency response of both M and P cells. Briefly, a sum of eight sinusoidal



frequencies (Fig. 2-5) was used as a signal to modulate the contrast of a sine grating, a spot, and/or an annulus. The signal is represented as:

$$M(t) = \sum_{n=1}^8 a_n \sin(2\pi f_n t + \phi_n) \quad (2-9)$$

where the subscript, n , indexes the individual frequencies. The frequencies, f_n , are chosen from one of two sets. The low temporal

frequency set spans the range 0.23-33.76 Hz. The high temporal frequency set which was used in the majority of experiments spans the range 2.71-41.25 Hz. Each stimulus episode lasted 30.356 seconds. The phases, ϕ_n , were designed to eliminate contamination by

responses of higher orders. Tables 2-3 and 2-4 show the frequencies and phases chosen from the sets designed by Victor and Shapley (1980). The frequencies are given as the number of cycles per repeat period and the phases as multiples of π .

Table 2-3. Low Frequency Sum-of-Sinusoids Set (Victor and Shapley, 1980).

f	Hz	Phase 1	Phase 2	Phase 4	Phase 4	Phase 5	Phase 6	Phase 7	Phase 8
7	0.23	0.5	0.5	0.5	0.5	0.5	0.5	0.5	0.5
15	0.49	0.5	1.5	1.5	0.5	0.5	1.5	1.5	0.5
31	1.02	0.5	0.5	0.5	0.5	1.5	1.5	1.5	1.5
63	2.08	0.5	1.5	0.5	1.5	1.5	0.5	1.5	0.5
127	4.19	0.5	0.5	1.5	1.5	1.5	1.5	0.5	0.5
255	8.41	0.5	0.5	1.5	1.5	0.5	0.5	1.5	1.5
511	16.86	0.5	1.5	1.5	0.5	1.5	1.5	0.5	1.5
1023	33.76	0.5	1.5	0.5	1.5	0.5	0.5	0.5	1.5

Table 2-4. High Frequency Sum-of-Sinusoids Set (Victor and Shapley, 1980)

f	Hz	Phase 1	Phase 2	Phase 3	Phase 4	Phase 5	Phase 6
82	2.71	0.5	1.167	1.833	1.50	0.167	0.833
162	5.35	0.5	1.167	1.833	1.50	0.167	0.833
270	8.91	0.5	1.167	1.833	1.50	0.167	0.833
450	14.85	0.5	1.167	1.833	0.50	1.167	1.833
566	18.68	0.5	1.167	1.833	0.50	1.167	1.833
750	24.75	0.5	1.167	1.833	0.50	1.167	1.833
982	32.41	0.5	1.167	1.833	1.50	0.167	0.833
1250	41.25	0.5	1.167	1.833	0.50	0.167	0.833

The zeroth, first-order, and second-order frequency kernels were calculated according to:

$$K_0 = \langle r(t) \rangle \quad (2-10)$$

$$K_1(f_n) = 2 \langle r(t) \cdot e^{-i(2\pi f_n t + \phi_n)} \rangle \quad (2-11)$$

$$K_2(f_n, f_m) = 2 \langle r(t) \cdot e^{-i(2\pi f_n t + \phi_n)} \cdot e^{-i(2\pi f_m t + \phi_m)} \rangle \text{ if } n \neq m \quad (2-12)$$

$$K_2(f_n, f_m) = 4 \langle r(t) \cdot e^{-i(2\pi f_n t + \phi_n)} \cdot e^{-i(2\pi f_m t + \phi_m)} \rangle \text{ if } n = m \quad (2-13)$$

where $r(t)$ is the response and $\langle \rangle$ represents an average over all initial phases and cycles of the stimulus (Victor, 1979). Frequently, only a partial set of phases was used in a experiment. This incompleteness may introduce anomalies into the kernels that are calculated (Victor and Knight, 1979). These discrepancies will be discussed later in the text. The sum-of-sinusoids signal was used to modulate the contrast of both luminance and chromatic gratings. In a typical experiment, a standard black-white grating was modulated at 4 contrast values. The maximum contrast for each of the sinusoids was $\frac{1}{8}$ of the maximum contrast of the stimulus. A range of contrasts was chosen: 0.01625, 0.03125, 0.0625, and 0.125. For (RG) P cells and M cells, several other stimuli were used: an L cone-isolating grating, an M cone-isolating grating, an L-M (isoluminant) grating, and an L+M grating. Similarly, for (YB) P cells, these conditions were used: an S cone-isolating grating, a yellow (Y) grating, Y+S grating, and Y-S grating. In addition, the gratings were usually assigned two spatial frequency values on different episodes, one low spatial frequency (typically, 0.145 c/d) and one high spatial frequency (2.181 c/d). The experiments were run under the UD73C program which gave an on-line analysis of cell responses during the experiment. After the experiment, further analysis was carried out on a PC.

In experiments designed to address the frequency responses of different parts of the cell's receptive field, the sum-of-sinusoids signal was used to modulate a small spot in the center of the CRT with the same contrast values as above. To excite the surround of the receptive field, an annulus was used instead of the spot. Typically, these experiments were done with the UD73C program. In some experiments, the spot and the annulus were modulated with the same sum-of-sinusoids signal but the contrast of the annulus was adjusted independently in a paradigm designed by Shapley and Victor (1981). These experiments addressed the effect of contrast in the surround of the receptive field on the response of the center (see Chapter 7 on M cells) and were performed with the MDX6RT program.

2.3.4 Perturbation Experiments

In some experiments the amplitude of one of the sinusoids in the sum-of-sinusoids signal was made larger than the others. This perturbation experiment (Shapley and Victor, 1978) provided a means to determine the temporal characteristics of the contrast gain control mechanism. Initially, a grating, typically 2.18 c/d, was modulated by a sum of eight sinusoids, each assigned a contrast of 0.0625. Then, in successive episodes, the contrast of one of the eight frequencies was increased to 0.35. These experiments were interleaved with each one of the eight frequencies, providing a higher amplitude signal. Each condition was interleaved with the seven others and progressed through the usual phase sets. The kernels were calculated for each one of these conditions and compared. These experiments were done with the UD73C program.

2.3.5 Step Response Experiments

In some experiments, the contrast of a grating, spot, or annulus was modulated by a simple square wave signal of several amplitudes at 1.0557 Hz. A peristimulus histogram of the cell's response was generated after the experiment. These experiments were handled by either UD73C or MDX6RT.

2.3.6 M-Sequence Experiments

The practical application of the multiple m-sequence method (Benardete and Victor, 1994) is discussed here while the theoretical aspects are postponed until Chapter 3.

In the m-sequence regime, it is important to recognize the discrete nature of the stimulus. The m-sequence signal, $m(t)$, which is cyclic and binary (Golomb, 1968), takes on a new value of 1 or -1 after a predetermined time step, ΔT . The contrast of a grating, spot, or annulus was modulated by this signal. For these experiments, a positive value indicates an increment in contrast while a negative value indicates a decrement. The modified m-sequence method uses a sum of two m-sequences as the signal. Thus, this new signal is ternary (2, 0, -2). The lengths of the two m-sequences are always of the form $2^N - 1$, where N is the order of the m-sequence. For the modified m-sequence method, the lengths of the sequences, integers of the form $2^N - 1$, are also chosen to be relatively prime, i.e. to share no common factors other than 1. As discussed in Chapter 3, this condition prevents certain kinds of kernel contamination. In these experiments, the time step was 14.8 ms. In a typical experiment, the sum of two m-sequences was used to reverse the contrast of a grating or other pattern. The contrast of the grating was

determined and scaled as described for the drifting gratings experiments. On successive episodes, the m-sequence signal was inverted to enable the use of the inverse repeat method (see Chapter 3). To calculate the m-sequence kernels, $\hat{h}_n(t)$, to a stimulus of unit power and unit time step, the response, $r(t)$, of the unit is cross-correlated with the input sequences. For the responses, $r_+(t)$, to the sequences in the usual polarity,

$$\hat{h}_1^{1+}(l) = \langle r_+(t) \cdot m_1(t-l) \rangle \quad (2-14)$$

$$\hat{h}_1^{2+}(l) = \langle r_+(t) \cdot m_2(t-l) \rangle \quad (2-15)$$

$$\hat{h}_2^{1,2+}(l_1, l_2) = \frac{1}{2} \langle r_+(t) \cdot m_1(t-l_1) \cdot m_2(t-l_2) \rangle \quad (2-16)$$

where $m_1(t)$ and $m_2(t)$ are the m-sequences in the sum-of-m-sequences signal. For the response to the inverted sequences, $r_-(t)$,

$$\hat{h}_1^{1-}(l) = \langle r_-(t) \cdot m_1(t-l) \rangle \quad (2-17)$$

$$\hat{h}_1^{2-}(l) = \langle r_-(t) \cdot m_2(t-l) \rangle \quad (2-18)$$

$$\hat{h}_2^{1,2-}(l_1, l_2) = \frac{1}{2} \langle r_-(t) \cdot m_1(t-l_1) \cdot m_2(t-l_2) \rangle \quad (2-19)$$

To take advantage of the inverse repeat, the above estimates are averaged as given by:

$$\hat{h}_1^1(l) = \frac{1}{2} \left(\hat{h}_1^{1+}(l) - \hat{h}_1^{1-}(l) \right) \quad (2-20)$$

$$\hat{h}_1^2(l) = \frac{1}{2} \left(\hat{h}_1^{2+}(l) - \hat{h}_1^{2-}(l) \right) \quad (2-21)$$

$$\hat{h}_1^{1,2}(l_1, l_2) = \frac{1}{2} \left(\hat{h}_1^{1,2+}(l_1, l_2) + \hat{h}_1^{1,2-}(l_1, l_2) \right) \quad (2-22)$$

In the actual experiment, the power, P , in the stimulus and the time step were both different from unity. In this case, the same calculations, performed as above (except for the factor of $\frac{1}{2}$ in the second-order kernel calculation), yield a measure of the first-order and second-order responses to the stimulus. The kernel is obtained, if desired, by dividing the response of order n by P^n and the time step. Frequently, in the results section, the analysis is presented as first-order and second-order responses for convenience and ease of discussion.

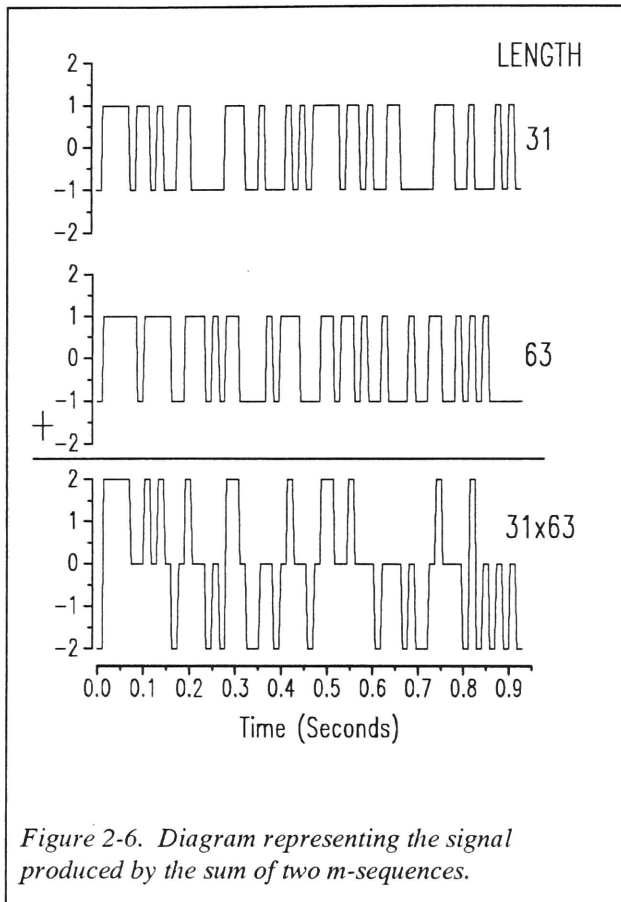
The modified m-sequence method was further exploited by using a shift of the same sequences to modulate a second grating or pattern simultaneously. This procedure allowed the calculation of a second set of first- and second-order kernels from the response to a single ambient stimulus as well as the calculation of a second-order cross-kernel. For example, in some experiments to be described, these two m-sequence signals were used to modulate both an L cone-isolating grating and an M cone-isolating grating simultaneously. The responses to this single presentation allows calculation of a first-order kernel and a second-order kernel for the L cone-driven mechanism, a first-order kernel and a second-order kernel for the M cone-driven mechanism, and a second-order cross-kernel for responses driven by nonlinear interactions between L and M cone-driven mechanisms.

The sum-of-m-sequences signal was generated from a sequence of length 31 and another of length 63. The total stimulus cycle was thus $(31 \cdot 63)$ 1953 time steps which was 28.9044 seconds. As part of the design of MDX6RT, there was an additional pre-stimulus of 5 seconds to avoid introducing transients into the response. Different conditions were interleaved, and successive presentations of the same stimulus used different generating polynomials for the m-sequence. This technique also reduces the anomalies in kernel estimates (see Chapter 3). The generating polynomials used in successive sets are given in Table 5. A shift of 16 was used with the length 31 sequence while a shift of 32 was used with the length 63 sequence.

Table 2-5. Generating Polynomials for M-Sequences

Set	Generating Polynomial (31)	Generating Polynomial (63)
1	$x^5 = x^2 + 1$	$x^6 = x + 1$
2	$x^5 = x^3 + 1$	$x^6 = x^4 + x^3 + x + 1$
3	$x^5 = x^3 + x^2 + x + 1$	$x^6 = x^5 + 1$
4	$x^5 = x^4 + x^2 + x + 1$	$x^6 = x^5 + x^2 + x + 1$

Figure 2-6 shows the composition of a sum-of-m-sequences signal from two relatively



prime-length m-sequences. The cross-correlations necessary for kernel calculation (Eqs. (2-14) - (2-19)) were done using the Fast M-Transform (FMT) described by Sutter (1992). I programmed the actual routine by modifying a Fast Hadamard Transform (Beauchamp, 1984) of Kunt (1975).

2.4 Classification of cells

All ganglion cell activity was attributed to either a P cell or an M cell based on several tests. The depth

of the penetration was a fairly reliable indication of the ganglion cell's target layer. The top of the LGN was nominally at 23 mm. The four P layers and two M layers were usually progressed through in order.

As an initial step in analyzing a cell's response to stimuli, the entire display was made a uniform red, green, or blue from the output of a single gun. Cells were thus classified as R+G-, R-G+, Y+B-, Y-B+, and achromatic (BB, broadband) based on the changes in their impulse rate to these stimuli. P cells are typically color opponent while M cells are broadband. For example, an R+G- unit would increase its maintained discharge in response to uniform red and decrease its output to uniform green. If the steady

discharge of an isolated unit increased in response to increased white light in its receptive field, the cell was classified as ON. If the rate decreased, the cell was classified as OFF.

The latency of the cell's S-potential following electrical stimulation of the optic chiasm was measured. The latencies of M cells fall in the range of 1-2.5 ms, and that of P cells between 2.5-4.5 ms (Kaplan and Shapley, 1982).

A luminance CRF was plotted as the amplitude of the cell's response at the drift frequency versus the value of the contrast of a grating stimulus on the x-axis. P cells show a contrast response function of shallow slope that is nearly a straight line with increasing contrast, while M cells demonstrate a steep slope at low contrast values (e.g. 0.01) and early saturation (Kaplan and Shapley, 1986). Figures 2-7 and 2-8 show the correspondence between the anatomical layers and the CRF from one of my experiments. In five such anatomical controls, the combination of the above criteria always correctly identified the type of cell that was marked.

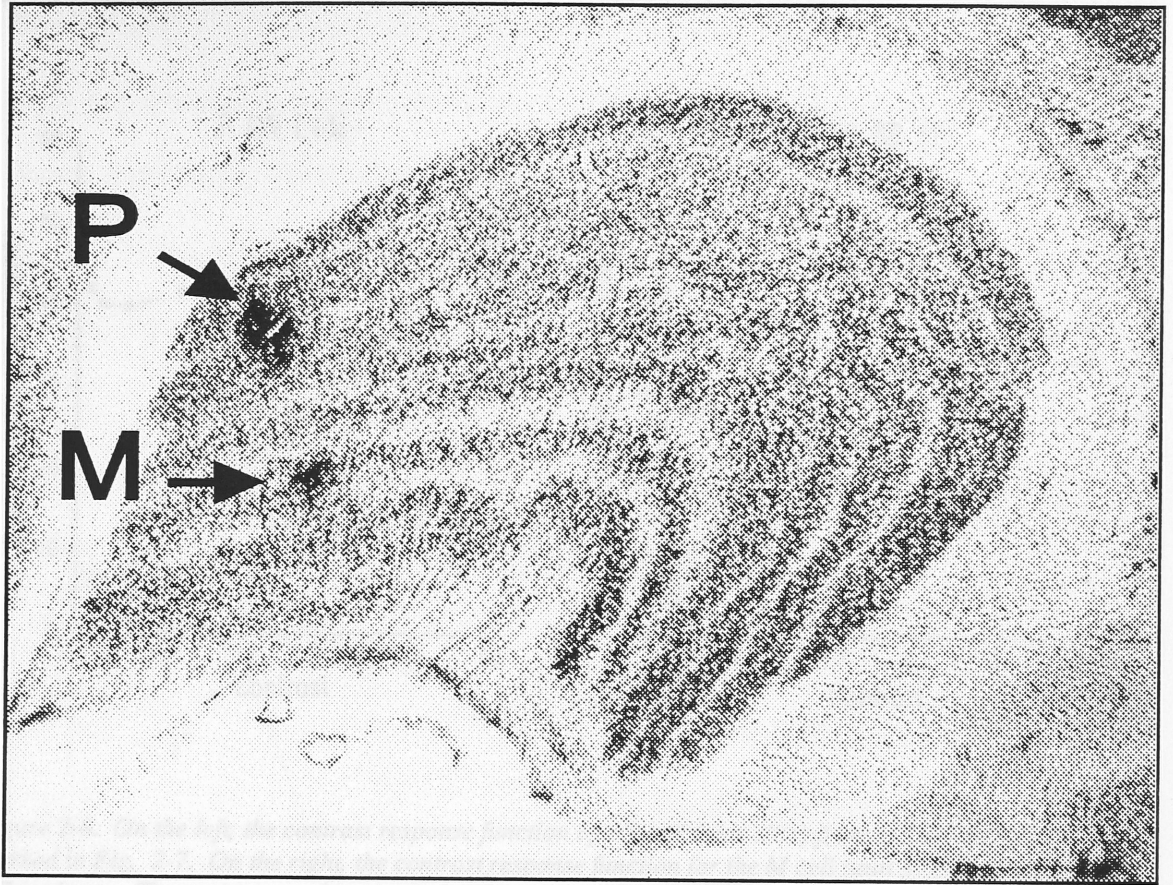


Figure 2-7. Electrolytic marking of the LGN identifies the anatomical layer of the units whose CRFs are shown in Fig. 2-8. Such controls assured that M and P cells were correctly differentiated by the physiological tests which were applied.

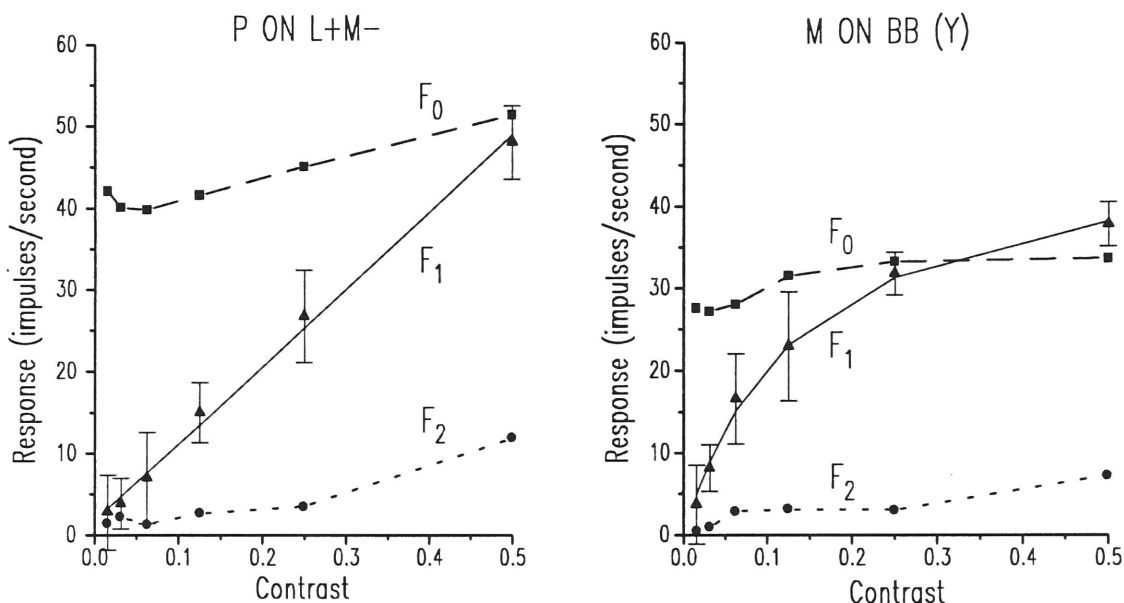


Figure 2-8. On the left, the contrast response function of a P cell (unit 37/1) from the recording site marked in Fig. 2-7. On the right, the contrast response function for the M cell (unit 37/5) marked in Fig. 2-7 is shown. The response at the stimulation frequency, 4.23 Hz, is labeled as F_1 . The response at twice the stimulation frequency is labeled F_2 , and the mean rate is labeled F_0 . The error bars show the 90% confidence interval around each data point using the T^2_{circ} statistic (Victor and Mast, 1991). The spatial stimulus was a drifting grating of 2.181 c/d. On the left, the regression line (solid) through the data has slope: 93.965 impulses/(second-unit contrast); and y-intercept: 1.725 impulses/second. On the right, the solid line represents a fit of the Michaelis-Menton function (Kaplan et al., 1990) to the F_1 amplitude: R_m : 48.749 impulses/second; b : 0.140 units of contrast.

2.4.1 Linearity of Spatial Summation

A contrast-reversing grating was used to test the spatial linearity of the cell's receptive field. The modified null test which is frequently used to distinguish X cells (linear) from Y cells (nonlinear) in the cat uses a high spatial frequency grating to probe for the presence of a second harmonic response (response at twice the stimulation frequency). Figure 2-9 shows the first (F_1) and second harmonic responses (F_2) of an M

cell that is clearly Y-like. Notice that at high spatial frequencies the ratio $F_2/F_1 \gg 1$.

Cells like this are extremely rare in the M layers of the primate LGN (Irvin *et al.*, 1993; Derrington and Lennie, 1984). Indeed, I found very few M cells that could be clearly classified as Y-like based on this test. More commonly, I found M cells with F_2/F_1 ratios near 1 at the high spatial frequencies. Typically, I called these cells X-like.

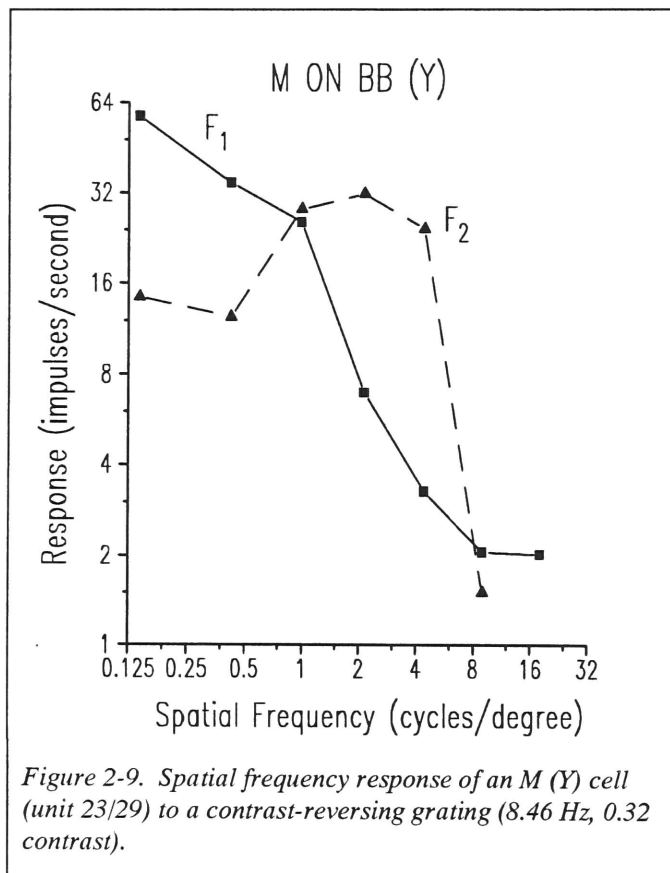


Figure 2-10 shows the results of a null test on a P cell and on an M (X) cell. Notice that F_1 goes through a minimum at one position of the grating. This “null” implies linearity of spatial summation. The second harmonic response, F_2 , for these two cells was essentially in the noise; the phase of F_2 was random at all positions of the grating. All P cells were classified as X-like (Kaplan and Shapley, 1982).

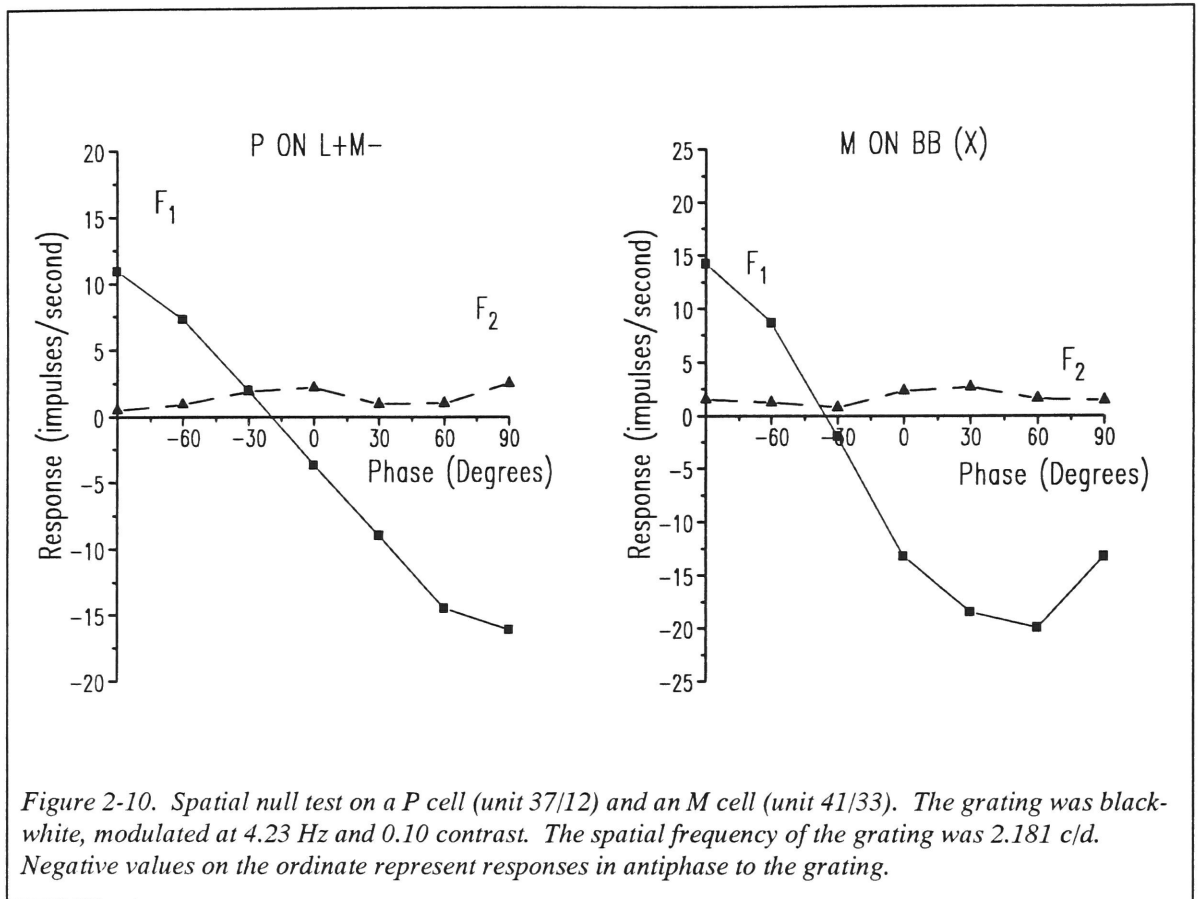
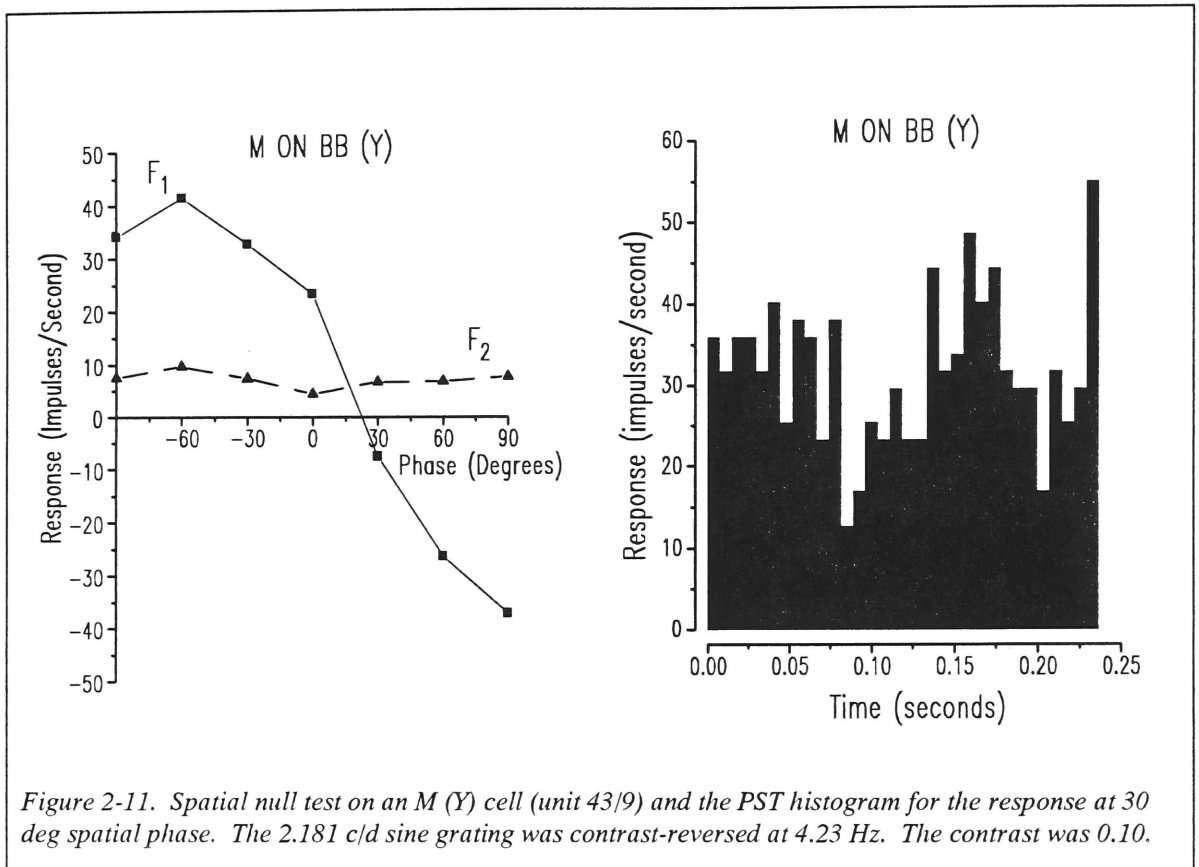
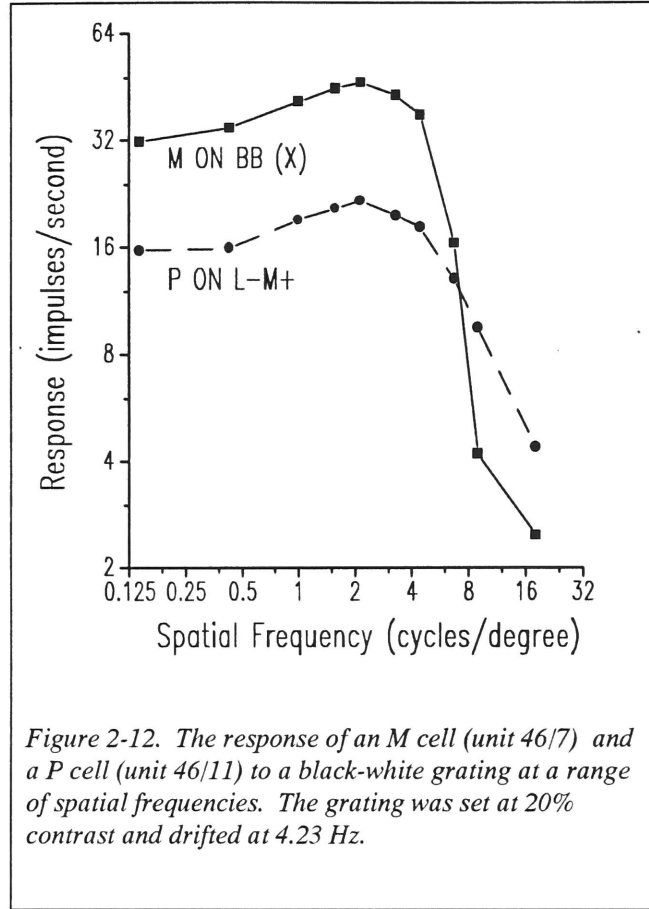


Figure 2-11 shows a null test on an M cell that was classified as Y-like. Here, even though F_2/F_1 was never $\gg 1$, a significant F_2 response was seen at all positions of the grating. The histogram on the right shows the cell's response at 30° phase (near the F_1 null). Notice that the response at twice the stimulation frequency is clear. Further work described in Chapter 6 suggests that M cells form a continuum between the strongly Y-like cell of Fig. 2-9 through the less strongly Y-like cell of Fig. 2-11 to the X-like M cells of Fig. 2-10. These results may mean that the X/Y (spatial linearity) classification has less significance in the M layers of the monkey LGN than it does in the cat.



2.4.2 Spatial Frequency Response

In addition, every cell had at least one spatial frequency response analyzed with a black-white grating. Results for a typical M cell and a typical P cell from the same primate and approximately the same eccentricity are shown in Fig. 2-12. This figure illustrates the lower spatial frequency cut-off of M cells compared to P cells and the higher contrast sensitivity of M cells relative to P cells for black-white (luminance) stimuli (Kaplan and Shapley, 1986). The spatial frequency response of retinal ganglion cells is determined by the size of their receptive field which is an increasing function of their eccentricity (distance from the fovea). Thus, in order to maintain some uniformity, all of the units analyzed in this work were in the parafoveal region (1-15 degrees of the fovea).



2.5 Model Fits

2.5.1 First-Order Kernels

A general-purpose model is used throughout this work to describe the temporal frequency responses of units that were analyzed. This model was used previously by Victor (1986) to describe the cat X-cell center. The model consists of two stages: a series of low-pass filters (“leaky” integrators) and a subtractive low-pass stage (Benardete *et al.*, 1992a):

$$K(\omega) = Ae^{-i\omega D} \left(1 - \frac{H_s}{1 + i\omega\tau_s} \right) \left(\frac{1}{1 + i\omega\tau_L} \right)^{N_L} \quad (2-23)$$

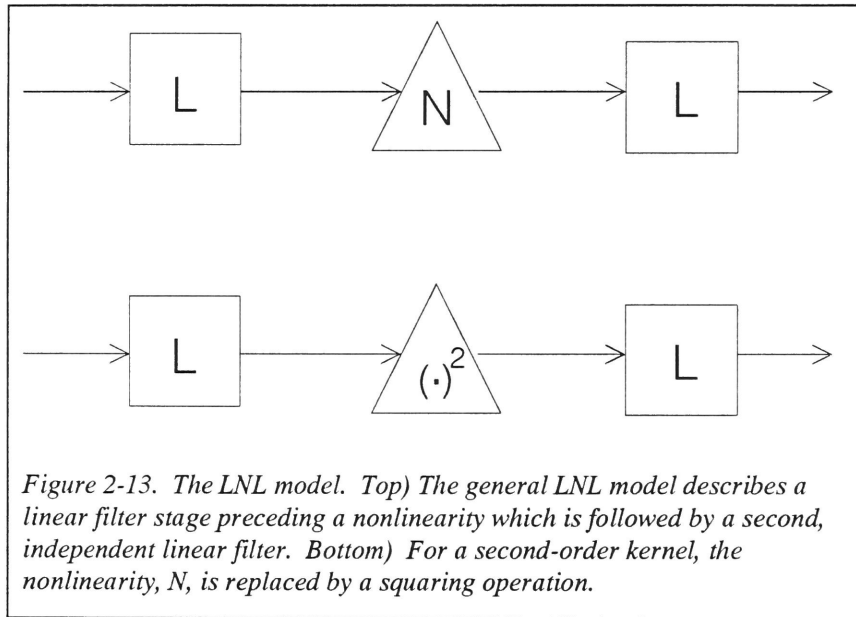
An initial delay, D , was the measured delay of transmission from the optic chiasm to the LGN. Five parameters determined the model: A , the overall gain; H_s the strength of the subtractive stage; τ_s , the time constant of the high-pass stage; τ_L , the time constant of the low-pass stages; and N_L , the number of low-pass stages. For data collected with the sum-of-sinusoids method, the model was fit to the data using either a custom version of the Levenberg-Marquardt routine (Press *et al.*, 1989) or a general-purpose commercial program (Excel, Microsoft Corporation). The response at each frequency, ω , is a complex number. The model was fit to the log of this complex quantity (log of the amplitude and the phase angle) by minimizing the sum of the squares of the difference between model and the data. The error at each frequency was weighted according to how much of the total response was accounted for by the response at that frequency (Shapley and Victor, 1981).

The first-order kernels from the m-sequence method were fit to the same model but two additional steps were required. First, the m-sequence kernel was transformed into the frequency domain using the FFT. Then the fit proceeded as above. Finally, the fitted model was transformed back into the time domain.

2.5.2 Second-Order Kernels

Two kinds of second-order kernels were measured in this work, one with the sum-of-sinusoids procedure, and the other with m-sequences. The fitting proceeded in the same manner for both methods except that the m-sequence fits were preceded by a Fourier transform and followed by its inversion (if desired). To reduce noise in the frequency measurement, values of the second-order kernel at which either of the two lags was

>120 ms were set to zero. The signal-to-noise ratio at these long lags was always small. The linear-nonlinear-linear (LNL) sandwich model provides a convenient approximate representation for Wiener white-noise kernels and kernels collected with Wiener-type methods of which the sum-of-sinusoids and the modified m-sequence methods are two examples (Victor and Knight, 1979; Korenberg and Hunter, 1986). For a second-order kernel, the structure of the model describes a linear filter stage preceding a quadratic nonlinearity followed by a second, independent linear filter (Fig. 2-13).



Following the scheme in the lower frame of the figure above, the quantitative analysis of the second-order kernels continued by fitting the general model as:

$$K_2(\omega_1, \omega_2) = Ae^{-iD(\omega_1 + \omega_2)} \cdot U(\omega_1) \cdot U(\omega_2) \cdot W(\omega_1 + \omega_2) \quad (2-24)$$

where A is an overall gain factor, D describes a delay as above, $U(\omega)$ is the transfer function of the pre-nonlinearity filter and $W(\omega)$ is the transfer function of the post-

nonlinearity filter. Both the pre-nonlinearity filter and the post-nonlinearity filter are given the same form as the linear filter described in the previous section. Thus, the overall fit is determined by 8 parameters plus an overall gain factor, A , and the delay, D . The 8 parameters are: $H_{S,U}$, $\tau_{S,U}$, $N_{L,U}$, $\tau_{L,U}$ and $H_{S,W}$, $\tau_{S,W}$, $N_{L,W}$, and $\tau_{L,W}$. Instead of fitting the model to the log of the measured response (as above), in this procedure, the model was fit to the data in the complex plane by minimizing the error between the measured real and imaginary parts of the response and the model output. Again, two methods were tried and compared: a custom-written program using the Levenberg-Marquardt procedure and a general-purpose algorithm in commercial software (Excel). Both methods yielded equivalent results.

In order to fit the LNL “sandwich” model to the m-sequence kernels, the m-sequence kernel, \hat{h}_2 , was transformed into the frequency domain. The measured m-sequence kernels are shown as surface plots in Fig. 2-14. The amplitude of the Fourier transform is shown at left as a contour plot in Fig. 2-15, and the fit of the LNL model is shown at right. In all the contour plots presented in this thesis the tick marks point in the downhill direction. Just as the second-order kernel, $\hat{h}_2(l_1, l_2)$, is defined at a pair of values l_1 and l_2 , the Fourier transform, $\hat{H}(\omega_1, \omega_2)$, is also defined at a pair of frequencies: ω_1 and ω_2 .

Because the kernel is symmetric, $\hat{H}(\omega_1, \omega_2) = \hat{H}(\omega_2, \omega_1)$. Similarly, since $\hat{h}_2(l_1, l_2)$ is real, $\left\| \hat{H}(\omega_1, \omega_2) \right\| = \left\| \hat{H}(-\omega_1, -\omega_2) \right\|$. For the phase, $\phi\left(\hat{H}(\omega_1, \omega_2)\right) = -\phi\left(\hat{H}(-\omega_1, -\omega_2)\right)$.

Thus to display $\hat{H}(\omega_1, \omega_2)$, it is only necessary to display the amplitude and the phase of the function in the upper right and lower right quadrants of the $(\omega_1 - \omega_2)$ plane. The amplitude of the transform is represented here as contours, and later the phase will be represented by the color of the contours. One can see here that the LNL model captures the major features of the kernel. Transforming the fitted model back into the time domain yields a close approximation to the data (Fig. 2-16). More will be said about the LNL model fits in Chapter 4.

For the center-surround cross-kernel, a modification of the LNL model was used. Instead of a single pre-nonlinearity filter, $U(\omega)$, the cross-kernel required two independent pre-nonlinearity filters, $U(\omega)$ and $V(\omega)$. These filters were of exactly the same type as above. $U(\omega)$ represents the linear filter for the center input, and $V(\omega)$ represents the filter for the surround input. The output of both filters then enters the quadratic nonlinearity in the model, and the output of the nonlinearity goes through a post-nonlinearity filter, $W(\omega)$. The fit of this LLNL model to the cross-kernel proceeds in the same way as above except that 4 additional parameters: $H_{S,V}$, $\tau_{S,V}$, $\tau_{L,V}$, and $N_{L,V}$ are required.

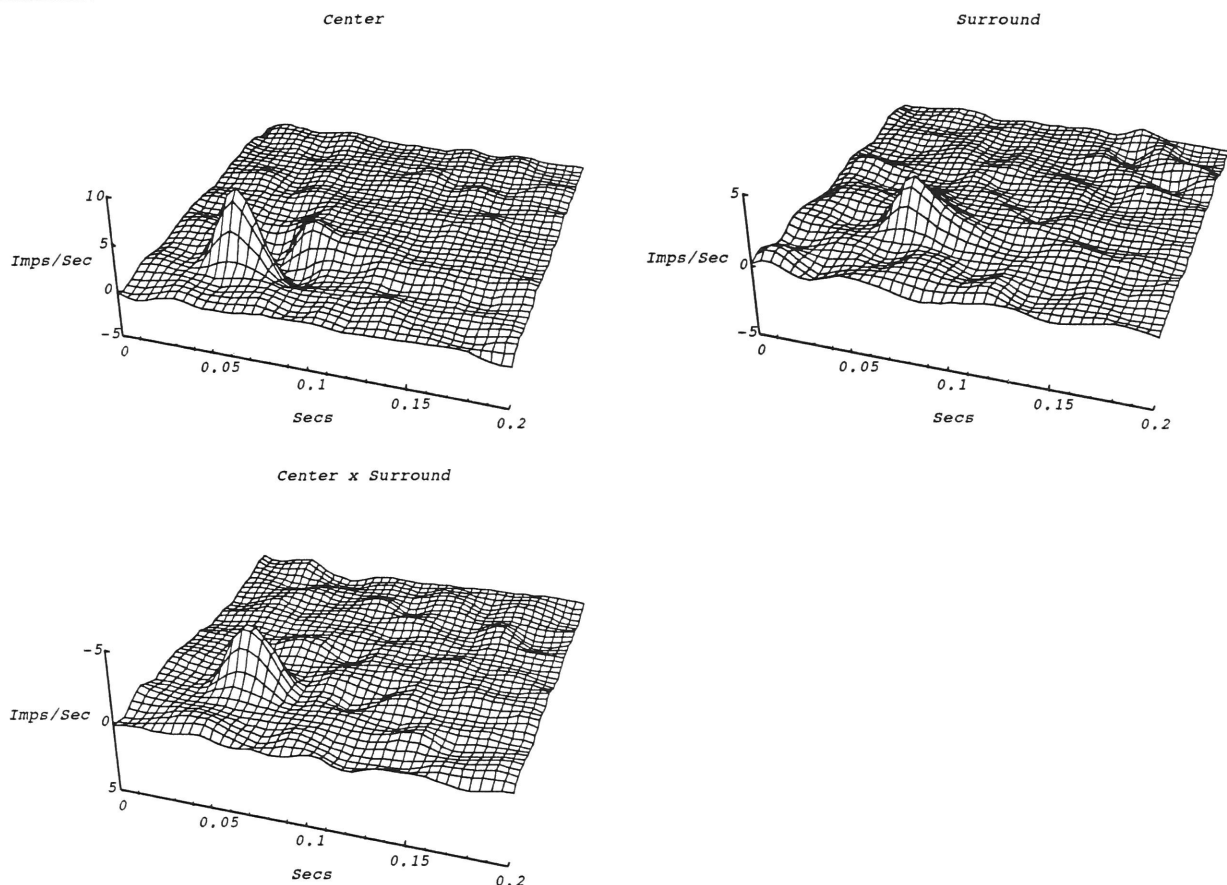
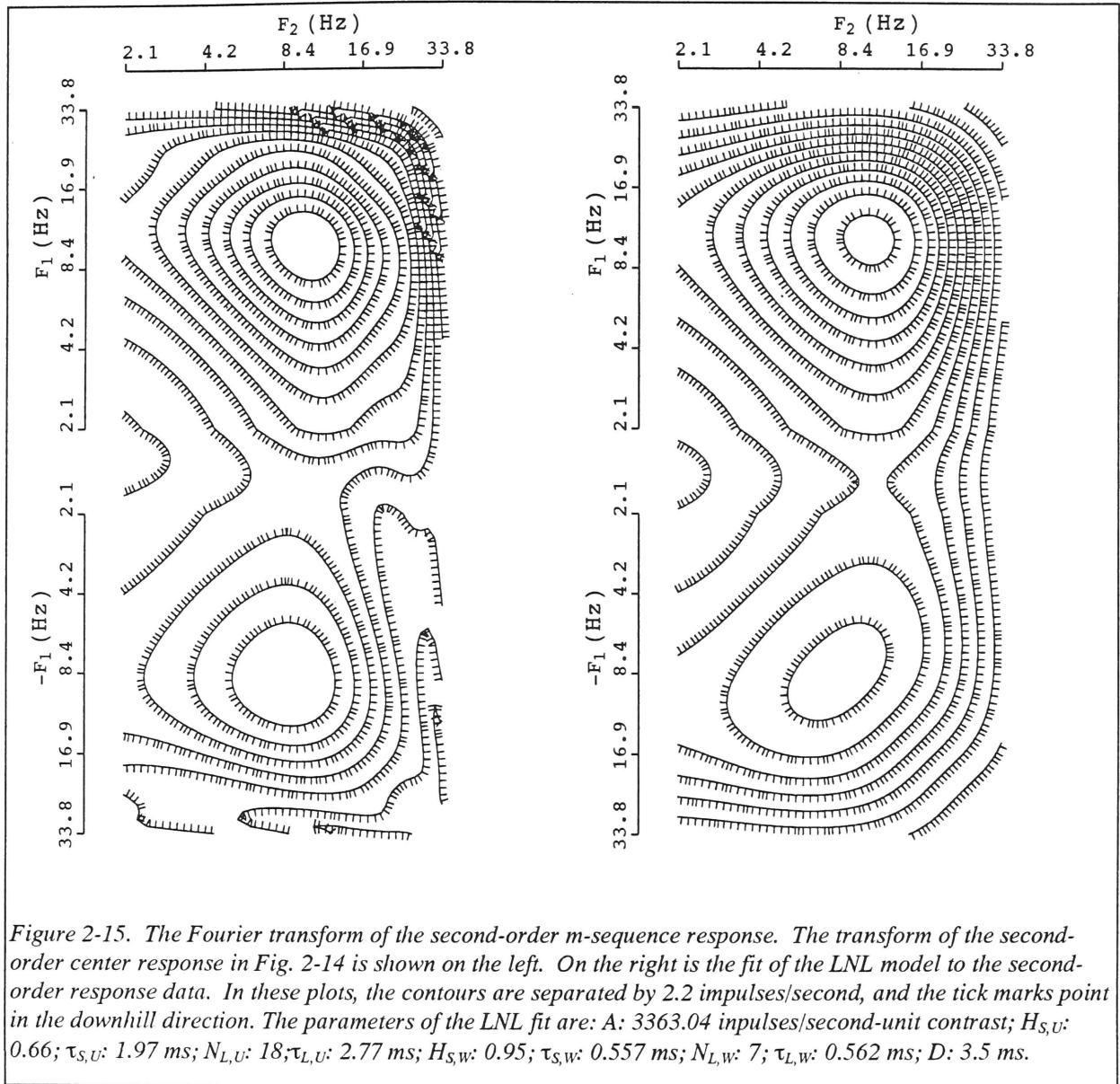
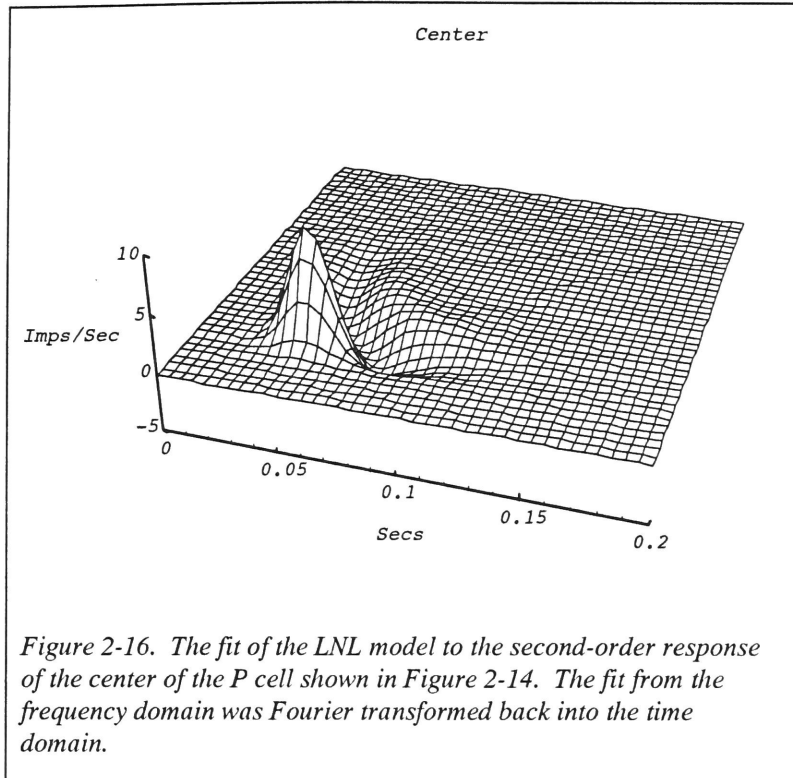


Figure 2-14. Surface plots of the second-order responses for the center, surround, and center-surround interaction calculated with the hybrid *m*-sequence method using the spot/annulus stimulus. The contrast was 0.5 (unit 36/7). A cubic spline procedure was performed on the estimated response values to fill in the surface. The *x*- and *y*-axes in the surface plots indicate the time from the origin of the response values. For the center and surround ("self-") kernels, both axes indicate the time for the center and surround signals respectively (i.e., the kernels are symmetric). For the center-surround ("cross-") kernel, the axis shows time from the origin for the center signal. The second time axis for all these kernels is hidden by the surface. Cross-kernels are not, in general, symmetric, as illustrated by the center-surround response of this P cell. The presence of these second-order kernels demonstrates nonlinear interactions in the center and surround mechanisms of P cells that have not previously been identified.





The Multiple M-Sequence Method

Overview

Introduction

Preliminaries

Types of Kernels

M-Sequences

Standard Approach

Elimination of Anomalies

The Hybrid M-Sequence Method

Higher-Order Systems

Multi-Input Systems

Relationship to Wiener Kernels

Relationship to the Sum-of-Sinusoids Approach

Discussion

Appendix I

Appendix II

3. The Multiple M-Sequence Method

3.1 Overview

This chapter describes the theoretical basis for the multiple m-sequence method that is used throughout much of this work. It also discusses the sum-of-sinusoids method briefly as it relates to the m-sequence method.

3.2 Introduction

Nonlinear systems analysis has widespread applications in biology. One of the most general approaches is Wiener white-noise analysis (Marmarelis and Marmarelis, 1978). Standard Wiener analysis in the time domain, based on the presentation of white noise to the system under study and dissection of the resulting response, has theoretical advantages (Wiener, 1958), but a straightforward application of the Wiener method is compromised by the impossibility of generating true white noise in the laboratory. For this reason, variations of the Wiener procedure, which share its theoretical framework but rely on alternative input signals, have been developed. These variations include frequency-domain methods (e.g. the sum of sinusoids technique (Victor and Knight, 1979)) and time-domain methods (e.g. band-limited Gaussian white noise (Marmarelis and Naka, 1972)).

The Wiener methods separate a system's response into "kernels," each of which is a component of a stereotyped mathematical description of the system's behavior. The order of the kernel function describes how many input values are simultaneously multiplied, weighted by that kernel, and summed into the total response. The fundamental

kernel representation of a system is that of Volterra (1932). The response, $r(t)$, of a single-input system to an input, $s(t)$, has a representation in terms of Volterra kernels which begins:

$$r(t) = L_0 + \int_0^\infty L_1(\tau)s(t-\tau)d\tau + \int_0^\infty \int_0^\infty L_2(\tau_1, \tau_1)s(t-\tau_1)s(t-\tau_2)d\tau_1d\tau_2 + \int_0^\infty \int_0^\infty \int_0^\infty L_3(\tau_1, \tau_2, \tau_3)s(t-\tau_1)s(t-\tau_2)s(t-\tau_3)d\tau_1d\tau_2d\tau_3 + \dots \quad (3-1).$$

Here, L_0 is the zeroth-order kernel, $L_1(\tau)$ is the first-order kernel, $L_2(\tau_1, \tau_2)$ is the second-order kernel, and $L_3(\tau_1, \tau_2, \tau_3)$ is the third-order kernel. The zeroth-order kernel describes the response of the system to no input. The first-order kernel function attaches a weight to values of the input at specific times in the past according to how much an input value affects the total response. For a linear system, the first-order kernel is known as the impulse response. The second-order kernel assigns weights to the product of two previous values. The third-order kernel assigns weights to the product of three previous input values and so on. The task for the experimenter is to determine the system kernels in an efficient, practical, and sufficiently complete manner.

3.3 Preliminaries

It is necessary to make some approximations and assumptions in order to estimate kernels experimentally. First, in the laboratory, the system's response is sampled at discrete time intervals, not continuously. The first measurement is usually considered to take place at time $t = 0$; the next at $t = \Delta T$, and the next at $t = 2\Delta T$, and so on, where ΔT is the sampling interval. Therefore, it is natural to expect that kernel values will only be

known at time lags which are a multiple of the sampling interval, ΔT ; and kernel values may be indexed by this integer multiplier. This corresponds to the assumption that the unit of time has been chosen so that $\Delta T = 1$.

Secondly, we assume that the system's kernels are of finite duration. In other words, an input at the present time will only affect the system's response for a limited amount of time in the future, not indefinitely. This length of time is generally referred to as the system's memory time, and will be denoted by T . This memory time may be determined from *a priori* knowledge of the system, or from pilot studies based on systems-analytic methods. Knowledge of the system's memory is important in designing a protocol to carry out a kernel measurement (see below). Furthermore, the only systems we will consider are those with kernels that are functions solely of past and present input, i.e. causal.

Finally, we assume that the system's kernels do not vary over the course of the experimental measurement. This system property is referred to as time-stationarity.

With this preface in mind, we take another look at the system in Eq. (3-1). Under the preceding assumptions, the integrals become summations indexed by the sampling interval:

$$\begin{aligned}
 r(t) = & L_0 + \sum_{k=0}^T L_1(k)s(t-k) + \sum_{k_1=0}^T \sum_{k_2=0}^T L_2(k_1, k_2)s(t-k_1)s(t-k_2) + \\
 & \sum_{k_1=0}^T \sum_{k_2=0}^T \sum_{k_3=0}^T L_3(k_1, k_2, k_3)s(t-k_1)s(t-k_2)s(t-k_3) + \dots
 \end{aligned} \tag{3-2}$$

where L_0 , $L_1(k)$, $L_2(k_1, k_2)$, and $L_3(k_1, k_2, k_3)$ are discrete versions of the kernels in Eq. (3-1) and T is the system's memory in discretized time units.

3.4 Types of Kernels

Having chosen to identify a physical system in terms of a functional expansion, it remains to determine the kernel functions that describe the properties of the system. To justify our efforts, the functional expansion that we derive should meet certain requirements.

One goal of modeling is to produce a mathematical formulation that will predict the physical system's behavior under certain conditions. A measure of how well the model mimics the actual system is the mean-squared error (MSE): the average of the square of the difference between the model's prediction and the physical system's output. Therefore, a natural requirement for a functional model is that it minimize this error in some sense. Furthermore, since polynomial functions may be poor approximations to biological nonlinearities (Victor and Shapley, 1979a,b), a kernel expansion should handle a variety of nonlinearities that may or may not be "analytic" in a mathematical sense.

The Volterra formalism introduced in (Eq. 3-1) cannot meet these requirements. First, the Volterra kernels do not meet the MSE criteria. For example, a cubic nonlinearity lacks a Volterra representation in the kernels of less than third-order. The first- and second-order kernels (L_1 and $L_2 = 0$) do not comprise the best-fitting first- and second-order models. In addition, measuring the Volterra kernels experimentally is very

difficult if not impossible (Victor, 1992), especially for biological systems with sharp nonlinearities.

The Wiener functional expansion is based on the system's response to white noise of a certain power (variance). The kernels are constructed in such a way that at every order the Wiener expansion of a system minimizes the difference between the model's response and the measured response to the white noise input upon which the expansion is based. The Wiener expansion thus depends on the power of the white noise input; Volterra series expansions are based on responses to infinitesimal inputs.

For analytic systems, the Volterra series representation can be rearranged into a Wiener representation, and vice-versa, but for all but a few special cases, Wiener and Volterra kernels are not identical. Wiener kernels of a given order, n , contain contributions from Volterra kernels not only of order n , but also of certain higher orders ($n + 2, n + 4, n + 6, \dots$). These contributions from Volterra kernels of higher order correspond to terms such as $L_4(k_1, k_2, k, k)$, where an even number of time lags are equal -- the "diagonal" elements.

For non-analytic systems which do not have a Volterra representation, the Wiener representation typically exists, and in principle can be measured (Schetzen, 1980). Furthermore, the Wiener kernels, once measured, provide a sound avenue for developing or verifying the validity of a variety of models of biological systems. (For a brief theoretical account of Wiener kernels, see Appendix I). In the following analysis, the goal of the hybrid m-sequence method will be to estimate the Wiener kernels of a system of interest.

3.5 M-Sequences

The properties of m-sequences that are needed for the hybrid m-sequence method are summarized below. A more extensive discussion of properties of m-sequences and procedures for generating them may be found elsewhere (Golomb, 1968; Sutter, 1987).

A binary m-sequence of order N is a cyclic sequence $\{b_k\}$ of 0's and 1's that satisfies a linear recurrence relation:

$$b_k \equiv \sum_{l=1}^N b_{k-l} r_l \quad (3-3),$$

where $\{r_1, \dots, r_N\}$ are the coefficients (either 0 or 1) of the recurrence relation, and \equiv denotes congruence (mod 2). An m-sequence has length $2^N - 1$. For use as a test signal,

$$m(k) = 1 - 2b_k \quad (\text{or equivalently } m(k) = (-1)^{b_k}) \quad (3-4).$$

For example, an m-sequence of length $(2^3 - 1)$ is the binary sequence $\{1, 0, 0, 1, 0, 1, 1\}$ which corresponds to the sequence $\{-1, 1, 1, -1, 1, -1, -1\}$ for $m(k)$. Thus, $m(1) = -1$, $m(2) = 1, \dots, m(7) = -1$. A time-shift of the m-sequence generates another m-sequence, which starts at a new initial position. The above sequence shifted by +5 reads $m(k + 5) = \{-1, -1, -1, 1, 1, -1, 1\}$. These shifts exploit the cyclic nature of the sequence. In what follows, we write the sequence as a function of the variable t , to indicate that it takes on a new value (1 or -1) after each unit of discrete time.

M-sequences satisfy certain properties that make them especially useful for systems analysis (Golomb, 1968). Three of these are frequently needed and so are stated here. First,

$$\langle m(t) \rangle = -\frac{1}{M} \quad (3-5),$$

where $\langle \rangle$ denotes the average over complete cycles of the m-sequence. That is, the sum of all the elements of an m-sequence divided by the length of the sequence is $-\frac{1}{M}$, where M is the length of the sequence. This property is based on the fact that every m-sequence has one more -1 than 1 in it.

For our purposes, it is also necessary to know how to compute the product of two shifts of the same m-sequence (multiplied together element by element). The second property gives this result:

$$m(t+a) \cdot m(t+b) = m(t+F(a,b)) \quad (3-6),$$

provided that $a \neq b$. (If $a = b$, then $m(t+a) \cdot m(t+b) = 1$, since $m(t)$ is always +1 or -1.) Eq. (3-6) states that the product of two distinct shifts of an m-sequence is a third shift of the same sequence. This shift is determined by a mapping, F , which depends on the choice of r 's in the recurrence relation in Eq. (3-3). To illustrate with the first example, $m(t) \cdot m(t+5) = \{1, -1, -1, -1, 1, 1, -1\} = m(t+4)$, thus $F(0,5) = 4$.

A third useful property, which is typically called the autocorrelation property of m-sequences, follows from the two above:

$$\langle m(t+a) \cdot m(t+b) \rangle = \begin{cases} 1 & \text{if } a = b \\ -\frac{1}{M} & \text{otherwise} \end{cases} \quad (3-7).$$

In Eq. (3-7), if the two shifts, a and b , are not equal, multiplication of the shifted m-sequences produces a third, the average of which is $-\frac{1}{M}$ as in Eq. (3-5). If $a = b$, multiplication produces a sequence of all 1's. The autocorrelation property establishes the m-sequences as a class of pseudorandom, quasi-white signals.

The ensemble average of the product of two signals may be considered to be an inner product. In this sense, two nonidentical shifts of the same m-sequence are nearly orthogonal since their inner product is small ($-\frac{1}{M}$). However, a shift of an m-sequence is not necessarily orthogonal to a product of two other shifts:

$$\langle m(t+a) \cdot m(t+b) \cdot m(t+c) \rangle = \begin{cases} 1 & \text{if } F(b,c) = a \\ -\frac{1}{M} & \text{otherwise} \end{cases} \quad (3-8).$$

These higher-order correlations are the source of the difficulty in the estimation of higher-order Wiener kernels via m-sequence methods.

3.6 Standard Approach

Lee and Schetzen (1965) showed that the Wiener kernels of a nonlinear system could be estimated by cross-correlating the response of the system with the white-noise input. Sutter (1987) has shown that for certain m-sequence inputs the Wiener kernels can also be approximated by cross-correlating the response of a system with the m-sequence test signal. Sutter has also developed a fast transform method for this cross-correlation, the Fast M Transform (FMT) (Sutter, 1991). The cross-correlation algorithm for the first few Wiener kernels is:

$$h_0 = \langle r(t) \rangle \quad (3-9),$$

$$h_1(l) = \langle r(t) \cdot s(t-l) \rangle \quad (3-10),$$

$$h_2(l_1, l_2) = \frac{1}{2!} \langle r(t) \cdot s(t-l_1) \cdot s(t-l_2) \rangle, l_1 \neq l_2 \quad (3-11),$$

$$h_3(l_1, l_2, l_3) = \frac{1}{3!} \langle r(t) \cdot s(t-l_1) \cdot s(t-l_2) \cdot s(t-l_3) \rangle, l_1, l_2, l_3 \text{ all unequal} \quad (3-12),$$

where h_0 , h_1 , h_2 , and h_3 are the zeroth-, first-, second-, and third-order Wiener kernels, and $\langle \rangle$ indicates an average over all values of the stimulus.

Consider the system whose input-output relationship is given by (3-2) truncated after second-order. The response of this system to the m-sequence $m_1(t)$ will be:

$$r(t) = L_0 + \sum_{k=0}^T L_1(k) m_1(t-k) + \sum_{k_1=0}^T \sum_{k_2=0}^T L_2(k_1, k_2) m_1(t-k_1) m_1(t-k_2) \quad (3-13).$$

Now we will use Eqs. (3-9) - (3-12) to measure the kernels h_0 through h_2 , with $m_1(t)$ playing the role of $s(t)$. We will denote these kernel estimates by $\hat{h}_0^1, \hat{h}_1^1, \hat{h}_2^1, \dots$, \hat{h}_n^1 to indicate that the estimates are derived from the cross-correlation algorithm (3-9) through (3-12) with an m-sequence, $m_1(t)$, as input, rather than with a white-noise input. From Eq. (3-9) and the above properties of m-sequences, the resulting estimate of h_0 is:

$$\hat{h}_0^1 = L_0 - \frac{1}{M} \sum_{k=0}^T L_1(k) + \sum_{k=0}^T L_2(k, k) - \frac{1}{M} \sum_{k_1 \neq k_2}^T L_2(k_1, k_2) \quad (3-14).$$

Eq. (3-14) shows that an average of the response produces an estimate, \hat{h}_0^1 , which has three kinds of contributions. First, there is a contribution from L_0 , which indicates the response of the system to zero input. Second, there is a small contribution due to the imperfect "randomness" of the m-sequence, whose size is inversely proportional to the length of the m-sequence. We denote the size of this contribution by $O(\frac{1}{M})$ to indicate that it approaches zero with the same rapidity as $\frac{1}{M}$, i.e. presenting the system with a longer m-sequence can further limit this contribution. With this notation, Eq. (3-14) takes the more compact form:

$$\hat{h}_0^1 = L_0 + O(\frac{1}{M}) + \sum_{k=0}^T L_2(k, k) \quad (3-15).$$

The third term in Eq. (3-15) is a contribution of the second-order Volterra kernel, L_2 , to the zeroth-order kernel estimate. This term is present in both the standard Wiener kernel h_0 and the m-sequence estimate \hat{h}_0^1 . It is a consequence (see above) of the relationship between the Volterra kernels and the Wiener kernels.

Now let us examine the estimate $\hat{h}_1^1(l)$ derived from the cross-correlation algorithm in Eq. (3-10) with $m_1(t)$ playing the role of $s(t)$. In order for $\hat{h}_1^1(l)$ to be a reasonable estimate of $h_1(l)$, the length, M , of the m-sequence should exceed the memory of the system, T ; otherwise, $\hat{h}_1^1(l)$ has contributions from $L_1(l)$ and other points on that kernel separated by the length of m-sequence. In what follows, we shall assume that a reasonable

estimate of the system's memory has been made such that an m-sequence of sufficient length ($>T$) can be selected.

For the system in Eq. (3-13), we apply the autocorrelation property of m-sequences given by Eq. 3-7 and Eq. 3-8 to obtain:

$$\hat{h}_1^1(l) = L_1(l) + O\left(\frac{1}{M}\right) + \sum_{k_1=0}^T \sum_{k_2=0}^T L_2(k_1, k_2) \delta(l, F_1(k_1, k_2)) \quad (3-16),$$

where \hat{h}_1^1 indicates the dependence of the estimate on the sequence $m_1(t)$ and where $\delta(l, k) = 1$ if $l = k$ and 0 otherwise. The above expression shows that \hat{h}_1^1 includes L_1 and a $O(\frac{1}{M})$ part, but also potential contributions from the second-order kernel, L_2 . These contributions to $\hat{h}_1^1(l)$ are not necessarily small. They depend on the size of the second-order kernel, $L_2(k_1, k_2)$, at the point at which $F_1(k_1, k_2) = l$. (F_1 is the mapping guaranteed by Eq. (3-6) to take the product of two shifts of $m_1(t)$ to a single shift of $m_1(t)$). These overlap contributions of the second-order kernel to the first-order kernel estimate do not correspond to Wiener/Volterra interrelationships, but rather are anomalies which are due solely to the algebraic properties of the m-sequence. The removal of these anomalies is the main benefit of the hybrid method.

The estimate \hat{h}_2^1 of h_2 is the cross-correlation of $r(t)$ with two shifts of the stimulus, as indicated in Eq. (3-11). Along the diagonal the fact that the input signal can only be ± 1 implies

$$\hat{h}_2^1(l, l) = \frac{1}{2} h_0 \quad (3-17).$$

Thus, this algorithm provides no information for points on the diagonal of h_2 , the second-order kernel.

Off the diagonal, we find from Eq. (3-11) that

$$\begin{aligned} \hat{h}_2(l_1, l_2) = & L_2(l_1, l_2) + O\left(\frac{1}{M}\right) + \frac{1}{2} \sum_{k=0}^T L_1(k) \delta(k, F_1(l_1, l_2)) + \\ & \frac{1}{2} \sum_{k_1=0}^T \sum_{k_2=0}^T L_2(k_1, k_2) \delta(F_1(k_1, k_2), F_1(l_1, l_2)) \end{aligned} \quad (3-18).$$

The estimate of $\hat{h}_2(l_1, l_2)$ has contributions from $L_2(l_1, l_2)$ and an $O(\frac{1}{M})$ part, but also contributions from L_1 and other points on L_2 , as determined by the mapping F_1 . These "overlaps" of first-order and second-order kernels amount to errors in the estimation of the Wiener kernel, again due to the algebraic properties of m-sequences.

Thus, estimates of kernels obtained by cross-correlation of responses to m-sequence inputs differ from Volterra kernels in three ways. One disparity corresponds to the slight difference in the number of +1's and -1's in the m-sequence. This is $O(\frac{1}{M})$, where M is the length of the m-sequence (typically > 1000), and will be ignored from now on. The second difference corresponds to the difference between Wiener kernels and Volterra kernels in general -- the "diagonal" terms discussed above. These are terms which are required by the fundamental differences between orthogonal (Wiener) series and power (Volterra) series. Finally, there are terms which relate specifically to anomalies in the higher-order statistics of m-sequences (i.e., triple correlations). These terms, which

depend on the choice of m-sequence through the mapping F , are the algebraic anomalies that we wish to control.

The above analysis readily extends to higher-order single-input systems. In general, higher-order kernel estimates obtained with m-sequences have numerous spurious contributions analogous to the lower-order anomalies already described.

The situation only worsens for a multi-input nonlinear system. For example, consider a two-input system with nonzero kernels up to second order. In the standard approach (Sutter 1987, 1992), a single m-sequence is the test signal for one input to this system and a long lag of this sequence is the second input. By an analysis exactly analogous to that above, it is straightforward to show that the estimate of the first-order kernels of this system will have contributions from all of the second-order kernels: two self-kernels and one cross-kernel. The estimates of these three second-order kernels will not only potentially contaminate one other but will also contain contributions from the first-order kernels for each input. Thus, for each second-order kernel, there are 5 kinds of anomalies, in addition to the $O(\frac{1}{M})$ parts.

3.7 Elimination of Anomalies

Several approaches to the anomaly problem have been developed. In this section, we focus on the inverse-repeat (IR) method (Sutter, 1992) which separates even- and odd-order kernel estimates from each other. In conjunction with the hybrid m-sequence method we describe, its effectiveness is expanded.

The IR method relies on measuring the second-order system's response Eq. (3-13) to the original m-sequence, $m(t)$, and to a second input given by $m(t)$ inverted in polarity: ($1 \rightarrow -1, -1 \rightarrow 1$). We denote the response to $m(t)$ by $r_+(t)$, and the response to the inverted input by $r_-(t)$. First-order contributions will be inverted in response to the inverted sequence, while the second-order contributions will maintain the same sign in both cases. Thus, subtraction of the first-order kernel estimate made with inverted sequence from the estimate made with the original sequence and averaging will produce an estimate of the first-order kernel that is free of second-order (and all higher, even-order) contamination. That is,

$$\hat{h}_1^{IR}(l) = \frac{1}{2} \left(\langle r_+(t) \cdot m(t-l) \rangle - \langle r_-(t) \cdot m(t-l) \rangle \right) \quad (3-19).$$

Adding two second-order estimates from $r_+(t)$ and $r_-(t)$ and averaging will annihilate aberrant contributions from first-order kernels:

$$\hat{h}_2^{IR}(l_1, l_2) = \frac{1}{2} \left(\langle r_+(t) \cdot m(t-l_1) \cdot m(t-l_2) \rangle + \langle r_-(t) \cdot m(t-l_1) \cdot m(t-l_2) \rangle \right) \quad (3-20).$$

For the second-order system in (3-13), this procedure would produce the estimates:

$$\hat{h}_1^{1+}(l) = L_1(l) + O\left(\frac{1}{M}\right) + \sum_{k_1=0}^T \sum_{k_2=0}^T L_2(k_1, k_2) \delta(l, F_1(k_1, k_2)) \quad (3-21),$$

$$\hat{h}_1^{1-}(l) = -L_1(l) + O\left(\frac{1}{M}\right) + \sum_{k_1=0}^T \sum_{k_2=0}^T L_2(k_1, k_2) \delta(l, F_1(k_1, k_2)) \quad (3-22),$$

$$\hat{h}_1^{IR(1)}(l) = L_1(l) + O\left(\frac{1}{M}\right) \quad (3-23),$$

$$\begin{aligned} \hat{h}_2^{1+}(l_1, l_2) &= L_2(l_1, l_2) + O\left(\frac{1}{M}\right) + \sum_{k=0}^T L_1(k) \delta(k, F_1(l_1, l_2)) + \\ &\sum_{k_1=0}^T \sum_{k_2=0}^T L_2(k_1, k_2) \delta(F_1(l_1, l_2), F_1(k_1, k_2)) \end{aligned} \quad (3-24),$$

$$\begin{aligned} \hat{h}_2^{1-}(l_1, l_2) &= L_2(l_1, l_2) + O\left(\frac{1}{M}\right) - \sum_{k=0}^T L_1(k) \delta(k, F_1(l_1, l_2)) + \\ &\sum_{k_1=0}^T \sum_{k_2=0}^T L_2(k_1, k_2) \delta(F_1(l_1, l_2), F_1(k_1, k_2)) \end{aligned} \quad (3-25),$$

$$\hat{h}_2^{IR(1)}(l_1, l_2) = L_2(l_1, l_2) + O\left(\frac{1}{M}\right) + \sum_{k_1=0}^T \sum_{k_2=0}^T L_2(k_1, k_2) \delta(F_1(l_1, l_2), F_1(k_1, k_2)) \quad (3-26),$$

where \hat{h}_2^{IR} denotes the estimates derived from applying (3-19) and (3-20), and \hat{h}_2^{1+} and \hat{h}_2^{1-} denote the estimates due to $m_1(t)$ and $m_1(t)$ inverted in polarity respectively. The IR method thus separates even- and odd-order kernel estimates from each other. However, it cannot resolve the problem of higher-order ($n \geq 2$) kernel estimates of the same parity (even or odd) from contaminating each other (see (3-26)).

Sutter has suggested the use of m-sequences with recursion terms that exceed the memory of the nonlinear system being tested to eliminate this kind of anomaly. For example, for a system with a memory of 15 time steps, an appropriate m-sequence would be of length $2^{15}-1$. Although this guarantees (via the nature of F) clean separation of all kernels up to order 15, this method becomes exceedingly onerous for multi-input nonlinear systems, or for a system whose memory is long. For a system with two inputs of memory 15, clean separation would require a single input of length $2^{30}-1$. For physiological experiments, such long sequences would exceed the period during which the preparation is stable. One motivation for the hybrid method is to remove contamination

without using exceedingly long sequences or requiring an intimate knowledge of the recursive structure of the stimulus.

3.8 The Hybrid M-Sequence Method

In this section, we examine the benefits of presenting a sum of m-sequences as a signal to a single-input system. That is, our input is $s(t) = m_1(t) + m_2(t)$, where $m_1(t)$ and $m_2(t)$ are distinct m-sequences whose lengths are relatively prime. This new stimulus can have three values: (-2, 0, and 2). This stimulus also requires a new algorithm for estimating the Wiener kernels, but the reader should easily see the similarities between the new algorithm and the Lee and Schetzen (1965) algorithm.

We begin by considering the system described by Eq. (3-2) truncated after kernels of second order. The response of this system to $s(t) = m_1(t) + m_2(t)$ is:

$$\begin{aligned}
 r(t) = & L_0 + \sum_{k=0}^T L_1(k)m_1(t-k) + \sum_{k=0}^T L_1(k)m_2(t-k) \\
 & + \sum_{k_1=0}^T \sum_{k_2=0}^T L_2(k_1, k_2)m_1(t-k_1)m_1(t-k_2) + \sum_{k_1=0}^T \sum_{k_2=0}^T L_2(k_1, k_2)m_2(t-k_1)m_2(t-k_2) \quad (3-27). \\
 & + 2 \sum_{k_1=0}^T \sum_{k_2=0}^T L_2(k_1, k_2)m_1(t-k_1)m_2(t-k_2)
 \end{aligned}$$

In Eq. (3-27), the system responds to each sequence individually and to pairwise combinations of inputs.

As before, to calculate the zeroth-order kernel, the response is averaged over an entire cycle of the combined signal:

$$\hat{h}_0 = \langle r(t) \rangle \quad (3-28).$$

The first-order kernel may be calculated by cross-correlating the response with either m-sequence in the input:

$$\hat{h}_1^1(l) = \langle r(t) \cdot m_1(t-l) \rangle \quad (3-29),$$

$$\hat{h}_1^2(l) = \langle r(t) \cdot m_2(t-l) \rangle \quad (3-30).$$

These are two independent estimates.

Estimates of the second-order kernel require that the lengths of $m_1(t)$ and $m_2(t)$ are relatively prime (i.e., they have no common factors apart from 1). As seen in Appendix I, this implies that

$$\langle m_1(t-l_1) \cdot m_2(t-l_2) \rangle = O\left(\frac{1}{M_1 \cdot M_2}\right) \quad (3-31),$$

where M_1 and M_2 are the lengths of the $m_1(t)$ and $m_2(t)$ respectively. In general, for the set of m-sequences, $\{m_1(t), m_2(t), m_3(t), \dots, m_n(t)\}$,

$$\langle m_1(t-l_1) \cdot m_2(t-l_1) \cdot m_3(t-l_1) \dots m_n(t-l_1) \rangle = O\left(\frac{1}{M_1 \cdot M_2 \dots M_n}\right) \quad (3-32),$$

if the lengths of each $m_i(t)$ are relatively prime to each other. Eq. (3-31) is the basis of an estimation formula for the second-order kernel:

$$\hat{h}_2^{12}(l_1, l_2) = \frac{1}{2!} \langle r(t) \cdot m_1(t-l_1) \cdot m_2(t-l_2) \rangle \quad (3-33).$$

That is, to calculate the second-order kernel, the response is cross-correlated with both sequences in the input. Along the diagonal $l_1 = l_2$, the same cross-correlation as (3-33)

can be used. The ability to measure the points on the diagonal of the kernel also distinguishes the hybrid method from the standard m-sequence method, to which these points are inaccessible.

We now see how this algorithm performs. Applying the cross-correlations Eqs. (3-28) - (3-30) and (3-33) to the system of Eq. (3-2) truncated at second-order leads to:

$$\hat{h}_0 = L_0 + O\left(\frac{1}{M}\right) + 2 \sum_{k=0}^T L_2(k, k) \quad (3-34),$$

$$\hat{h}_1^1(l) = L_1(l) + O\left(\frac{1}{M}\right) + \sum_{k_1=0}^T \sum_{k_2=0}^T L_2(k_1, k_2) \delta(l, F_1(k_1, k_2)) \quad (3-35),$$

$$\hat{h}_1^2(l) = L_1(l) + O\left(\frac{1}{M}\right) + \sum_{k_1=0}^T \sum_{k_2=0}^T L_2(k_1, k_2) \delta(l, F_2(k_1, k_2)) \quad (3-36),$$

$$\hat{h}_2^{1,2}(l_1, l_2) = L_2(l_1, l_2) + O\left(\frac{1}{M_1 \cdot M_2}\right) \quad (3-37).$$

The first-order kernels have second-order contributions, but these may be eliminated by an inverse repeat. The key point is that anomalies in the estimate of $\hat{h}_2^{1,2}(l_1, l_2)$ due to algebraic anomalies of the m-sequence have been completely eliminated (compare Eqs. (3-26) and (3-37)).

This analysis is somewhat artificial in that it is unlikely that a real system has a Volterra representation which is truncated after order 2. Contributions from third-order Volterra terms will necessarily overlap on first-order estimates, even with this hybrid approach. However, comparing the two estimates, $\hat{h}_1^1(l)$ and $\hat{h}_1^2(l)$ gives a convenient

experimental check on the presence of such "kernel noise" in the estimates of $h_1(l)$, because this "noise" depends on different mappings, F_1 and F_2 .

3.9 Higher-Order Systems

We have shown that the hybrid approach (a sum of m-sequences) can remove anomalous contributions which have the same parity as the kernel of interest. This is in contrast to the IR method, which can only remove anomalies on the basis of parity. This advantage of the hybrid approach extends to higher-order nonlinearities, provided that a longer input sequence is used. We consider the estimation of a third-order kernel via an input signal $s(t) = m_1(t) + m_2(t) + m_3(t)$, where the lengths of the three m-sequences are relatively prime in pairs (for example, 31, 63, and 127). We will see that this provides for estimates of the third-order kernel to lag 31, free of anomalies due to the algebraic properties of the m-sequences. (The length of the stimulus $s(t)$, $31 \cdot 63 \cdot 127$, though long, is nevertheless approximately 1/8000th as long as an m-sequence of order 31, which would be required by the use of a single m-sequence whose order exceeds the maximum lag of the kernel to be extracted).

The response of a third-order Volterra system to the input $s(t) = m_1(t) + m_2(t) + m_3(t)$ is:

$$r(t) = L_0 + \sum_{k=0}^T L_1(k) \left(\sum_{p=1}^3 m_p(t-k) \right) + \sum_{k_1=0}^T \sum_{k_2=0}^T L_2(k_1, k_2) \left(\sum_{p,q=1}^3 m_p(t-k_1) m_q(t-k_2) \right) + \sum_{k_1=0}^T \sum_{k_2=0}^T \sum_{k_3=0}^T L_3(k_1, k_2, k_3) \left(\sum_{p,q,r=1}^3 m_p(t-k_1) m_q(t-k_2) m_r(t-k_3) \right). \quad (3-38).$$

Applying Eq. (3-28), the estimated zeroth-order kernel is:

$$\hat{h}_0 = L_0 + O\left(\frac{1}{M}\right) + 3 \sum_{k=0}^T L_2(k, k) \quad (3-39).$$

The first-order kernel can be estimated three ways by cross-correlating the response with any one of the m-sequences Eq. (3-29). The three estimates are:

$$\hat{h}_1^p(l) = \langle r(t) \cdot m_p(t-l) \rangle \quad (3-40).$$

Substitution of Eq. (3-38) into Eq. (3-40) yields:

$$\begin{aligned} \hat{h}_1^p(l) = & L_1(l) + O\left(\frac{1}{M}\right) + \sum_{k_1=0}^T \sum_{k_2=0}^T L_2(k_1, k_2) \delta(F_p(k_1, k_2), l) + \\ & \sum_{k_1=0}^T \sum_{k_2=0}^T \sum_{k_3=0}^T L_3(k_1, k_2, k_3) \delta(F_p(k_1, k_2, k_3), l) + 3 \sum_{k=0}^T L_3(l, k, k), \end{aligned} \quad (3-41),$$

where $F_p(k_1, k_2, k_3) = F_p(k_1, F_p(k_2, k_3))$. Note that the first-order kernel estimate has potential contributions from both the second- and third-order kernels. The last term is a contribution from the third-order kernel diagonal terms. This contribution is a proper part of the Wiener kernel. The second-order contribution can be removed by IR. The IR method does not remove the third-order, nondiagonal contribution since it is of the same parity (odd) as the kernel being estimated. The disparities between the three estimates \hat{h}_1^1 , \hat{h}_1^2 , and \hat{h}_1^3 can be used to gauge the significance of this higher-order overlap, since in each estimate, the third-order overlap depends on a different mapping F (either F_1 , F_2 , or F_3).

With three m-sequences, it is possible to obtain three estimates of h_2 . To estimate the second-order kernels, the response is cross-correlated with any two of the component m-sequences:

$$\hat{h}_2^{p,q}(l_1, l_2) = \frac{1}{2!} \langle r(t) \cdot m_p(t - l_1) \cdot m_q(t - l_2) \rangle \quad (p \neq q) \quad (3-43).$$

Substitution of Eq. (3-38) into Eq. (3-42) yields:

$$\begin{aligned} \hat{h}_2^{p,q}(l_1, l_2) &= L(l_1, l_2) + O\left(\frac{1}{M}\right) + \frac{3}{2} \sum_{k_1=0}^T \sum_{k_2=0}^T L_3(l_1, k_1, k_2) \delta(F_p(k_1, k_2), l_1) + \\ &\frac{3}{2} \sum_{k_1=0}^T \sum_{k_2=0}^T L_3(l_2, k_1, k_2) \delta(F_q(k_1, k_2), l_2)). \end{aligned} \quad (3-44).$$

Thus, there are three estimates for the second-order kernel, $\hat{h}_2^{1,2}$, $\hat{h}_2^{2,3}$, and $\hat{h}_2^{1,3}$. The third-order contamination of the second-order kernel can be estimated by comparing the quantities, or can be removed by IR, e.g.

$$\hat{h}_2^{IR(1,2)} = \frac{1}{2} (\hat{h}_2^{1+2+} + \hat{h}_2^{1-2-}) \quad (3-45).$$

For the third-order kernel, the estimate is evaluated by cross-correlating the response with three m-sequences:

$$\hat{h}_3^{1,2,3}(l_1, l_2, l_3) = \frac{1}{3!} \langle r(t) \cdot m_1(t - l_1) \cdot m_2(t - l_2) \cdot m_3(t - l_3) \rangle \quad (3-46).$$

Substitution of eq. (39) into eq. (46) yields

$$\hat{h}_3^{1,2,3}(l_1, l_2, l_3) = L_3(l_1, l_2, l_3) + O\left(\frac{1}{M_1 \cdot M_2 \cdot M_3}\right) \quad (3-47).$$

The general form of the hybrid algorithm may now be stated: The input signal is a sum of n distinct m-sequences of relatively prime lengths. The n th-order kernel is estimated by cross-correlating the response with the product of these n m-sequences. The k th-order kernel ($k < n$) has $\frac{n!}{(n-k)!k!}$ estimates, each obtained by cross-correlation with a product of k of the input m-sequences. By comparing these estimates, one can judge whether overlaps are significant and whether to average these estimates or combine them with IR measurements. Formally, for an input $s(t)$ consisting of a sum of n m-sequence inputs, all of relatively prime length to the others ($s(t) = m_1(t) + m_2(t) + m_3(t) + \dots + m_n(t)$), the kernel calculations are made as follows:

$$\hat{h}_0 = \langle r(t) \rangle \quad (3-48),$$

$$\hat{h}_1^p(l) = \langle r(t) \cdot m_p(t-l) \rangle \quad (3-49),$$

$$\hat{h}_2^{p,q}(l_1, l_2) = \frac{1}{2!} \langle r(t) \cdot m_p(t-l_1) \cdot m_q(t-l_2) \rangle \quad (3-50),$$

$$\hat{h}_n^{1,2,\dots,n}(l_1, l_2, \dots, l_n) = \frac{1}{n!} \langle r(t) \cdot m_1(t-l_1) \cdot m_2(t-l_2) \dots m_n(t-l_n) \rangle \quad (3-51).$$

The FMT can be used to calculate each one of these cross-correlations in exactly the same way that the FFT can be used to calculate the Fourier transform in more than one dimension (see below).

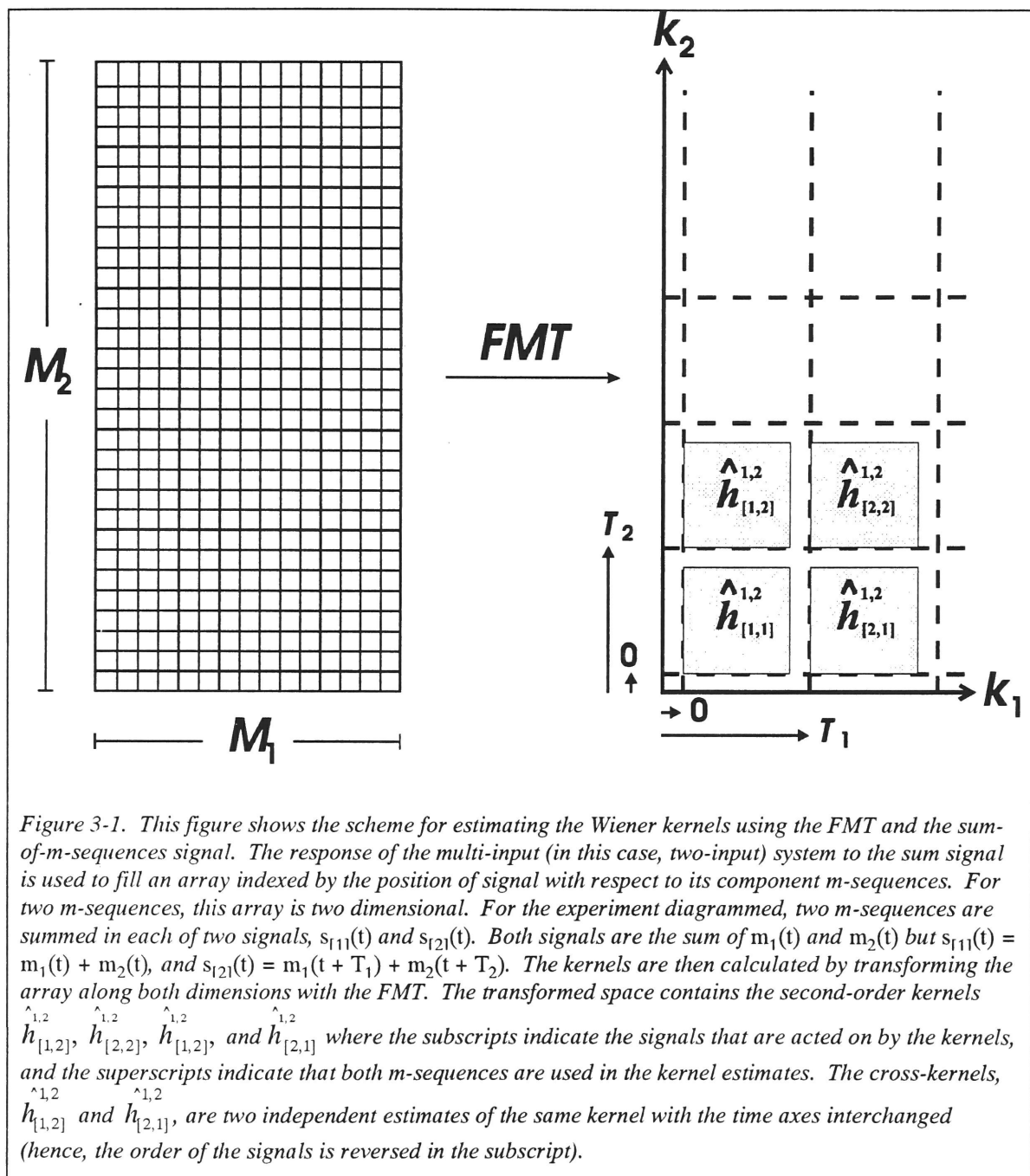
3.10 Multi-Input Systems

The final step in the development of this method is to apply it to the identification of a multi-input nonlinear system. This extension is straightforward now that the foundations have been laid. To measure the kernel of a single-input system above, it is necessary that each m-sequence is longer than the system's memory. To extend this technique to a multi-input nonlinear system, each sequence must have a length which exceeds the system's memory multiplied by the number of inputs. Then each input is assigned a tap, or lag, which is longer than the system's memory. The cross-correlation analysis proceeds exactly as before, and the kernels for each input are represented in the resulting cross-correlation shifted by an amount corresponding to its associated input lag.

Consider, for example, a two-input, second-order system. There are two first-order kernels, one for each input. There are three distinct second-order kernels; one involving the product of two values of the first input, one involving the product of two values of the second input, and a third that involves the product of the first and second inputs together. To resolve the second-order kernels, a sum of two relatively prime m-sequences is chosen for the input. Each individual sequence is of length at least $2T$ (where T as before is the system's memory in discretized time units). The signal applied to the first input is $s_{[1]}(t) = m_1(t) + m_2(t)$, i.e. the sum of two m-sequences. The signal applied to the second input is $s_{[2]}(t) = m_1(t + T_1) + m_2(t + T_2)$, where T_1 and T_2 are lags which are greater than the memory of the system. These lags separate the contributions of the two inputs. The cross-correlation formulae, Eqs. (3-48) - (3-50), yield estimates of the zeroth-, first- and second-order kernels except the combinatorial factor on the left-hand

side must be adjusted for the second-order cross-kernel. Instead of $\frac{1}{2!}$, the coefficient is simply 1. For the n th-order multi-input kernel with k different inputs, this coefficient is $\frac{k!(n-k)!}{n!}$.

The two-dimensional cross-correlation analysis (facilitated by the FMT) that yields estimates of the second-order kernels is graphically represented in Fig. 3-1. The response of the system is recorded and used to fill a two-dimensional array, the rows and columns of which are indexed by the position of the signal with respect to each of the two m-sequences at the time of the response. This array is transformed in one dimension by the FMT corresponding to the sequence, $m_1(t)$, and in the other dimension according to $m_2(t)$. The second-order kernels are separated by the lags T_1 and T_2 in the transformed array.



For higher-order, multi-input, nonlinear systems, the analysis proceeds the same way. For an n th-order system with k inputs and memory T , n lagged m -sequences are summed and applied to each of the k inputs. Lags assigned to different inputs must differ

by at least an amount T . Each sequence, therefore, is of length at least kT , and the length of the sequences, as above, must be relatively prime.

3.11 Relationship to Wiener Kernels

Above we have discussed the measurement of system kernels with a stimulus made up of a sum of relatively prime-length m-sequences. In the original Wiener framework, the kernels form an orthogonal set of functions with respect to Gaussian white noise of a particular power. The measured kernels are then orthogonal with respect to this Gaussian (Klein, 1987, 1992). The orthogonality assures that truncating this series at any given order minimizes the estimation error in a least squares sense.

The hybrid m-sequence method, on the other hand, uses a stimulus that is neither white nor strictly Gaussian. However, biological systems generally have a finite bandwidth, and stimulus frequencies that exceed this bandwidth will not influence the response. The highest frequency in the stimulus is determined by the length of the time interval between steps in the m-sequence. The shorter this interval the wider the bandwidth of the signal. The lowest frequency in the stimulus is determined by the length of the m-sequence since the stimulus repeats after this interval. As long as these two parameters are set to span the frequency range of the system under study, the frequencies present in the stimulus are a good approximation to those present in Gaussian white noise.

Figures 3-2 - 3-5 illustrate these two points for the experiments in this thesis . First, Fig. 3-2 and Fig. 3-3 show that despite the fact that the sum of two m-sequences is far from Gaussian as it enters the retina, when a linear filter stage, represented by the

impulse response of a cone (Schnapf *et al.*, 1990) acts before the first nonlinearity, then the signal reaching the nonlinearity is much more Gaussian (Victor, 1991). Compare the histograms in Fig. 3-3. One measure of “Gaussianness” is the ratio of the kurtosis in the signal to the variance (power). For a true Gaussian signal, this ratio is 0. For the original m-sequence stimulus, it is -0.499; for the filtered signal, it is -0.002256, a 200-fold improvement. Since photoreceptors act like linear filters over a broad range of illumination levels, and they also form the first stage in vision, the modified m-sequence kernels are much closer to true Wiener kernels than they would be if there were no initial linear stage.

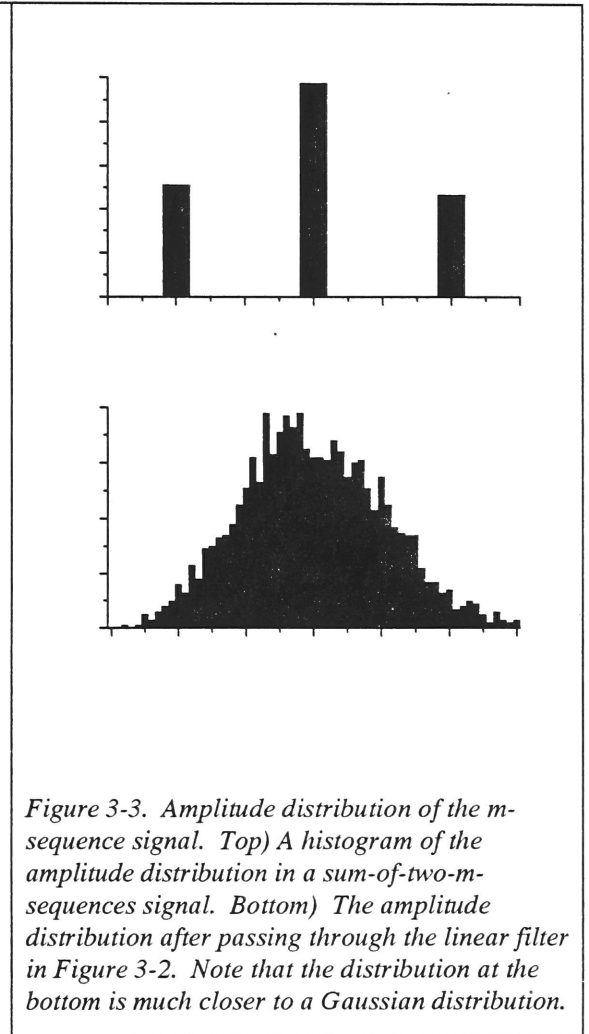
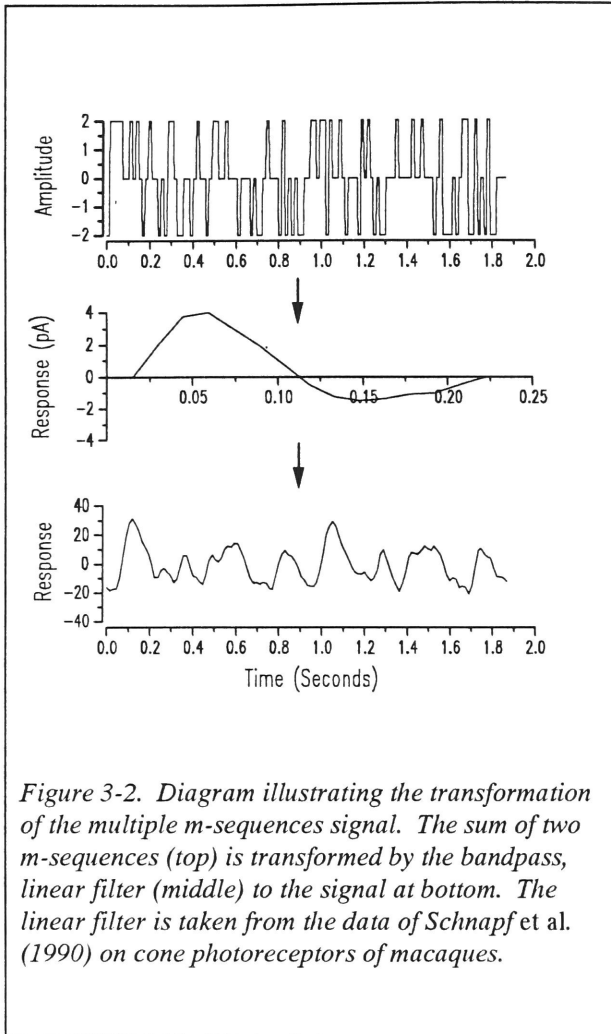
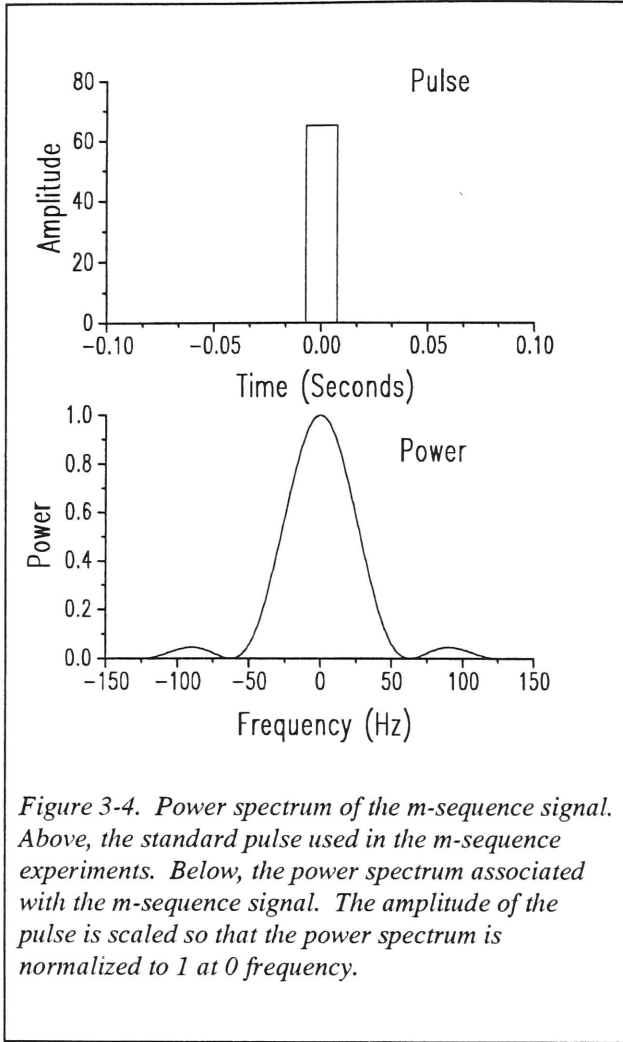


Figure 3-4 illustrates the relationship between the width of the m-sequence pulse used in these experiments and the distribution of power in different frequencies. The amplitude is approximately 70% of maximum at 32 Hz.



In the above analysis, we have noted where diagonal elements have contributed to lower order kernels. These contributions depend on the power in the stimulus. Thus the Wiener kernels and the kernels estimated by the hybrid m-sequence are dependent on the power level of the stimulus used to estimate the kernels. For example, we noted above that the diagonal elements of the second-order kernel, h_2 , contribute to h_0 . If the stimulus is made up of two m-sequences of unit amplitude then this contribution is

$2 \sum_{k=0}^T h_2(k, k)$ (Eq. 3-34). For a Gaussian white-noise stimulus of power, P , the

corresponding contribution is $P \sum_{k=0}^T h_2(k, k)$. Thus the zeroth-order kernel measured with the sum of two m-sequences is an estimate of the Wiener kernel of equal power. In general, Wiener kernel estimates derived from a sum of n m-sequences are matched for a Gaussian white noise of power n . As the number of m-sequences in the stimulus is increased, the number of kernels that can be estimated grows. This is because the statistics of the stimulus becomes more and more like those of a Gaussian distribution --

each value of the stimulus is a sum of independent random variables, and thus the Central Limit Theorem of probability applies (Feller, 1968).

Thus stimulus design depends in part on *a priori* knowledge of the system one is trying to study. The choice of time interval and m-sequence length requires knowledge of the frequency response and memory of the system. Furthermore, it is helpful to know approximately the highest-order interaction likely to be present in the system's response. A hybrid routine involving k inputs can only rigorously measure kernels up to order k . Components of higher order in the response will confound the calculation of lower-order kernels. Indeed, one must always bear in mind that "noise" in a kernel measurement may represent contamination of the measurement by some kernel whose order exceeds the resolution of the analytical technique.

3.12 Relationship to the Sum-of-Sinusoids Approach

In the sum-of-sinusoids method, separation of nonlinear contributions of different orders is achieved by choosing a set of input frequencies which are nearly incommensurate. This provides an input signal which densely samples the input phase space. The condition of near-incommensurateness makes the component sinusoids nearly independent, and thus guarantees orthogonality of kernel estimates of different orders. The hybrid m-sequence method likewise uses a sum of m-sequences of relatively prime lengths. The component m-sequences can be thought of as the time-domain analogues of the nearly incommensurate frequencies. They sample the time-lag space densely and independently, and thus allow calculation of Wiener kernels with little kernel cross-contamination. Although the frequency approach promises better kernel separation, the

hybrid m-sequence method offers a simpler routine for multi-input nonlinear system identification, since shifts of the same m-sequences that are used as the signal to one input can be used as the signal to another input.

3.13 Discussion

The theoretical framework of Wiener nonlinear systems analysis provides an attractive and precise formalism for categorizing and modeling any system. Direct application of this approach is impractical. This has led to several efforts at designing more practical system identification algorithms that retain the theoretical advantages of the Wiener approach.

Deterministic signals offer certain advantages in this context, since the experimenter knows in advance the statistical deviations of the signal from a Gaussian white noise. Within the deterministic framework, one of the most promising approaches is the m-sequence method, as developed by Sutter (1987, 1992). However, the algebraic structure of the m-sequences leads to anomalies in kernel estimates for nonlinear systems, especially for those with many inputs. In this paper, we show how many of these anomalies can be eliminated by a method analogous to the sum-of-sinusoids method (Victor and Shapley, 1980). By choosing a sum of m-sequences of relatively prime lengths, the cross-correlation properties of the stimulus were refined to enable a simple and accurate estimation of multi-input nonlinear kernels.

The goal in designing a useful Wiener-like system identification procedure is to separate the system into kernels of various orders. Reduction of the cross-contamination

of the calculated kernels can be achieved by appropriate stimulus design, but since the stability of physiological preparations is limited, the recording times are also best kept as short as possible. The sum-of-m-sequences is economical in this regard as well since it samples the pertinent region of stimulus space densely and uniformly.

3.14 Appendix I

This appendix is a brief introduction to generalized Wiener kernels from the point of view of Victor and Knight (1979).

A Volterra series defines a physical system in terms of a hierarchy of kernels, each of which can be thought of as a transducer, μ_j , of a particular order j . The order refers to the number of time lags of the stimulus that are multiplied and weighted by the transducer.

The transducers, μ_j , are members of a vector space, M_j , of transducers of Volterra order j . Basis functions for this vector space are:

$$D_{j, \vec{\tau}}(s)(t) = \prod_{k=1}^j s(t - \tau_k) \quad (\text{A1.1}),$$

which take the product of j time lags, τ_k , of the stimulus, $s(t)$. For a single-input system, the ordering of the $s(t - \tau_k)$ is irrelevant so that the $D_{j, \vec{\tau}}$ are symmetric functions of their arguments. For stimuli $s(t)$ whose value at each time is independently chosen, the $D_{j, \vec{\tau}}$ form a set of linearly independent basis elements only as long as each of the time lags is different. The space of time-invariant transducers has a natural inner product given by the product of the responses of two transducers averaged over the signal ensemble, Ω :

$$(\mu, \nu) = \langle \mu(s)(0) \cdot \nu(s)(0) \rangle_{\Omega} \quad (\text{A1.2}),$$

where μ and ν are transducers and $s(0)$ is the signal at the initial time.

The vector spaces M_j are not orthogonal. However, each M_j can be projected onto a new set of orthogonal vector spaces, K_j , in which each basis function has lower order correction terms. Each transducer in the K_j space is orthogonal to any transducer in a subspace K_l of a different order.

The Wiener characterization of an unknown transducer is the projection of that transducer onto the vector spaces, K_j . The projection of a transducer μ_j in M_j into its corresponding orthogonal space K_j can be written:

$$\mu_j = \sum_{k=0}^j \mu_j^{(k)} \quad (\text{A1.3}),$$

as sum of a j th-order term, $\mu_j^{(j)}$, and lower order correction terms, $\mu_j^{(k)}, 0 \leq k < j$. These lower-order correction terms depend on the power in the stimulus. They differentiate the kernels of the Wiener orthogonal functional expansion from those of the Volterra series.

3.15 Appendix II

The goal of this section is to show that a sum of m-sequences is an especially useful signal for nonlinear systems analysis if the lengths of the component m-sequences are **relatively prime** (i.e., their lengths are numbers that share no common factor except for 1). We show that the n th-order Wiener kernel of a system can be estimated by cross-

correlating the response to this test signal with the product of its n component m-sequences.

We require that each component m-sequence have a length greater than the memory of the system, T . We denote the length of each component signal, $m_i(t)$, by M_i . The relative primality condition implies that the length of the sum signal M^* , is given by $M_1 \cdot M_2 \cdots M_n$.

Consider the response of a second-order system to a sum of two m-sequences, $m_1(t) + m_2(t)$:

$$\begin{aligned} r(t) = & L_0 + \sum_{k=0}^T L_1(k) m_1(t-k) + \sum_{k=0}^T L_1(k) m_2(t-k) \\ & + \sum_{k_1=0}^T \sum_{k_2=0}^T L_2(k_1, k_2) m_1(t-k_1) m_1(t-k_2) + \sum_{k_1=0}^T \sum_{k_2=0}^T L_2(k_1, k_2) m_2(t-k_1) m_2(t-k_2) \quad (\text{A2.1}) \\ & + 2 \sum_{k_1=0}^T \sum_{k_2=0}^T L_2(k_1, k_2) m_1(t-k_1) m_2(t-k_2) \end{aligned}$$

To estimate the second-order Wiener kernel, $h_2(l_1, l_2)$, the following cross-correlation,

$$\hat{h}_2^{1,2}(l_1, l_2) = \frac{1}{2!} \langle r(t) \cdot m_1(t-l_1) \cdot m_2(t-l_2) \rangle \quad (\text{A2.2}),$$

is valid as long as no other points on h_2 contribute to the estimate (see Eq. 3-18). In order for this to be true, products of shifts of $m_1(t)$ and $m_2(t)$ must be uncorrelated with any other shifts of $m_1(t)$ and $m_2(t)$. We will show that this is the case:

$$\langle m_1(t-l_1) \cdot m_2(t-l_2) \cdot m_1(t-k_1) \cdot m_2(t-k_2) \rangle = O\left(\frac{1}{M^*}\right) \text{ if } l_1 \neq k_1, l_2 \neq k_2 \quad (\text{A2.3}),$$

where $\langle \rangle$ denotes an average over the whole sum-of-m-sequences signal. From Eq. (3-6), the product of two shifts of the same m-sequence is another shift of the same m-sequence. Thus, (A2.3) is equivalent to:

$$\langle m_1(t - q_1) \cdot m_2(t - q_2) \rangle = O\left(\frac{1}{M^*}\right) \quad (\text{A2.4}),$$

where $q_1 = F_1(l_1, k_1)$ and $q_2 = F_2(l_2, k_2)$. Because of the relative-primality condition (see below) each element of $m_1(t)$ occurs once and only once with each element of $m_2(t)$ in composite sequence of length $M^* = M_1 \cdot M_2$. That is, the values of the m-sequences are independent over the cycle length, and the average in Eq. (A2.4) separates:

$$\begin{aligned} \langle m_1(t - q_1) \cdot m_2(t - q_2) \rangle &= \langle m_1(t - q_1) \rangle_1 \cdot \langle m_2(t - q_2) \rangle_2 \\ &= \frac{1}{M_1 \cdot M_2} \end{aligned} \quad (\text{A2.5}),$$

where $\langle \rangle_1$ indicates an average over $m_1(t)$ and $\langle \rangle_2$ indicates an average over $m_2(t)$. Note that if $l_1 = k_1$ but $l_2 \neq k_2$, then the correlation of A2.3 is still small but it is $O\left(\frac{1}{M_2}\right)$ since one term in Eq. (A2.5) is eliminated.

The fact that every element of $m_1(t)$ appears once and only once with every element of $m_2(t)$ in a cycle of length $M_1 \cdot M_2$ can be seen as follows: Let x represent the position of an element in the sum-of-m-sequences signal. That is, for the first element of the sum signal, $x = 0$; for the second, $x = 1$, and so on. Let a and b represent the corresponding quantity for $m_1(t)$ (length M_1) and $m_2(t)$ (length M_2) respectively. Then, there is a unique x in the range from 0 to $(M_1 \cdot M_2 - 1)$ that solves the congruence equations:

$$x \equiv (a \bmod M_1) \quad (\text{A2.6}),$$

$$x \equiv (b \bmod M_2) \quad (\text{A2.7}),$$

if and only if M_1 and M_2 are relatively prime. This is a restatement of the Chinese Remainder Theorem of elementary number theory (Pinter, 1990). Figure A2.1 illustrates how the sum of m -sequences signal presents every element of one component m -sequence in conjunction with every element of the other component m -sequence once and only once. The sum signal, as shown in Fig. A2.1, traces out a path which samples the plane of pairwise values evenly and exhaustively.

For a signal which is the sum of n m -sequences, these ideas generalize to a system of n congruence equations, provided that M_1, M_2, \dots, M_n are relatively prime. This leads to:

$$\langle m_1(t - q_1) \cdot m_2(t - q_2) \cdots m_n(t - q_n) \rangle = O\left(\frac{1}{M^*}\right) \quad (\text{A2.8}).$$

Consequently,

$$\langle m_1(t - l_1) \cdot m_2(t - l_2) \cdots m_n(t - l_n) \cdot m_1(t - k_1) \cdot m_2(t - k_2) \cdots m_n(t - k_n) \rangle = O\left(\frac{1}{M^*}\right) \quad (\text{A2.9}),$$

if $l_1 \neq k_1, \dots, l_n \neq k_n$. As in the second-order case discussed above, if some but not all of the l_i 's and k_i 's are equal, the cross-correlation in Eq. (A2.9) is still small. Equation (A2.2) generalizes to provide an estimate of the n th-order Wiener kernel measured with a sum-of- n - m -sequences signal:

$$\hat{h}_n^{1,2,\dots,n}(l_1, l_2, \dots, l_n) = \frac{1}{n!} \langle r(t) \cdot m_1(t - l_1) \cdot m_2(t - l_2) \cdots m_n(t - l_n) \rangle \quad (\text{A2.10}).$$

Equation (A2.9) guarantees near elimination of overlaps in this estimate.

The main point is that the relatively prime lengths of the component m-sequences allow for averages over the entire stimulus cycle to be broken down into independent averages over each component m-sequence.

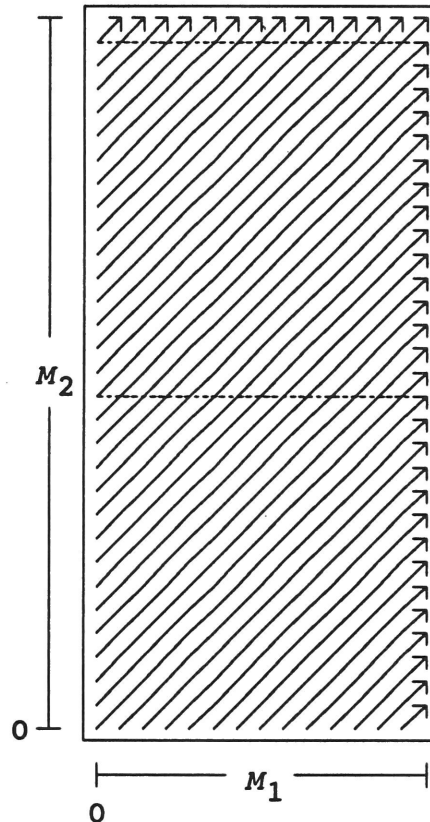


Figure 3-5. A geometric rendering of the sum-of-m-sequences signal for the sum of two m-sequences of relatively prime length. The horizontal and vertical axes indicate the position of the elements of the sum signal in the sequences $m_1(t)$ (length M_1) and $m_2(t)$ (length M_2), respectively. The sum signal starts out in the bottom left hand corner $(0, 0)$ and continues to the far right and then wraps around to $(0, M_1)$ (dashed line). As time progresses, the signal continues to move up and to the right, wrap around, and so on. In this way, the entire space is filled by the sum signal of length $M_1 \cdot M_2$. Each element of $m_1(t)$ appears once and only once with each element of $m_2(t)$ in the signal cycle. This structure provides statistical independence of the two component signals and improves Wiener kernel estimates.

P CELLS: CENTER AND SURROUND

Introduction

Linearity of Center and Surround

Effect of Dynamic Contrast on the First-Order Responses

Model Fits

Nonlinear Responses

LNL Model Fits

Center-Surround Interaction Experiments

Surround Effect in M cells

Circuit Model of the Nonlinear Surround Effect

Mathematical Development of the Circuit Model

Zeroth-Order Kernel

First-Order Kernels

Second-Order Kernels

The Relationship of the Kernels to the Model Fits

Kernel Predictions

Summary

4. P Cells: Center and Surround

4.1 Introduction

The center and the surround of a retinal ganglion cell are the most fundamental divisions of the receptive field (Kuffler, 1953). As a first step to understanding the responses of retinal ganglion cells, it is necessary to understand the dynamics of the center and surround. This chapter discusses experiments done on P cells to study the dynamics of the P cell center and surround and the interactions between these two opponent mechanisms in the P cell receptive field.

First, this chapter addresses the dynamics of the P cell center and surround as they were explored with luminance spots and annuli modulated with the multiple m-sequence method. The dynamics of P ON and OFF cells are compared. The linear filter model (Eq. (2-23)) is fit to the first-order kernels from the center and surround and a comparison of the fitted parameters is made across different P cell types. The basically linear nature of the center and surround first-order responses is demonstrated. Unlike M cells, there is very little effect of surround modulation on the first-order responses of the P cell center.

Next, the second-order responses derived from these spot/annulus experiments are discussed. The second-order kernels are fit to the LNL model and the relevant parameters are compared. The second-order kernels are evidence of a nonlinear interaction in the P cell receptive field. The center region and the surround region of the P cell's receptive

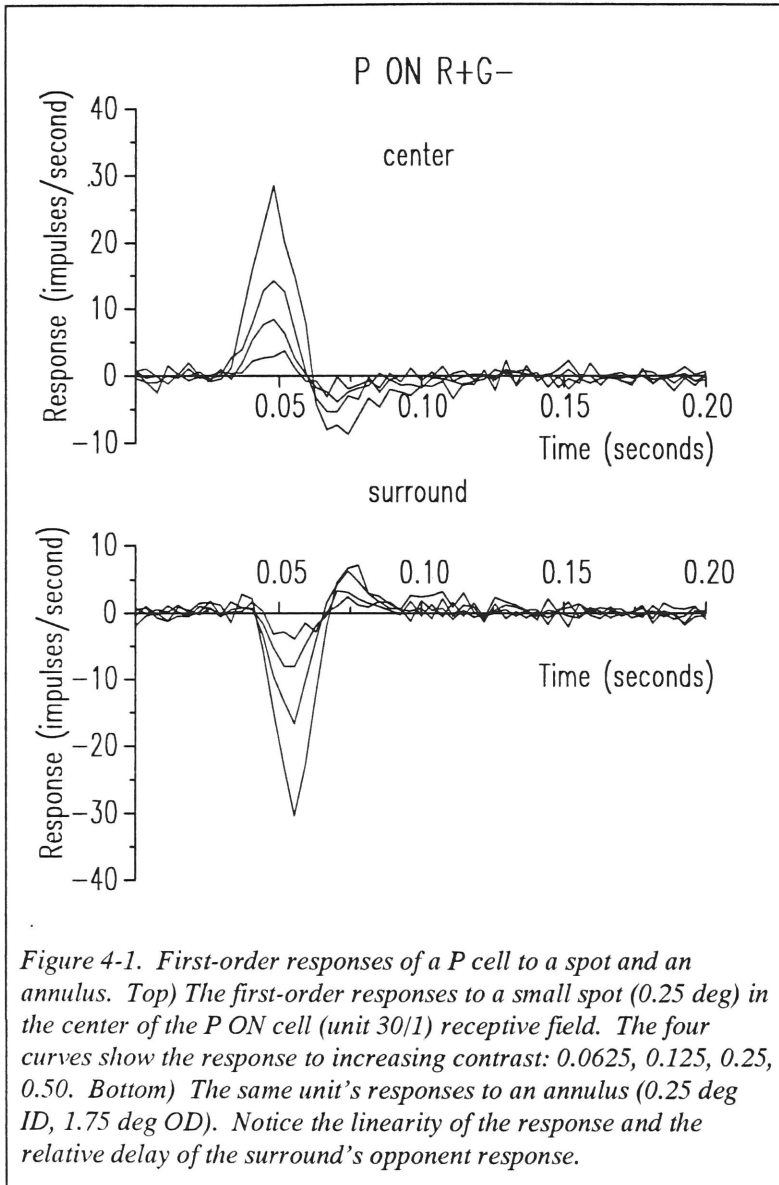
field interact nonlinearly with themselves (the “self-kernels”) as well as with each other (the “cross-kernels”).

The third section discusses the nonlinear effect on center dynamics of steady illumination in the surround of the P cell receptive field. The data show that as surround illumination increases, the gain and dynamics of the center mechanism change. These changes correspond to changes in 2 parameters of the linear filter model. The data suggest a simple electrical model based on biophysics that is discussed in the next section.

Last, the biophysical model is discussed and the relevant mathematical formulations are worked out for the relationship between the center gain and dynamics and the surround illumination. In addition, the Volterra kernels for this model are calculated and related to the previous results. Finally, these results are briefly discussed as they relate to P cell function and known physiology.

4.2 Linearity of Center and Surround

Small spots and annuli were used to analyze the response of the center and the



surround of parafoveal P

cells (Figs. 4-1 - 4-3).

Twenty-one P cells, for

which separation of the

center and surround

response was attained

using this stimulus, were

studied in detail.

Although it is difficult to

investigate the dynamics

of the center and surround

of P cells separately, the

m-sequence technique

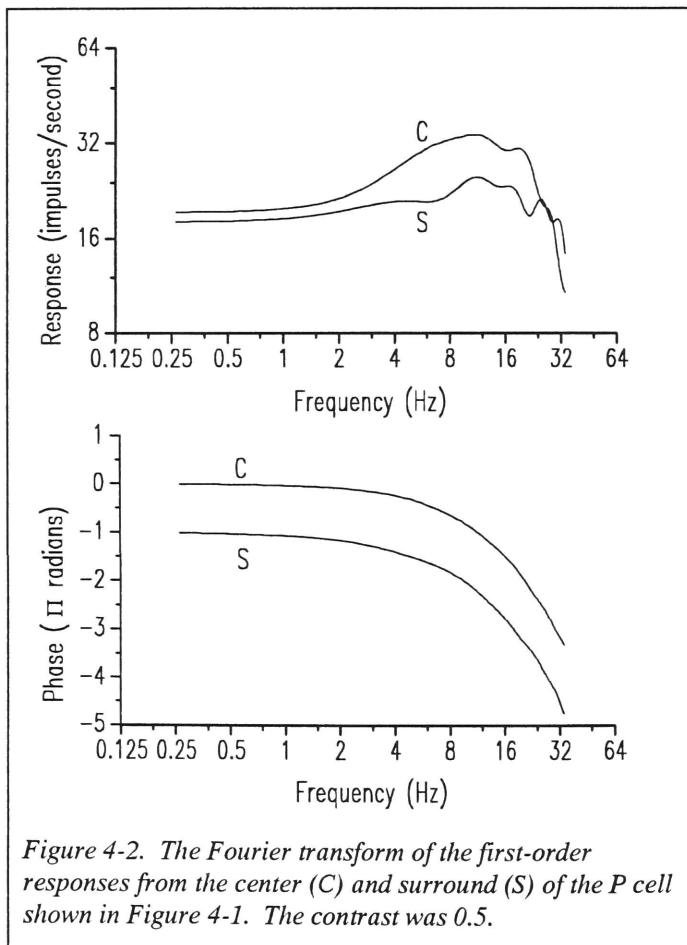
makes such separation

possible.

At the top, Fig. 4-

1 shows the first-order responses of a P ON cell stimulated with a small spot (0.25 deg) in the center of its receptive field. The curves (from bottom to top) show the responses to four doublings in contrast of the spot. Notice that doubling the contrast almost exactly doubles the response, and that there are only slight changes in the time course of the

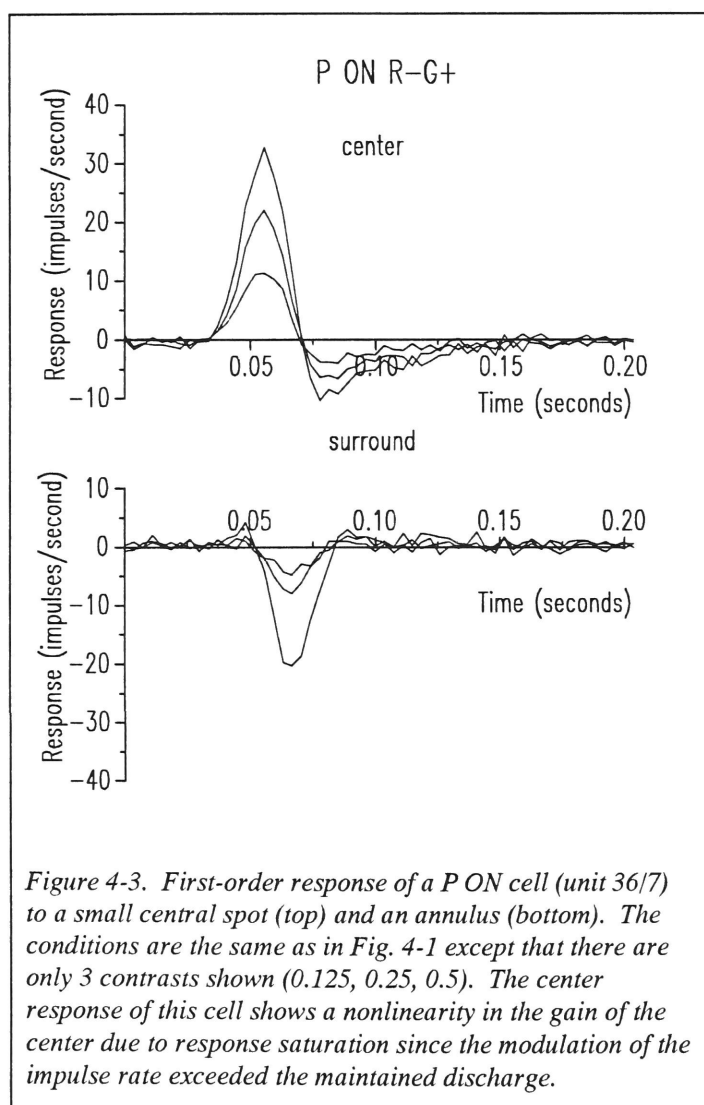
response with increasing contrast. There is a small shift in the point where the curves cross the x-axis (the “zero-crossing”). At bottom, the first-order responses to a large annulus that stimulates the surround are shown. Notice that the surround response also scales near linearly with contrast. In addition, one can see that the peak of the surround response is delayed approximately 7 ms with respect to the center response. Both the center and surround responses show some undershoot after the initial peak of the response. The frequency response of the center and the surround can be calculated by Fourier-transforming the first-order m-sequence responses (Fig. 4-2).



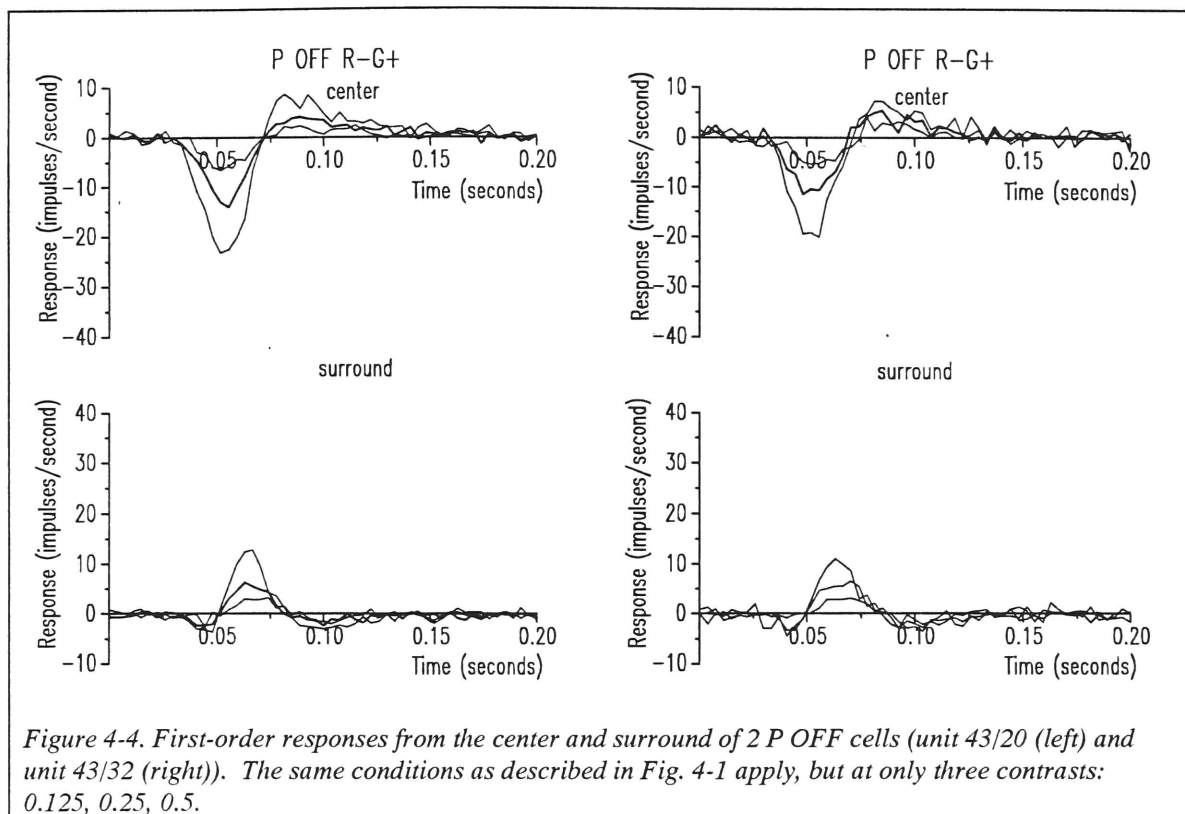
The responses of some P ON cells did not scale linearly at high contrasts (Fig. 4-3). This effect is due to the fact that the amplitude of the cell’s response exceeded the maintained discharge. The fact that the response of a spiking neuron can never be less than 0 spikes/second introduces a truncation nonlinearity into a retinal ganglion’s cell response when it is modulated at high enough contrast levels. In this cell (Fig. 4-3), at the

highest contrast, saturation (mean rate: 41.8 impulses/second) lowers the gain of the

center for the signal which was a spot modulated by the sum of 2 m-sequences. Notice, however, that there is no change in the time course of the response, which is another indication that the nonlinearity in this cell is due to saturation rather than to the action of a gain control mechanism. The kernels from the surround of this cell show at most small deviations from linearity; it is apparent that since the gain of the surround is lower than the center, there is no saturation.



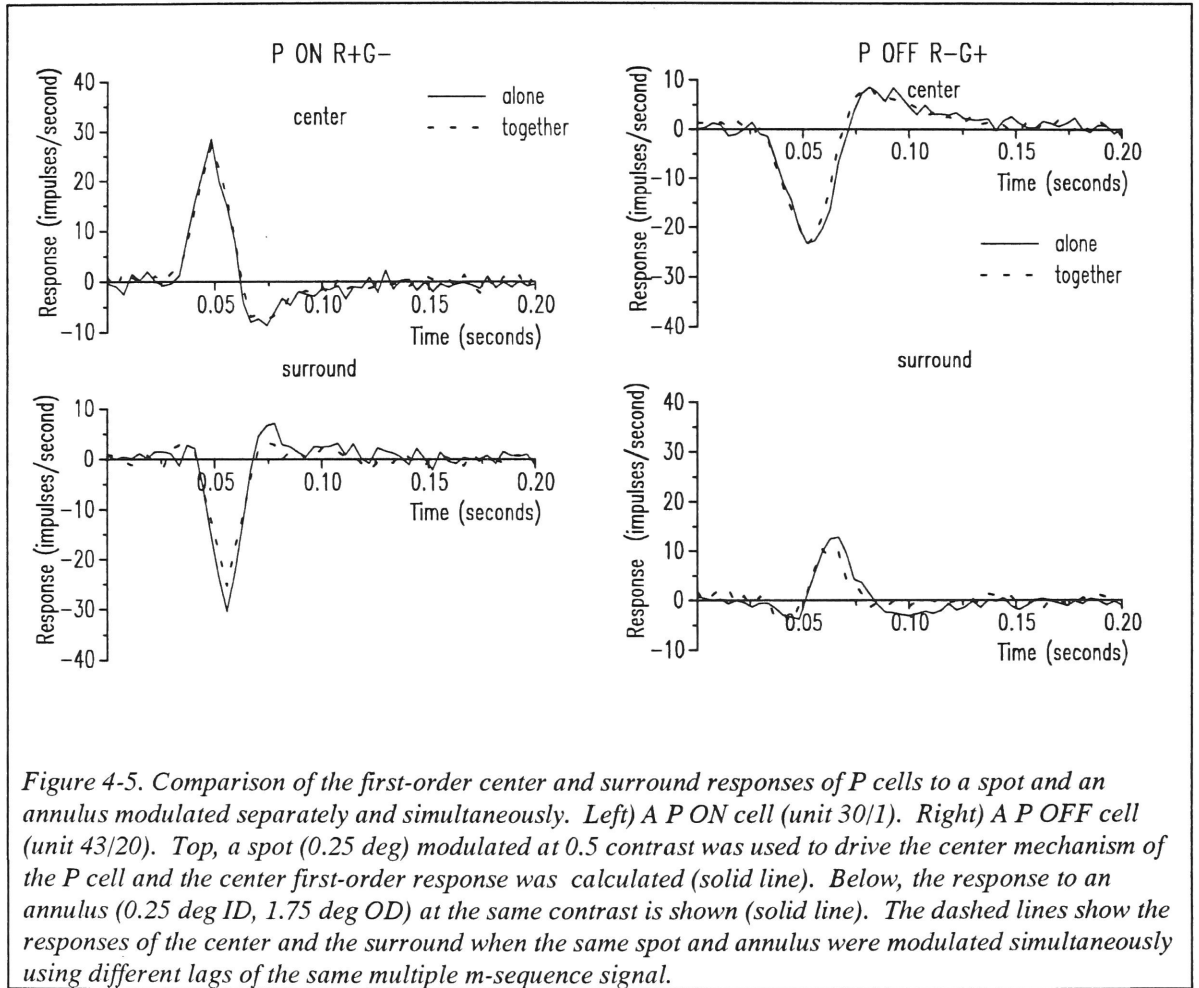
P OFF cells demonstrate the same linearity in their responses (Figs. 4-4 - 4-5). For these two cells, the center response is primarily negative and the opponent surround response is positive. The P OFF units' center response in Fig. 4-4 is linear; the surround response shows small deviations from linearity.



4.3 Effect of Dynamic Contrast on the First-Order Responses

The next results demonstrate an important difference between P cells and M cells. The detailed discussion of the M cell results is postponed until Chapter 6. In Fig. 4-5, there is a comparison of the first-order responses from the center and surround of a P cell when the center and surround are stimulated separately and when they are stimulated together. The modified m-sequence technique permits the calculation of a separate center and surround response from the cell's response to the spot and annulus modulated simultaneously. As shown, there is no significant effect of an annulus modulated by m-sequences on the center's first-order response. Similarly, there is hardly any effect of the modulated center on the surround's response. In this way, P cells differ from M cells or cat retinal ganglion cells, which demonstrate a substantial effect of a dynamically

modulated surround on the center response. These data also suggest that the major center-surround interactions in the P cell are even-order, e.g. the second-order cross-kernel, not odd-order as in cat retinal ganglion cells where the rectified response of the surround modifies the response of the center (Shapley and Victor, 1981).



4.4 Model Fits

The linear filter model (Eq. (2-23)) was used to quantify and describe the first-order kernels from P cells. To fit the model, the points on the first-order kernel were transformed into the frequency domain. The model was fit as described in Methods. The

model's response in the frequency domain was transformed back into the time domain to judge the goodness of fit. Figure 4-6 shows the fits (solid lines) along with the data for a P ON cell and a P OFF cell.

For the analysis shown in Fig. 4-6, the model for the center and for the surround was fit to the data at the highest contrast (0.5). Then, the curves for the lower contrast responses were generated by scaling response of the model for the lower contrast. For both the ON and the OFF cell, the model describes the dynamics well.

For certain cells, the annulus elicited a mixed center-surround response (Fig. 4-7). Data like these were not fit to the model. Thus, the parameters generated by fitting the model are only for P cells from which clear center and surround responses could be isolated. In this sample, there are fewer model fits to isolated surround responses.

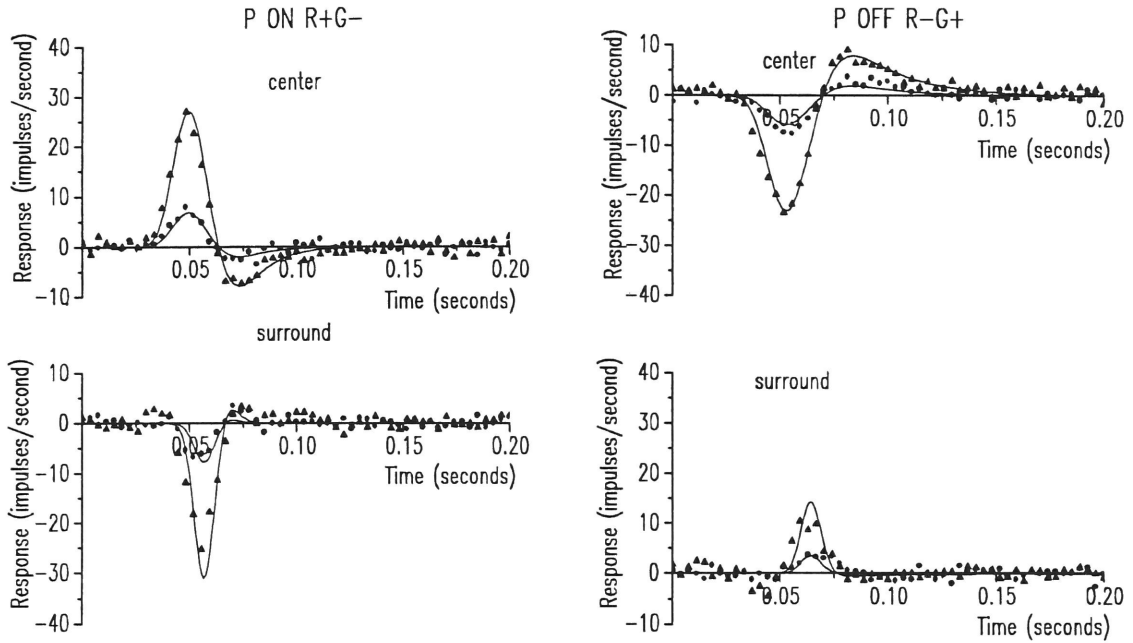
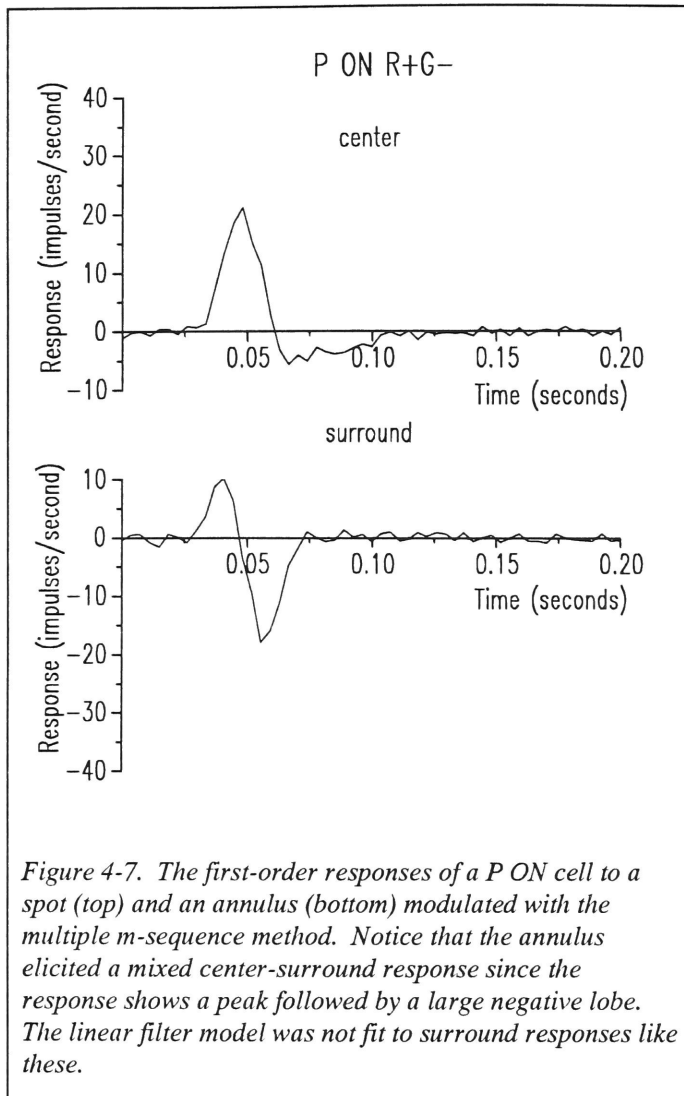


Figure 4-6. Comparison of the fit of the linear filter model and the first-order response data for P cells. Left) The responses of a P ON cell (unit 30/1) to a small spot and an annulus are shown at two contrasts (0.5: triangles; 0.125: circles). The smooth curves show the model's response. The model was fit at the highest contrast, and then the response was scaled to fit the data at the lower contrast. Right) The responses of a P OFF cell (unit 43/20) to the same stimuli and the corresponding model fits are shown. The parameters of the P ON center fit are: A : 116.27 impulses/second-unit contrast, H_S : 0.69; τ_S : 11.9 ms; N_L : 30; τ_L : 1.63 ms; D : 4.0 ms. The parameters of the P ON surround fit are: A : -517.01 impulses/second-unit contrast, H_S : 0.92; τ_S : 0.44 ms; N_L : 98; τ_L : 0.57 ms; D : 4.0 ms. The parameters of the P OFF center fit are: A : 114.12 impulses/second-unit contrast, H_S : 0.82; τ_S : 24.9 ms; N_L : 25; τ_L : 2.12 ms; D : 3.5 ms. The parameters of the P OFF surround fit are: A : 23.84 impulses/second-unit contrast, H_S : 0.18; τ_S : 40.0 ms; N_L : 168; τ_L : 0.36 ms; D : 3.5 ms.



Tables 4-1 and 4-2

summarize the fitted parameters from the model for the center and surround first-order kernels of P cells, respectively. Table 4-3 summarizes the population data for the mean rate and the eccentricity of the cells in this sample.

The combination of parameters, $N_L\tau_L$, gives an estimate of the peak of the first-order kernel. The average of the parameter, $N_L\tau_L$, for the P cell center was 49.22 ms, and there was no significant difference between

ON and OFF cells ($P > 0.1$). The peak of the surround response was 58.16 ms. The typical center-surround delay, which is labeled in Table 4-2 as $N_L\tau_{L,surround} - N_L\tau_{L,center}$ was 8.41 ms. The only parameter which showed a significant difference between ON and OFF cells was the mean rate. The mean rate for OFF cells was significantly lower than that of ON cells (25.13 impulses/second vs. 38.12 impulses/second; $p < 0.0002$). The overall gain, A , of the fits showed a fair amount of dispersion in the population. The overall gain in the model is coupled to the number of stages and the overall time constant of the low-

pass stages. In addition, the subtractive stage was more variable in the surround than in the center population. Indeed, the fit of the model to some surround kernels has no subtractive stage.

The large number of low-pass stages in the fits to the center and especially the surround kernels suggests that the lumped low-pass filter stages in the model represent the action of several different synaptic and electrochemical circuits in the P cell pathway. It is difficult to make any direct inferences from these numbers themselves. Rather, the combined parameter, $N_L\tau_L$, is a much better gauge of the overall dynamics. Furthermore, the fitted parameters do not vary with contrast since the shapes of the kernels as shown above are nearly invariant under these conditions.

Some investigators have suggested differences between the dynamics of the L-cone and M-cone pathways; for example, the M-cone pathway may be faster (Hamer and Tyler, 1992). To test this suggestion with these data, the parameter, $N_L\tau_L$, was compared for R-center (15) and G-center (9) P cells, and no significant differences were found. In addition, the other dynamical parameters including the gain of the center were compared across these two population, and no significant differences were found.

Table 4-1. P Cell Center Parameters

$N_{TOTAL} = 26$; $N_{ON} = 14$; $N_{OFF} = 12$; $N_{RG} = 24$; $N_{YB} = 2$

Parameter	P cell	Minimum	Maximum	Median	Mean	S.D.	C.V.
A (impulses/s-unit contrast)	ON	19.41	128.10	68.71	65.19	32.26	0.49
	OFF	29.58	114.05	53.42	63.30	28.05	0.44
	ALL	19.41	128.10	56.34	64.02	29.32	0.46
$N_L \tau_L$ (ms)	ON	39.64	55.10	48.15	48.36	4.131	0.09
	OFF	42.39	55.40	50.38	50.85	3.65	0.07
	ALL	39.64	55.40	49.63	49.22	4.15	0.08
N_L (dimensionless)	ON	20	46	38	35.71	6.84	0.19
	OFF	21	41	27	27.18	5.83	0.21
	ALL	20	46	30.5	31.73	7.57	0.24
H_S (dimensionless)	ON	0.5728	0.8585	0.6936	0.6868	0.078	0.12
	OFF	0.4999	0.8229	0.7462	0.7132	0.08	0.11
	ALL	0.4998	0.8586	0.7118	0.6990	0.09	0.13
τ_S (ms)	ON	11.9	60.2	30.63	33.31	14.85	0.45
	OFF	20.84	88.20	35.68	41.39	21.94	0.53
	ALL	11.9	101.77	33.55	39.36	22.03	0.56
D (ms)	ON	2.5	4	3.5	3.47	0.48	0.14
	OFF	2.5	4	3.75	3.58	0.58	0.16
	ALL	2.5	4	3.5	3.52	0.50	0.14

Table 4-2. P Cell Surround Parameters

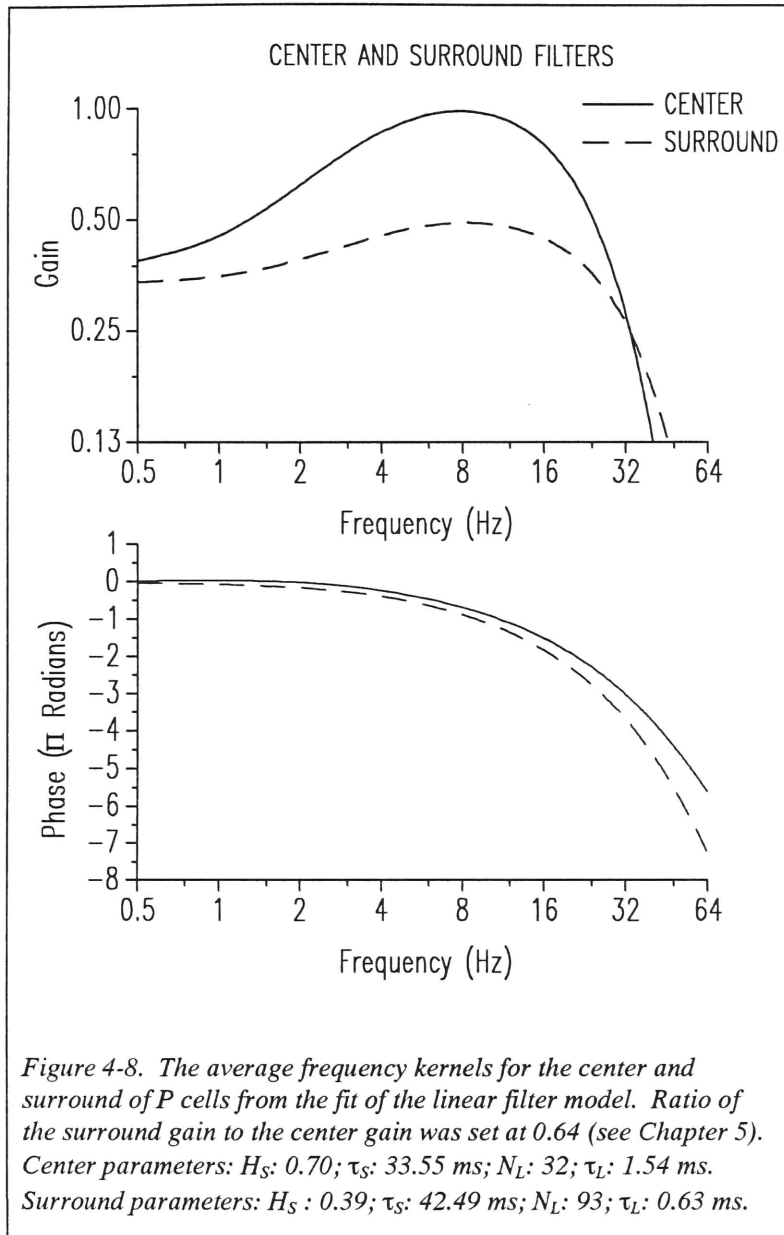
The same values for the delay, D , were used (See Table 4-1). $N_{TOTAL} = 14$; $N_{ON} = 6$; $N_{OFF} = 8$; $N_{RG} = 14$

Parameter	P cell	Minimum	Maximum	Median	Mean	S.D.	C.V.
A (impulses/s-unit contrast)	ON	29.68	517.00	49.97	126.02	192.16	1.52
	OFF	12.53	398.01	25.22	76.01	131.25	1.73
	ALL	12.53	517.00	40.13	97.45	155.36	1.59
$N_L\tau_L$ (ms)	ON	47.79	63.99	55.02	55.84	5.37	0.10
	OFF	53	64.20	60.33	59.89	3.61	0.06
	ALL	47.79	64.20	58.68	58.16	4.73	0.08
N_L (dimensionless)	ON	98	133	111	111.5	13.19	0.12
	OFF	45	168	67	78.88	41.45	0.53
	ALL	45	168	98	92.86	35.67	0.38
H_S (dimensionless)	ON	0	0.9184	0.4764	0.4343	0.3204	0.74
	OFF	0	0.6471	0.3512	0.3510	0.2402	0.69
	ALL	0	0.9184	0.4536	0.3867	0.2690	0.69
τ_S (ms)	ON	0	38.71	18.62	18.93	20.38	1.08
	OFF	0	14.05	51.99	60.15	42.79	0.71
	ALL	0	14.04	37.08	42.49	39.92	0.94
$N_L\tau_{L,surround}-N_L\tau_{L,center}$ (ms)	ON	8.93	4.51	7.24	7.04	1.45	0.21
	OFF	14.84	4.76	10.22	9.43	3.17	0.34
	ALL	14.84	4.51	7.52	8.41	2.78	0.33

Table 4-3. The Mean Rate and Eccentricity of the P Cell Sample

Parameter	P cell	Minimum	Maximum	Median	Mean	S.D.	C.V.
M (impulses/second)	ON	23.13	51.97	38.12	38.94	9.18	0.24
	OFF	16.48	39.38	24.68	25.13	6.83	0.27
	ALL	16.48	52	30.41	32.43	10.69	0.33
Eccentricity (deg)	ON	2.25	28	5.5	7.55	6.33	0.84
	OFF	1	7	4.5	4.34	1.87	0.43
	ALL	1	28	5	6.17	4.98	0.81

From the pooled fitted parameters, consensus center and surround frequency kernels were calculated (Fig. 4-8). The figure illustrates the major differences between the center and surround dynamics. The center is more bandpass than the surround although both responses peak at almost the same temporal frequency. The phases show that the surround is more delayed than the center and consequently lags more behind the center response as temporal frequency increases. Similar conclusions were reached by Gouras and Zrenner (1979) using entirely different methods.



4.5 Nonlinear Responses

This section discusses the second-order kernels calculated with the multiple m-sequence signal. This signal was used to modulate a small spot in the center of the P cell receptive field and an annulus in the surround. The first-order responses to this stimulus have already been discussed. There are three kinds of second-order responses to the spot and annulus stimulus. First, there is a second-order response from the center mechanism

of the P cell. The associated kernel is called the center x center kernel because it describes how the contrast signal at two previous times affects the center response. Similarly, there is also a surround x surround second-order kernel in response to the annulus. Finally, a third second-order kernel, the center x surround kernel, describes how contrast signals in the center and the surround interact. Figures 4-9 and 4-10 display the second-order responses for a P ON cell and a P OFF cell as surface plots. The 15 x 15 grid of calculated values was splined in two dimensions and used to plot the surface. These second-order kernels are typical for ON and OFF P cells. Another set of second-order responses for a P ON cell was shown in Chapter 2 (Fig. 2-14).

Notice in Fig. 4-9 that along the diagonal, the second-order center response for the P ON cell has a positive-going lobe followed by a small depression, and then followed by a small peak. A simple linear filter followed by a trivial nonlinearity like truncation or a quadratic nonlinearity of any kind will produce only positive lobes along the diagonal in the second-order response. Thus, the shape of the kernel suggests that an LNL sandwich is a minimal model necessary to describe all of the second-order kernel features.

The second-order surround response has much the same form as the center x center response in P ON cells, although the first positive lobe is more delayed (similar to the first-order surround response).

The second-order center-surround response is also shown. The major peak of this response is negative although it is plotted upward here for clarity. This kernel shows that the center and the surround do interact in a multiplicative way to affect the response of P cells. This kind of nonlinear interaction is a new observation not previously made in

studies limited to linear methods of analysis (e.g. Derrington and Lennie, 1984). The large negative-going peak of the cross-kernel suggests that the center and surround interact to reduce each other's response.

The previous section showed that the first-order responses from the center and surround of P cells are not affected by the m-sequence modulation of the other region. This is because the negative and positive steps in contrast average out over an entire m-sequence stimulus cycle. However, the second-order cross-kernel shows that the signed contrast in either the center or surround region does affect the gain of the other region. Thus, positive contrast in the surround reduces the response of the center and negative contrast increases the response. The negative lobe of the cross-kernel signifies this relationship. The next section discusses a more direct evaluation of this effect.

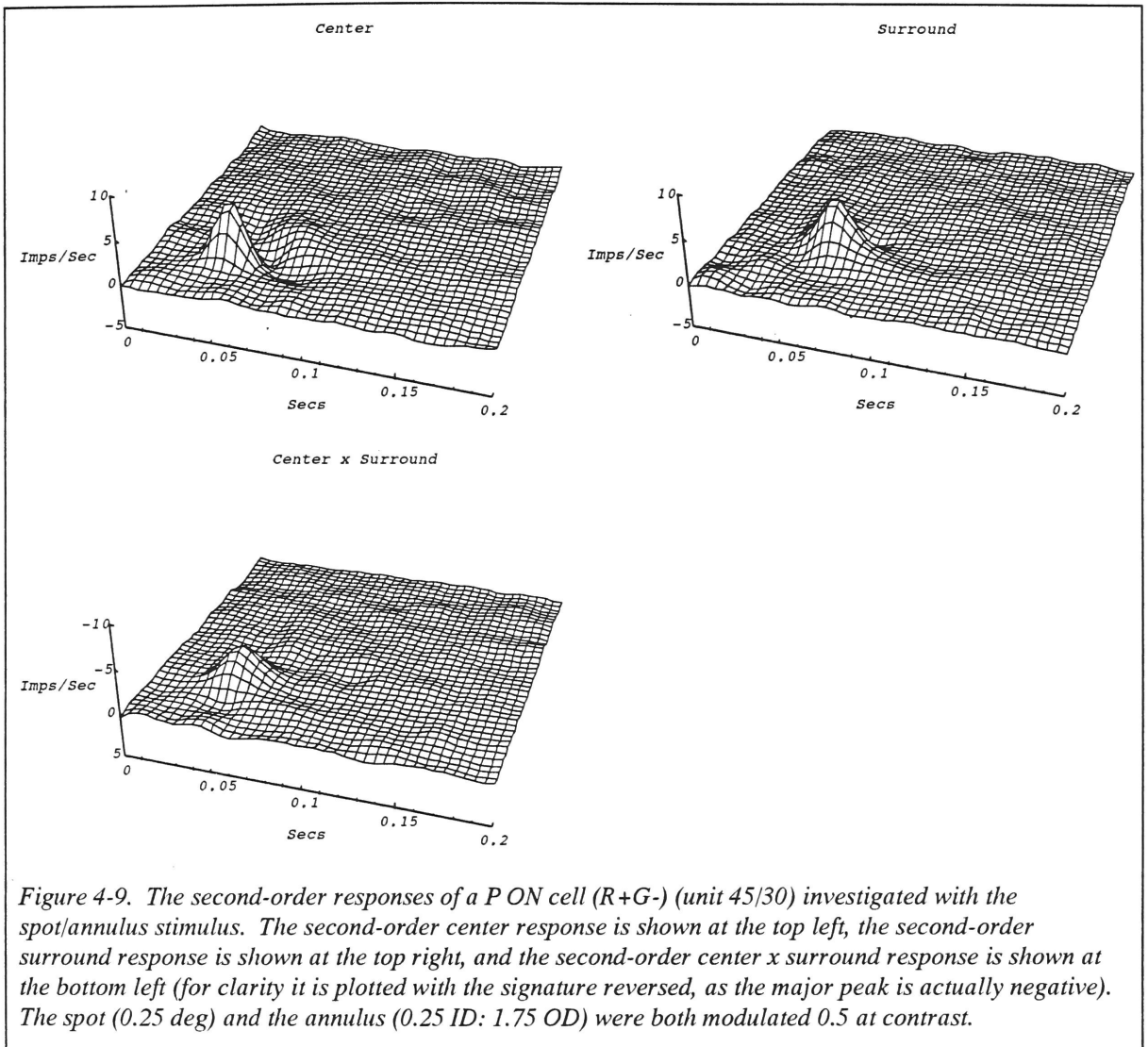


Fig. 4-10 shows the same set of three second-order responses for a P OFF cell.

The center x center and the center x surround responses are very similar to that of the P ON cell. The second-order surround response of the P OFF cell shows instead of a peak, a depression which is typical for P OFF cells.

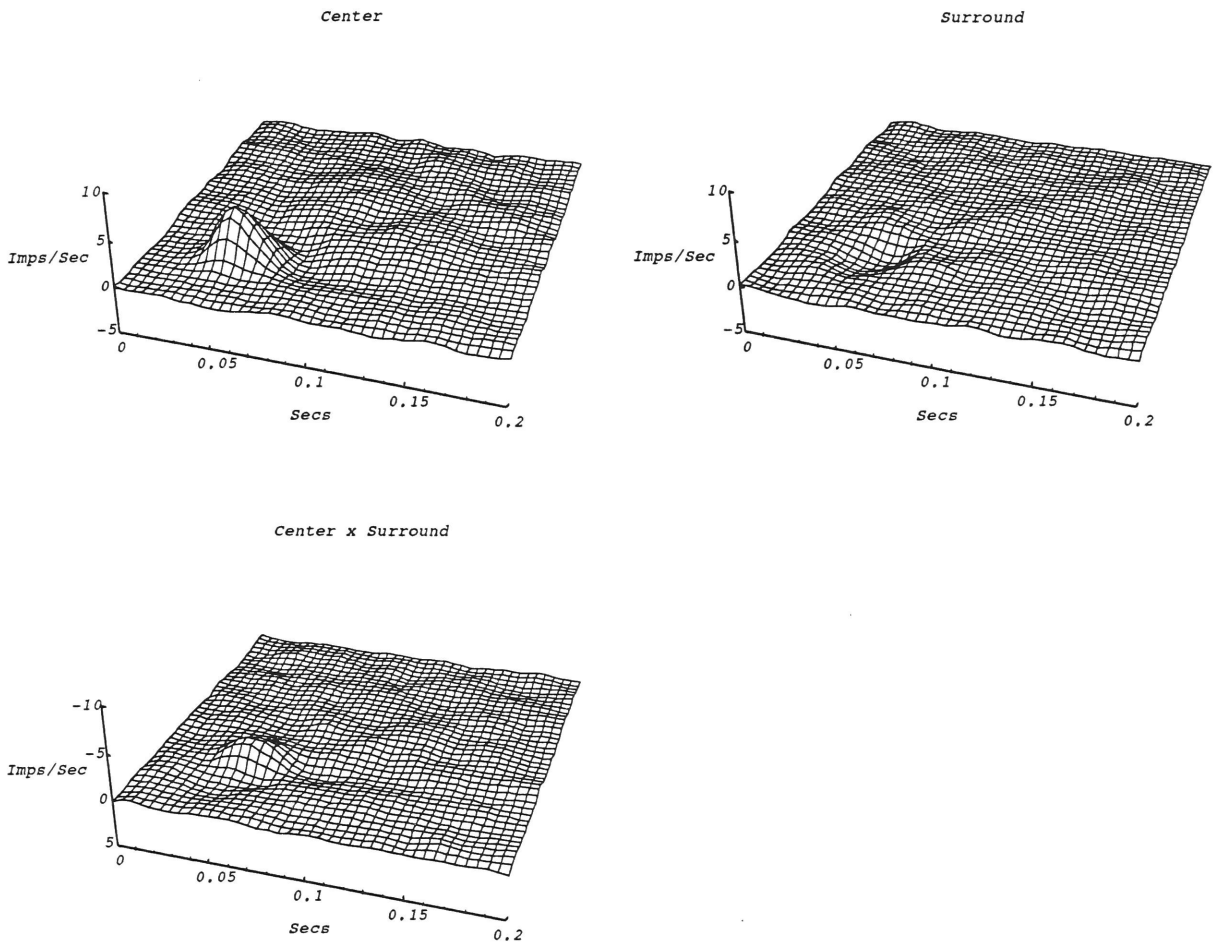


Figure 4-10. The second-order responses of a P OFF cell (R-G+) (unit 45/23) investigated with the same spot/annulus stimulus as described in Fig. 4-9. The center (top left), surround (top right), and the center x surround (bottom) second-order responses are shown.

4.6 LNL Model Fits

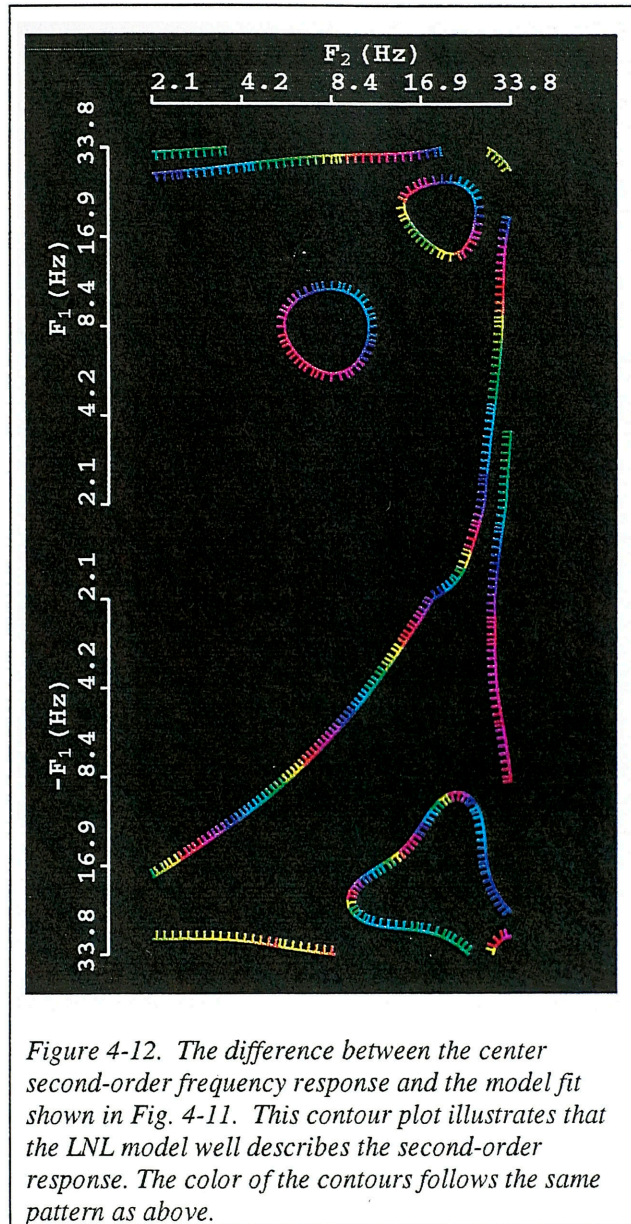
The second-order kernels from the m-sequence experiments were transformed into the frequency domain, and the LNL model was fit to the data as described in Methods. Figures 4-11 - 4-13 show the frequency domain data and the model fits for the P ON cell center. Figure 4-11 shows the center second-order frequency response data on the right and the model fit on the left. The contours represent the height of the surface and the

colors of the contours code for the phase of the response as described in the legend. One can see that the model captures the major features of the data.

Each frequency response can be divided into an upper and a lower half: the upper half being the F_1+F_2 (“sum”) frequency region and the lower half being the $-F_1+F_2$ (the “difference”) frequency region. The asymmetry of these two regions reflects the same biphasic shape seen in the time domain kernel.



Figure 4-11. The Fourier transform of the second-order center response of the P ON cell (unit 45/30) shown in Figure 4-9 (left). The LNL model is fit to 1024 complex data points from the Fourier transform of the second-order response (right). Each contour is separated by 1.8 impulses/second, and the tick marks point in the downhill direction. The legend at the top shows how the colors of the contours relate to the phase. The 0°-180° axis is real; the 90°-270° axis is imaginary. The parameters of the LNL fit are: A : 693.77 impulses/second-unit contrast²; $H_{S,U}$: 0.65; $\tau_{S,U}$: 15.7 ms; $N_{L,U}$: 20; $\tau_{L,U}$: 2.03 ms; $H_{S,W}$: 0.86; $\tau_{S,W}$: 1.80 ms; $N_{L,W}$: 7; $\tau_{L,W}$: 1.80 ms; D : 3.0 ms.



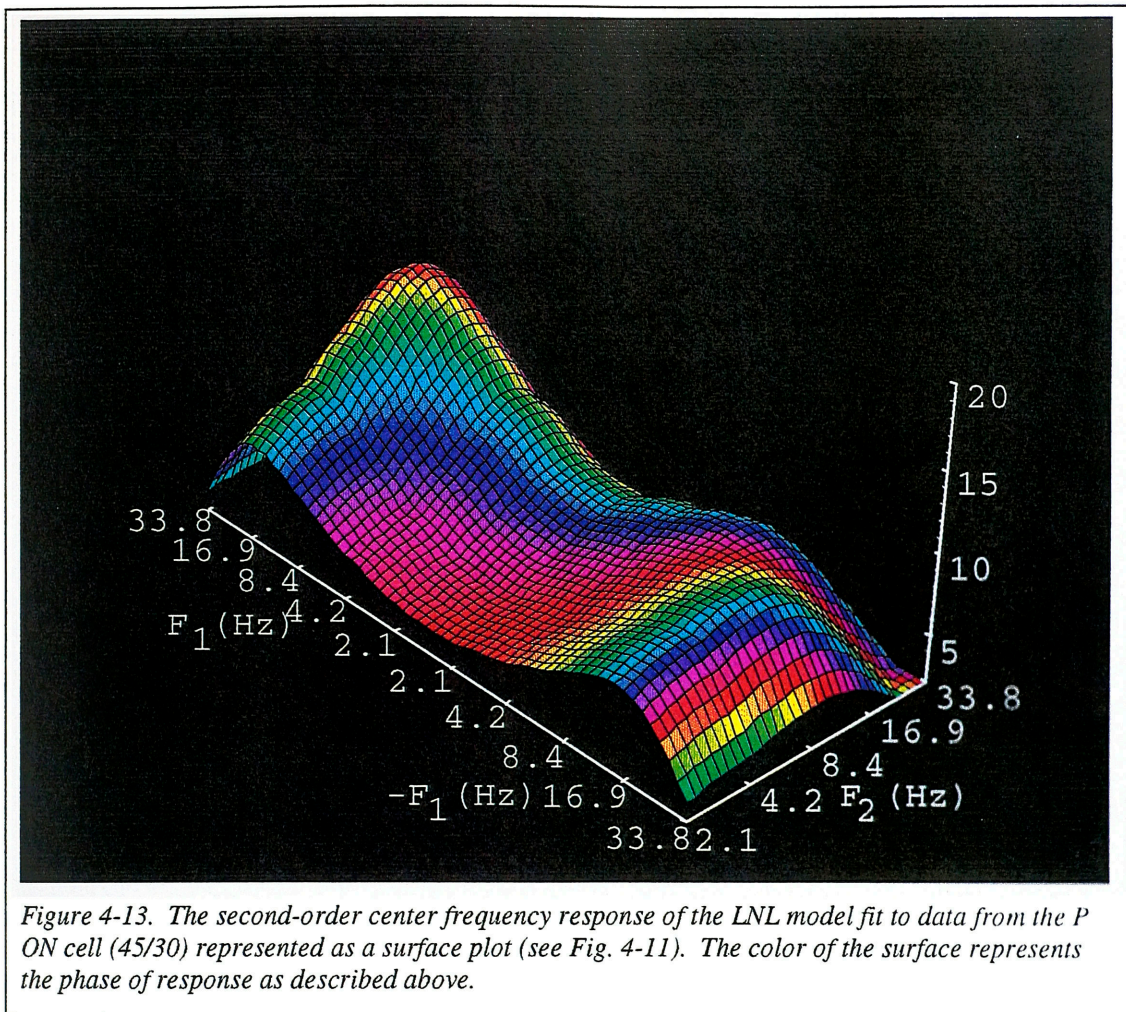


Figure 4-13 shows the LNL fit to the center x center response as a surface plot using the same color code as the contour plots to label the phases.

Similarly, the second-order center- surround frequency response is shown in Fig. 4-14 along with the corresponding fit of the LLNL model. Figure 4-15 shows the difference between the data and the model fit, demonstrating the accuracy of the fit.

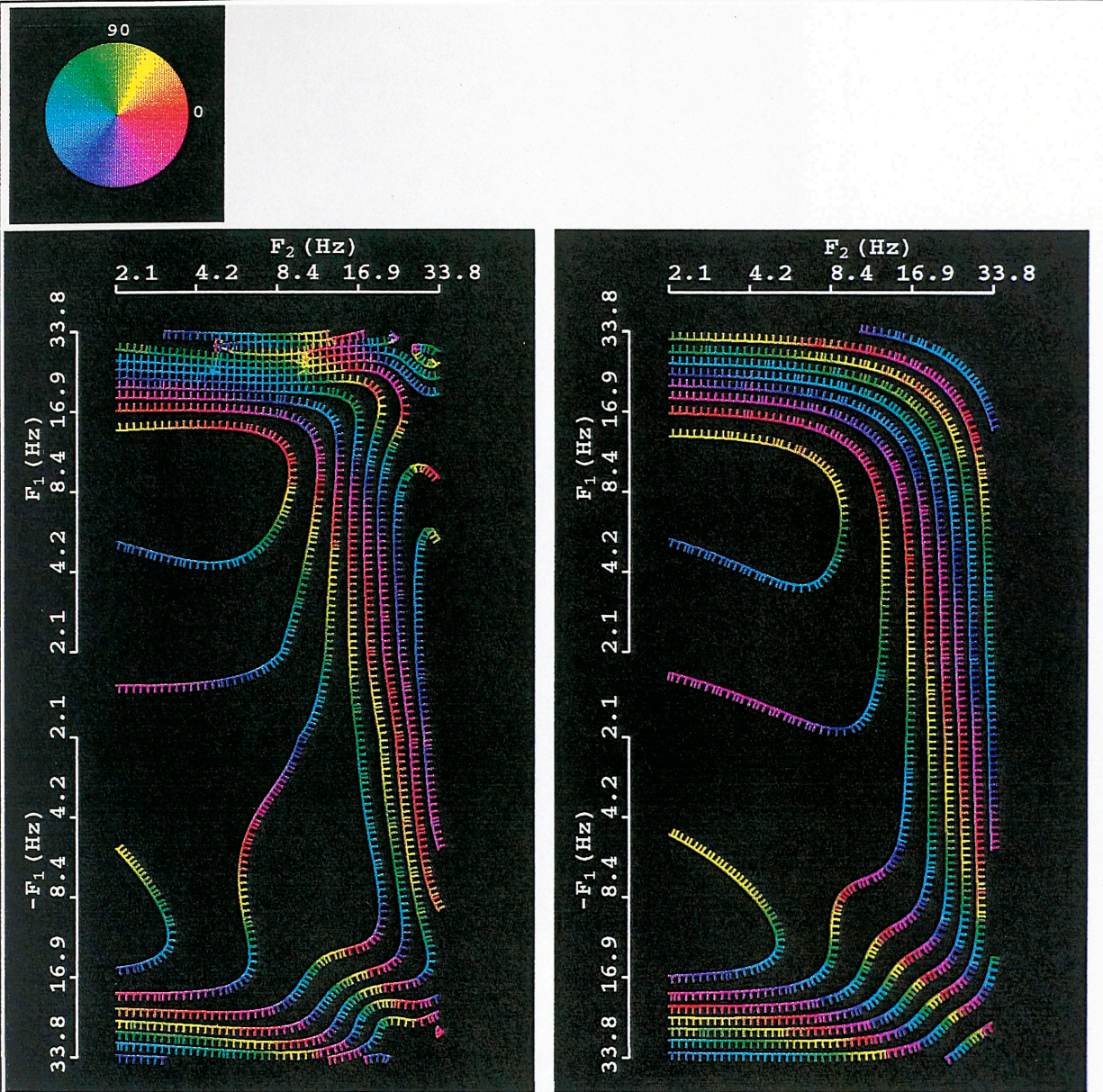


Figure 4-14. The second-order center \times surround frequency response of a P ON cell (unit 45/30) (left) and the fit of the LLNL model (right). The m -sequence kernel is shown in Fig. 4-9. The contours are separated by 1.0 impulses/second. The color of the contours corresponds to the legend above. The surround frequencies are represented on the F_1 axis; the center frequencies are represented on the F_2 . This kernel is clearly not symmetric. The parameter of the LLNL fit are: -293.44 impulses/second-unit contrast²; $H_{S,V}$: 0.57; $\tau_{S,V}$: 5.77 ms; $N_{L,V}$: 18; $\tau_{L,V}$: 2.49 ms; $H_{S,U}$: 0.56; $\tau_{S,U}$: 2.56 ms; $N_{L,U}$: 14; $\tau_{L,U}$: 2.56 ms; $H_{S,W}$: 0.45; $\tau_{S,W}$: 1.90 ms; $N_{L,W}$: 7; $\tau_{L,W}$: 9.60 ms; D : 3.0 ms. The linear filter, V , operates on the surround signal; U operates on the center signal. W is the post-nonlinearity linear filter.

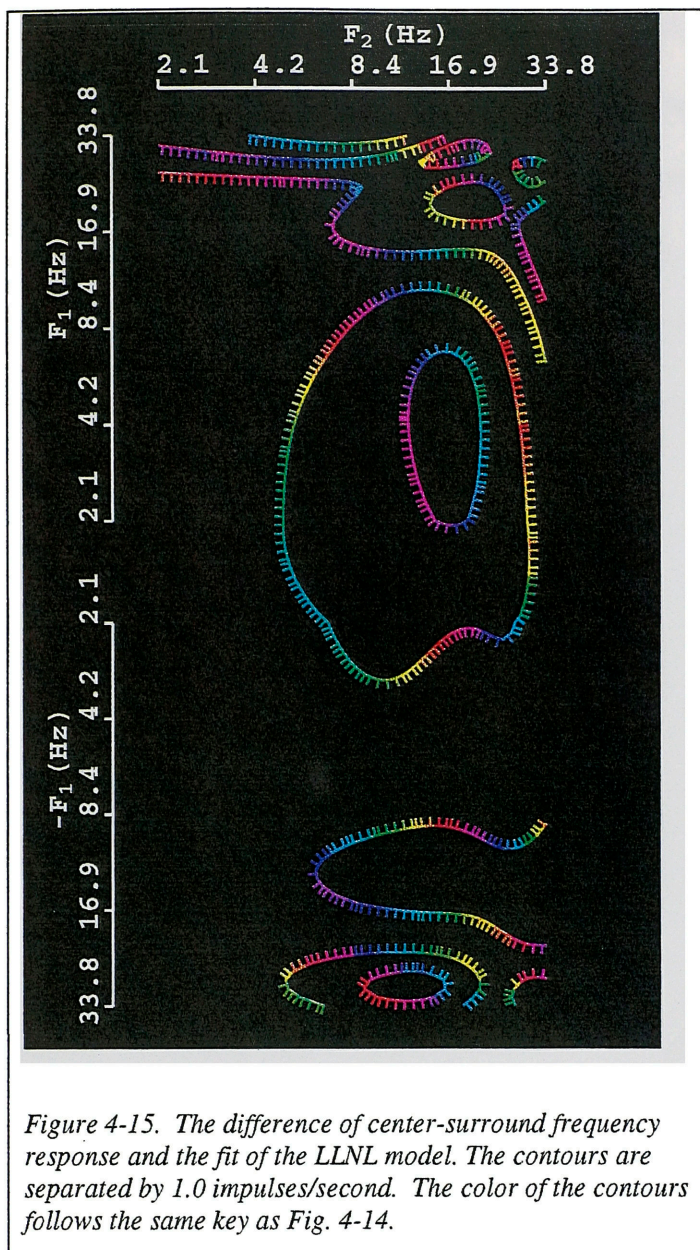


Figure 4-15. The difference of center-surround frequency response and the fit of the LLNL model. The contours are separated by 1.0 impulses/second. The color of the contours follows the same key as Fig. 4-14.

The same analysis as above was performed on the responses of the P OFF cell shown in Fig. 4-11. Notice in Fig. 4-16 that the center x center frequency response of the P OFF cell has a slightly different appearance than that of the P ON cell. Quantitatively, this difference corresponds to a statistically different second linear stage in the LNL sandwich model for the P OFF cell population. The center x surround (Fig. 4-17) interaction is qualitatively the same in the P OFF population as in the P ON population, although the interaction tends to be less strong.

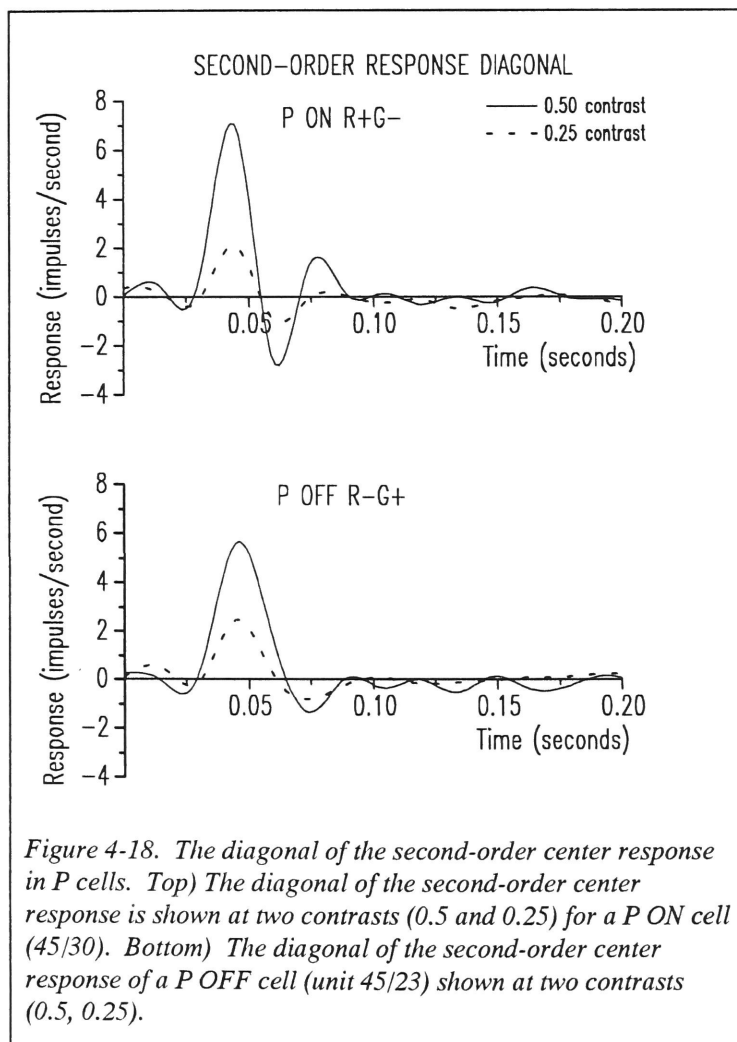


Figure 4-16. The second-order frequency response of the center of a P OFF cell (unit 45/23) (left) and the fit of the LNL model (right). The *m*-sequence kernel is shown in Fig. 4-10. The contours are separated by 1.8 impulses/second. The color of the contours reflects the phase of the response as indicated by the color circle in the legend. The parameters of the LNL fit are: A : 194.96 impulses/second-unit contrast², $H_{S,U}$: 0.51; $\tau_{S,U}$: 15.6 ms; $N_{L,U}$: 18; $\tau_{L,U}$: 2.78; $H_{S,W}$: 0.36; $\tau_{S,W}$: 20.3 ms; $\tau_{L,W}$: 0 ms; D : 3.5 ms.



Figure 4-17. The center \times surround frequency response of a P OFF cell (45/23) (left) and the LLNL model fit (right). The m -sequence kernel is shown in Fig. 4-10. The contours are separated by 1.0 impulses/second. The color of the contours represents the phase as shown above. F_1 represents surround frequencies; F_2 represents center frequencies. A: -2773.49 impulses/second-unit contrast², $H_{S,V}$: 0.85; $\tau_{S,V}$: 2.32 ms; $N_{L,V}$: 20; $\tau_{L,V}$: 2.32; $H_{S,U}$: 0.90; $\tau_{S,U}$: 4.99 ms; $N_{L,U}$: 8; $\tau_{L,U}$: 4.99; $H_{S,W}$: 0.81; $\tau_{S,W}$: 3.87 ms; $\tau_{L,W}$: 3.87 ms; D: 3.5 ms. The linear filter, V, operates on the surround signal; U operates on the center signal. W is the post-nonlinearity linear filter.

Figure 4-18 demonstrates how the size of the second-order response scales with increasing contrast. This relationship also was explored with a simple test. The values of the diagonal of the second-order center response were squared and summed. The ratio of this value at 0.5 contrast to this value at 0.25 contrast was calculated. For a system with a purely quadratic nonlinearity, this value would be 4. For the P ON cell shown, this value is 3.11. For the OFF cell, it is 2.27. Over the whole population of P cells, there was some dispersion in these values; the mean was 2.17 (S.D. 0.58). There was no significant difference between the ON and OFF populations.



These values reflect the nature of the operating characteristic of the nonlinearity in P cells. The second-order kernel reflects an expansion of this nonlinearity up to terms of second-order. The last section of this chapter will suggest the possible origin of this nonlinearity.

Table 4-4 summarizes the fitted parameters of the LNL model for the second-

order center kernels of P cells. The parameters $N_L\tau_L$, H_S , and τ_S describe the characteristics of the pre- and post-nonlinearity linear filters, U and W , respectively.

Figure 4-19 shows the average characteristics of these filters. There was no difference between the ON and OFF populations or the R-center or the G-center populations in these parameters. The first filter, $U(\omega)$, can be seen to have the same general gentle bandpass characteristics as the first-order frequency response of the P cell. The post-filter, $W(\omega)$, on the other hand, has a relatively sharp band-pass characteristic.

Table 4-4. The Parameters of the LNL Model for the Second-Order Center Response of P cells
 $N_{TOTAL} = 18$; $N_{ON} = 9$; $N_{OFF} = 9$; $N_{RG} = 16$; $N_{YB} = 2$

Parameter	Minimum	Maximum	Median	Mean	S.D.	C.V.
A (impulses/(s-unit contrast ²))	59.59	3476.00	305.47	777.44	997.40	1.28
$N_{L,U}\tau_{L,U}$ (ms)	26.64	49.98	38.09	39.43	7.46	0.19
$H_{S,U}$ (dimensionless)	0.2995	0.6490	0.6812	0.6541	0.1930	0.30
$\tau_{S,U}$ (ms)	4.21	28.41	11.00	13.02	7.00	0.54
$N_{L,W}\tau_{L,W}$ (ms)	0	24.53	9.93	10.76	7.63	0.71
$H_{S,W}$ (dimensionless)	0.3673	0.9672	0.8159	0.7644	0.1880	0.25
$\tau_{S,W}$ (ms)	1.70	23.21	3.91	8.76	7.88	0.90

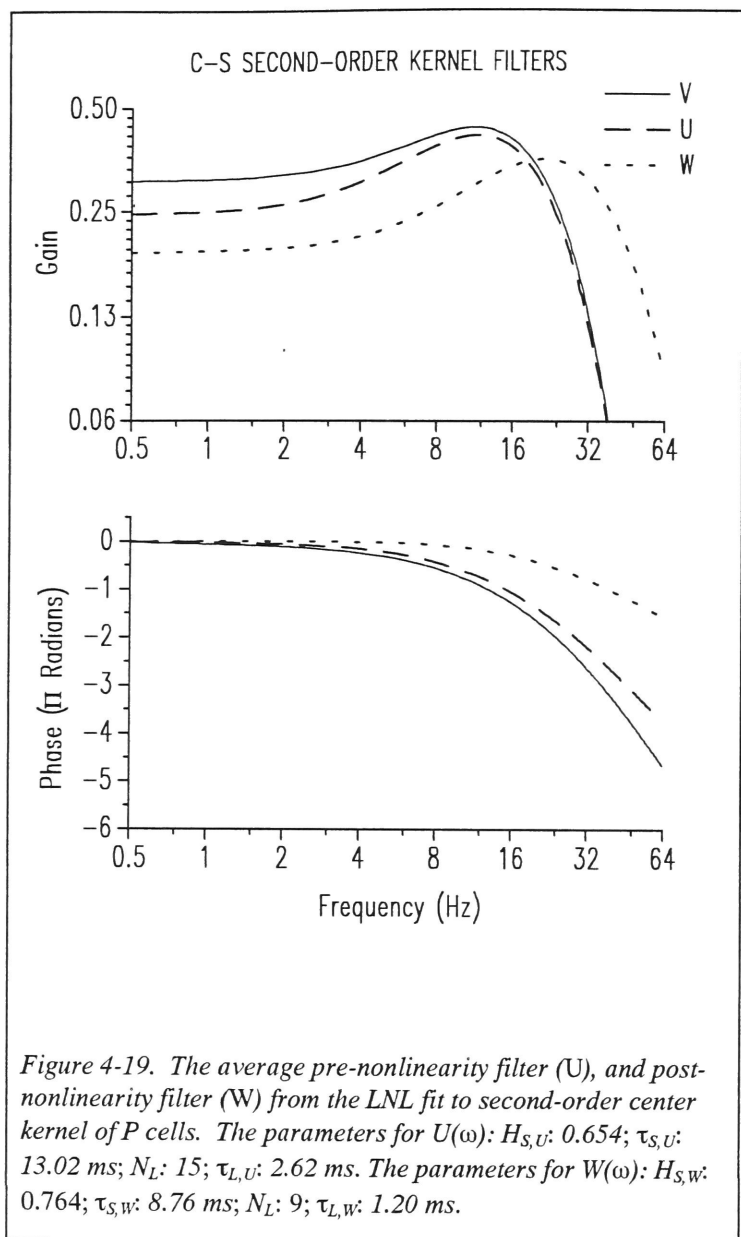


Table 4-5 summarizes the results of the fit of the LLNL model to the center x surround kernel data. The filter, V , which is the surround filter and the filter, U , which is the pre-nonlinearity filter for the center input, both have gentle bandpass characteristics. The post-nonlinearity filter, W , shows a sharper bandpass feature than the pre-nonlinearity filter and peaks at a higher temporal frequency (Fig. 4-20).

Table 4-5. The Parameters of the LLNL Model for the Second-Order Center-Surround Kernel of P Cells
 $N_{TOTAL} = 13$; $N_{ON} = 7$; $N_{OFF} = 6$; $N_{RG} = 13$

Parameter	Minimum	Maximum	Median	Mean	S.D.	C.V.
A (impulses/(s-unit contrast ²))	-23053.5	-1208.7	-7124.4	-9010.7	6592.4	-0.73
$N_{L,U}\tau_{L,U}$ (ms)	34.18	62.14	44.54	45.88	8.36	0.18
$H_{S,U}$ (dimensionless)	0.2835	0.9359	0.7232	0.6934	0.1996	0.29
$\tau_{S,U}$ (ms)	0.47	29.4	3.20	8.29	9.03	1.09
$N_{L,V}\tau_{L,V}$ (ms)	25.28	54.38	39.44	40.03	8.39	0.21
$H_{S,V}$ (dimensionless)	0.3332	0.9582	0.8687	0.7558	0.2122	0.28
$\tau_{S,V}$ (ms)	0.15	38.14	2.64	8.41	12.5	1.49
$N_{L,W}\tau_{L,W}$ (ms)	4.10	27.10	15.51	16.88	6.92	0.41
$H_{S,W}$ (dimensionless)	0.4506	0.9582	0.8214	0.8096	0.1353	0.17
$\tau_{S,W}$ (ms)	1.28	9.60	3.30	4.03	2.73	0.68

4.7 Center-Surround Interaction Experiments

The second-order kernels

derived with the m-sequence

technique demonstrate that there

are nontrivial nonlinearities in the

receptive fields of primate P

retinal ganglion cells. Previous

work by Kaplan and Shapley

(1989) had shown that the level

of steady illumination of the

surround of P cells affects the

center response in a way that was

strictly nonlinear. I developed a

similar paradigm, which uses a

spot modulated by a sum of two

m-sequences and a steady

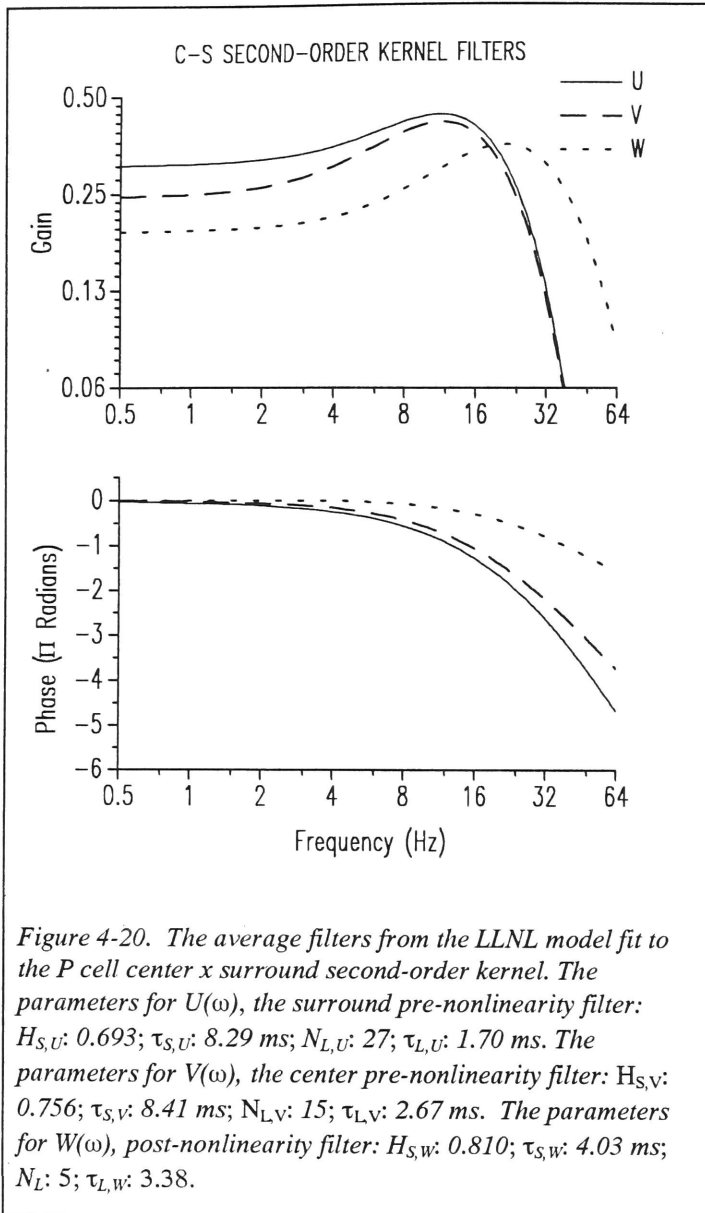


Figure 4-20. The average filters from the LLNL model fit to the P cell center \times surround second-order kernel. The parameters for $U(\omega)$, the surround pre-nonlinearity filter: $H_{S,U}$: 0.693; $\tau_{S,U}$: 8.29 ms; $N_{L,U}$: 27; $\tau_{L,U}$: 1.70 ms. The parameters for $V(\omega)$, the center pre-nonlinearity filter: $H_{S,V}$: 0.756; $\tau_{S,V}$: 8.41 ms; $N_{L,V}$: 15; $\tau_{L,V}$: 2.67 ms. The parameters for $W(\omega)$, post-nonlinearity filter: $H_{S,W}$: 0.810; $\tau_{S,W}$: 4.03 ms; $N_{L,W}$: 5; $\tau_{L,W}$: 3.38.

annulus, to investigate this effect. This technique permitted the observation of both a

change in gain and a change in response dynamics that was difficult to evaluate without

these more advanced techniques.

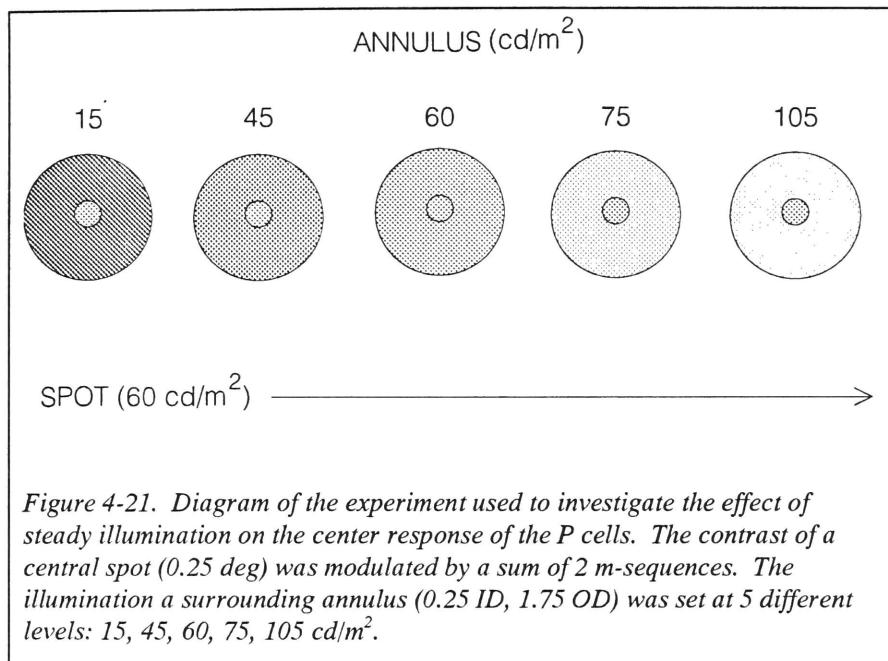
Figure 4-21 diagrams the basic experiment. The central spot is modulated by the

m-sequence signal around a steady level of mean illumination. In five experimental

conditions, the steady illumination of a surrounding annulus is increased from a level

below (0.25-fold) the mean illumination of the spot to well above that level (1.75-fold).

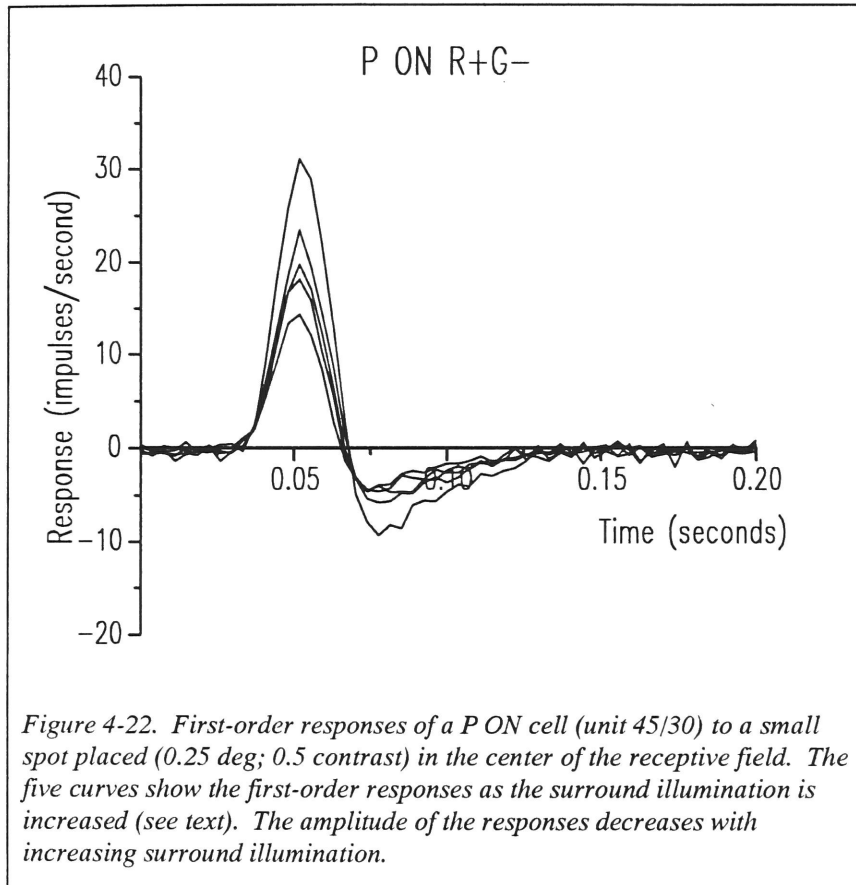
For each of these conditions, the first-order response of the center mechanism was calculated and fit to the linear filter model.



The first-order responses of three P ON cells and the model fits under these conditions are shown in Figs. 4-22 - 4-31. For the first P ON cell, the

calculated first-order responses to the spot are shown in Fig. 4-22. The lowest amplitude response corresponds to the highest surround illumination. As the surround illumination decreases, the amplitude of the response increases. The data from three cells are shown to demonstrate the reproducibility of this effect. Figure 4-23 shows the calculated first-order center response at the lowest (Fig. 4-22, top) and highest (Fig. 4-22, bottom) level of illumination for a P ON cell. These data show that increasing the surround illumination reduces the gain of the center and slightly speeds up the response as can be judged from the position of the zero-crossing. The solid curves in Fig. 4-22 show the fit of the linear filter model. All of the model parameters were initially fit at each level of surround illumination. However, empirically, it was found that as the surround illumination

increases, it was only necessary to vary the overall gain, A , and the time constant of the lowpass stages, τ_L , to generate fits to the responses at higher levels of surround illumination.



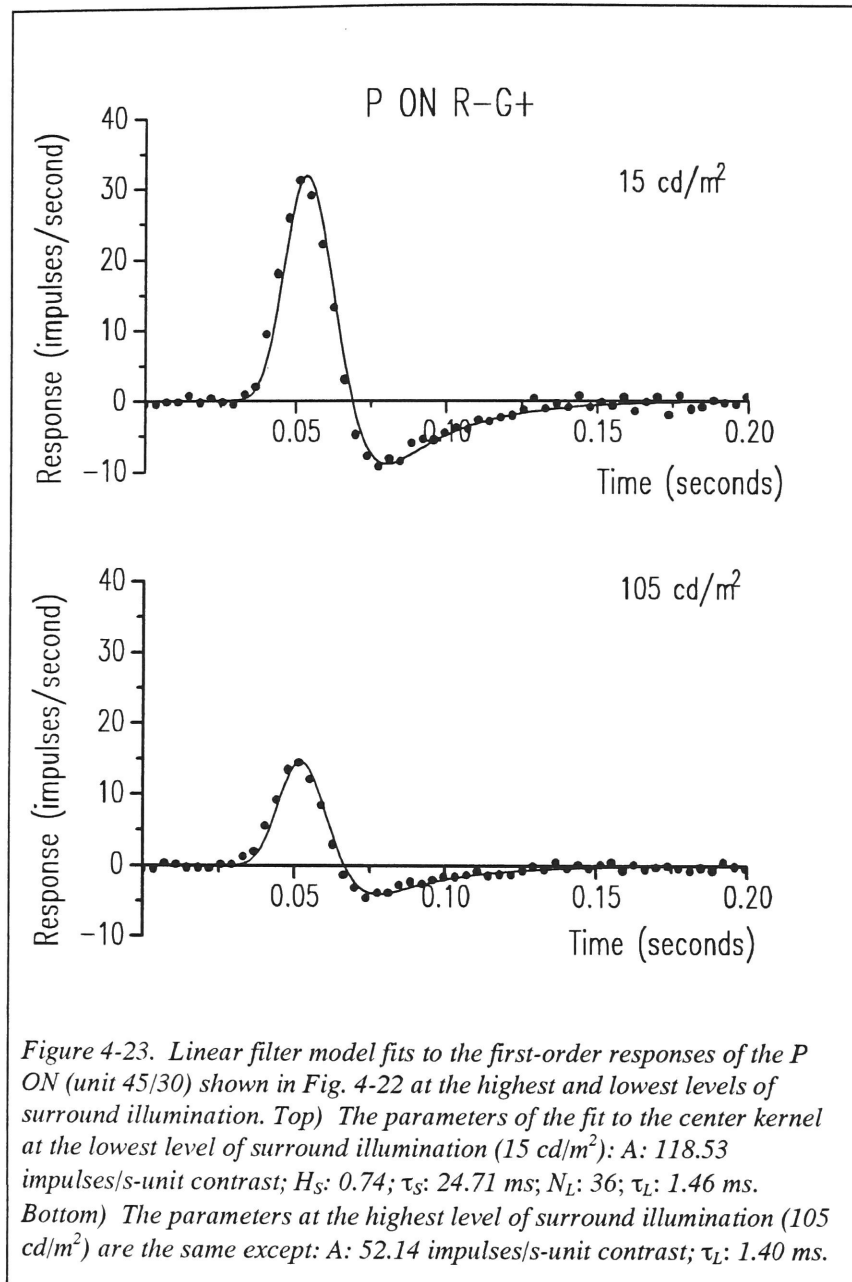


Figure 4-24

shows the family of fitted curves from the model (without the associated data points for clarity).

Figures 4-25 -

4-27 and Figs. 4-28 - 4-30 show the same sets of data for two other P ON cells. The gain and time course changes among the three P ON cells are very similar. Figures 4-31 - 4-33 show the effect on the first-

order center response of a P OFF cell. This effect is somewhat less pronounced in P OFF cells. For the P OFF cell, increasing the surround illumination **increases** the center gain but still speeds up the time course of the response of the first-order response.

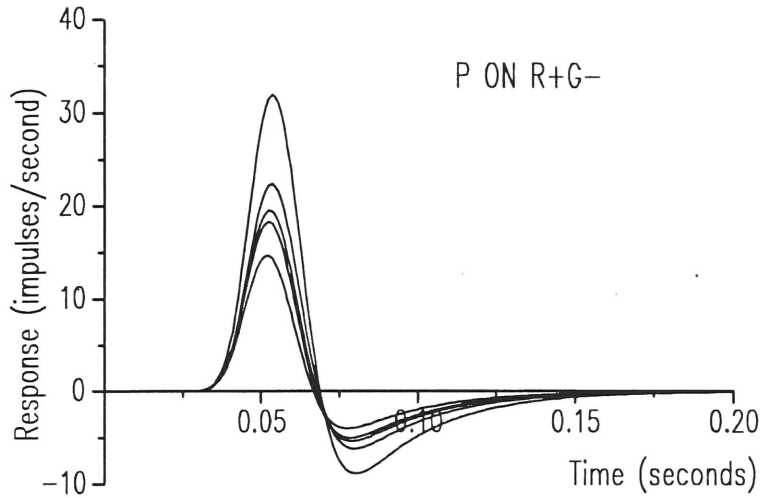


Figure 4-24. The family of curves that show the fits of the linear filter model to the first-order responses of the center of the P ON cell (unit 45/30) under conditions of increasing surround illumination (see Fig. 4-21). These curves are obtained by fitting only two parameters, A and τ_L , at each level of surround illumination after the entire model was fit at the lowest level of surround illumination. These model responses show the characteristic decrease in gain and speed-up in time course associated with increasing surround illumination in P ON cells. For the exact values of the parameters, see Fig. 4-23 and Fig. 4-34.

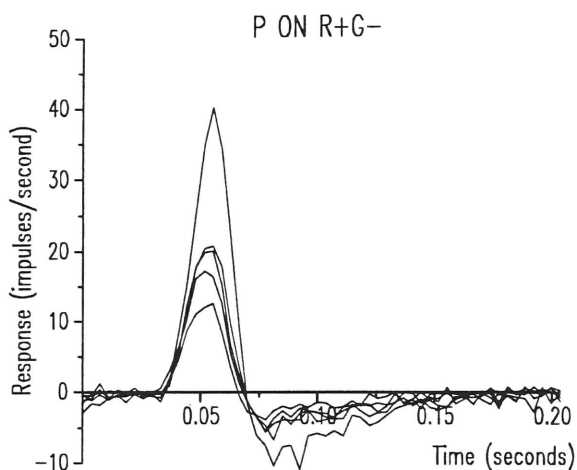


Figure 4-25. The first-order responses of a P ON cell (unit 43/27) to a 0.5 contrast spot (0.25 deg) as surround illumination increases (see Fig. 4-21). The amplitude of the response decreases and the time course speeds up as the surround illumination increases.

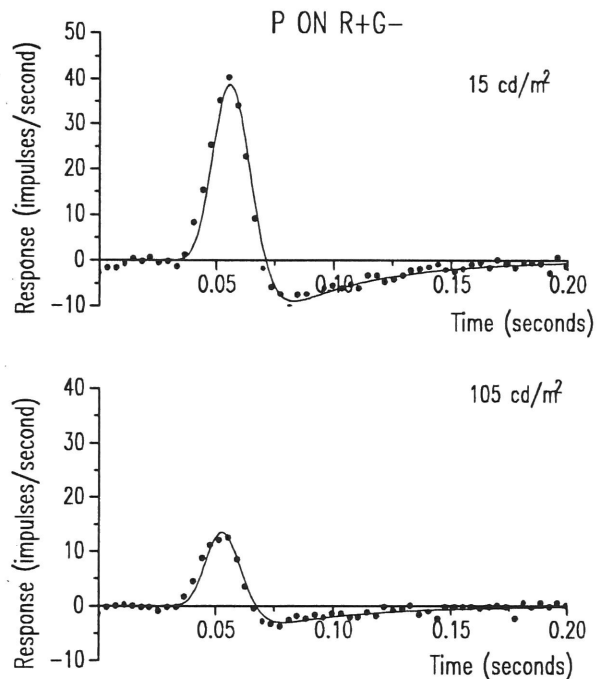


Figure 4-26. Fits to the first-order responses of a P ON cell (unit 43/27) obtained at the highest (bottom) and lowest (top) levels of surround illumination. The parameters at the lowest level of surround illumination (15 cd/m^2) are: A : 129.19 impulses/s-unit contrast; H_S : 0.79; τ_S : 40.81 ms; N_L : 42; τ_L : 1.27 ms. At the highest level (105 cd/m^2) of surround illumination: A : 41.84 impulses/s-unit contrast; τ_L : 1.19 ms.

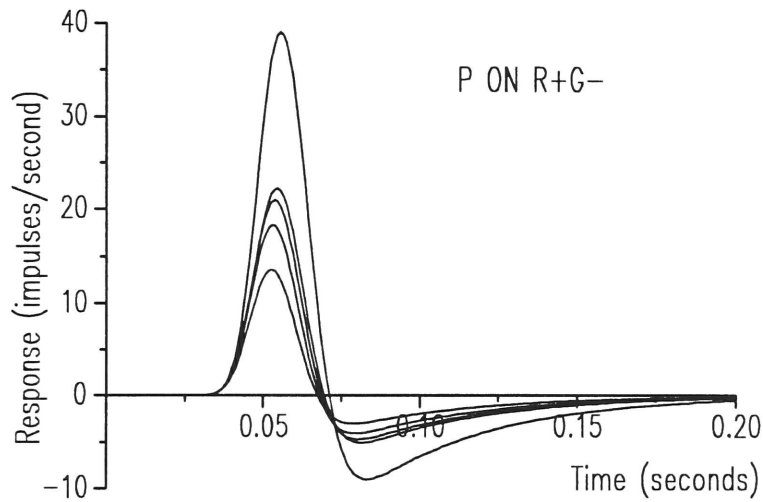


Figure 4-27. The fits of the linear filter model to the first-order responses of a P ON cell (unit 43/27) (see Fig. 4-25 and 4-26) as surround illumination is increased. The response at the lowest level of surround illumination has the largest amplitude; the response at the highest level, the smallest. For the exact values of the fitted parameters, see Fig. 4-25 and Fig. 4-35.

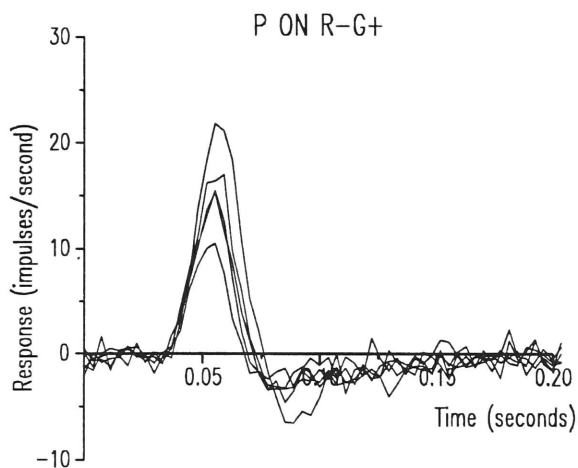


Figure 4-28. First-order center responses of a P ON (R-G+) cell (unit 43/25) at five levels of steady surround illumination (see Fig. 4-21) to a 0.5 contrast spot (0.25 deg).

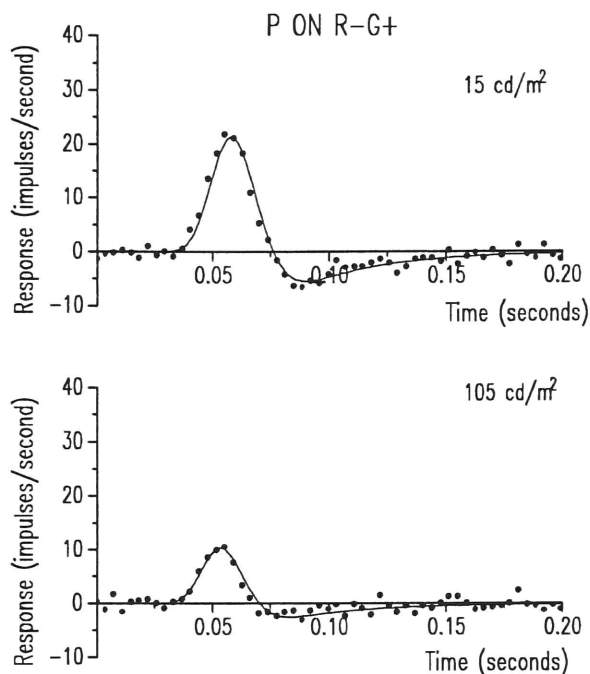


Figure 4-29. Fits of the linear filter model to the first-order responses of a P ON cell (unit 43/25) at the lowest (15 cd/m^2) (top) and highest (105 cd/m^2) (bottom) level of surround illumination. The parameters of the fit at the lowest level of surround illumination are: A : 91.0866/s-unit contrast; H_S : 0.734; τ_S : 34.45 ms; N_L : 31; τ_L : 1.83 ms. At the highest level of surround illumination, the parameters are the same except: A : 39.73 impulses/s-unit contrast; τ_L : 1.67 ms.

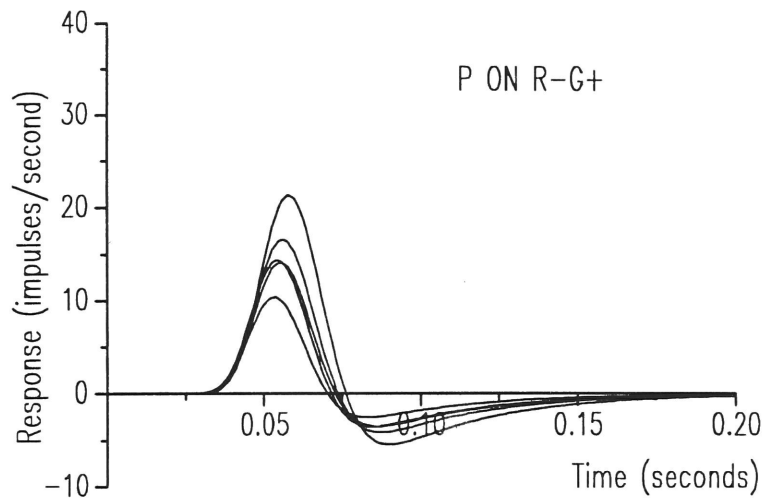


Figure 4-30. The linear model fits to the first-order responses of a P ON cell at five levels of surround illumination (unit 43/20). Increasing the surround illumination decreases the amplitude of the response. For the actual parameters, see Fig. 4-29 and Fig. 4-35.

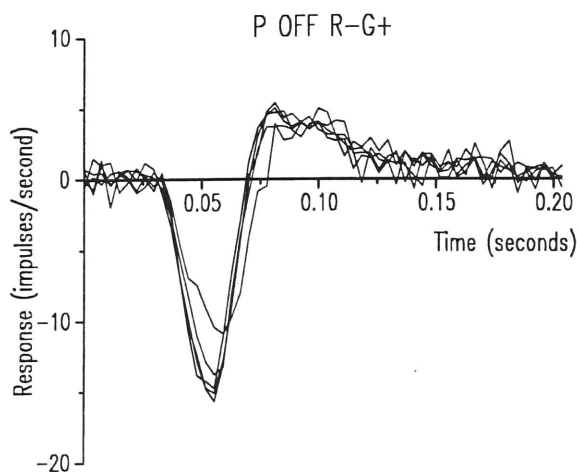


Figure 4-31. First-order center responses of a P OFF cell (unit 43/20) at five levels of surround illumination to a central spot (0.25 deg) at 0.25 contrast. As the level of surround illumination increases, the amplitude of the response increases. The time course of the response also speeds up with increasing illumination.

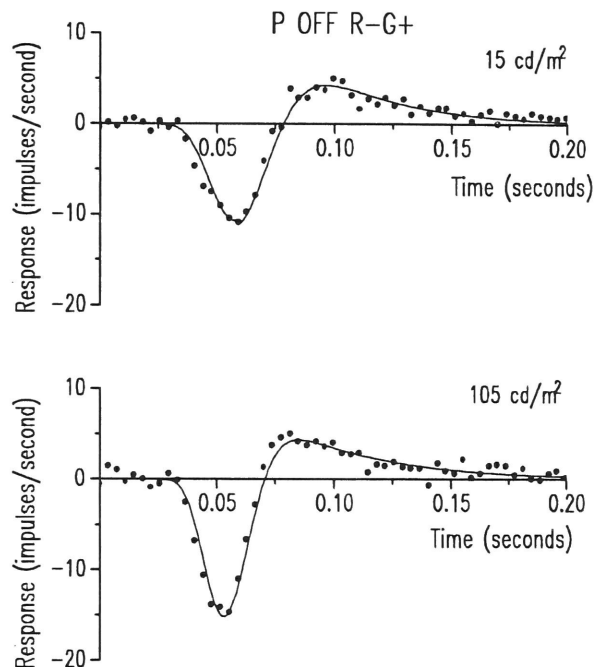


Figure 4-32. Fits of the linear filter model to the first-order responses of a P OFF cell (unit 43/20) at the lowest (top) (15 cd/m^2) and highest (bottom) (105 cd/m^2) levels of surround illumination. The parameters of the fit at the lowest level of surround illumination are: A : 64.191 impulses/s-unit contrast; H_S : 0.926; τ_S : 36.26 ms; N_L : 20; τ_L : 2.96 ms. At the highest level of surround illumination: A : 62.97 impulses/s-unit contrast; H_S : 0.870; τ_S : 41.68 ms; N_L : 27; τ_L : 1.91 ms.

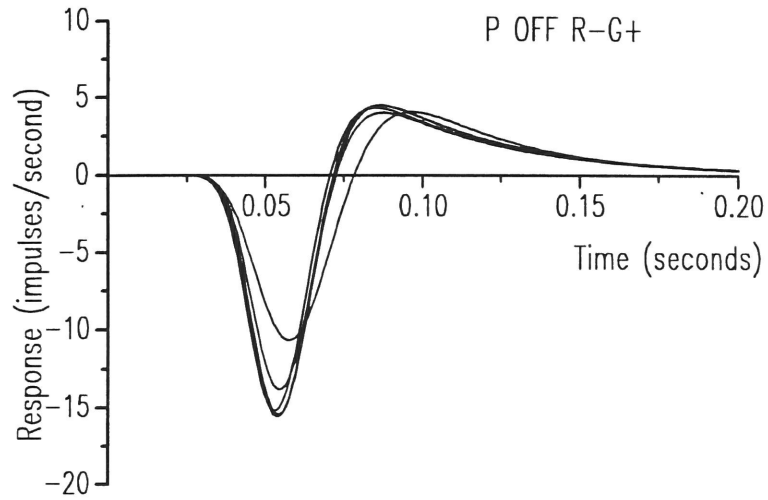
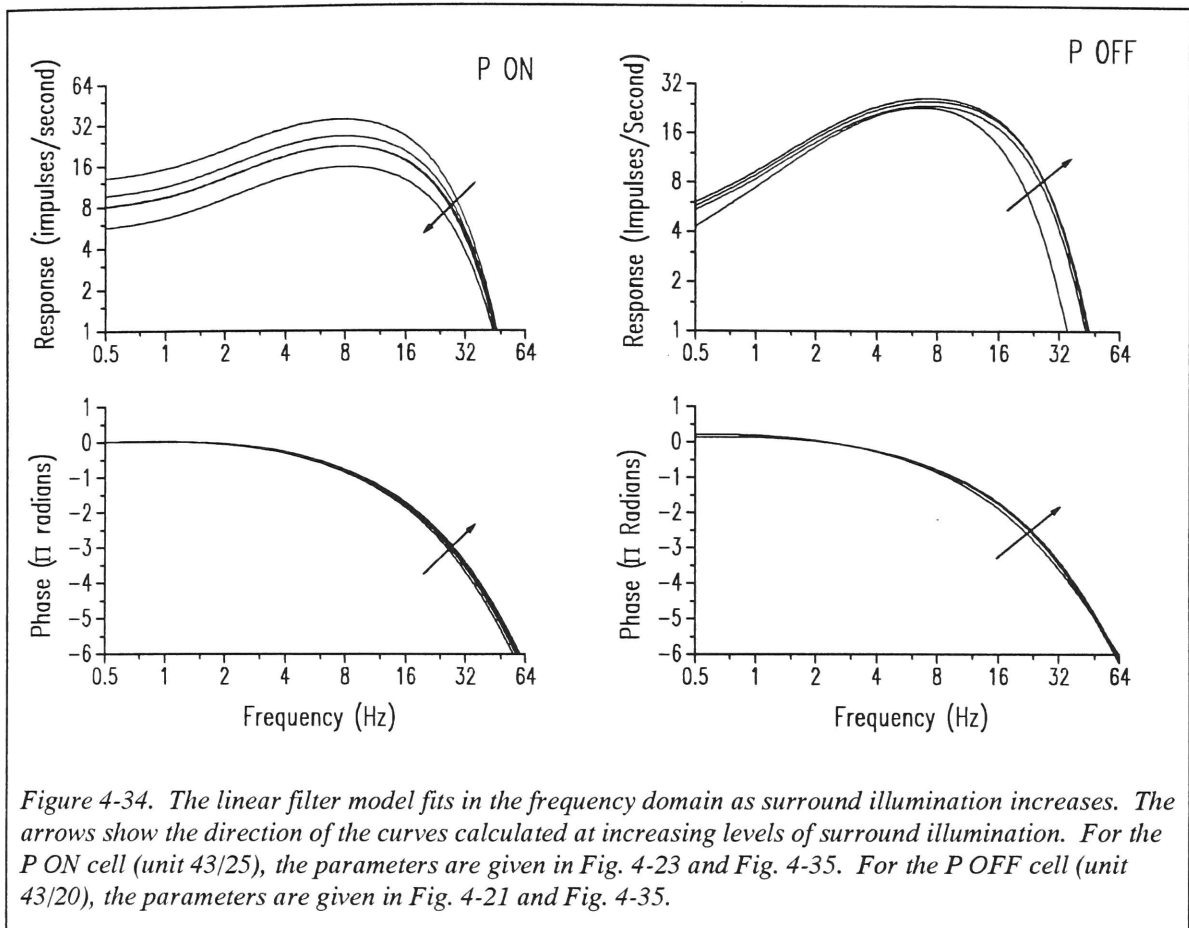


Figure 4-33. The fits of the linear filter model to the first-order center responses of a P OFF cell (unit 43/20) at five levels of surround illumination (see Figs. 4-31 and 4-32). The response amplitude increases as the surround illumination increases. The parameters of the fits are given in Fig. 4-32 and Fig. 4-35.



In the frequency domain (Fig. 4-34), the changes in the gain and dynamics under the conditions of increasing surround illumination affect the amplitude and phase of the response. The parameters A , τ_L , and the mean rate, M , vary with the level of surround illumination for each cell above (Fig. 4-35). For the ON cells, it can be seen that, with increasing surround illumination the gain, A , decreases along a gradually sloping curve. The time constant, τ_L , on the other hand, decreases nearly linearly. The mean rate in the first 2 P ON cells was higher at the lowest level of surround illumination (due to the release of surround inhibition), but flattened out at the 4 higher levels. For the third P ON cell, the mean rate stayed relatively flat across all levels of surround illumination. The truncation nonlinearity, described in the section on the P cell center, is a function of the

mean rate, but that nonlinearity cannot be responsible for the change in gain and dynamics; for the third P ON cell, the gain and time constant changes occur in the absence of changes in the mean rate. Measurements made with lower contrast stimulation, where saturation could not be a factor, showed the same effect. In addition, pilot studies with annuli of different spatial extents showed that the nonlinear surround effect is nearly maximal when the outer diameter of the annulus is 1.75 deg. Larger annuli do not increase the effect.

In Fig. 4-35, smooth curves are shown plotted through the overall gain parameter, A , at the 5 levels of surround illumination. This smooth curve is a fit to the data of the function:

$$A(I) = A_{\max} \cdot \frac{1}{1 + kI} \quad (4-1)$$

The parameters, A_{\max} and k , were adjusted using a least-squares fitting routine to give the best fit of the hyperbola (Eq. (4-1)) to the data. In addition, a regression line was fit to the time constant, τ_L . The parameters from the fit of the regression line and the hyperbola for a population of 8 P ON cells are summarized in Table 4-6.

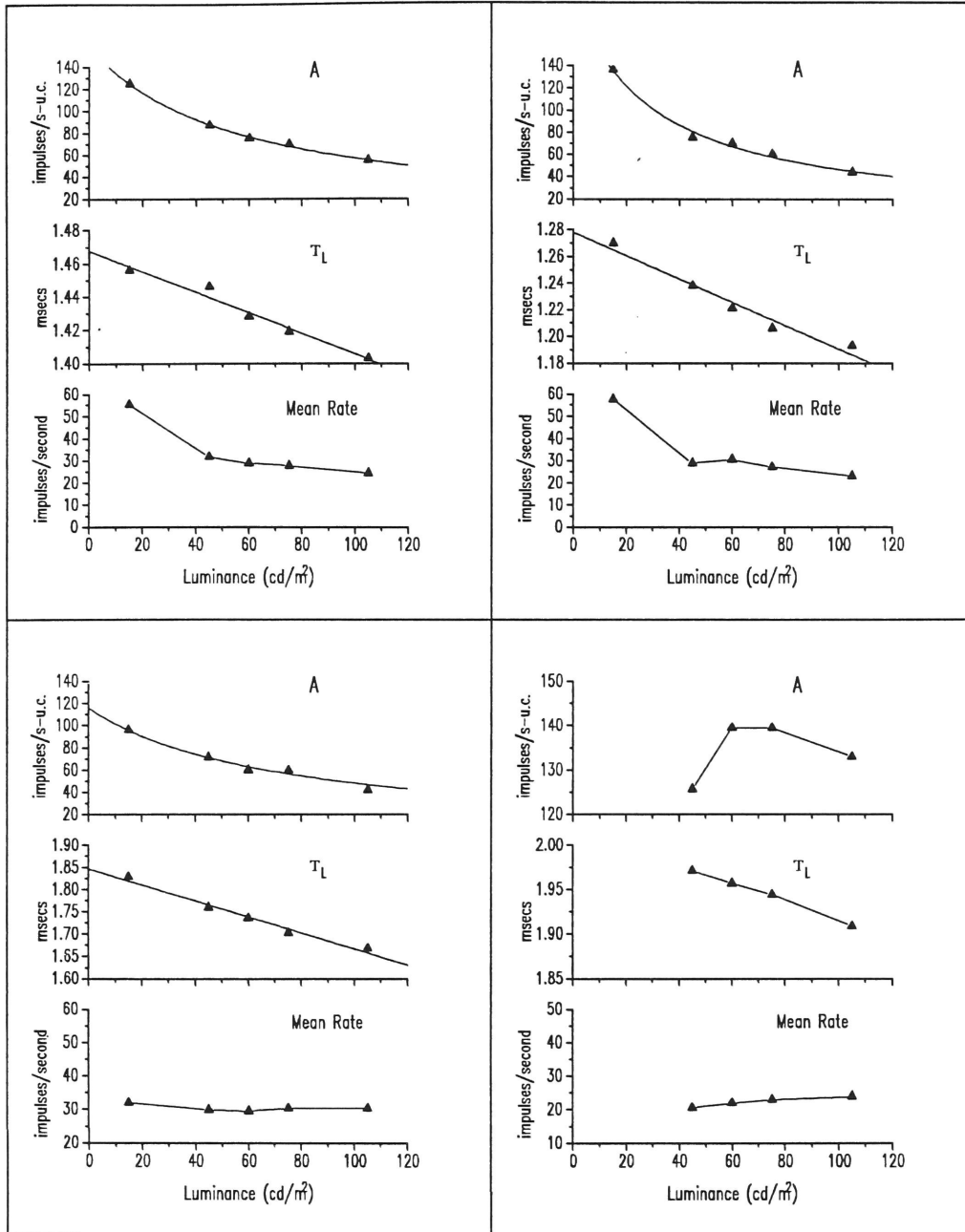


Figure 4-35. The variation of the gain, A , τ_L , and the mean rate, M , with increasing surround illumination for 3 P ON cells (unit 45/30: top left; 43/27: top right; 43/25: bottom left) and 1 P OFF cell (unit 43/20: bottom right). Notice that for the P ON cells, the gain, A , follows a hyperbolic course while the time constant, τ_L , decreases linearly with surround illumination. For each ON cell, Eq. (4-1) was fit to the parameter, A , and a regression line was fit to τ_L . The fits are shown as solid lines. For Eq. 4-1, the parameters are: unit 45/30: A : 149.90 impulses/s-unit contrast; k : $0.017 (\text{cd/m}^2)^{-1}$. unit 43/27: A : 193.93 impulses/s-unit contrast; k : $0.034 (\text{cd/m}^2)^{-1}$; unit 43/25: A : 109.73 impulses/s-unit contrast; k : $0.014 (\text{cd/m}^2)^{-1}$. For the regression lines, the parameters are: Unit 45/30: intercept: 1.47 ms; slope: $-0.0062 \text{ ms}/(\text{cd/m}^2)$. Unit 43/27: intercept: 1.28 ms; slope: $-0.0088 \text{ ms}/(\text{cd/m}^2)$. Unit 43/25: intercept: 1.85 ms; slope: $-0.018 \text{ ms}/(\text{cd/m}^2)$.

Table 4-6. Parameters Fit for 8 P ON Cells to Eq. (4-1) and a Regression Line for τ_L

$N_{RG} = 8$

Parameter	Minimum	Maximum	Median	Mean	S.D.	C.V.
A_{max} (impulses/(s-u.c.))	32.84	193.93	88.18	99.30	51.71	0.52
k (cd/m ²) ⁻¹ x 10 ⁻³	5.52	33.99	16.08	17.87	9.17	0.51
τ_L slope (ms/(cd/m ²)) x 10 ⁻³	-34.43	-6.02	-11.82	-13.89	9.11	-0.66
τ_L intercept (ms) x 10 ¹	9.35	22.60	13.85	14.79	4.13	0.28

4.8 Surround Effect in M cells

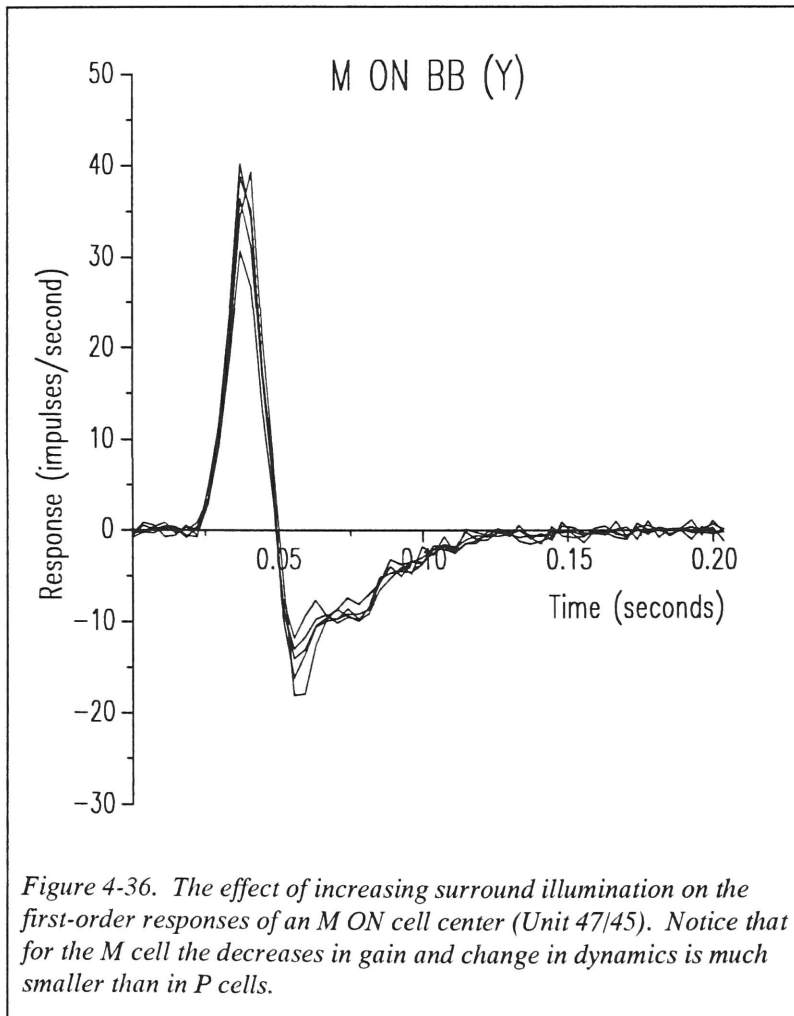
The same nonlinear effect of the surround was investigated in a few M cells (3) as

a preliminary study.

Previous work by Kaplan and Shapley (1989) suggested that M cells show a weak effect of surround illumination on center dynamics or completely lack this effect.

The data shown in Fig. 4-36 confirm this idea. The

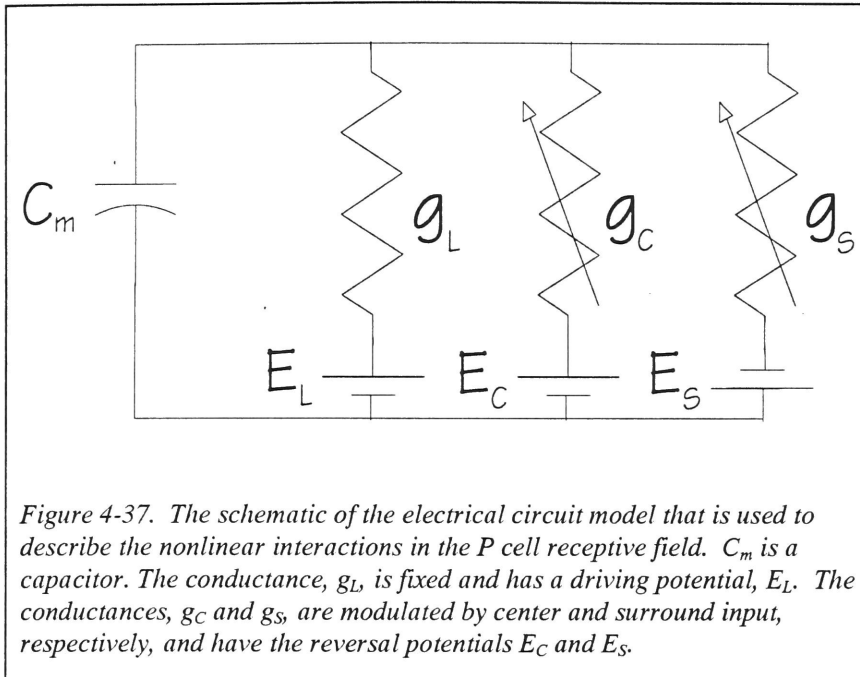
figure shows the first-order responses due to modulation of a central spot (0.25 deg) at five



levels of surround illumination as above. The first-order responses are all plotted and can be seen to show no dramatic changes in gain and time course unlike the P cells. The peak of one response can be seen to fall slightly below that of the others. This is the peak of the response at the highest level of surround illumination. The slight reduction in gain here may be due to a small variation like the P cell surround effect discussed above although there is no apparent change in dynamics. More likely, this effect is due to some scattered light from the bright surround perhaps slightly reducing the contrast of the spot in the large M (Y) cell receptive field.

4.9 Circuit Model of the Nonlinear Surround Effect

The above effect of a reduction in gain of the center accompanied by a decrease in the time constant, τ_L , suggested a possible biophysical model for the interaction of center and surround signals (Koch and Poggio, 1992; Borg-Graham and Grzywacz, 1992). Figure 4-38 depicts the equivalent circuit for a hypothetical mechanism in the P cell where center and surround signals are combined.



The circuit has a capacitor, C_m . There are three conductances: g_L , g_C , and g_S , each of which can be thought of as controlling an ionic current, the equilibrium

potential of which is represented by the batteries E_L , E_C , and E_S . In this development, the conductances g_C and g_S will be assumed to be modulated by a signal coming from the center and surround, respectively. For this model, we will show that as the level of surround illumination increases, the gain of the center first-order Volterra kernel decreases and that the time constant of the center kernel decreases. Also, the second-order kernels for this model will be evaluated to see how they compare with those measured.

4.10 Mathematical Development of the Circuit Model

First, it is necessary to write down a differential equation for the voltage, V , across the capacitor C_m . This voltage, $V(t)$, will represent the output of model; the membrane voltage of a neuron typically controls its output. It is not unreasonable to suppose that such a voltage might control the release of transmitter from an interneuron or spike

generation by a retinal ganglion cell. By analyzing the current flowing in the circuit, the differential equation describing the circuit is determined to be:

$$C_m \frac{dV(t)}{dt} = g_L(t) \cdot (E_L - V(t)) + g_C(t) \cdot (E_C - V(t)) + g_S(t) \cdot (E_S - V(t)) \quad (4-2)$$

Now, we can take a variational approach (Barrett, 1963) to solve for the zeroth-, first-, and second-order responses, V_0 , $V_1(t)$, and $V_2(t)$, of this system. Let

$$V = V_0 + \epsilon V_1(t) + \epsilon^2 V_2(t) + \dots \quad (4-3)$$

$$g_L(t) = \bar{g}_L \quad (4-4)$$

$$g_C(t) = \bar{g}_C + \epsilon \hat{g}_C(t) \quad (4-5)$$

$$g_S(t) = \bar{g}_S + \epsilon \hat{g}_S(t) \quad (4-6)$$

where ϵ is a small parameter. Notice that the conductance, g_L , maintains a steady value, \bar{g}_L , while the center, $g_C(t)$, and the surround, $g_S(t)$, conductances have a variation, $\hat{g}_C(t)$ and $\hat{g}_S(t)$, around a mean level, \bar{g}_C and \bar{g}_S , respectively. Thus, the conductances, $g_C(t)$ and $g_S(t)$, are time-varying. Obviously, the variation of these conductances is assumed to be dependent on the light falling in the center and surround regions, $I_C(t)$ and $I_S(t)$, respectively. For now, that dependence will be left implicit. Next, we can solve for the Volterra kernels by substituting Eqs. (4-3) - (4-6) into Eq. (4-2) and equating powers of ϵ :

$$\begin{aligned} C_m \frac{d(V_0 + \epsilon V_1 + \epsilon^2 V_2 + \dots)}{dt} &= \bar{g}_L \cdot (E_L - V_0 + \epsilon V_1 + \epsilon^2 V_2 + \dots) \\ &+ (\bar{g}_C + \epsilon \hat{g}_C) \cdot (E_C - V_0 + \epsilon V_1 + \epsilon^2 V_2 + \dots) + (\bar{g}_S + \epsilon \hat{g}_S) \cdot (E_S - V_0 + \epsilon V_1 + \epsilon^2 V_2 + \dots) \end{aligned} \quad (4-7)$$

4.10.1 Zeroth-Order Kernel

To calculate the zeroth-order kernel, K_0 , we equate powers of ϵ^0 on either side of Eq. (4-7):

$$0 = \bar{g}_L \cdot (E_L - V_0) + \bar{g}_C \cdot (E_C - V_0) + \bar{g}_S \cdot (E_S - V_0) \quad (4-8)$$

Thus,

$$V_0 = \frac{\bar{g}_L E_L + \bar{g}_C E_C + \bar{g}_S E_S}{\bar{g}_L + \bar{g}_C + \bar{g}_S} \quad (4-9)$$

The expression for V_0 is also the zeroth-order Volterra kernel, K_0 , and is the familiar expression, known to electrophysiologists, which defines the mean voltage in many membrane models (Kandel and Schwartz, 1985).

4.10.2 First-Order Kernels

Equating ϵ^1 on both sides of Eq. 4-7 leads to:

$$C_m \frac{dV_1}{dt} = -\bar{g}_L V_1 - \bar{g}_C V - \bar{g}_S V + \hat{g}_C (E_C - V_0) + \hat{g}_S (E_S - V_0) \quad (4-10)$$

Separating terms in V_1 , we find that

$$\frac{dV_1}{dt} + \frac{(\bar{g}_L + \bar{g}_C + \bar{g}_S)}{C_m} V_1 = \hat{g}_C \frac{(E_C - V_0)}{C_m} + \hat{g}_S \frac{(E_S - V_0)}{C_m} \quad (4-11)$$

Equation (4-11) is a first-order ordinary differential equation. Notice that the voltage on the left side, V_1 , is driven by two signals, one from the center, \hat{g}_C , and one from the surround, \hat{g}_S . Let

$$\lambda = \frac{\bar{g}_L + \bar{g}_C + \bar{g}_S}{C_m} \quad (4-12)$$

λ is the eigenvalue of the homogeneous equation. Furthermore, to see the general structure of the solution, for now, set $B(t)$ equal to the right side of Eq. (4-11). The solution of equation then takes the form (Hirsch and Smale, 1974):

$$V_1(t) = \int_0^\infty e^{-\lambda\tau} B(t - \tau) d\tau \quad (4-13)$$

Substituting for $B(t)$, the two first-order kernels, one for the center input and one for the surround input, are:

$$K_{1,\hat{g}_C}(t) = \frac{(E_C - V_0)}{C_m} \exp\left(-\left(\frac{\bar{g}_L + \bar{g}_C + \bar{g}_S}{C_m}\right)t\right) \quad (4-14)$$

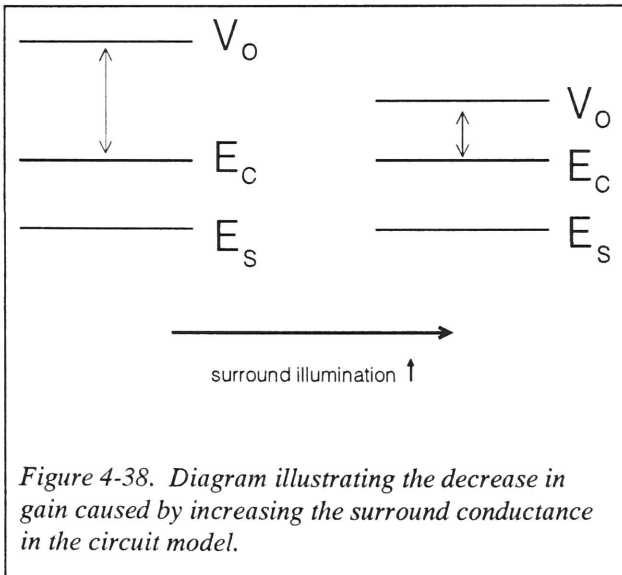
$$K_{1,\hat{g}_S}(t) = \frac{(E_S - V_0)}{C_m} \exp\left(-\left(\frac{\bar{g}_L + \bar{g}_C + \bar{g}_S}{C_m}\right)t\right) \quad (4-15)$$

These first-order kernels deserve a brief comment. First, notice that the gain of the kernel is set by the term $\frac{(E_C - V_0)}{C_m}$ for the center kernel and $\frac{(E_S - V_0)}{C_m}$ for the surround kernel. Thus, the mean level, V_0 , adjusts the gain.

To better understand this relationship, we have to explicitly state the relationship between the illumination on center and surround and the changes in these conductances. For example, let A_C represent the gain of the center first-order kernel, then

$$A_c = \frac{(E_c - E_L)\bar{g}_L + (E_c - E_s)\bar{g}_s}{C_m(\bar{g}_L + \bar{g}_c + \bar{g}_s)} \quad (4-16)$$

Consider, for example, that increased surround illumination increases the surround conductance \bar{g}_s and that the equilibrium potential of the surround conductance is more negative than the resting potential, V_0 . Likewise let the center conductance be decreased by the illumination of the center and the equilibrium potential of this mechanism be intermediate between V_0 and E_s . Figure 4-38 shows how increasing the surround conductance will decrease the gain of the center mechanism by bringing V_0 closer to E_c . Over a broad range of parameters, the gain of the first-order kernel shows a hyperbolic relationship with increasing surround illumination exactly as shown in the data for ON cells. For OFF cells, a different set of equilibrium potentials and conductances will increase the gain of the center when the surround is illuminated.



Notice that the time constant of the kernel, $\frac{(\bar{g}_L + \bar{g}_c + \bar{g}_s)}{C_m}$, is also affected by the mean level of the conductances. In the linear filter model, the time constant of the low-pass stages, τ_L , represents the product of a resistance (the inverse of

conductance) and a capacitance. Increasing the surround conductance will decrease this time constant in the model as shown in the data.

4.10.3 Second-Order Kernels

By equating the terms in ϵ^2 , the second-order kernel is obtained:

$$\frac{dV_2}{dt} + \left(\frac{\bar{g}_L + \bar{g}_C + \bar{g}_S}{C_m} \right) V_2 = -\frac{\hat{g}_C}{C_m} V_1 - \frac{\hat{g}_S}{C_m} V_1 \quad (4-17)$$

Again, let $\lambda = \frac{\bar{g}_L + \bar{g}_C + \bar{g}_S}{C_m}$, then the solution for $V_2(t)$ is:

$$V_2(t) = \int_0^\infty e^{-\lambda\tau} \left(\frac{-\hat{g}_C(t-\tau) - \hat{g}_S(t-\tau)}{C_m} \right) V_1(t-\tau) d\tau \quad (4-18)$$

Substituting for V_1 leads to an expression for the three second-order kernels.

The second-order center kernel is:

$$K_{2, \hat{g}_C, \hat{g}_C}(t_1, t_2) = -\frac{(E_C - V_0)}{C_m^2} \frac{e^{-\lambda t_1} e^{-\lambda t_2}}{2} \quad (4-19)$$

The second-order surround kernel is:

$$K_{2, \hat{g}_S, \hat{g}_S}(t_1, t_2) = -\frac{(E_S - V_0)}{C_m^2} \frac{e^{-\lambda t_1} e^{-\lambda t_2}}{2} \quad (4-20)$$

Since the second-order center-surround cross-kernel is not symmetric, it has a slightly more complex expression:

$$K_{2, \hat{g}_C, \hat{g}_S}(t_1, t_2) = -\frac{(E_S - V_0)}{C_m^2} e^{-\lambda t_1} e^{-\lambda t_2}, \quad t_1 > t_2 \quad (4-21)$$

$$K_{2, \hat{g}_S, \hat{g}_C}(t_1, t_2) = -\frac{(E_C - V_0)}{C_m^2} e^{-\lambda t_1} e^{-\lambda t_2}, \quad t_1 > t_2 \quad (4-22)$$

For these cross-kernels, $K_{2,\hat{g}_c,\hat{g}_s}$ and $K_{2,\hat{g}_s,\hat{g}_c}$, the subscripts of the kernels indicate the

signals that are interacting. The first signal in the subscript (e.g. \hat{g}_c in Eq. (4-21)) has t_1 as its associated time, and t_2 is the time of the second signal in the subscript.

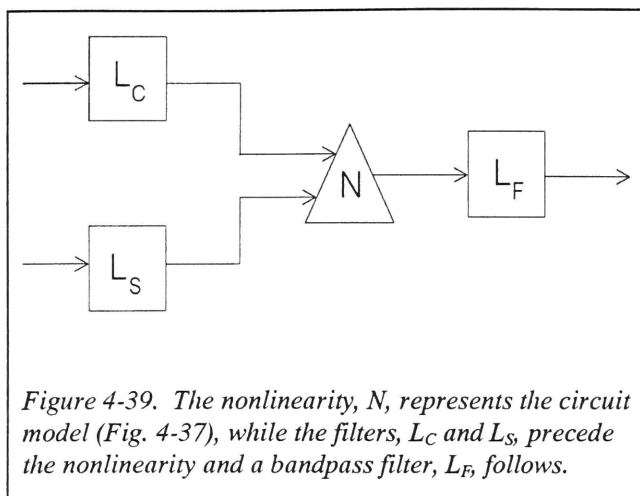
4.11 The Relationship of the Kernels to the Model Fits

The kernels derived above can be simply related to the linear filter model and the LNL model that were fit to the m-sequence data above. The first-order kernels of the circuit model show how the gain and the time constant will change with surround illumination. The linear filter model can be thought of as appending some additional low-pass stages and a subtractive high-pass stage to this nonlinearity. For example, for the center kernel, let the center conductance be modulated by the illumination of the center filtered by a series of linear stages:

$$\hat{g}_c(t) = L_c(t) * I_c(t)$$

where $L_c(t)$ is a series of filter stages and $I_c(t)$ is illumination of the center, and the symbol “*” stands for convolution (as in the integral of Eq. (4-13)). This signal, \hat{g}_c , enters the nonlinear stage in the circuit model where the gain and the time constant of this stage can be modulated. The subtractive stage may occur after this stage, or may be distributed before and after the nonlinearity.

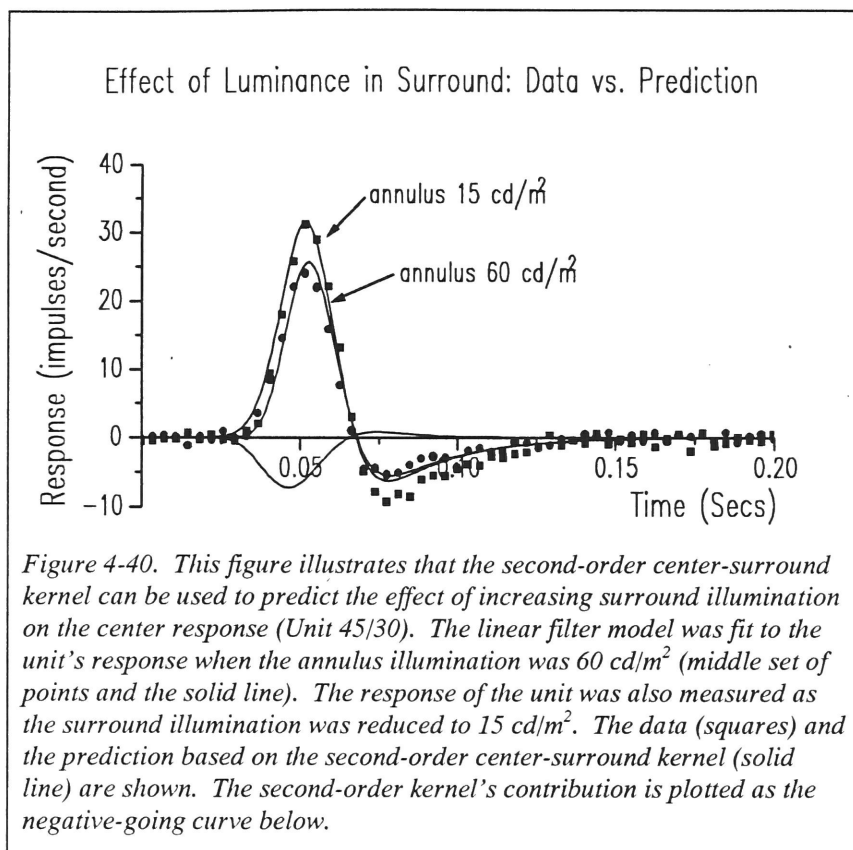
Similarly for the second-order kernels, the signals from the center and the surround are first linearly filtered then enter the nonlinear circuit. The output of the nonlinear stage then enters another linear stage as illustrated in Fig. 4-39.



4.12 Kernel Predictions

Figure 4-40 demonstrates that the center-surround cross-kernel can predict the results of the effect of surround illumination on center gain and dynamics further supporting the idea that the results from the two

experimental paradigms reflect the same underlying nonlinearity. The response of the unit was measured at all 5 levels of surround illumination. The response at 60 cd/m^2 of surround illumination was fit to the linear filter model. The fit to the second-order center-surround kernel was used to predict the response at a surround illumination level of 15 cd/m^2 by calculating the response of the second-order kernel fit to steady illumination in the surround and an impulse in the center. For low levels of surround illumination, the agreement is good; however, the prediction is not as good for high levels of surround illumination (not shown). This discrepancy probably reflects at least two effects. First, the second-order kernel is just a first approximation to the center-surround nonlinearity which actually shows a hyperbolic relationship with surround illumination. Second, the very low frequencies are not well represented in the m-sequence kernel and these low frequency values provide the best predictions of the effect of the steady surround on the center.



4.13 Summary

This chapter explored the linear and nonlinear dynamics of P cells using the multiple m-sequence technique. These results can be summarized as follows:

1. The first-order responses of the center and surround of P cells show similar dynamics except for a delay associated with the surround response.
2. When isolated with small spots and annuli, the size of the center and surround responses of the P cell show a linear relationship with increasing contrast. The gain and dynamics of the first-order response are not changed by white-noise-type modulation in the opposing subregion suggesting that the major nonlinear interaction must involve the signed contrast in the other region.

3. Using the m-sequence technique, clear and reproducible second-order responses can be obtained from the center and surround regions of the P cell receptive field. There is also a significant multiplicative interaction between the center and surround evident in the center-surround second-order response.

4. Steady illumination of the surround of P cells changes the gain and dynamics of the center region. With increasing surround illumination, P ON cells show a characteristic decrease in gain and a shortening of time course that is well described by the variation of only two parameters in the five parameter linear filter model. P OFF cells show an increase in gain with increasing surround illumination accompanied by a shortened time course.

5. The data from these experiments suggested an electrical circuit model the design of which was strongly influenced by biophysical reality. The behavior of the model mimics that shown by real P cells, and links the kernel data together with the nonlinear effects. Furthermore, the kernel data can be used to predict the general effect of surround illumination on center dynamics in P cells.

P Cell Responses to Chromatic and Achromatic Stimuli

Introduction

Responses to Chromatic and Achromatic Gratings

Frequency Responses

Comparison with M Cell Chromatic and Achromatic Responses

Model Fits

M vs. P Comparison

Prediction of P Cell Chromatic and Achromatic Responses

Nonlinear Responses

Spatiotemporal Responses

Summary

5. P Cell Responses to Chromatic and Achromatic Stimuli

5.1 Introduction

One of the most interesting features of P cells is their color opponency. The anatomical basis for this effect is still incompletely understood. It is clear that midget bipolars conduct the signal from a single cone to a midget ganglion cell near the fovea. This relationship can account for the chromatic specificity of the center mechanism, but the P cell surround also seems to carry the signature of a single cone type (e.g. Reid and Shapley, 1992). The question remains, how is the surround generated given that horizontal cells make connections to a mixture of cone types (Boycott *et al.*, 1987; Dacheux and Raviola, 1990)?

The science of color vision (Boynton, 1992) depends greatly on the linearity that human subjects display when making judgments about color. Presumably, as the functional correlates of precortical color processing, P cells should display the same linearity in response to color mixtures. To better understand the functional role and organization of P cells, the dynamics of their responses to chromatic and achromatic gratings were studied. The dynamics can answer some of these outstanding questions about P cell organization and function. The results of this chapter show that the responses of P cells to chromatic gratings that selectively stimulate either the center or surround are very similar except for an opposite signature and a slight delay, suggesting that two

opponent signals may share a common anatomical substrate (e.g. bipolars). Furthermore, the basic linearity of combination of cone signals found by other workers is confirmed (e.g. Gielen *et al.*, 1982), but only for weak chromatic stimuli.

In detail, this chapter discusses experiments that were done to explore the responses of P cells to chromatic and achromatic stimuli using sine gratings modulated by the multiple m-sequence signal (Benardete *et al.*, 1992c). A comparison is also made between the P cell response to these stimuli and the M cell responses to similar stimuli. P cell responses to cone-isolating gratings are also used to try to predict the response to other chromatic and achromatic gratings as a basic test of P cell linearity. Finally, using an entirely different stimulus, drifting gratings, the basic results about the P cell center and surround are confirmed.

5.2 Responses to Chromatic and Achromatic Gratings

Since the work of DeValois *et al.* (1966), LGN cells in the parvocellular layers have been known to produce chromatically opponent responses. P retinal ganglion cells are also chromatically opponent. For example, a P ON cell might produce ON responses to a long wavelength (red) stimulus and OFF responses to a middle wavelength (green) stimulus. Using the multiple m-sequence method and cone-isolating gratings, it was possible to elicit from a P cell the first- and second-order responses to two chromatic and/or achromatic gratings simultaneously. From the response to a single ambient stimulus, this method provided a means to directly compare the dynamics of P cells' responses to these two classes of stimuli. Figures 5-1 - 5-7 show typical results for 2 P ON cells and 2 P OFF cells.

The responses of a P ON R-G+ cell to low spatial frequency gratings (0.145 c/d) of several types are shown in Fig. 5-1. In the far left column, the first-order responses to gratings that selectively stimulate L cones and M cones are shown. (These are cone-isolating gratings as described in Chapter 2). Notice that, for this cell, the L cone and M cone responses are of opposite signature i.e. opponent. These two first-order responses were calculated from the response to a single stimulus, namely a multiple m-sequence signal modulating two gratings, one L cone- and one M cone-isolating. Notice that the time course of the L cone response is delayed in comparison with that of the M cone response.

The middle column shows the responses of the same cell to an isoluminant (L-M) grating (top) and an L cone and an M cone mixture (L+M) stimulus (bottom). Recall that for the L-M stimulus, the luminance of the L cone-isolating and M cone-isolating gratings are set equal and opposite in luminance so that there is only a chromatic signal in this stimulus. This purely chromatic (isoluminant) stimulus produces a slightly more delayed response than the response to the L+M stimulus.

Finally, the last column shows the response of the P cell to a black-white grating. The response here is noticeably more transient than the others.

Figure 5-2 shows the responses of the same cell to higher spatial frequency gratings (2.181 c/d) of the same types. In this series, the relative amplitudes of L and M cone responses have changed. The L cone response has become disproportionately weaker indicating that the L cone mechanism is broader in space. Since the work of Wiesel and Hubel (1966), it has been known that for most parvocellular cells (type I), the color opponent mechanisms of the receptive field are also spatially opponent and adhere to

a center-surround organization. In this cell, the L cone driven mechanism has clear surround spatial characteristics. The M cone driven mechanism which comes from the center has the same signature as the overall response (ON). The second and third columns show that the isoluminant response has become relatively weaker at this higher spatial frequency compared to the L+M or the achromatic response. This loss of chromatic response has been noted before both physiologically and psychophysically (Ingling and Martinez-Uriegas, 1983; Mullen, 1985). The m-sequence analysis makes the reason for this clear. As the response of the L cone driven surround grows weaker at higher spatial frequencies, the responses that rely on the two mechanisms working in synchrony diminish. At this higher spatial frequency, the first-order response to an achromatic grating becomes less transient as a result of less surround antagonism. Figures 5-3 and 5-4 show responses from another P ON (R-G+) cell that demonstrates the same types of relationships.

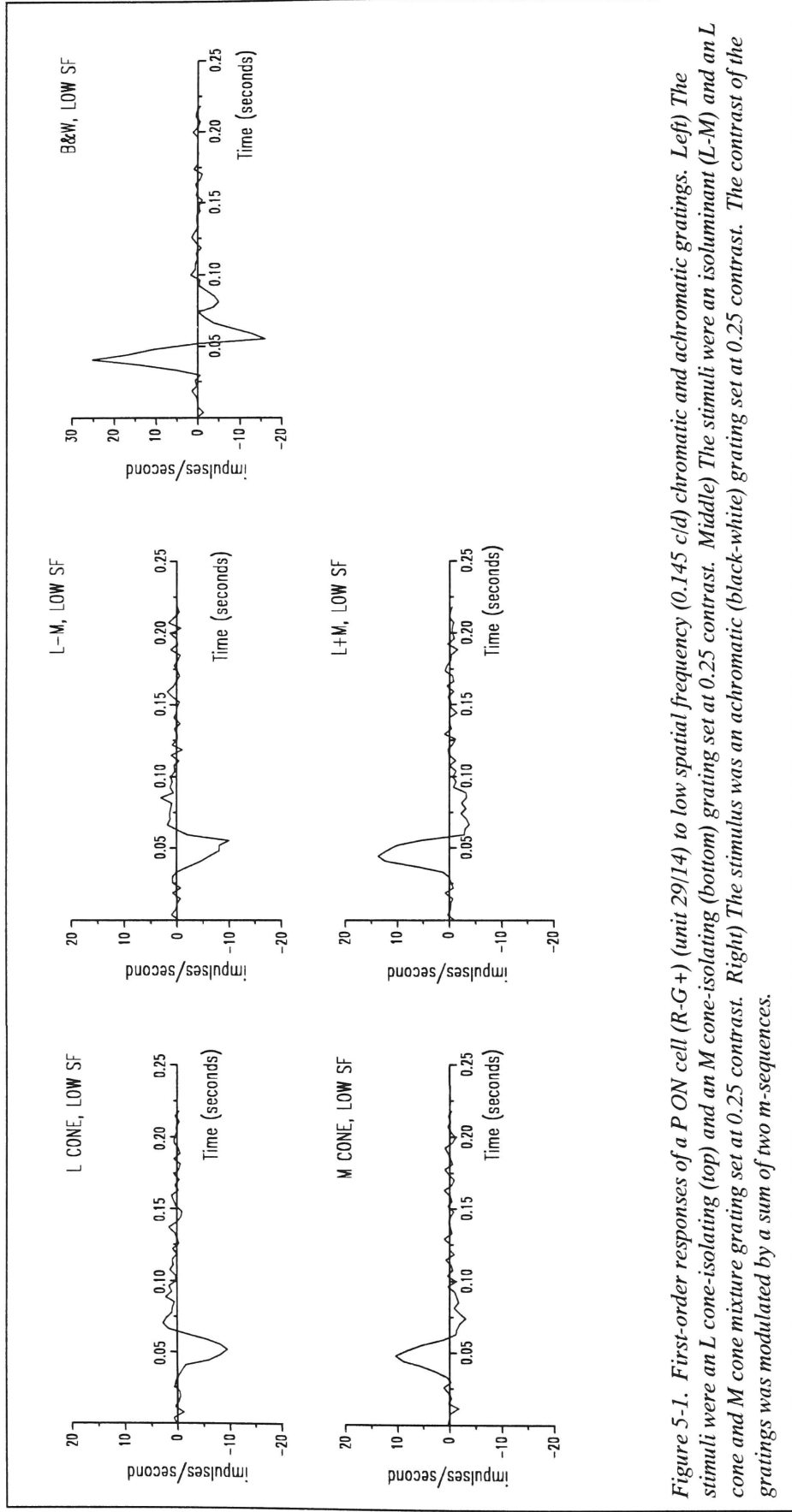


Figure 5-1. First-order responses of a P ON cell (R-G +) (unit 29/14) to low spatial frequency (0.145 c/d) chromatic and achromatic gratings. Left) The stimuli were an L cone-isolating (top) and an M cone-isolating (bottom) grating set at 0.25 contrast. Middle) The stimuli were an isoluminant (L-M) and an L cone and M cone mixture grating set at 0.25 contrast. Right) The stimulus was an achromatic (black-white) grating set at 0.25 contrast. The contrast of the gratings was modulated by a sum of two m-sequences.

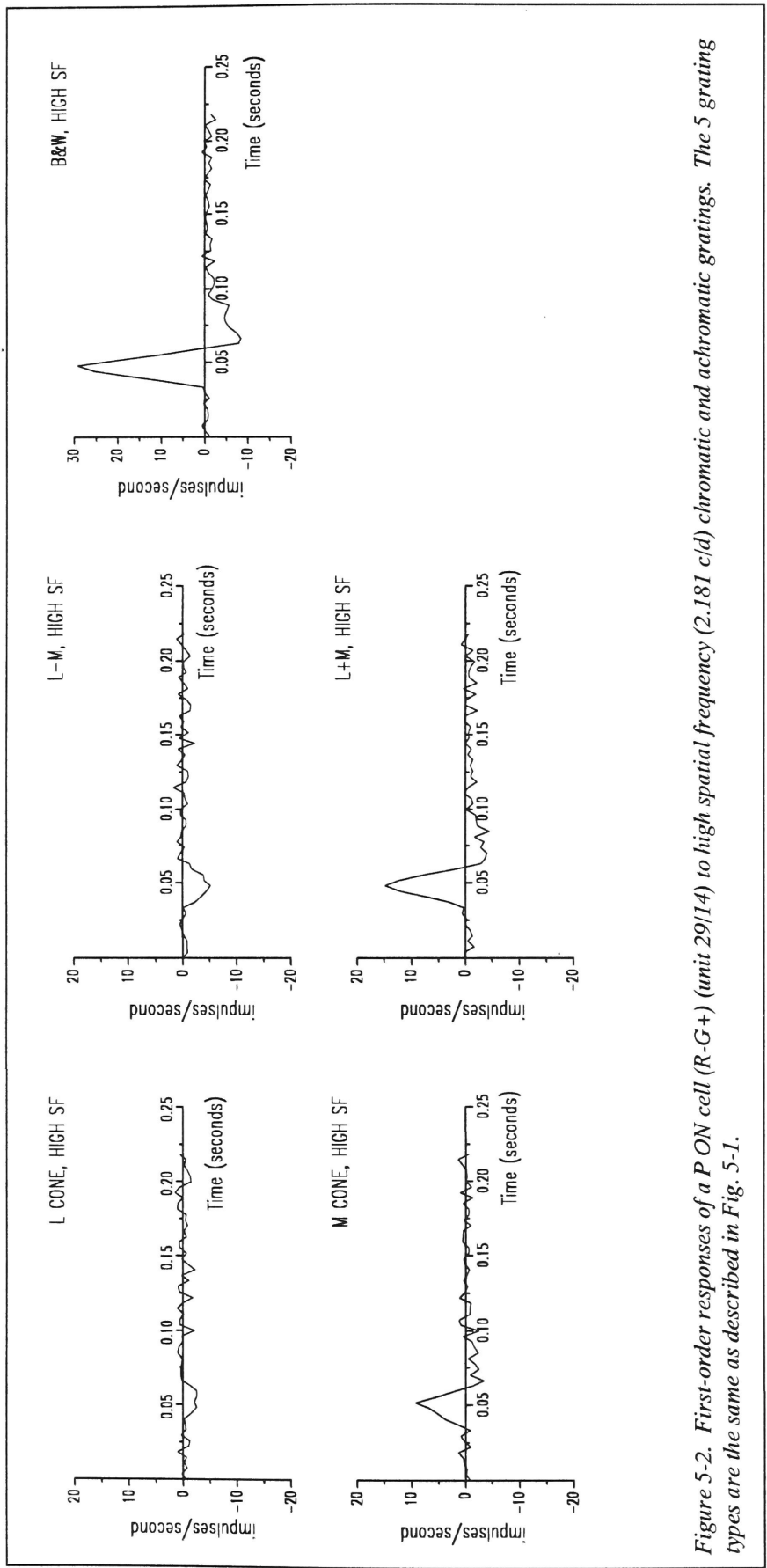


Figure 5-2. First-order responses of a P ON cell (R-G+) (unit 29/14) to high spatial frequency (2.181 c/d) chromatic and achromatic gratings. The 5 grating types are the same as described in Fig. 5-1.

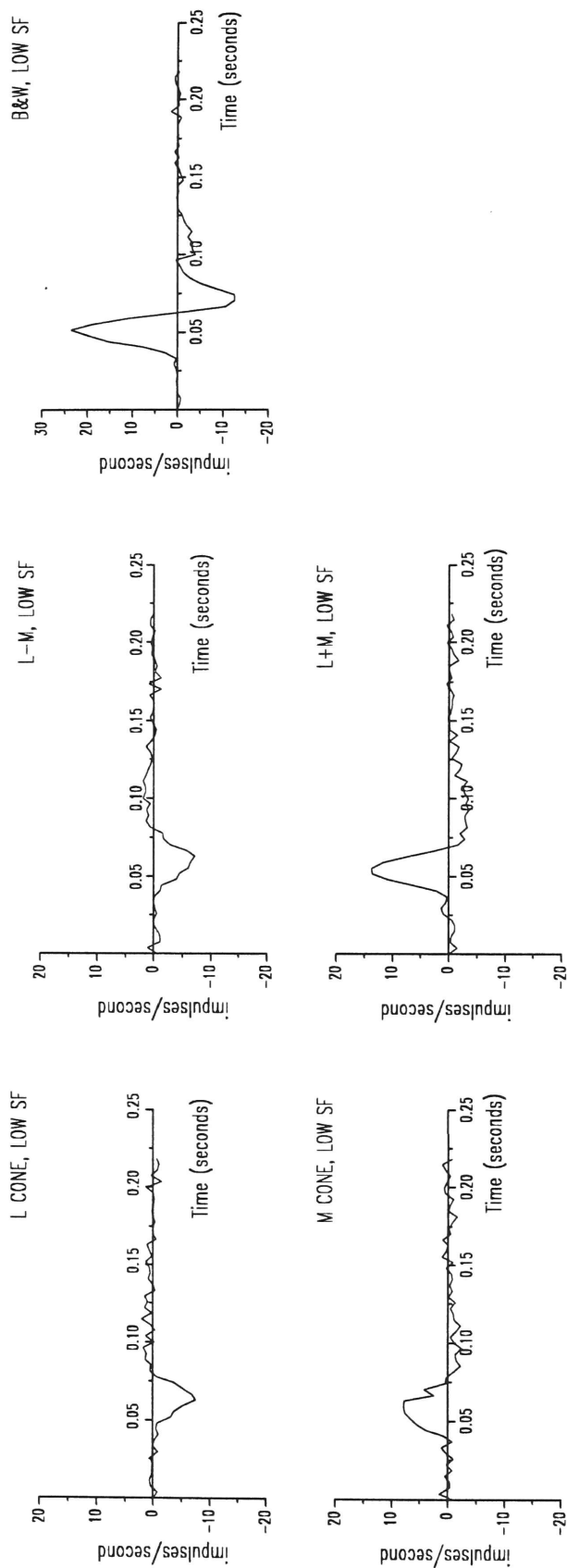


Figure 5-3. First-order responses of a P ON cell (R-G+) (unit 36/7) to low spatial frequency (0.141 c/d) chromatic and achromatic gratings. The stimuli are the same as Fig. 5-1.

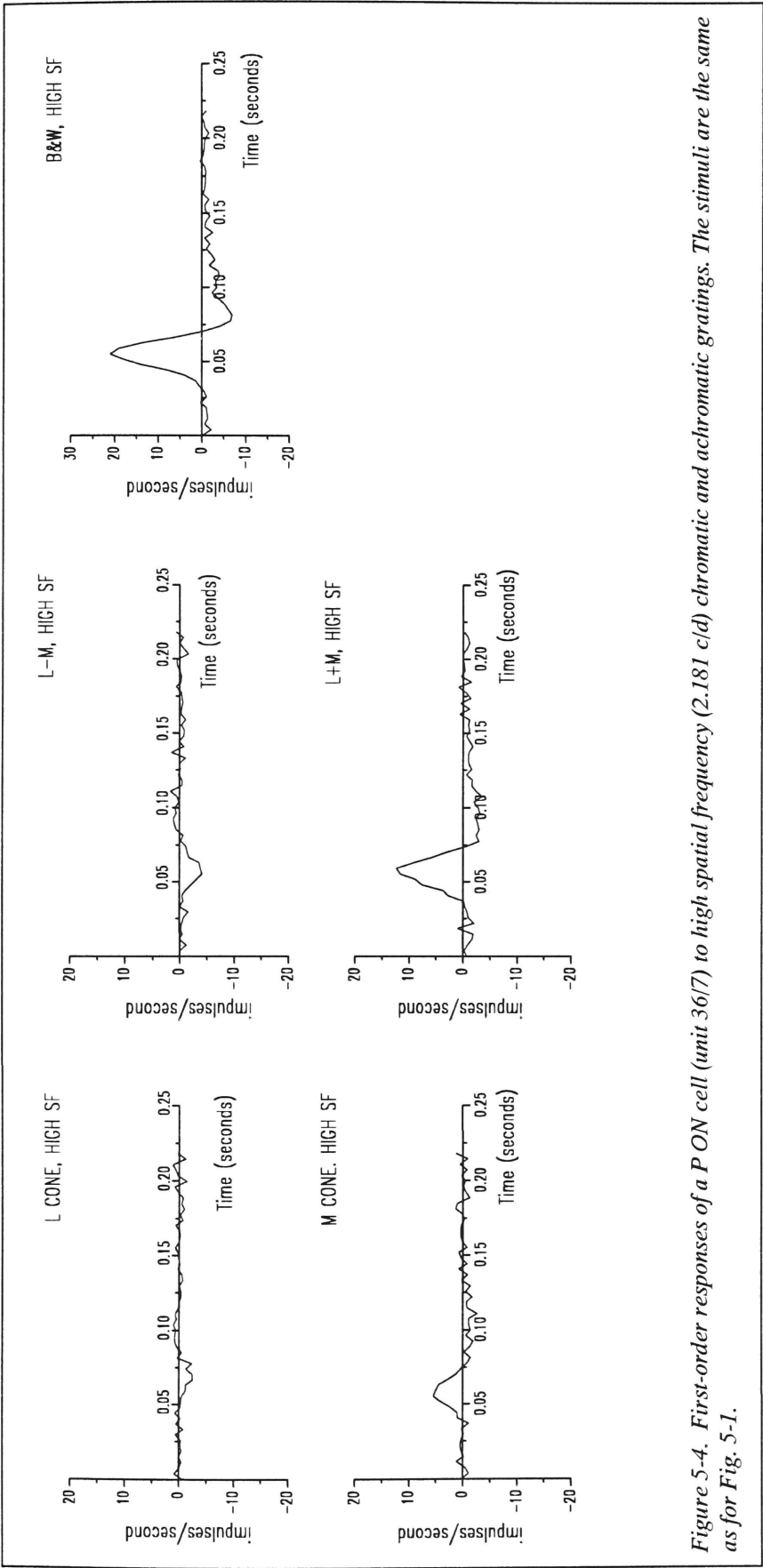


Figure 5-4. First-order responses of a P ON cell (unit 36/7) to high spatial frequency (2.181 c/d) chromatic and achromatic gratings. The stimuli are the same as for Fig. 5-1.

Figure 5-5 shows the low spatial frequency response of a P OFF cell (R+G-). For this cell, the signature of the response to the L cone- and the M cone-isolating stimuli is opposite to that of the two previous ON cells, and the response to the achromatic grating is also inverted. However, the same relationship of the center and the surround responses still holds as the M cone driven center response which carries the sign of the overall response (OFF) slightly precedes the response of the surround. The isoluminant response is also more delayed than that of the achromatic or mixed responses. This cell had very weak high spatial frequency responses (not shown).

Figures 5-6 and 5-7 show the first-order responses of another P OFF cell; however, this one is R-G+. Here, the signature of the L cone response is the same as that of the overall response, and it clearly leads the M cone driven response. At high spatial frequency, all of the chromatic responses are small except for the L cone driven center response and the response to the black-white stimulus remains large.

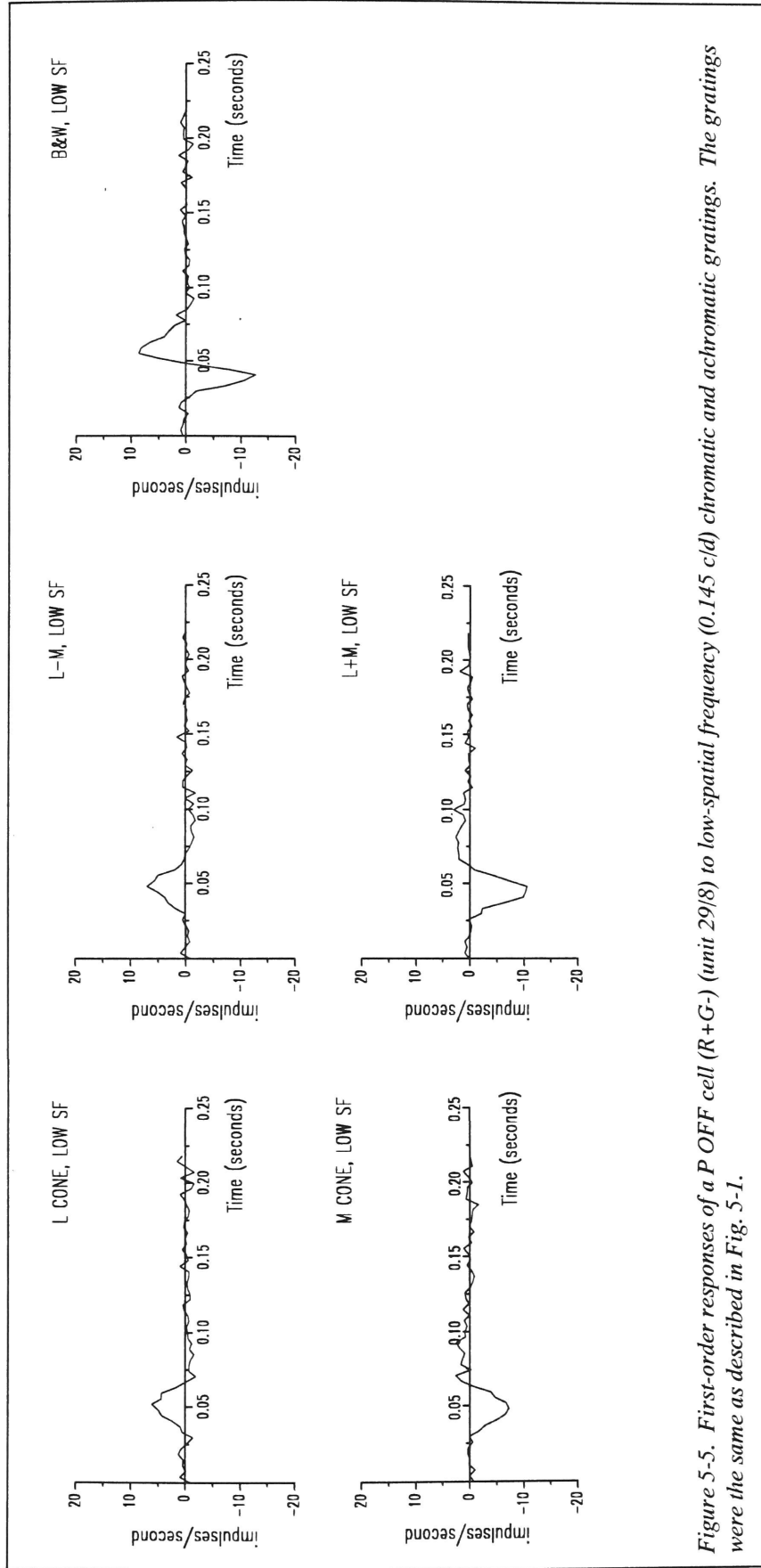


Figure 5-5. First-order responses of a P OFF cell (R+G-) (unit 29/8) to low-spatial frequency (0.145 c/d) chromatic and achromatic gratings. The gratings were the same as described in Fig. 5-1.

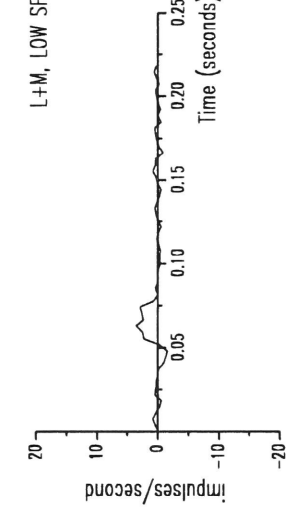
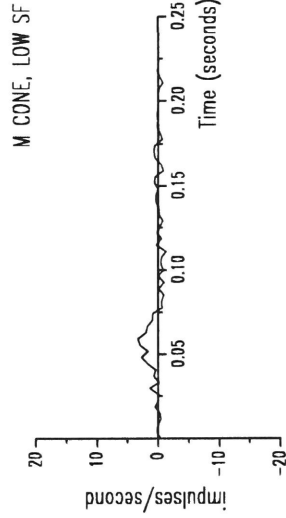
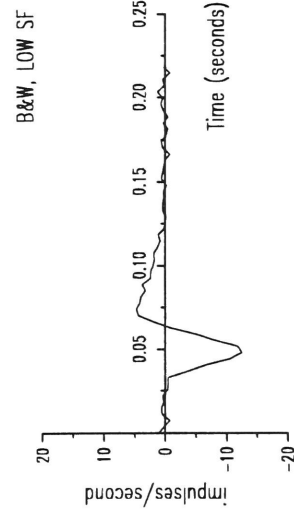
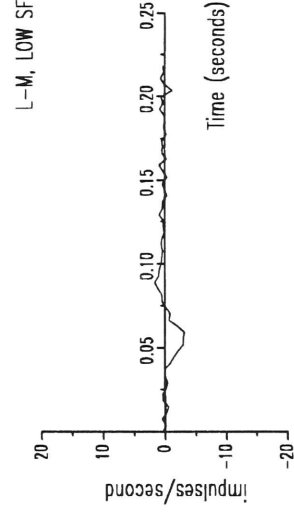
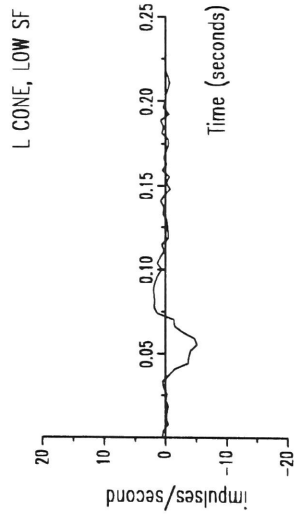


Figure 5-6. First-order responses of a P OFF (R-G+) cell (unit 43/20) to low spatial frequency (0.145 c/d) chromatic and achromatic gratings (see Fig. 5-1).

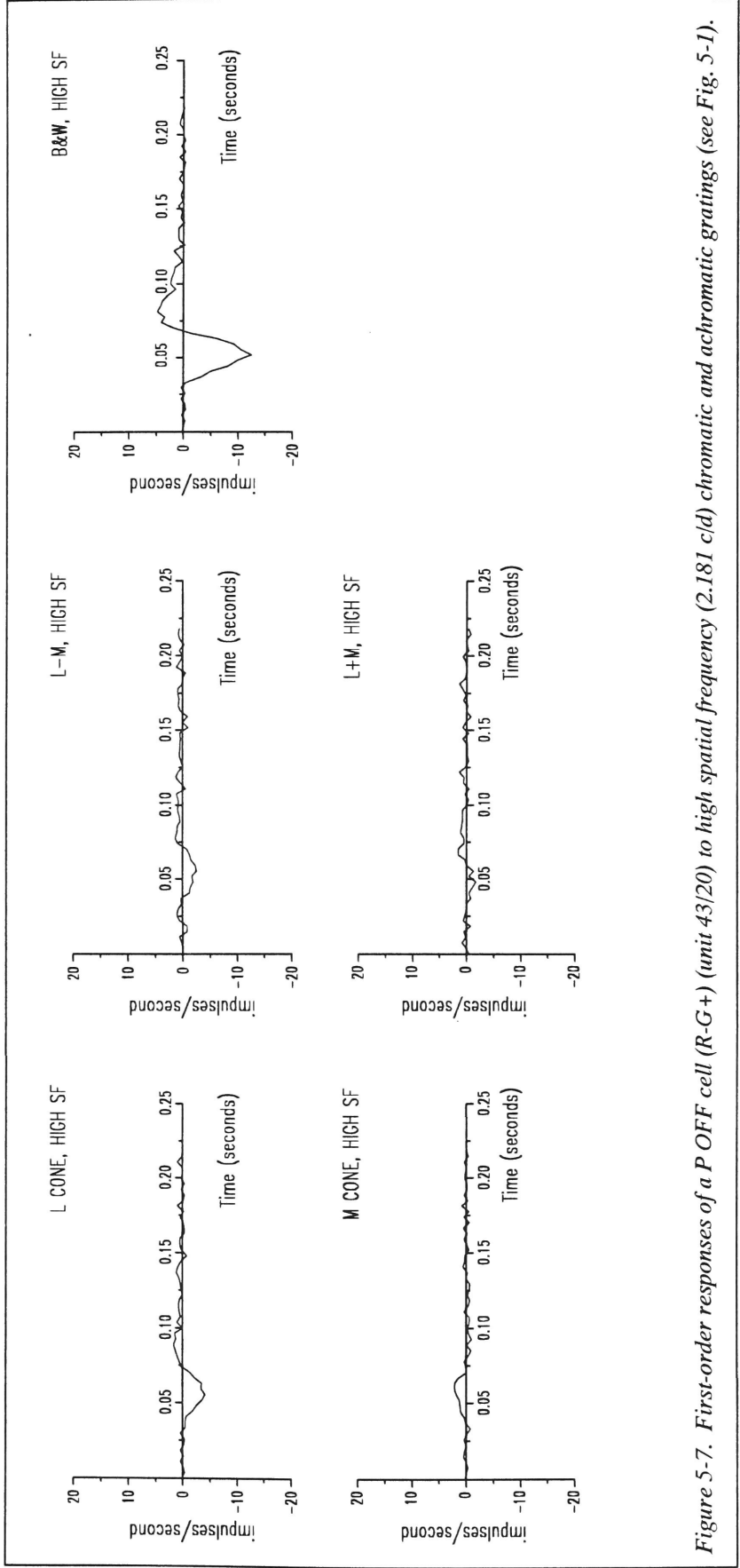


Figure 5-7. First-order responses of a P OFF cell (R-G+) (unit 43/20) to high spatial frequency (2.181 c/d) chromatic and achromatic gratings (see Fig. 5-1).

The basic linearity of a typical P cell's chromatic and achromatic responses is shown in Fig. 5-8. The response to the low spatial frequency L cone-isolating stimulus is shown at three contrasts (0.0625, 0.125, and 0.25), each a two-fold increase. In addition, the responses to both low and high spatial frequency achromatic gratings are shown at the same contrasts. Except for the high spatial frequency black-white stimulus which caused response truncation at the highest contrast, the linearity was nearly exact. This result illustrates again the same linearity of first-order responses that was found in Chapter 4 for spots and annuli.

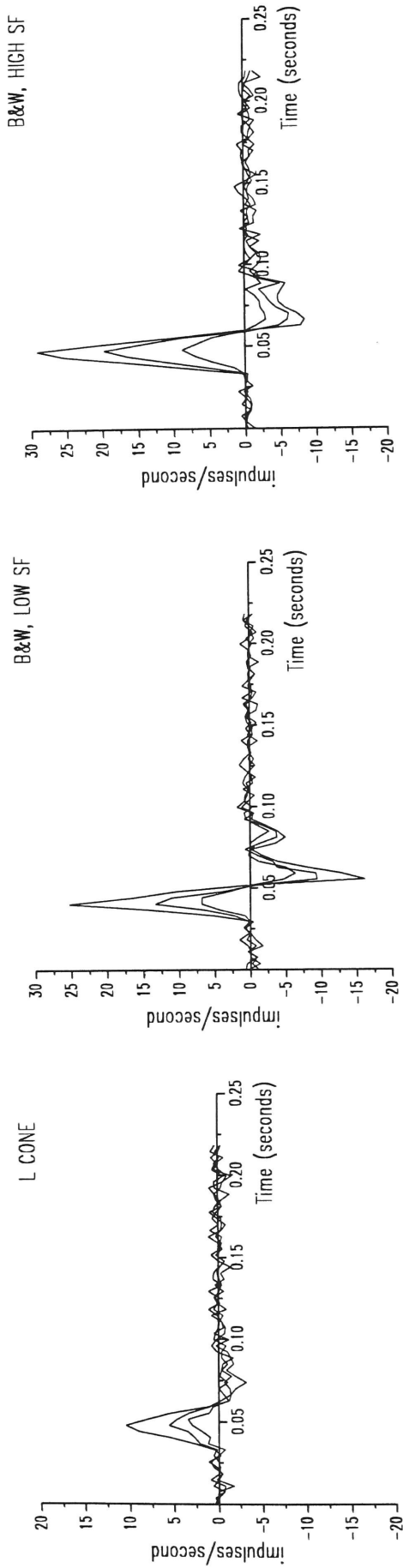


Figure 5-8. The first-order responses of a P ON (R-G+) cell (unit 29/14) to chromatic and achromatic gratings at several contrasts (0.0625, 0.125, 0.25). The chromatic grating was L cone-isolating set 0.145 c/d (left). The achromatic gratings were black-white and set at 0.145 c/d (middle) and 2.181 c/d (right).

5.3 Frequency Responses

The first-order responses of a typical P cell (shown in Figs. 5-1 - 5-2) were transformed into the frequency domain and are shown in Fig. 5-8. The sets of curves in each figure show two levels of contrast (0.125 and 0.25) and emphasize the basic linearity of the response. The upper two panels show the frequency response to 2 chromatic stimuli, L cone- and M cone-isolating gratings. For this R-G+ cell, the response to the L cone-isolating stimulus has an additional phase shift of $-\pi$ radians because of the OFF response to L cone stimulation. The responses to both chromatic stimuli demonstrate a gentle bandpass shape with a peak around 8-12 Hz. The response to the achromatic gratings demonstrates a more bandpass shape with a higher peak temporal frequency. The response to the achromatic stimuli is more transient. However, at high spatial frequencies, this difference becomes less pronounced because the surround antagonism is increasingly diminished since the large surround averages out the bright and dark bars of the grating. The shape of the response amplitude and the phase plots vs. frequency does not change with increased contrast, and this indicates that P cells do not have the contrast gain control phenomenon found in cat retinal ganglion cells and M cells (see Chapter 6).

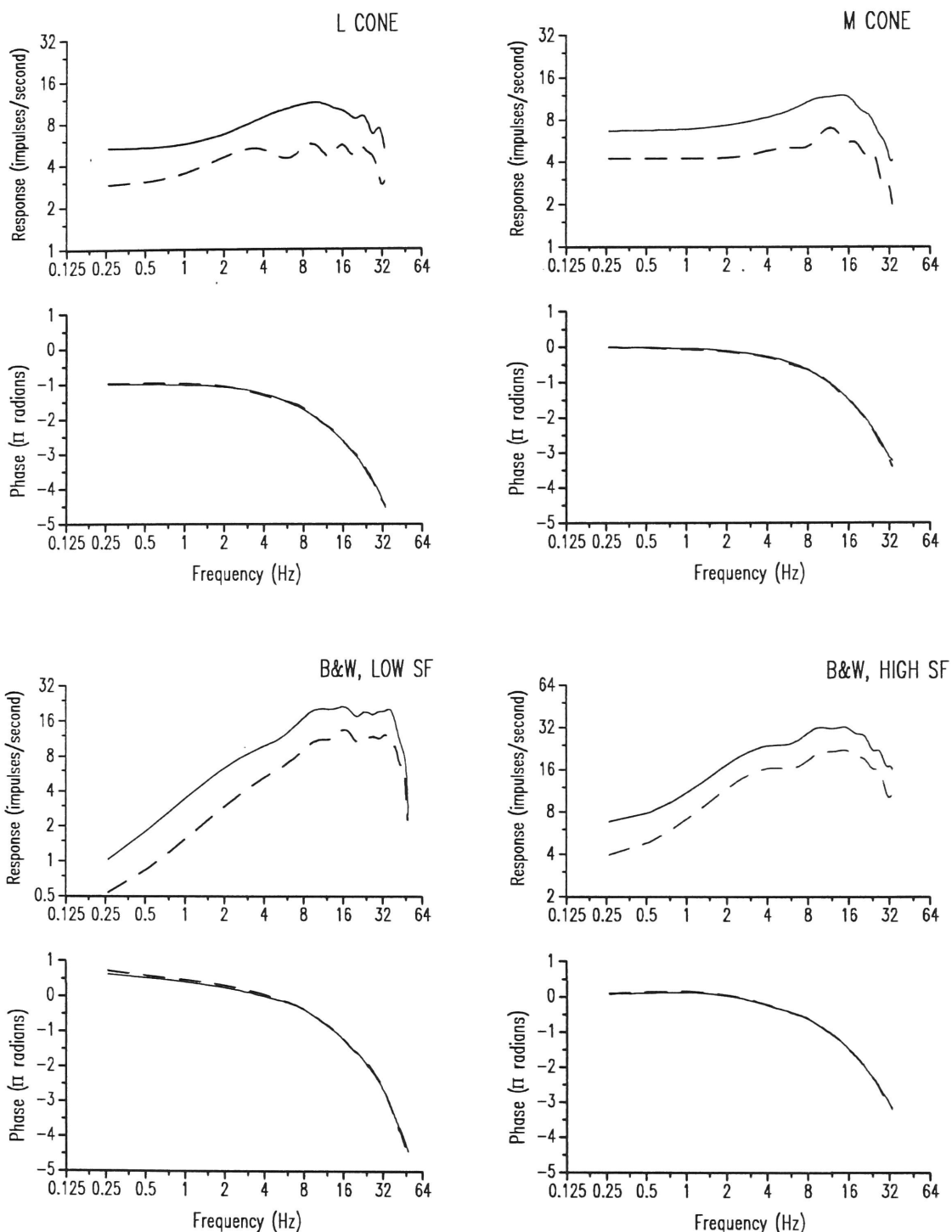


Figure 5-9. The frequency responses of a P ON (R-G+) cell (unit 29/14) derived from Fourier transforming the first-order responses from the multiple m -sequence method. The responses to low spatial frequency (0.141 c/d) L cone-isolating (top, left) and M cone-isolating (top, right) gratings at 0.125 (dashed line) and 0.25 (solid) contrast were Fourier transformed to yield the frequency responses shown. Similarly, the frequency responses to black-white gratings (0.125 and 0.25 contrast; 0.145 c/d (bottom, left) and 2.141 c/d (bottom, right)) are shown.

5.4 Comparison with M Cell Chromatic and Achromatic Responses

In Chapter 6, the responses of M cells to chromatic and achromatic stimuli are discussed in detail. However, at this point, it is appropriate to make a brief comparison between P cell and M cell responses to the same type of stimuli since their different characteristics underlie important visual functions (Kaplan *et al.*, 1990). Figure 5-10 shows the first-order responses of a typical broadband M ON cell. At the far left, first-order responses to the low spatial frequency L cone- and M cone-isolating gratings are shown. Notice that for the M cell, the response to the L cone- and M cone-isolating gratings is not opponent. Consequently, there is no response to the isoluminant grating (middle column, top) while achromatic stimuli (L+M, and black -white low spatial frequency, and black-white high spatial frequency gratings) produce large, phasic responses. The responses to the low spatial frequency black-white gratings are noticeably more phasic than the high spatial frequency response. A comparison of the frequency response of the M cell and the P cell emphasizes these points. Figure 5-11 displays the frequency responses corresponding to the responses in Fig. 5-10. The M cell responses are noticeably more transient than the corresponding P cell responses. The M cell frequency response also tends to peak at a slightly higher temporal frequency. Chapter 6 discusses how the first-order responses of M cells differ from those of P cells in another fundamental way; M cell frequency responses become increasingly bandpass and phase-advanced with higher contrast. This phenomenon which was previously identified in the

cat (Shapley and Victor, 1978) is termed the contrast gain control and is notably absent in P cell responses.

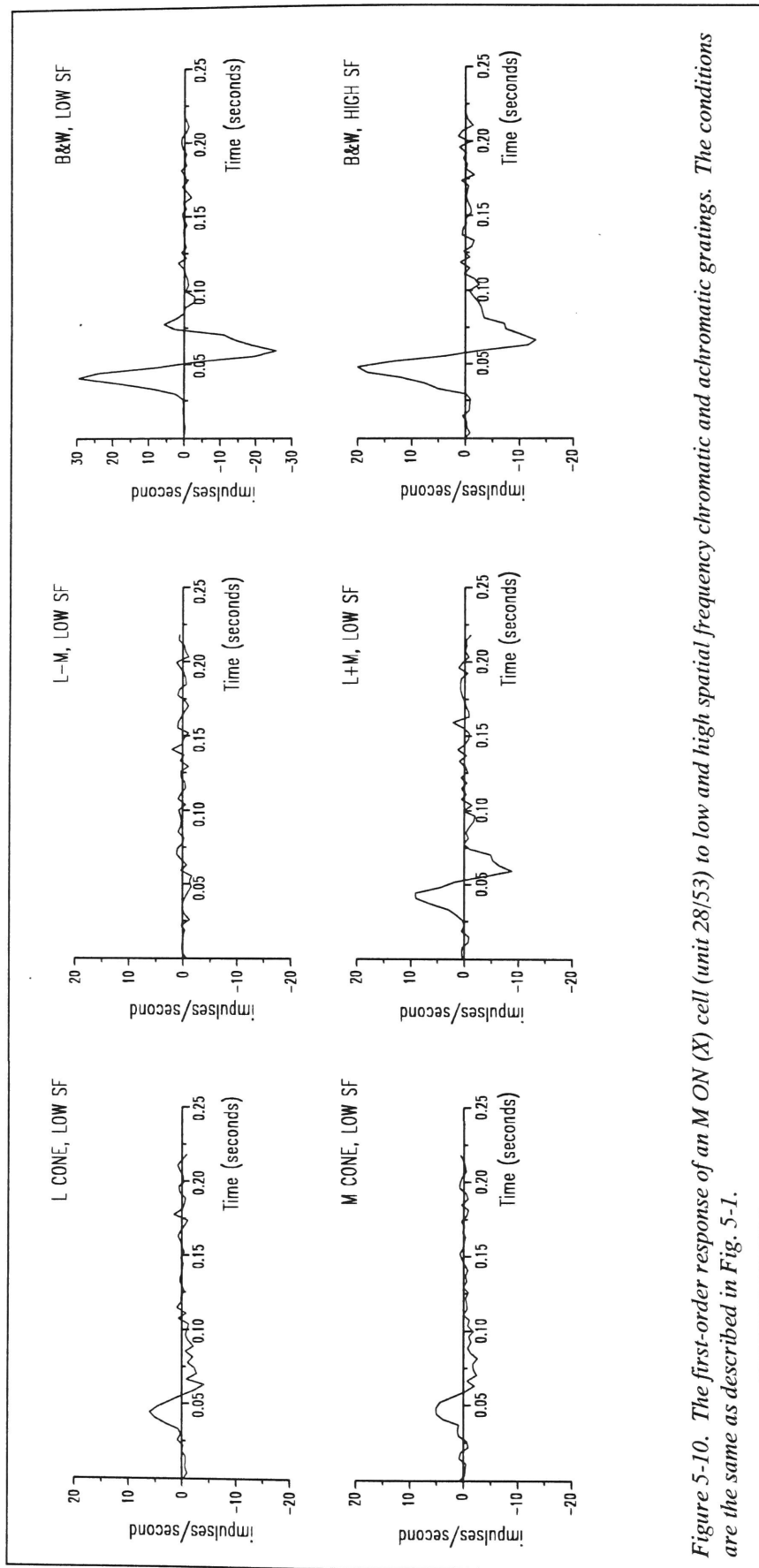


Figure 5-10. The first-order response of an M ON (X) cell (unit 28/53) to low and high spatial frequency chromatic and achromatic gratings. The conditions are the same as described in Fig. 5-1.

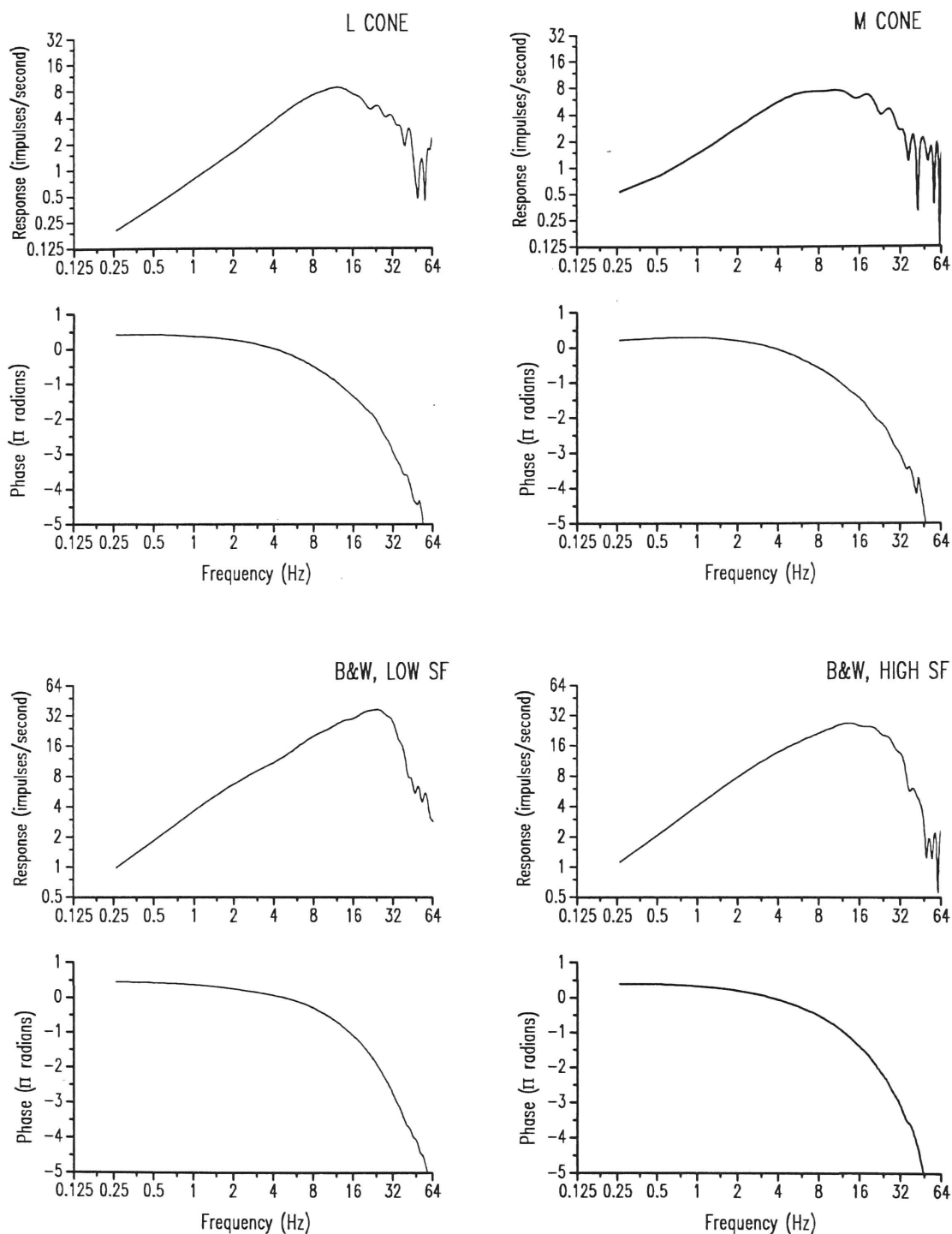
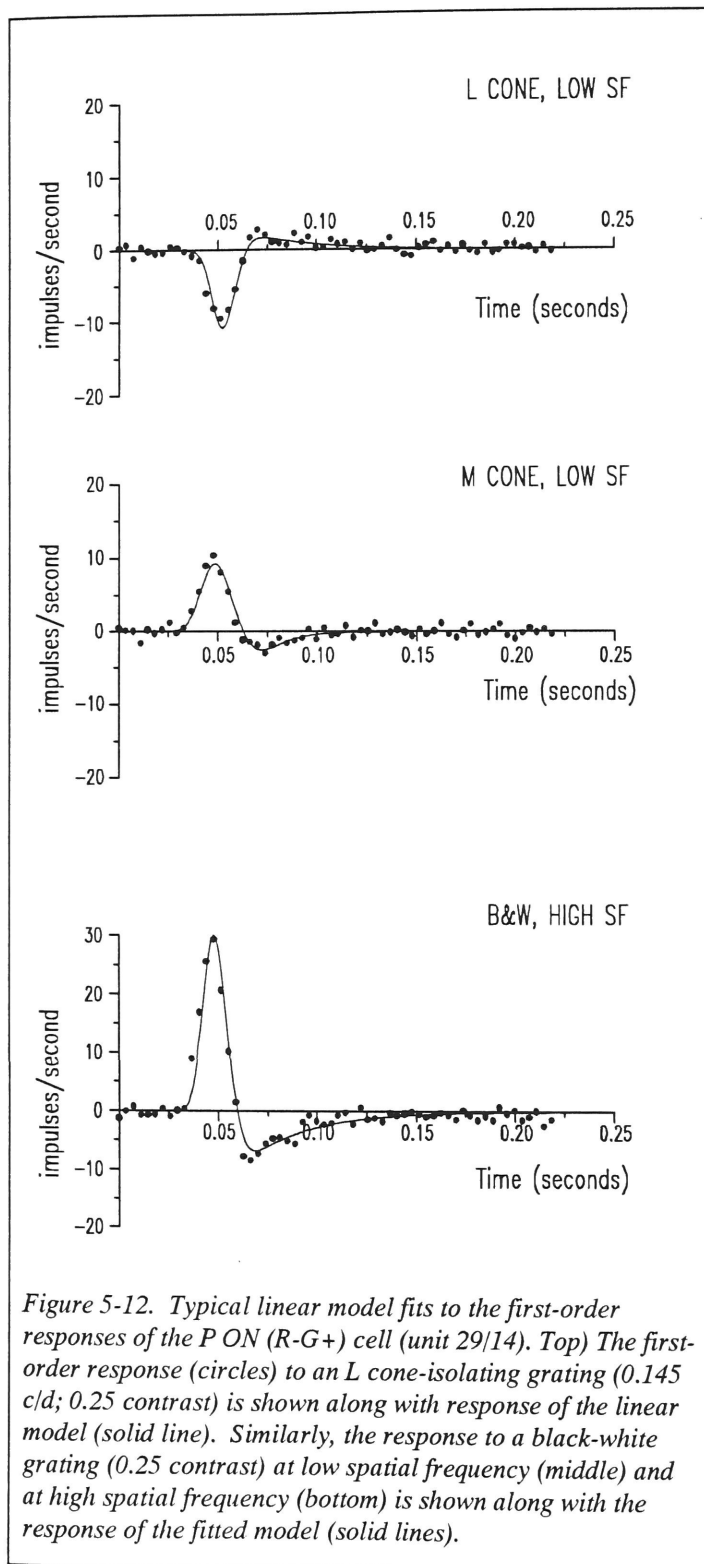


Figure 5-11. The frequency responses of the M ON (X) cell (unit 28/53) derived from the first-order responses from the multiple m-sequence method. The responses to low spatial frequency L cone and M cone-isolating gratings modulated at 0.25 contrast were transformed into the frequency domain and are shown in the top row. Similarly, the bottom row shows the frequency responses of the same M cell to a low (0.145 c/d) and a high spatial frequency (2.181 c/d) black-white grating modulated at 0.25 contrast.

5.5 Model Fits



The linear filter model was fit to the first-order responses of P cells to chromatic and achromatic gratings. Typical fits are shown in Figure 5-12. The model was fit to responses of 15 P cells to cone-isolating gratings. Although several (YB) P cells were encountered in these experiments, not enough data was collected from these cells to allow reliable fits to their responses; therefore, the parameters from these fits were not included in this sample. However, qualitatively, the dynamics of (YB) P cells are very similar to those of (RG) P cells. Furthermore, pilot studies showed that (RG) P cells respond negligibly to S cone-isolating gratings so that the responses to these gratings were not routinely recorded for (RG) P cells.

The parameters of the center and surround responses were tabulated separately (Tables 5-1 and 5-2). The responses to the cone-isolating gratings corresponding to the center cone type were less delayed than the surround responses. The mean difference in delay, however, is only 3.02 ms. In the model fits, there were on average more surround stages than center stages (44 vs. 26, $P < 0.002$). However, the time constants of the surround low-pass stages was significantly shorter ($P < 0.02$). It is interesting to note that the center-surround delay is less when measured with chromatic gratings than when measured with spots and annuli. This fact probably indicates that the delay from regions of the surround that are preferentially stimulated by the annulus is greater than the average delay of the entire surround. Low spatial frequency chromatic gratings can stimulate the whole chromatically opponent surround, part of which probably overlaps the center. The linear filter model was also fit to P cell response to black - white gratings set near the optimal spatial frequency for the cell. These parameters (Table 5-3) are similar to those from the center-isolating responses.

Table 5-1. P Cell Chromatic Center Parameters

$N_{TOTAL}=15$; $N_{ON} = 12$; $N_{OFF} = 3$; $N_{RED-CENTER}=8$; $N_{GREEN-CENTER} = 7$

Parameter	Minimum	Maximum	Median	Mean	S.D.	C.V.
A (impulses/s)	7.48	111.42	14.99	22.24	25.17	1.13
N_L	16	36	26	26.40	4.32	0.16
$N_L\tau_L$ (ms)	44.28	64.53	55.32	53.14	5.49	0.10
H_S (dimensionless)	0.4069	0.9421	0.6765	0.6771	0.1444	0.21
τ_S (ms)	1.78	51.85	16.31	20.56	13.57	0.69

Table 5-2. P Cell Chromatic Surround Parameters

$N_{TOTAL}=15$; $N_{ON} = 12$; $N_{OFF} = 3$; $N_{RED-CENTER}=8$; $N_{GREEN-CENTER} = 7$

Parameter	Minimum	Maximum	Median	Mean	S.D.	C.V.
A (impulses/s)	2.41	65.13	10.44	15.80	16.38	1.04
N_L	20	101	39	44.07	20.50	0.47
$N_L\tau_L$ (ms)	46.82	65.31	55.90	56.16	5.44	0.10
H_S (dimensionless)	0.4810	0.8952	0.5963	0.6374	0.1252	0.20
τ_S (ms)	2.04	40.92	23.64	24.13	12.19	0.51
$N_L\tau_{L,surround}-N_L\tau_{L,center}$ (ms)	-2.59	11.27	2.27	3.02	3.26	1.08

Table 5-3. P Cell Optimal Spatial Frequency Parameters

$N_{TOTAL}=9$; $P_{ON} = 8$; $P_{OFF}=1$

Parameter	Minimum	Maximum	Median	Mean	S.D.	C.V.
A (impulses/s-u.c.)	134.26	3498.59	593.74	844.91	1045.14	1.24
N_L	24	54	36	38.44	9.96	0.26
$N_L\tau_L$ (ms)	44.47	56.84	51.55	51.60	3.62	0.07
H_S (dimensionless)	0.6405	0.9649	0.8071	0.8196	0.1141	0.14
τ_S (ms)	0.97	42.56	23.61	20.95	16.00	0.76

5.5.1 M vs. P Comparison

In order to quantify the comparison that has already been made graphically in Figs. 5-1 - 5-7 and Figs. 5-10 - 5.11, Table 5-4 compares the fitted parameters for P cell and M cell centers from the linear filter model. The M cell parameters are averages of the fitted parameters derived from model fits to the sum-of-sinusoids data described in Chapter 6. The P cell center data come from the large sample described in Chapter 4. The M and P populations differ significantly in every parameter (two sample T-test).

In these data, the average gain of the M cell center is approximately 7.5 times higher than the P cell center gain (Kaplan and Shapley, 1986). The degree of transience of the response is quantified by the parameter H_S . This parameter is significantly larger for the M cell population (0.96 vs. 0.70, $P < 0.0001$). In addition, the number of low-pass stages (N_L) and the overall delay ($N_L\tau_L$) of the M cell response is significantly smaller for M cells. The time constant, τ_S , as shown in Chapter 6 varies with contrast for M cells.

The values given here (for an intermediate level of contrast: 0.0625) are significantly shorter for M cell centers than for P cells which is an indication of the high peak temporal frequency and bandpass nature of the M cell response.

Table 5-4. M vs. P Center Parameters
 $N_M = 21; N_P = 26$

Parameter	M cell	P cell	P
A (impulses/s-u.c.)	504.70	67.59	1.2×10^{-8}
H_S (dimensionless)	0.9666	0.6990	2.9×10^{-14}
τ_S (ms)	20.64	39.36	0.0009
N_L	22.71	39.36	0.000013
$N_L \tau_L$ (ms)	41.99	49.22	0.0000056

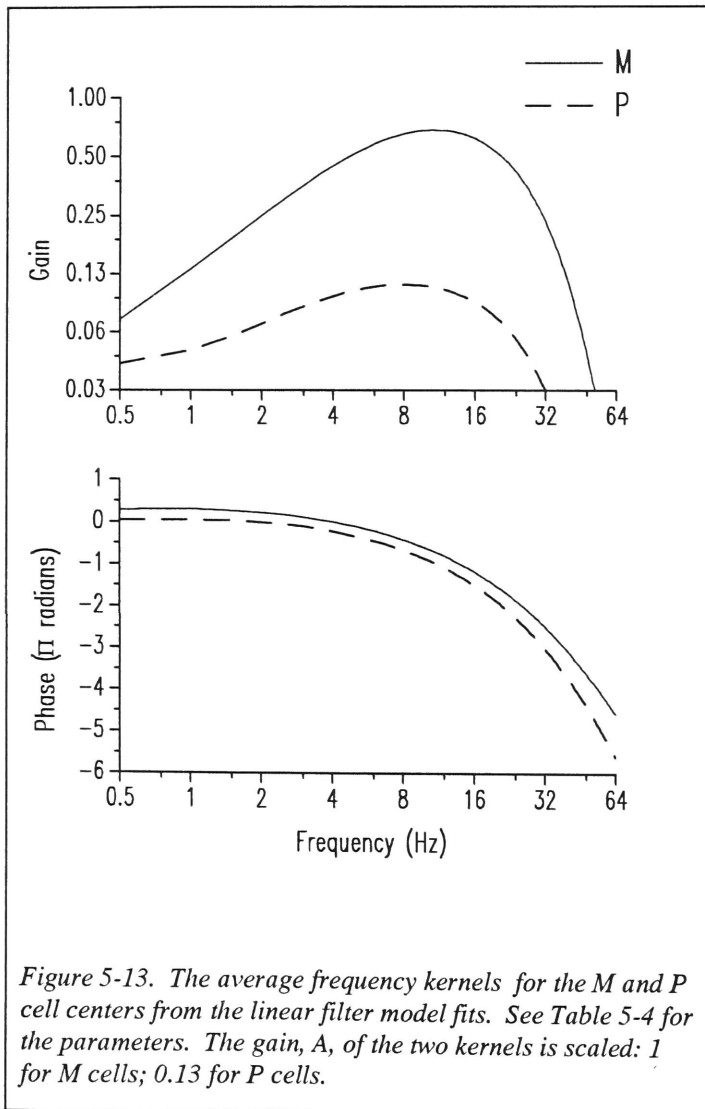
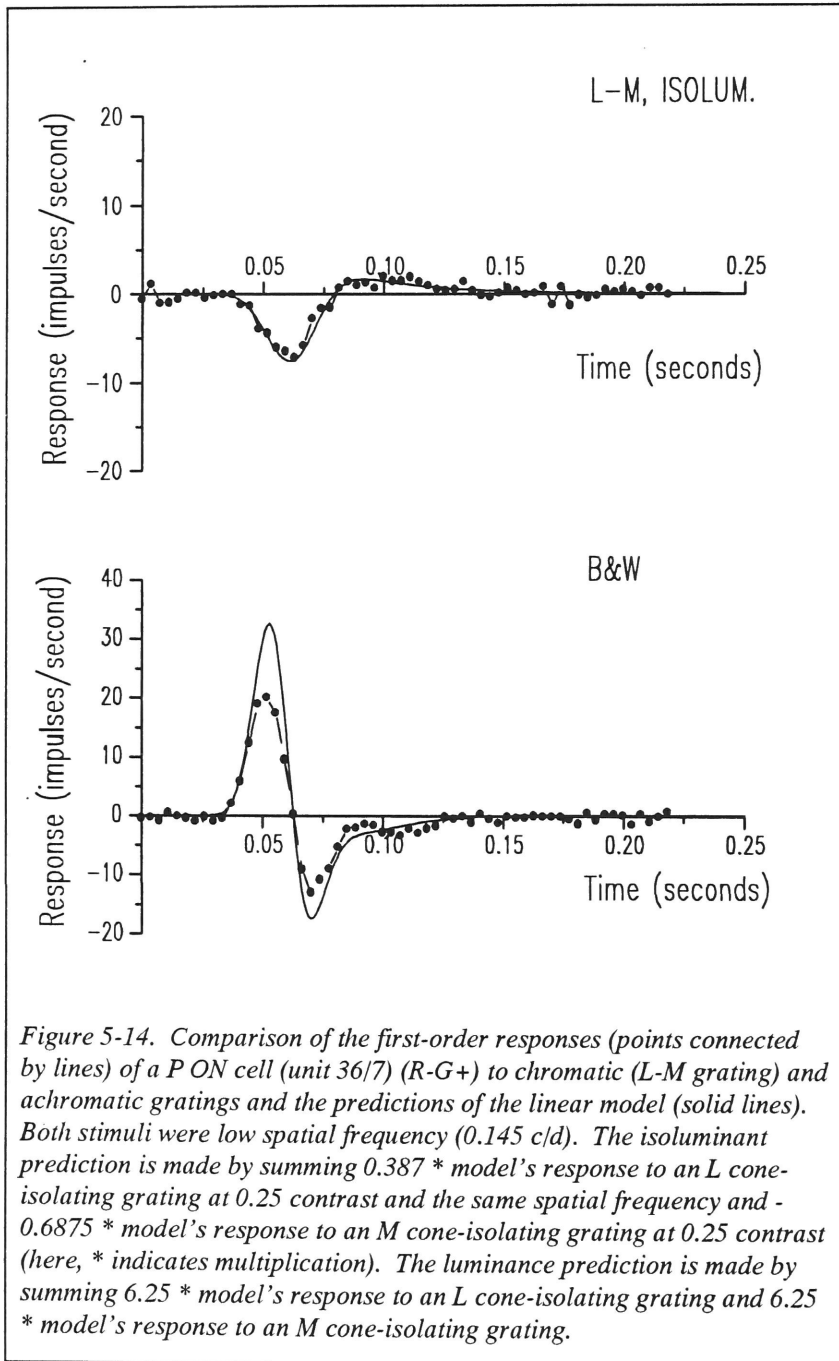


Figure 5-13 summarizes these differences by plotting the population average of the fitted linear filters for M and P cells. The M cell frequency kernel has noticeably higher gain and is more bandpass. In addition, the M cell frequency kernel is relatively phase-advanced which reflects the approximately 8 ms difference in the peak of the M and P cell responses. A qualitative analysis by Derrington and Lennie (1984) reached similar conclusions.

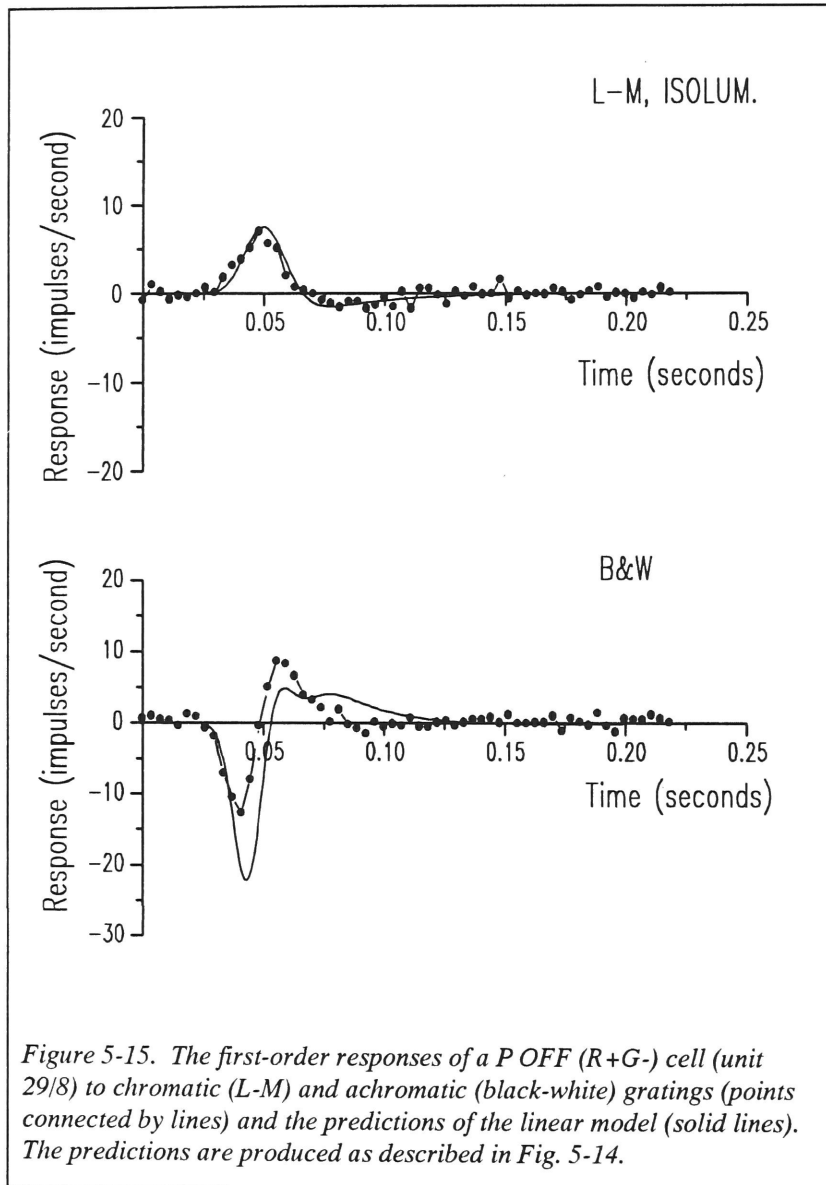
5.6 Prediction of P Cell Chromatic and Achromatic Responses

P cells are widely believed to sum their inputs linearly, and their linearity is critical for theories about their function (e.g. Ingling and Martinez-Uriegas, 1983). The first-order responses of P cells to the L and M cone-isolating gratings can be used to try to



predict the responses of the same cells to other stimuli based on simple assumptions that are consistent with linear P cell models (e.g. Derrington *et al.*, 1984). This will be illustrated with two typical examples (Figs. 5-14 and 5-15). Consider a P cell that has inputs from L cones and from M cones that are summed linearly by the P cell. Stimuli that excite a

combination of L and M cones will produce a response that is a linear combination of the response to pure L and M cone-isolating stimuli. Furthermore, as described in Methods, each stimulus used in these studies produces a known amount of L and M cone



stimulation. Figures

5-14 and 5-15

compare these linear predictions with the measured responses.

For a P ON R-

G+ cell, the linear

prediction for the

isoluminant (L-M)

response is in excellent

agreement with the

data (Fig. 5-14). This

is a typical result for

an isoluminant

condition. However,

for larger responses to

achromatic stimuli, the

prediction typically overestimates the size of the actual response. Figure 5-15 shows the

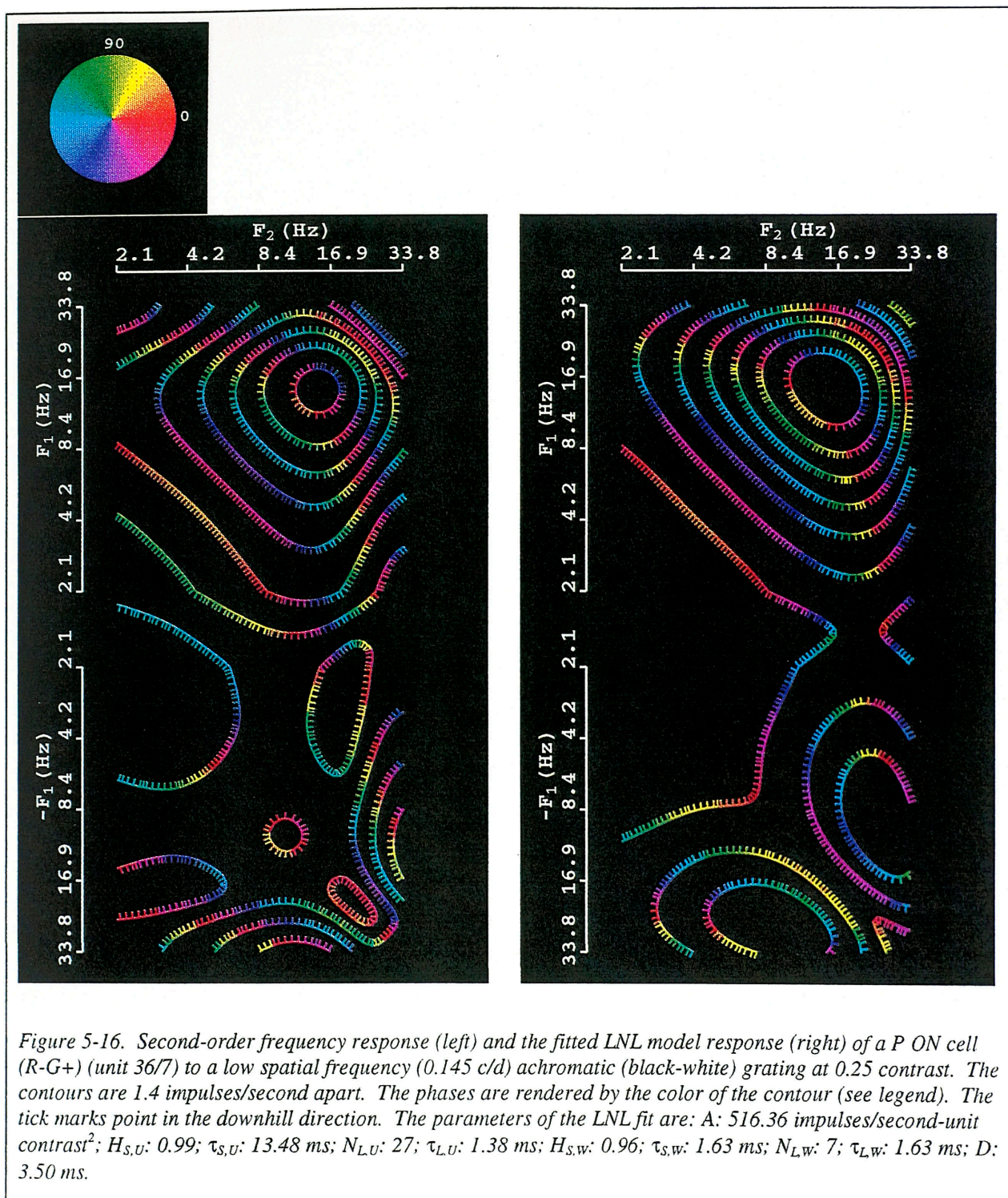
same typical results for a P OFF R+G- cell. The responses of these two cells were not

saturating or truncating under the achromatic condition, indicating that the failure of the linear prediction is not due to overmodulation of the cell's response. Fifteen cells were tested in this way, and all fell into this general pattern, namely that the responses to achromatic stimuli were overestimated by the linear prediction. This result suggests that the same kind of shunting gain control demonstrated in Chapter 4 may also play a role in the interaction of chromatic signals in the P cell receptive field. Indeed, although the P cell receptive field is chromatically and spatially opponent, as previously recognized (Wiesel and Hubel, 1966, Derrington *et al.*, 1984), the subregions of the P cell receptive field interact in a nonlinear manner. This nonlinearity is reported here for the first time.

5.7 Nonlinear Responses

The previous section dealt with the linear summation of the cone inputs. It is naturally interesting to inquire about the nonlinear responses of P cells to grating stimuli. Second-order responses obtained from P cells with black-white gratings were very similar to those obtained with spots and annuli. This section shows an example of those responses obtained as described in Methods by taking the Fourier transform of the second-order m-sequence kernel from the time domain into the frequency domain. Figures 5-16 and 5-17 show these second-order frequency responses at low and high spatial frequency obtained with an achromatic grating modulated by a sum of 2 m-sequences. The fits of the LNL model accompany the data. At low spatial frequency, the power in the second-order response can be seen to be concentrated in the sum region ($F_1 + F_2$) of the second-order frequency response, while at high spatial frequency the power is still asymmetrical but more evenly distributed. From an analysis of the LNL fits, this variation can be seen

to be primarily due to the less bandpass nature of the pre-filter $U(\omega)$ at high spatial frequency rather than to a significant change in the second filter $W(\omega)$ which is consistently bandpass and peaks at a higher frequency as shown in Chapter 4. In general, P cells gave insignificant second-order responses to chromatic gratings (L cone-isolating, M cone-isolating, and isoluminant gratings) probably due to the lower overall cone-modulation available with these stimuli.



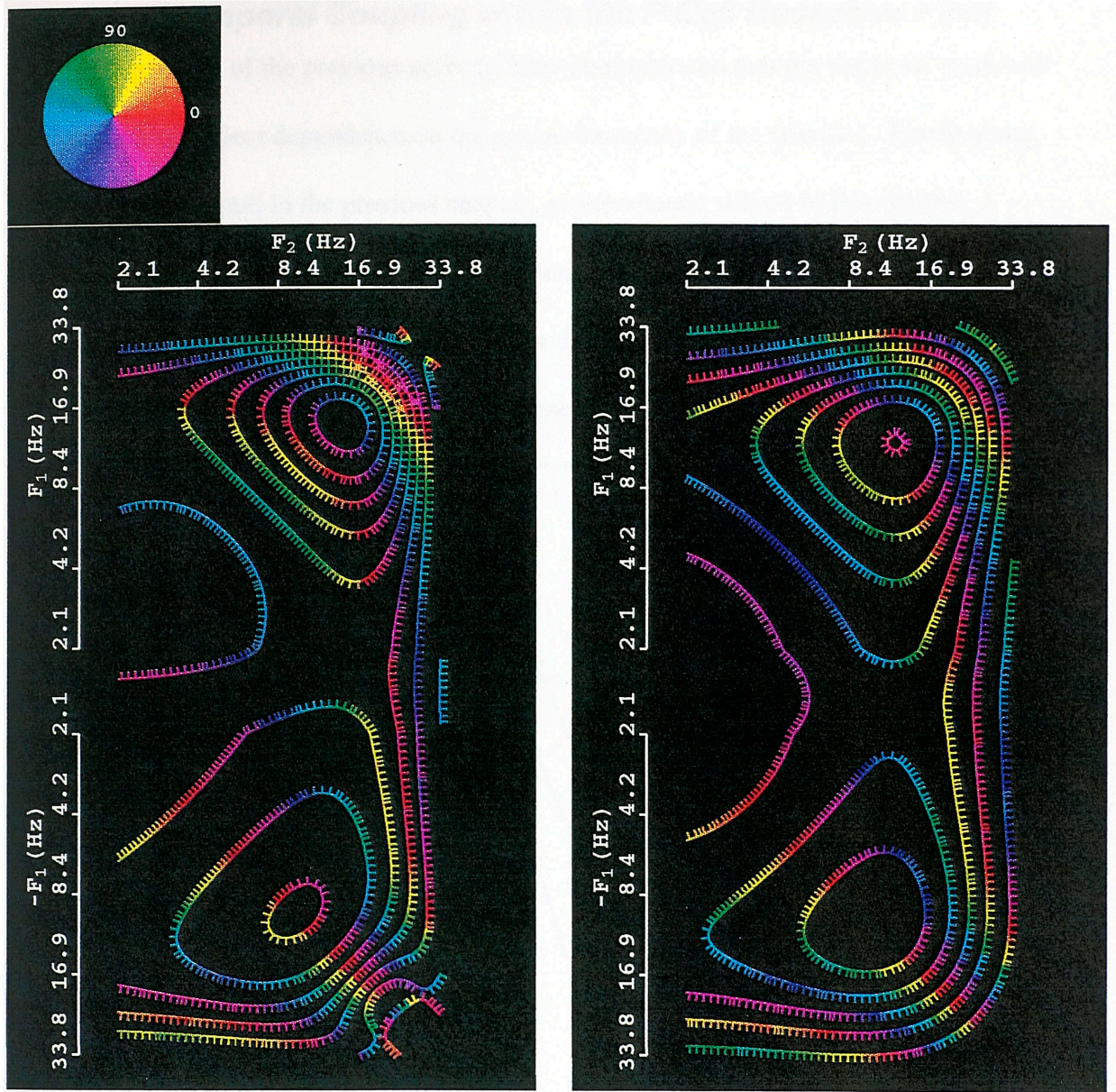


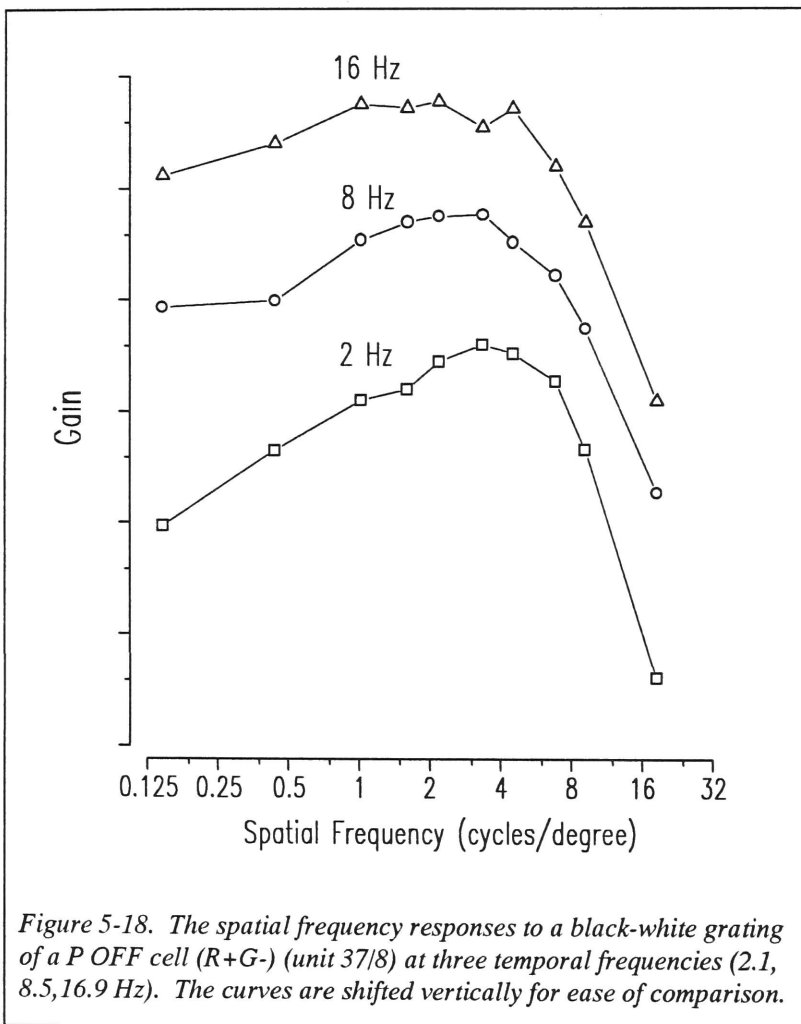
Figure 5-17. Second-order frequency response (left) and the fitted LNL model response (right) of a P ON cell (R-G+) (unit 36/7) to a high spatial frequency (2.18 c/d) achromatic grating at 0.25 contrast. The contours are 1.4 impulses/second apart. The phases are rendered by the color of the contour (see legend). The tick marks point in the downhill direction. The parameters of the LNL fit are: A : 12490.64 impulses/second-unit contrast²; $H_{S,U}$: 0.90; $\tau_{S,U}$: 3.87 ms; $N_{L,U}$: 18; $\tau_{L,U}$: 3.19 ms; $H_{S,W}$: 0.92; $\tau_{S,W}$: 0.53 ms; $N_{L,W}$: 7; $\tau_{L,W}$: 0.16 ms; D : 3.50 ms.

5.8 Spatiotemporal Coupling within the P Cell Receptive Field

The results of the previous sections have demonstrated that the temporal responses of P cells show a clear dependence on the spatial frequency of the stimulus. Furthermore, using spots and annuli in the previous chapter, and chromatic stimuli in this chapter, a delay in the surround response was demonstrated. These findings indicate that the parameters of space and time are inseparable in describing the P cell receptive field. In this section, I briefly discuss a completely independent technique that corroborates these

results.

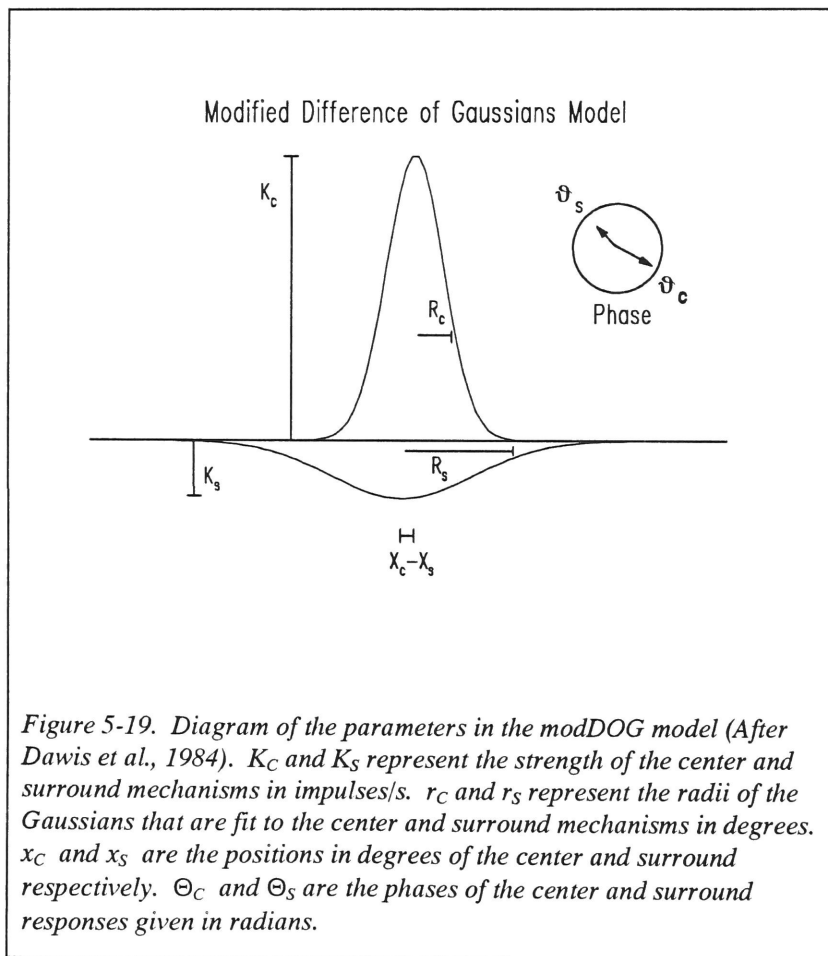
The responses of P cells to drifting gratings at several spatial frequencies were measured as described in Methods. This section will discuss responses to achromatic gratings. The resulting spatial frequency responses show a characteristic variation with temporal frequency (Fig. 5-18).



As the drift frequency increases, the spatial frequency response curves become less bandpass. Using a paradigm developed by Dawis *et al.* (1984), the spatial frequency

responses of P cells were used to fit the modified Difference-of-Gaussians (modDOG) model to the data (see also Enroth-Cugell *et al.*, 1983). The model used for the fit is shown in Figure 5-19. For the present discussion, the phases of the center and surround, θ_c and θ_s , and the strength of the center and surround, K_c and K_s , are most important.

For each of 3 temporal frequencies, the phase of the center and surround responses were estimated by fitting the modDOG model to the data (Benardete and Kaplan, 1993). A line was then fit to the phase data, the slope of which represents the delay of the center and the surround response respectively. The difference of these two values represents the relative delay between the center and the surround.



As temporal frequency increases, the overall flattening of the P cell spatial frequency response can be explained by a diminution of surround strength at higher temporal frequencies, or by a relative delay of the surround mechanism so that at high temporal frequencies the center

and surround responses becomes more in phase and less opponent. Fits to the modDOG model (Fig. 5-20) allow the relative center-surround delay to be estimated. A summary (Fig. 5-21) of these experiments shows that, according to the modDOG model, the surround strength does not appreciably weaken relative to the center strength even at 16 Hz. Indeed, the surround contributions, although still weaker than those of the center, increase at high temporal frequencies. However, the phase difference between the center and surround lessens such that by 16 Hz, the center-surround phase difference is much less than one half of a cycle. A smaller phase difference implies weaker center-surround antagonism and a flatter spatial frequency response. The weakening of the surround's ability to oppose the center weakens the chromatic opponency of P cells as temporal frequency is increased, as suggested by Gouras and Zrenner (1979).

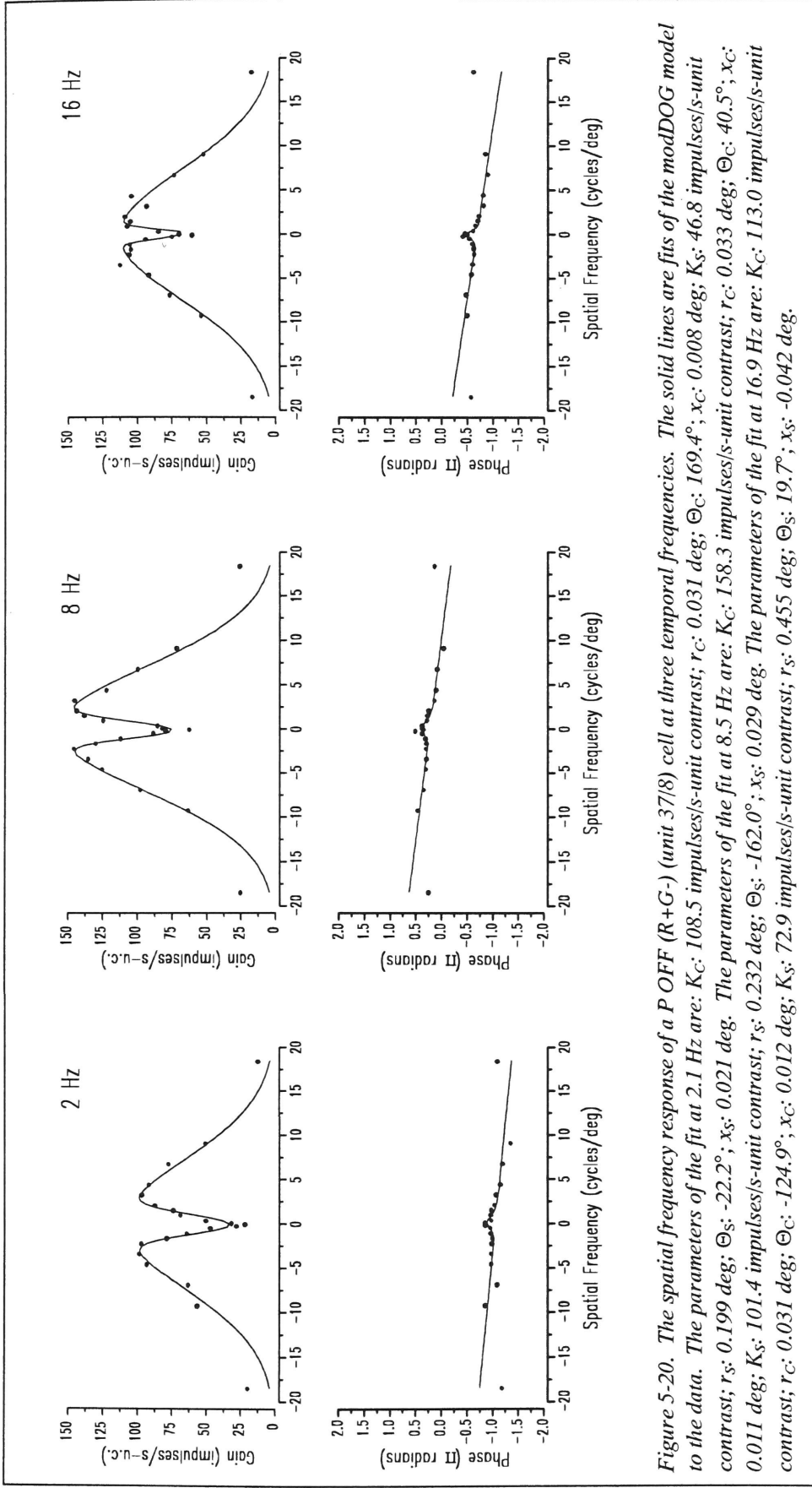


Figure 5-20. The spatial frequency response of a P OFF (R+G-) (unit 37/8) cell at three temporal frequencies. The solid lines are fits of the modDOG model to the data. The parameters of the fit at 2.1 Hz are: K_C : 108.5 impulses/s-unit contrast; Θ_C : 169.4°; x_C : 0.008 deg; K_S : 46.8 impulses/s-unit contrast; r_S : 0.199 deg; Θ_S : -22.2°; x_S : 0.021 deg. The parameters of the fit at 8.5 Hz are: K_C : 158.3 impulses/s-unit contrast; Θ_C : 40.5°; x_C : 0.011 deg; K_S : 101.4 impulses/s-unit contrast; r_S : 0.232 deg; Θ_S : -162.0°; x_S : 0.029 deg. The parameters of the fit at 16.9 Hz are: K_C : 113.0 impulses/s-unit contrast; Θ_C : -124.9°; x_C : 0.012 deg; K_S : 72.9 impulses/s-unit contrast; r_S : 0.455 deg; Θ_S : 19.7°; x_S : -0.042 deg.

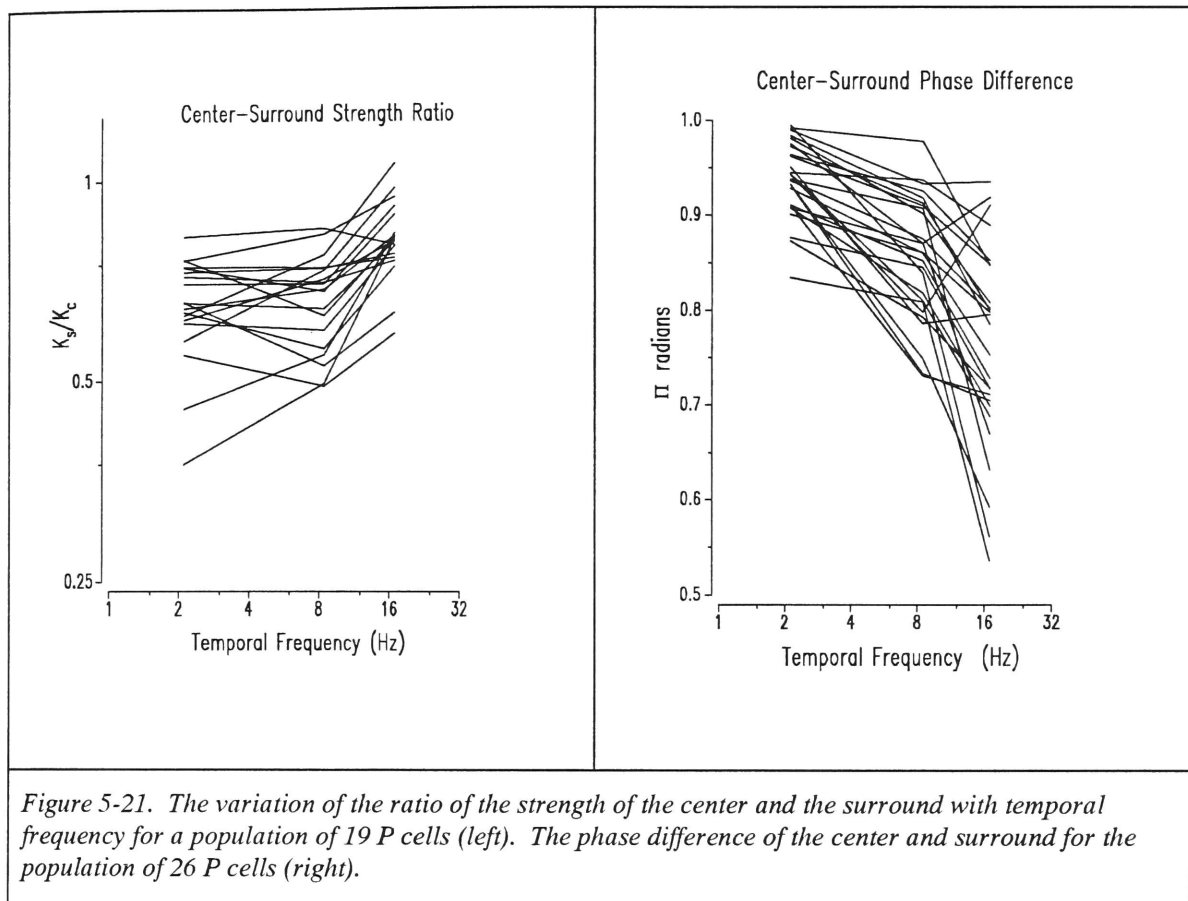


Table 5-5 summarizes some of the parameters obtained with the modDOG fits. This sample of cells in the same parafoveal region (mean eccentricity 4.9 deg; S.D. 3.38 deg), has an average center radius of approximately 0.05 deg, while the average radius of the surround was almost 5 times as large. The average delay of the center response with respect to the stimulus was 54.34 ms, slightly longer than the delay measured with the multiple m-sequence techniques above. But, of course, the estimate here is based only on fitting a line to 3 phase values, so the agreement is reasonable. Similarly, the average surround delay is approximately 60 ms, close to the m-sequence estimate. Finally, the average delay of the surround with respect to the center was 6 ms estimated by this

technique, compared with the value of 8.4 ms obtained with spots and annuli in Chapter 4. As mentioned above, the spot/annulus paradigm probably slightly overestimates the delay since only the outer regions of the surround mechanisms are stimulated by the annulus.

Table 5-5. Parameters from the Fit of the modDOG Model to P Cell Spatial Frequency Responses
 $N_{TOTAL} = 26$; $N_{ON} = 16$; $N_{OFF} = 10$; $N_{RG} = 22$; $N_{YB} = 4$

Parameter	Minimum	Maximum	Median	Mean	S.D.	C.V.
r_c (deg)	0.0300	0.1047	0.0538	0.05455	0.01624	0.30
r_s (deg)	0.10905	0.6874	0.1941	0.2396	0.1480	0.62
r_c/r_s	1.7476	14.8599	3.5492	4.7044	3.2439	0.69
K_s/K_c	0.2385	0.9933	0.6506	0.6406	0.1545	0.24
$Delay_C$ (ms)	47.81	64.62	53.25	54.34	4.10	0.08
$Delay_S$ (ms)	48.49	74.69	59.18	60.47	6.45	0.11
$Delay_{C,S}$ (ms)	0.67	14.75	5.82	6.07	3.26	0.54

5.9 Summary

This chapter examined the response of P cells to achromatic and chromatic gratings. The major results are as follows:

1. The responses of P cells to cone-isolating gratings demonstrate the chromatically and spatially opponent nature of their receptive fields.
2. Fourier transforms of the first-order m-sequence responses show how the temporal frequency responses of P cells vary with chromaticity and spatial frequency. For a single kind of stimulus (chromatic or achromatic), the response of P cells are linear with increasing contrast.
3. The linear filter model fit to P cell responses to chromatic stimuli shows that the color opponent mechanisms in the receptive field are similar in their temporal characteristics although there is a small delay associated with the surround mechanism.
4. The responses of P cells to cone-isolating gratings can be used to predict the responses of these cells to other chromatic and luminance stimuli. In general, the predictions based

on linear assumptions work well for other chromatic stimuli but fail for strong luminance stimuli.

5. P cells demonstrate second-order responses to achromatic grating stimuli that are similar to those already described for spots and annuli. The variation of the second-order responses of P cells with spatial frequency is dependent more on the changing characteristics of the pre-filter than the post-filter in the LNL fit.

6. The modDOG model was fit to the responses of P cells to drifting gratings. From the fit of the modDOG model, the calculated relative delay of center and surround supports the results obtained with the multiple m-sequence method.

7. Taken together, we find in the P cell's receptive field previously unreported nontrivial nonlinearities, and clear evidence for spatiotemporal coupling. The functional implications of these findings will be taken up in the discussion.

M CELL DYNAMICS

Introduction

Frequency Responses

Spatiotemporal Coupling

Model Fits

Step Responses

M Cell Chromatic Responses

Spatial Profile of the Contrast Gain Control

Temporal Characteristics of Contrast Gain Control

Nonlinear Responses

Summary

6. M Cell Dynamics

6.1 Introduction

Just as contrast-processing by P cells is important for understanding their structure and function, the same information is critical for addressing M cell structure and function. Some of the work presented in this chapter has been published in Benardete *et al.* (1992a).

The functional and anatomical division of primate retinal ganglion cells into M and P types has led to a fuller understanding of visual processing based on the similarities and differences between the two groups. Since contrast in the visual scene provides the substrate for pattern vision, the mechanisms that M and P cells use to signal contrast provide clues to their separate roles. For instance, it is well established that the M and P populations show a clear difference in their sensitivity to contrast, M cells being on average 8-10 times more sensitive than P cells (Kaplan and Shapley, 1986; Smith *et al.*, 1991).

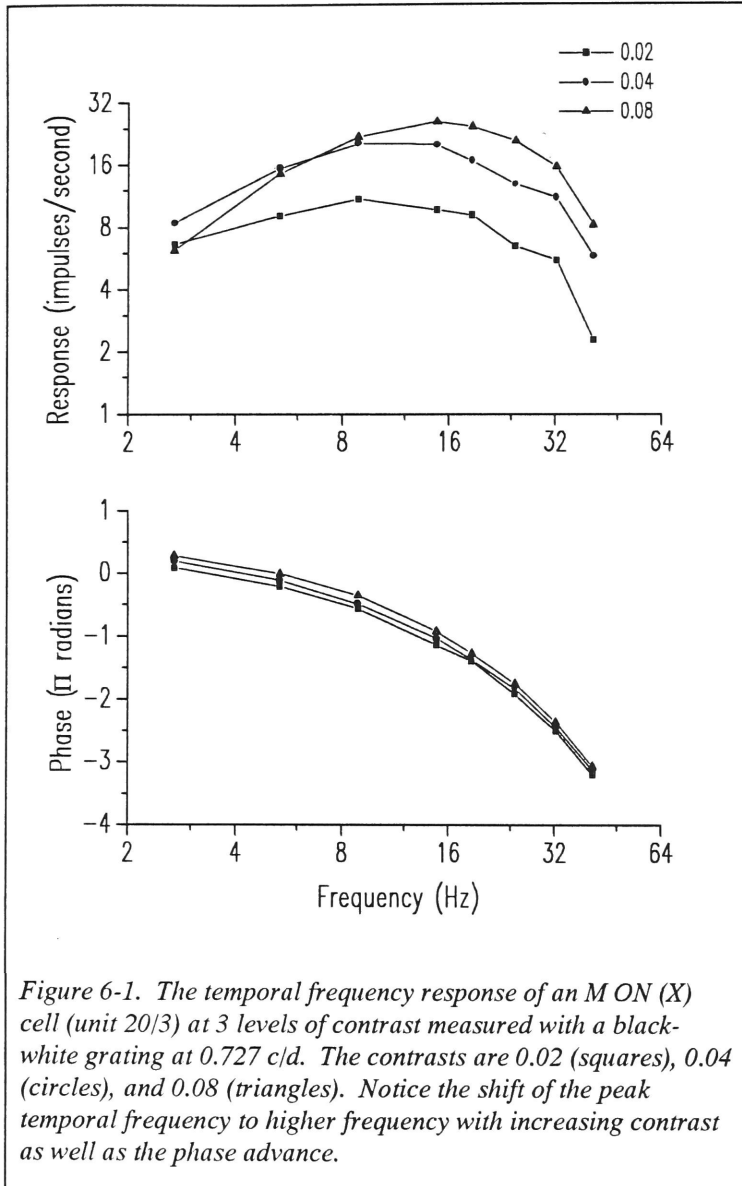
Two of the major functional subdivisions of retinal ganglion cells in the cat retina, X and Y, express a common motif in contrast processing. The temporal frequency response of both X and Y cells is modified by contrast. As contrast increases, the peak of the temporal frequency response is shifted to higher temporal frequencies due to a greater attenuation of the response at low temporal frequencies. The mechanism responsible for this phenomenon has been termed the contrast gain control (Shapley and Victor, 1978,

1979a, 1981). The generality of this feature in the cat led me to explore the temporal frequency response of primate retinal ganglion cells for the presence of a similar process in a visual system close to that of man (DeValois *et al.*, 1974a,b). The responses of retinal ganglion cells were assessed with sine wave gratings modulated in time by a sum of sinusoids. By measuring the responses of the cells at several contrasts, I show that M cells share the characteristic features of a contrast gain control mechanism, while P cells do not.

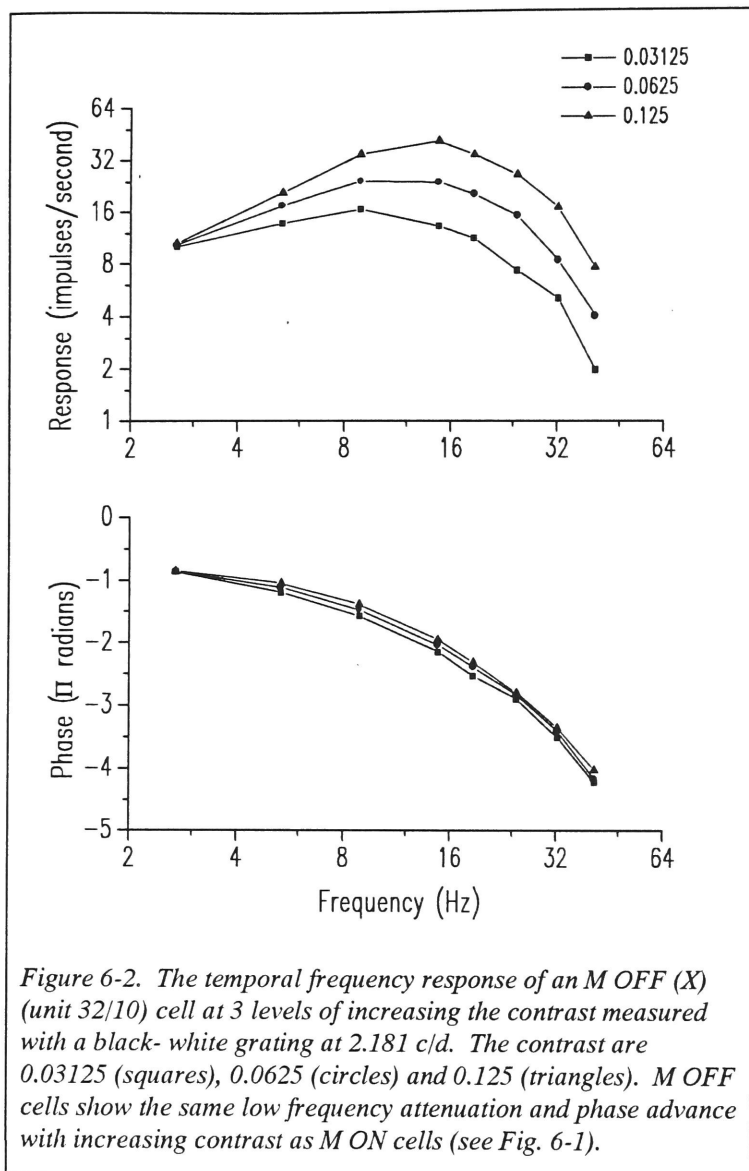
This chapter will first discuss the data that demonstrate the contrast gain control effect. Next, the fits of the linear filter model to the data are discussed as they provide a concise description of the phenomenon and a way to predict how an M cell will respond to a step of contrast. Next, M cell responses are analyzed with respect to chromatic contrast, and these results are related to the contrast gain control model. Finally, the spatial aspects of contrast gain control mechanism are discussed, and these results are related to the nonlinear response of M cells.

6.2 Frequency Responses

The temporal frequency responses of an M ON and an M OFF cell, measured with



a sum of sinusoids, are shown at three levels of contrast (Figs. 6-1 and 6-2). Notice that, for both cells, as the contrast in the stimulus increases, the peak of the temporal frequency response shifts from about 8 Hz at the lowest contrast to 14 Hz at the highest contrast. By comparison, the P cell (Fig. 6-3) shows a temporal frequency response that is invariant with contrast (Benardete *et al.*, 1991).



Notice that at low temporal frequencies, the M cells' response barely increases with contrast. In fact, in these two M cells (Figs. 6-1 and 6-2), the response amplitude at the lowest temporal frequency is almost identical at 3 different contrast levels while the amplitude of the response at higher frequencies increases with contrast. This phenomenon has important implications for the contrast gain of M cells, since it shows that the response of M cells at

low temporal frequencies is preferentially attenuated as contrast increases.

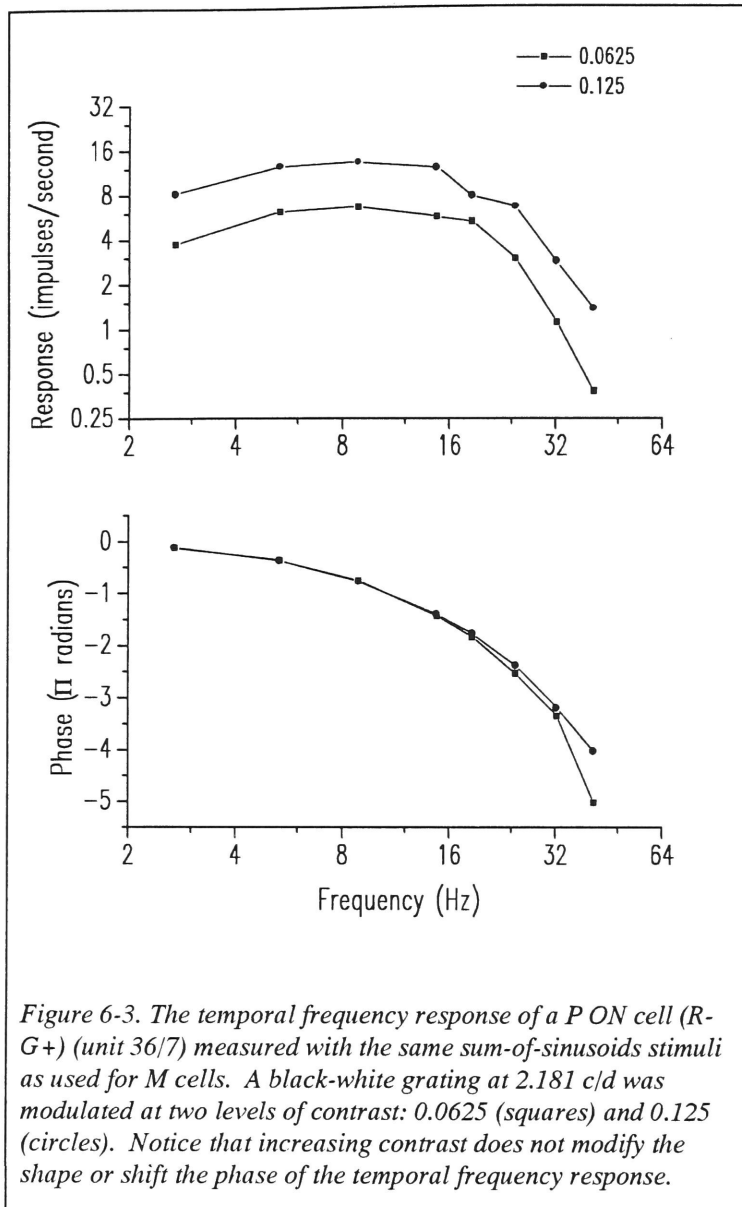


Figure 6-3. The temporal frequency response of a P ON cell (R-G+) (unit 36/7) measured with the same sum-of-sinusoids stimuli as used for M cells. A black-white grating at 2.181 c/d was modulated at two levels of contrast: 0.0625 (squares) and 0.125 (circles). Notice that increasing contrast does not modify the shape or shift the phase of the temporal frequency response.

The phase of the M cell response also demonstrates an interesting dependence on contrast (Figs. 6-1 and 6-2). As contrast increases, the phase of the response advances in the middle frequency range (in some cells by nearly 40°). By comparison, the phase of the P cell response is invariant with contrast (Fig. 6-3).

The M cell responses shown demonstrate the major features of the contrast gain control, but it was also found

uniformly across the sample of M cell responses analyzed in detail (21 M cells).

6.3 Spatiotemporal Coupling

Spatially, the gratings used in the experiments above (Figs. 6-1 - 6-3) were set near the optimal spatial frequency for each cell. However, for a typical M cell, the temporal frequency responses change with the spatial frequency of the grating stimulus (Fig. 6-4). At low spatial frequency, the peak of the temporal frequency response is higher than at

higher spatial frequencies; however, even at low spatial frequency the peak of the temporal frequency response is still shifted to higher frequency by the contrast gain control. There is also a clear phase advance at all spatial frequencies. At higher spatial frequencies, even greater than the optimal spatial frequency, the peak temporal frequency is still shifted to higher frequency by the contrast gain control effect. Thus, these data suggest that the source of the contrast gain control has a spatial scale at least as small as the center of the M cell although one cannot say at this point from what part of the receptive field or from what retinal elements the contrast gain control signal may come. Later, evidence is presented that the contrast gain control signal is collected from a broad region of the retina in the surround of the M cell receptive field.

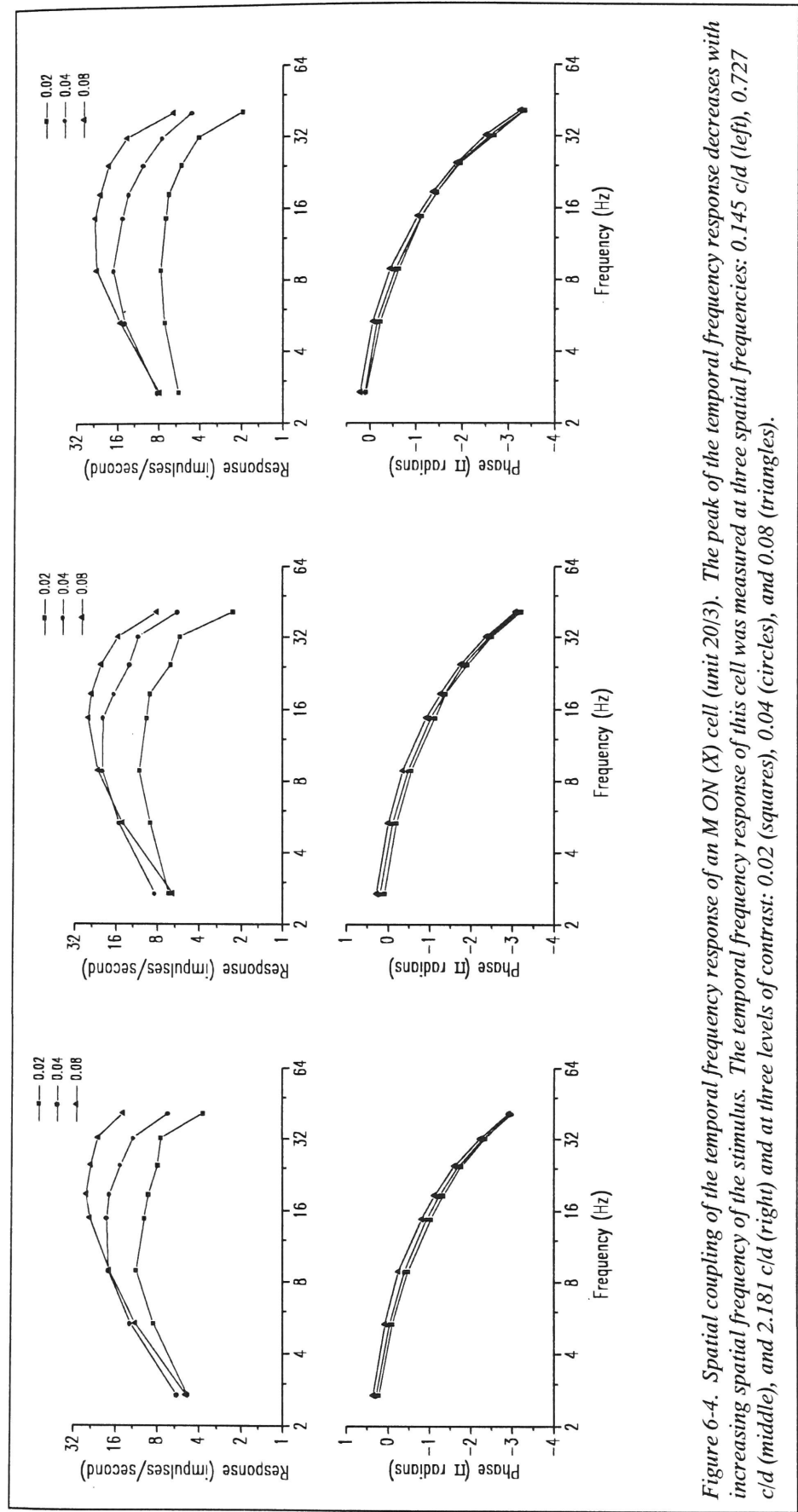
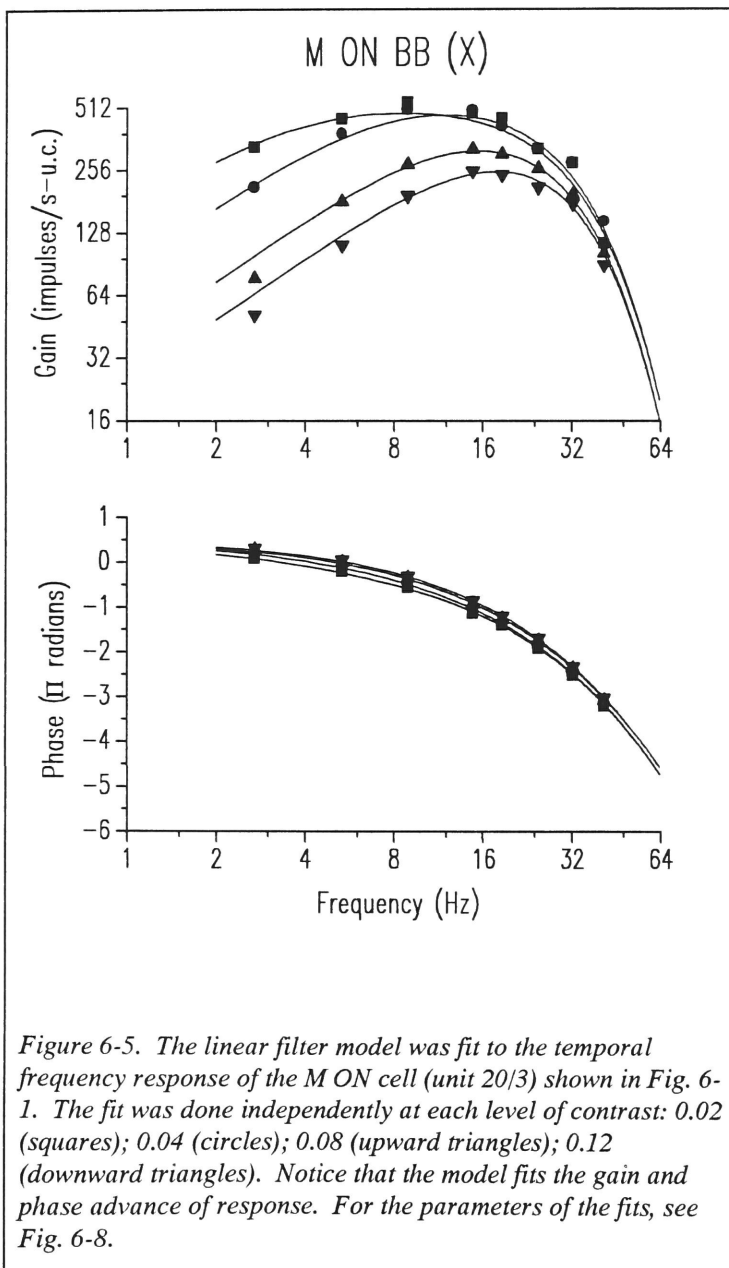


Figure 6-4. Spatial coupling of the temporal frequency response of an M ON (X) cell (unit 20/3). The peak of the temporal frequency response decreases with increasing spatial frequency of the stimulus. The temporal frequency response of this cell was measured at three spatial frequencies: 0.145 c/d (left), 0.727 c/d (middle), and 2.181 c/d (right) and at three levels of contrast: 0.02 (squares), 0.04 (circles), and 0.08 (triangles).

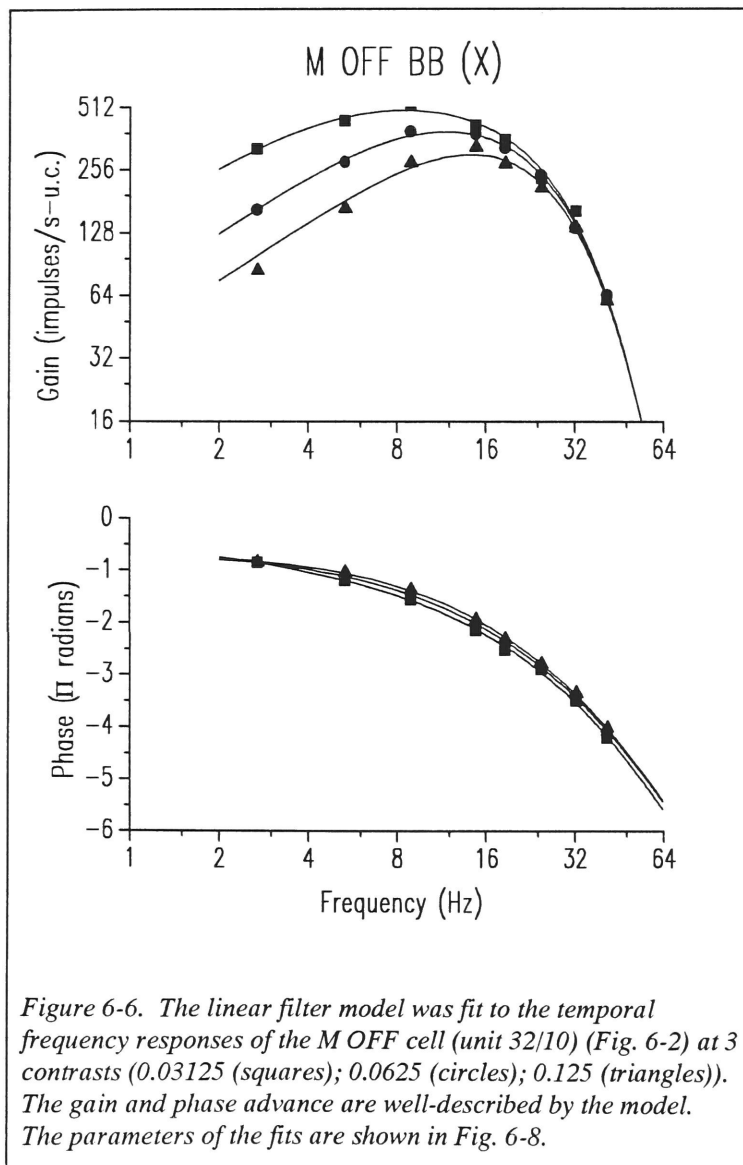
6.4 Model Fits

By now, it is clear that the magnitude of the contrast signal has a profound effect on the M cell temporal frequency response. Thus, the contrast gain control mechanism measures a quantity similar to the RMS contrast signal and adjusts the temporal frequency response of the cell (Victor, 1987).

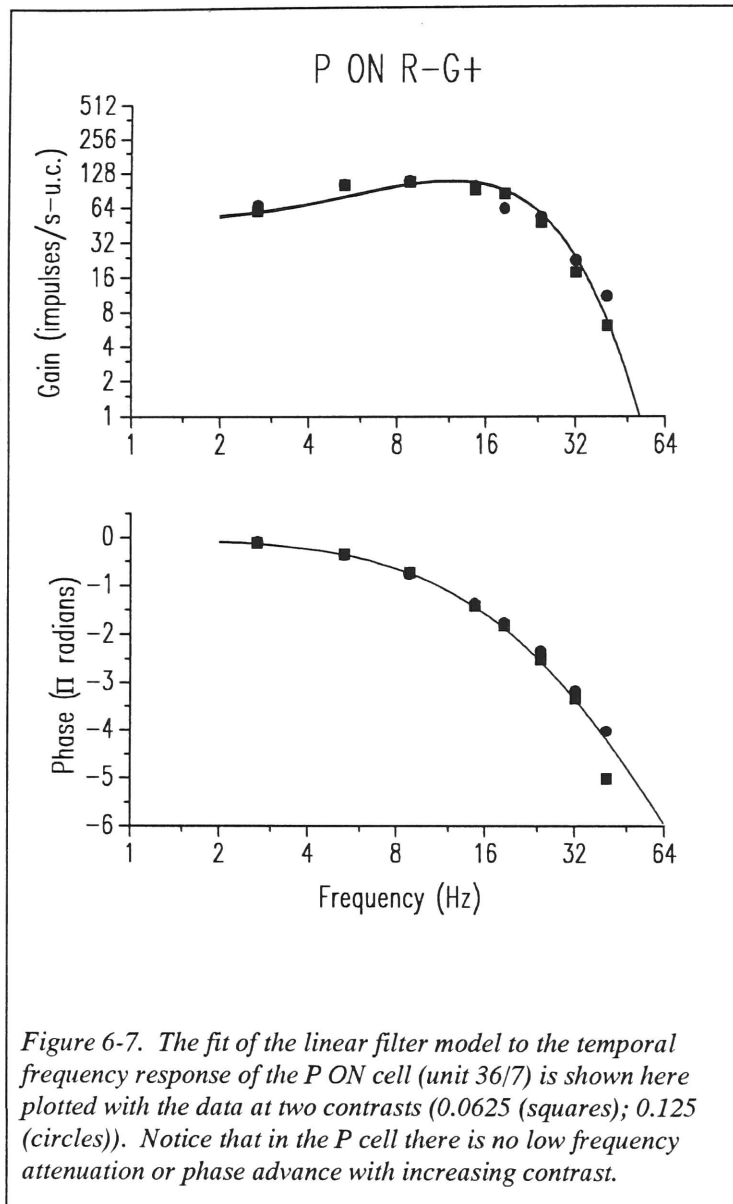


In modeling the responses of the cat X-cell center, Victor (1987) proposed the linear filter model that has been previously introduced (see Methods). This same model was fit to the M cell data and the parameters were studied in order to better understand how contrast modifies the response of M cells (Figs. 6-5 - 6-7). The responses have been converted to gain by dividing by the contrast in the stimulus. The solid curves in the figures show the fit of the

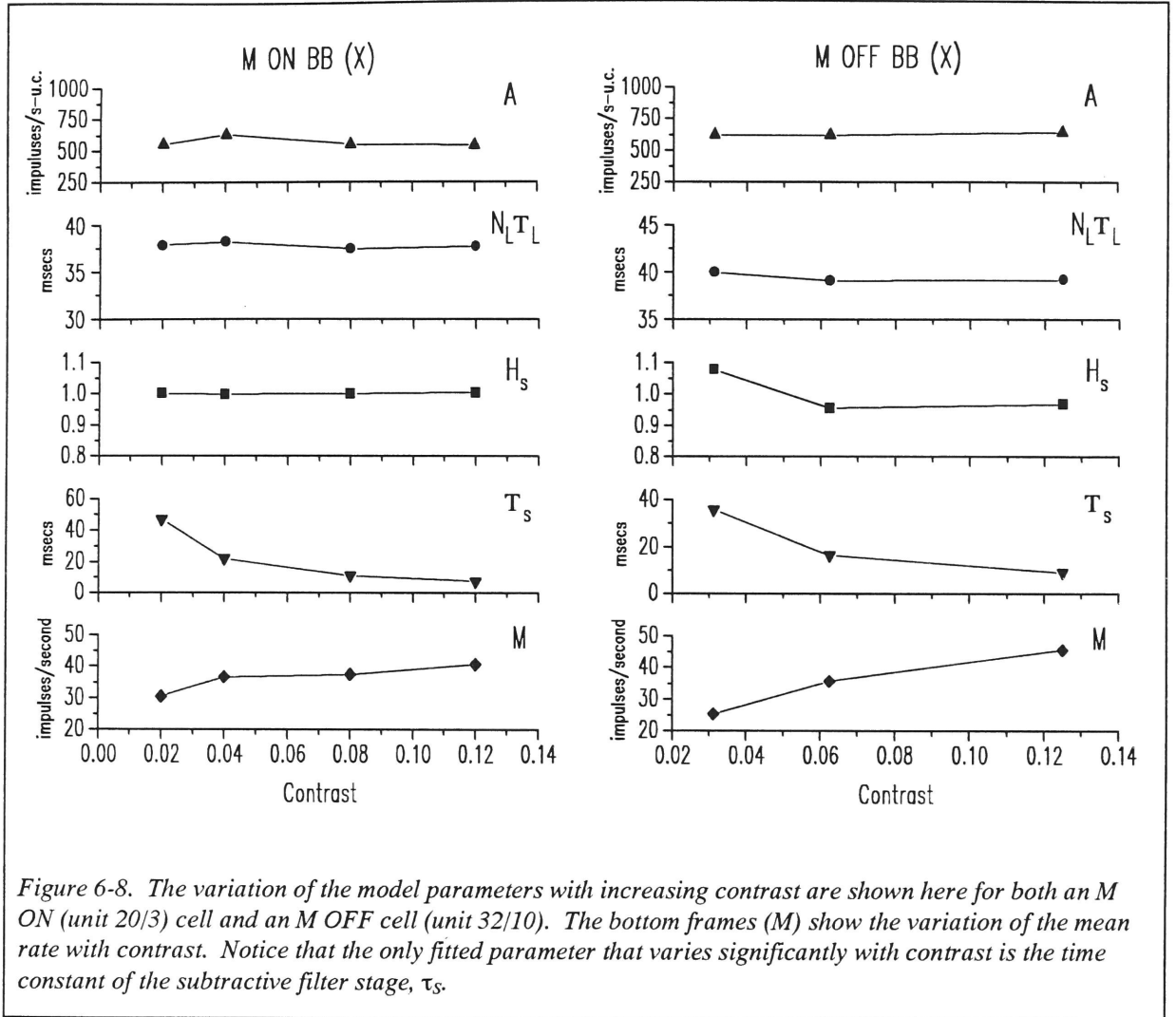
model to the data. In the figures for the 2 M cells, the lowest curve and the lowest set of points show the values of the gain at the highest contrast. As contrast increases the low frequency gain decreases progressively, although the gain remains nearly constant at the highest temporal frequency. The model also fits the phase of the response, which shows a progressive advance with increasing contrast for both M cells. The P cell's response (Fig. 6-7), on the other hand, demonstrates that the gain and phase of the P cell does not change with increasing contrast.



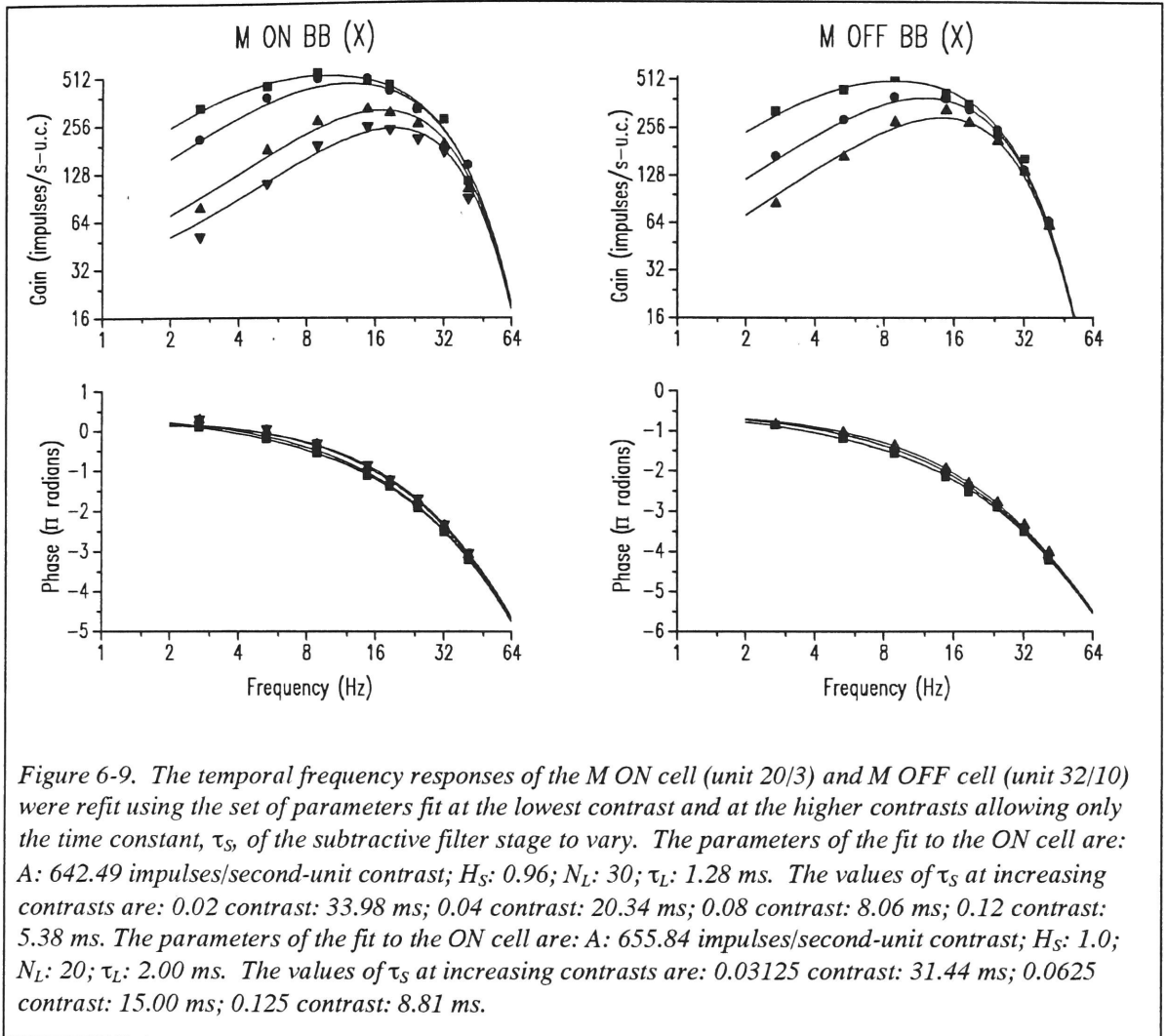
It is important to examine how the parameters in the model fits to M cell responses change with contrast (Fig. 6-8). The five fitted parameters, A , N_L , τ_L , H_S , and τ_S are shown in 4 graphs: this is because $N_L\tau_L$ is taken as a single parameter since the two parameters, N_L and τ_L , are strongly coupled, and it is their product which is the robust parameter. Also shown is the mean rate, M . The parameter of the model



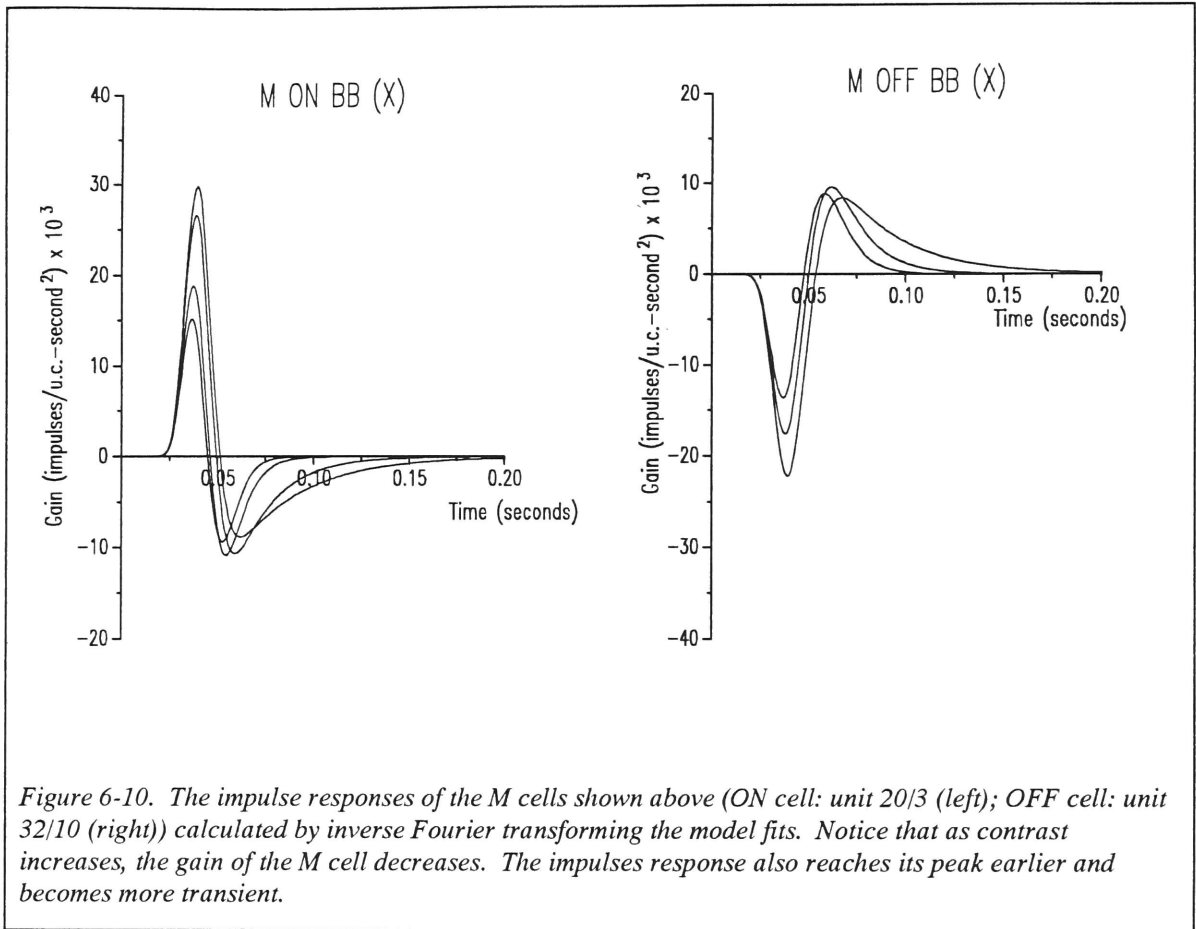
which deviates significantly with increasing contrast is τ_s which decreases. Thus, the influence of contrast is expressed in the model as a decrease in the time constant of the subtractive stage.



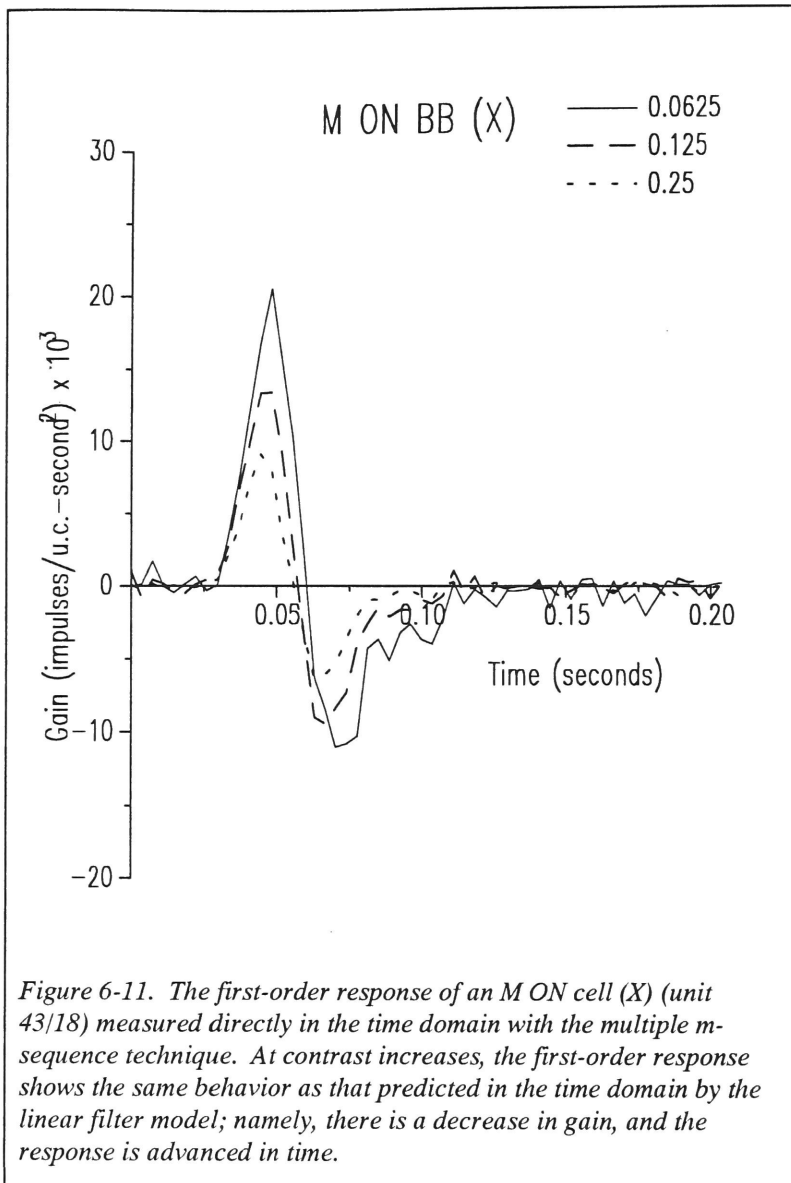
To be consistent with this contrast dependence of τ_s , the data sets, collected with increasing contrast, were fit at the lowest contrast and then a family of curves was generated by allowing only τ_s to vary as contrast increased (Fig. 6-9). Notice that these one-parameter fits generate results in close agreement with the data and the full five-parameter fit. Thus, just as in the cat retinal ganglion cells, the subtractive filter time constant is a good descriptor of the contrast gain control mechanism.



The fits of the temporal frequency data were transformed into the time domain to show how contrast modifies the impulses response of M cells (Fig. 6-10). For both the M ON and M OFF cells, increasing contrast lowers the overall height of the impulse response as well as slightly advances the peak, making the M cell response more transient and faster.



The impulse responses were observed in a different *M* cell using the m-sequence technique (Fig. 6-11). Here, the first-order time-domain kernels directly measured show the decrease in gain and the speed up of the response shown in the inverse Fourier-transformed data.



A population of 21 M cells were investigated with optimal sine gratings modulated with a sum of sinusoids signal. Table 6-1 is a summary of the fitted parameters. Since the spatial frequency of the stimulus was optimal for the M cell, it is probable that these parameters largely reflect the center dynamics of the M cell and are worth comparing across M cell subclasses. The M ON and OFF

population show significant differences in the degree to which they are transient (ON more transient than OFF) reflected in the parameters H_S and τ_S . In addition, there were slightly more stages needed to fit the ON cell data, although the overall delay in the ON cell response is not longer than the delay of the OFF cell response. The peak of the M cell response peaks on average at 40 ms. By comparison, the responses of P cell centers on average peak around 48 ms.

Table 6-1. The Fitted Parameters of the Linear Model to M cell Responses (at 0.0625 contrast)

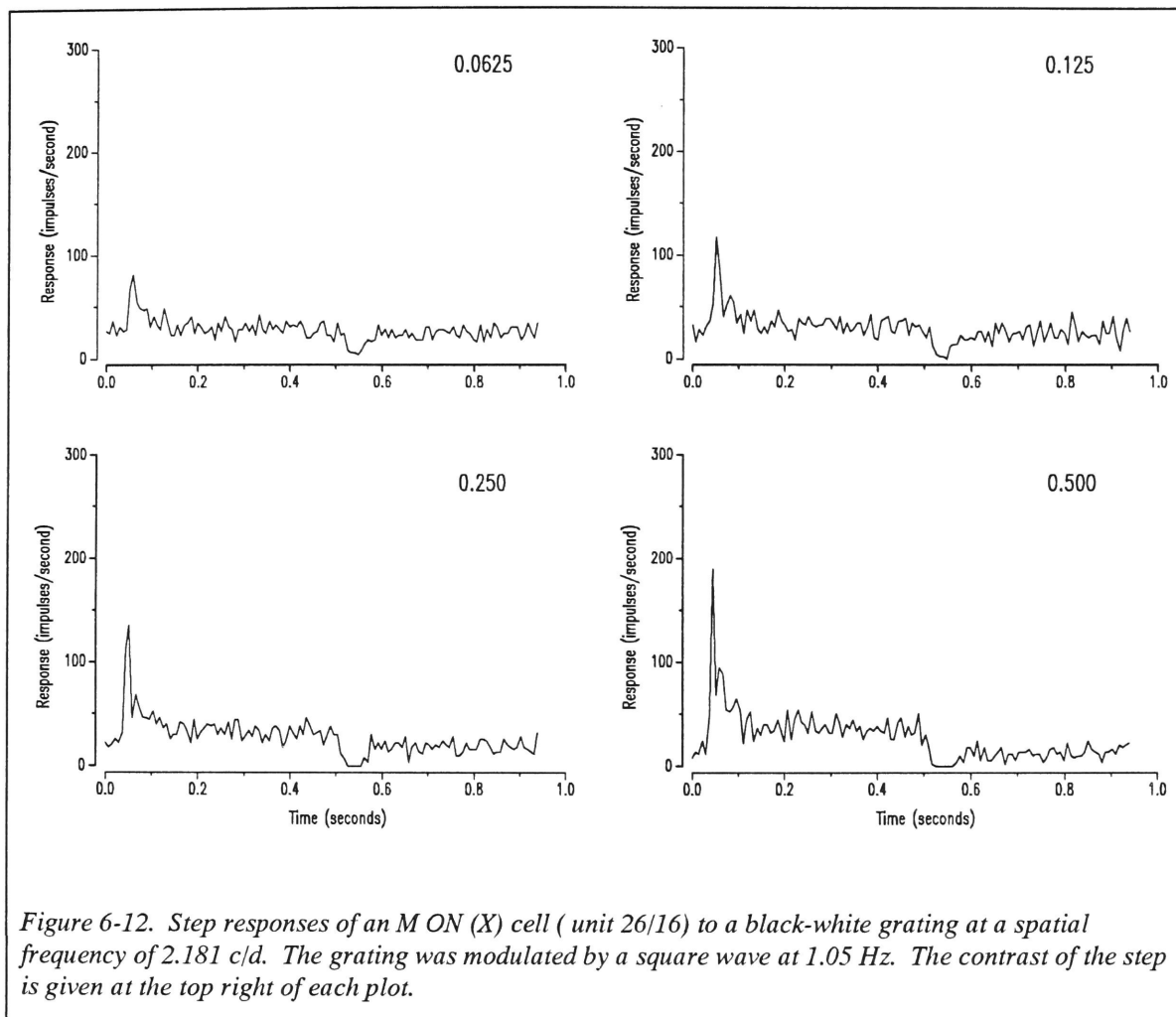
$N_{TOTAL} = 21$ $N_{ON} = 11$ $N_{OFF} = 10$ $N_Y = 2$ $N_X = 19$. P is the likelihood that the difference in mean between ON and OFF subsets occurred by chance.

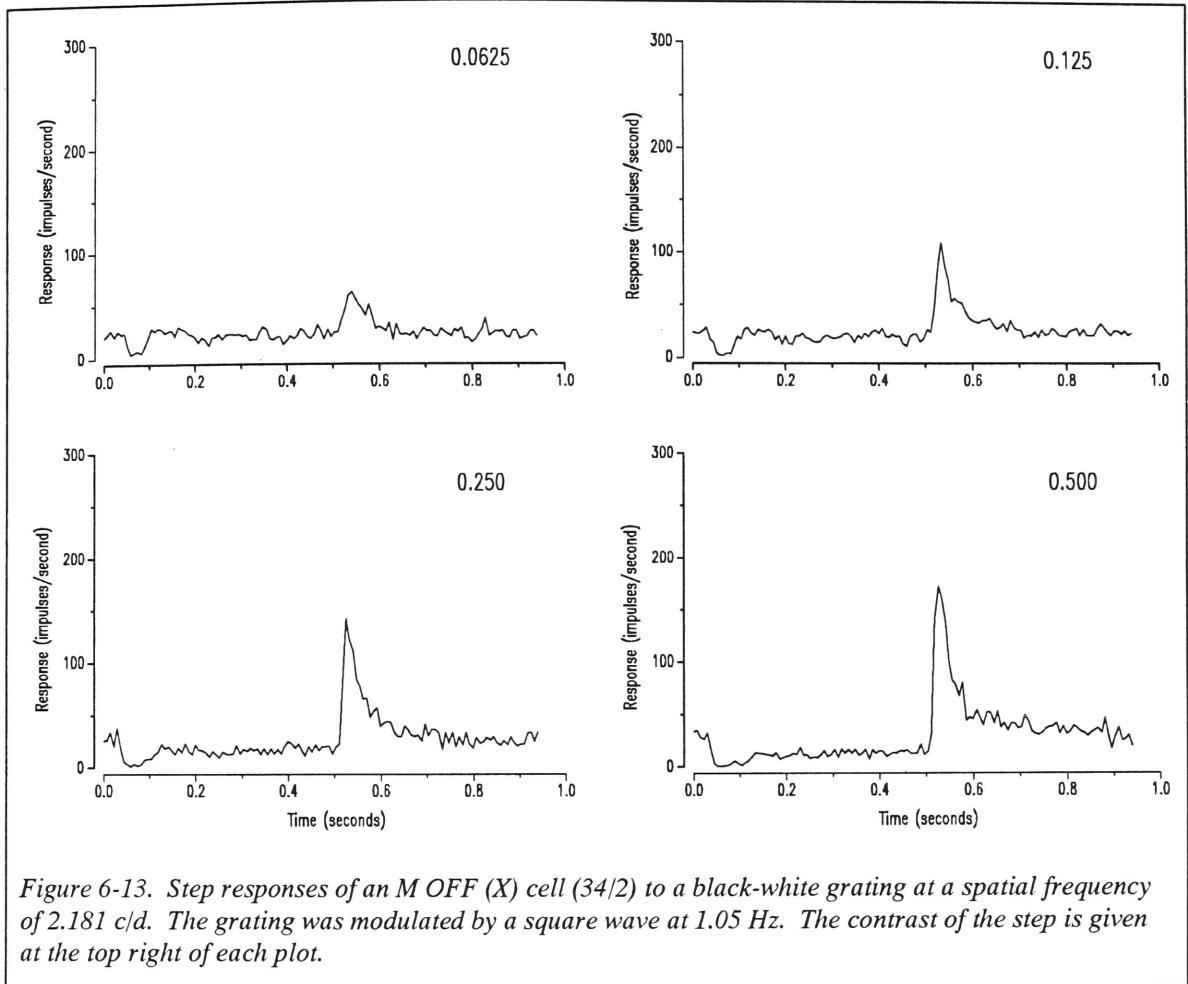
Parameter	M cell	Minimum	Maximum	Median	Mean	S.D.	C.V.	P
A (impulses/s-u.c.)	ON	273.05	984.26	419.00	513.67	213.46	0.42	> 0.1
	OFF	151.26	982.70	468.58	494.84	239.83	0.48	
	ALL	151.26	984.26	465.19	504.70	220.81	0.44	
$N_L \tau_L$ (ms)	ON	32.89	50.62	39.68	41.71	6.26		> 0.1
	OFF	37.327	53.65	41.17	42.31	4.77	0.15	
	ALL	32.89	53.65	41.05	41.99	5.47	0.11	
N_L (dimensionless)	ON	19	29	24	25	3.26	0.13	0.0023
	OFF	13	26	20	20.2	3.58	0.13	
	ALL	13	29	23	22.71	4.14	0.18	
H_S (dimensionless)	ON	0.95	1.21	1.00	1.01	0.07	0.18	0.0005
	OFF	0.82	0.98	0.92	0.91	0.05	0.07	
	ALL	0.82	1.21	0.97	0.97	0.08	0.05	
τ_S (ms)	ON	9.28	28.24	14.76	15.27	5.79	0.08	0.0068
	OFF	10.89	49.63	22.57	26.54	12.35	0.38	
	ALL	9.28	49.63	17.08	20.64	10.89	0.47	
D (ms)	ON	1	2.5	2	2.05	0.48	0.53	> 0.1
	OFF	2	2.5	2.4	2.31	0.23	0.23	
	ALL	1	2.5	2.25	2.17	0.40	0.10	
M (impulses/second)	ON	23.99	54.23	35.96	36.12	9.79	0.18	> 0.1
	OFF	23.8	48.62	29.85	32.12	7.54	0.27	
	ALL	23.8	54.23	30.89	34.22	8.81	0.23	
Eccentricity	ON	1	13	2.5	4.02	3.54	0.26	> 0.1
	OFF	1.5	4.5	3.13	3.33	1.11	0.88	
	ALL	1	13	2.5	3.69	2.64	0.33	

6.5 Step Responses

As illustrated by studies of the horseshoe crab, *Limulus*, (Brodie *et al.*, 1978a,b) and of the cat (Victor, 1987), step responses are a good way to test the predictive power of a dynamical model. The response to an optimal spatial frequency grating modulated by a square-wave at 1.05 Hz was measured for several M cells in addition to their responses to the sum of sinusoids stimulus. The step responses of an M ON and an OFF cell are shown in Figs. 6-12 and 6-13. The responses of each cell are shown at 4 contrasts. The increasing low frequency attenuation of the M cell response at higher contrasts is shown

here in a new way. As the contrast of the step increases, the responses of both the ON and the OFF M cell become more sharply peaked. These data illustrate why M cells were originally designated phasic cells by Gouras (1968).





The data shown here for M cells suggest that the overall contrast is used by the M cell to modify its temporal frequency response. As demonstrated in the cat (Victor, 1987), to a first approximation, the frequency response measured at a given level of contrast can be used to predict the response of the cat X cell center to a step in contrast. However, the further the contrast of the step deviates from the RMS level contrast used to measure the frequency response, the less accurate the prediction. The frequency responses at low contrast accurately predict low contrast step responses; however, at high contrast, they overestimate the height of the response and underestimate the sharpness of the peak. By

comparison, frequency responses obtained at high contrast underestimate the response to low contrast steps and predict a faster time course than the measured response (Figs. 6-14 and 6-15). In every respect, these data mimic the results found in the cat X cell by Victor (1987) and suggest that M cells use a dynamic measurement of contrast to modify their frequency responses.

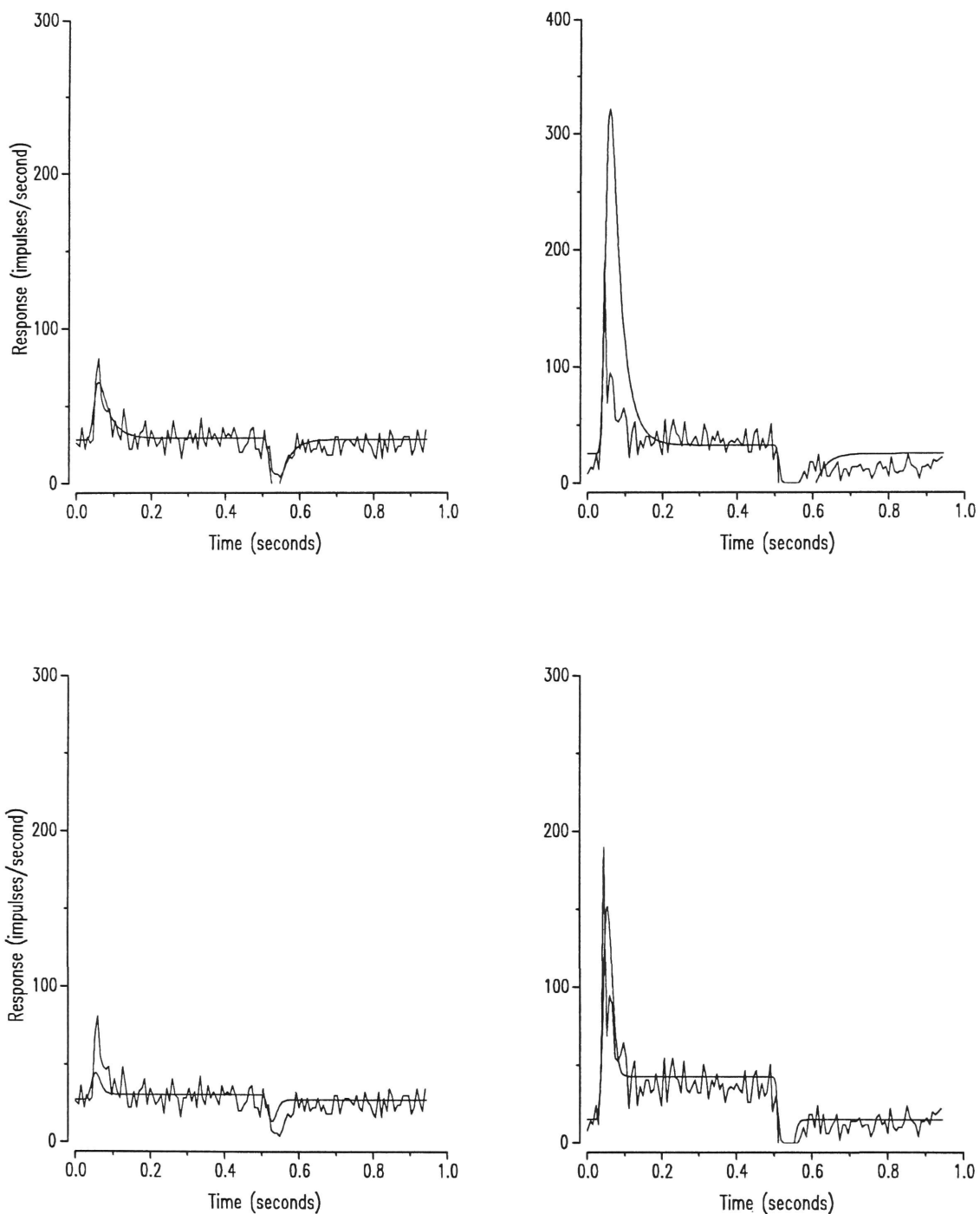


Figure 6-14. Comparison of the step responses of an M ON cell (unit 26/16) at two levels of contrast (0.0625 left column; 0.5 right column). The solid lines show the predictions of the fitted linear filter model using Fourier synthesis. The top row shows the predictions of the model fit at 0.03125 contrast. On the bottom, the prediction of the model fit at 0.0125 contrast is shown. Notice that the low contrast model overpredicts the high contrast step and is too sustained. Conversely, the high contrast model underpredicts the low contrast step and is too transient.

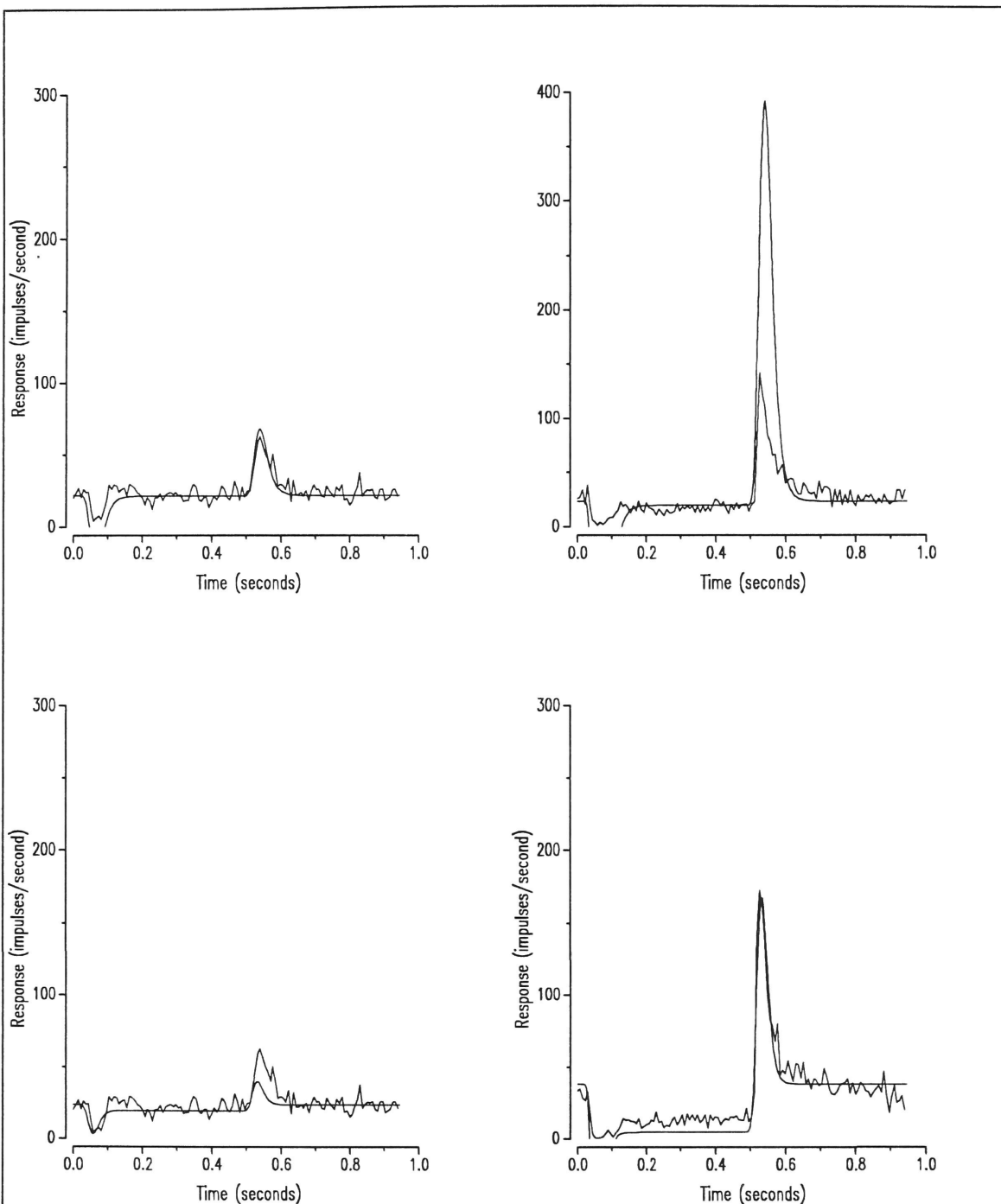


Figure 6-15. Comparison of the step responses of an M OFF cell (unit 34/2) at two levels of contrast (0.0625 left column; 0.50 right column). The solid lines show the predictions of the fitted linear filter model using Fourier synthesis. The top row shows the predictions of the model fit at 0.03125 contrast. On the bottom, the prediction of the model fit at 0.125 contrast is shown. Notice that the low contrast model overpredicts the high contrast step and is too sustained. Conversely, the high contrast model underpredicts the low contrast step and is too transient.

6.6 M Cell Chromatic Responses

Having explored the basic aspects of the contrast gain control in M cells, it was also of interest to explore how M cells respond to chromatic contrast and how that might relate to the contrast gain control. Recall that Derrington *et al.* (1984) concluded that LGN magnocellular cells are both spatially and spectrally opponent. Low spatial frequency gratings that stimulated L and M cones selectively as well as an isoluminant grating and a grating that stimulated a combination of L and M cones in synchrony were used to explore these questions. Using these gratings, an *ad hoc* classification scheme identified 3 types of M cell, 14 of which were analyzed in detail. The first type had significant responses to both L and M cone-isolating gratings (8 of 14). Unlike P cells, however, these responses were not opponent (Fig. 6-16). The relative magnitude of the response to the L cone- and M cone-isolating gratings is approximately proportional to the luminance energy in these stimuli. The response to the L cone-isolating grating being approximately twice that of the M cone-isolating grating. The responses of this cell type to an isoluminant grating are weak and unreliable. However, the response to an L+M grating is large and resembles the response to an achromatic (black-white) grating.

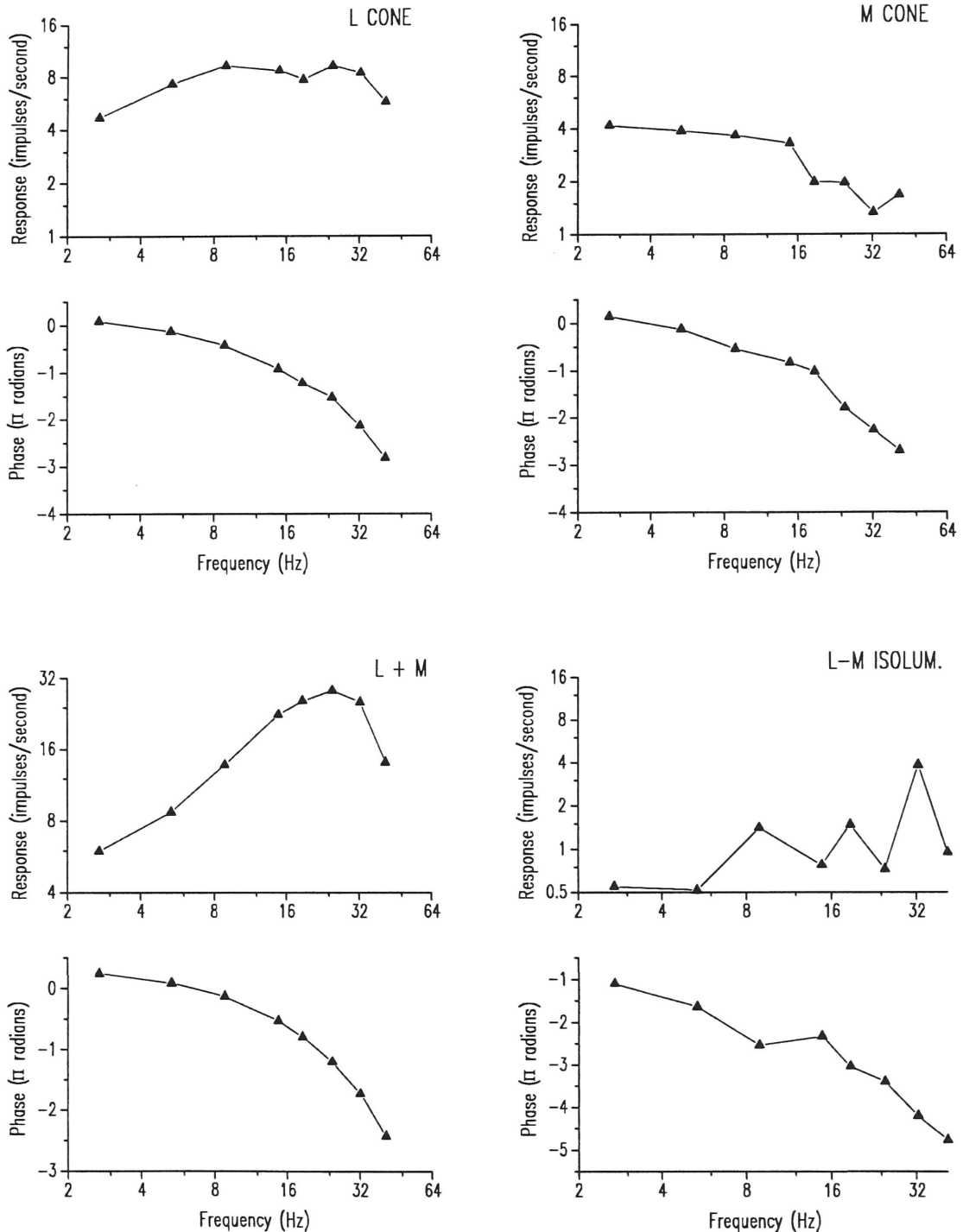


Figure 6-16. The temporal frequency responses of an M ON (X) cell (unit 37/5) to chromatic gratings modulated by a sum-of-sinusoid stimulus. The gratings were modulated by a sum of sinusoids. The contrast of the gratings was 0.125 per sinusoid. The spatial frequency was 0.145 c/d. This cell shows responses to both L and M cone-isolating gratings, but the response is nulled by the isoluminant (L-M) grating. The cell also shows a strong response to the L+M grating.

The next class of M cells (5 of 14) had responses to L cone-isolating gratings that were much greater than the weak or insignificant responses to M cone-isolating gratings (Fig. 6-17). Notice that, for this cell, the isoluminant grating produces a significant response because this cell has little M cone input that would otherwise null the L cone input.

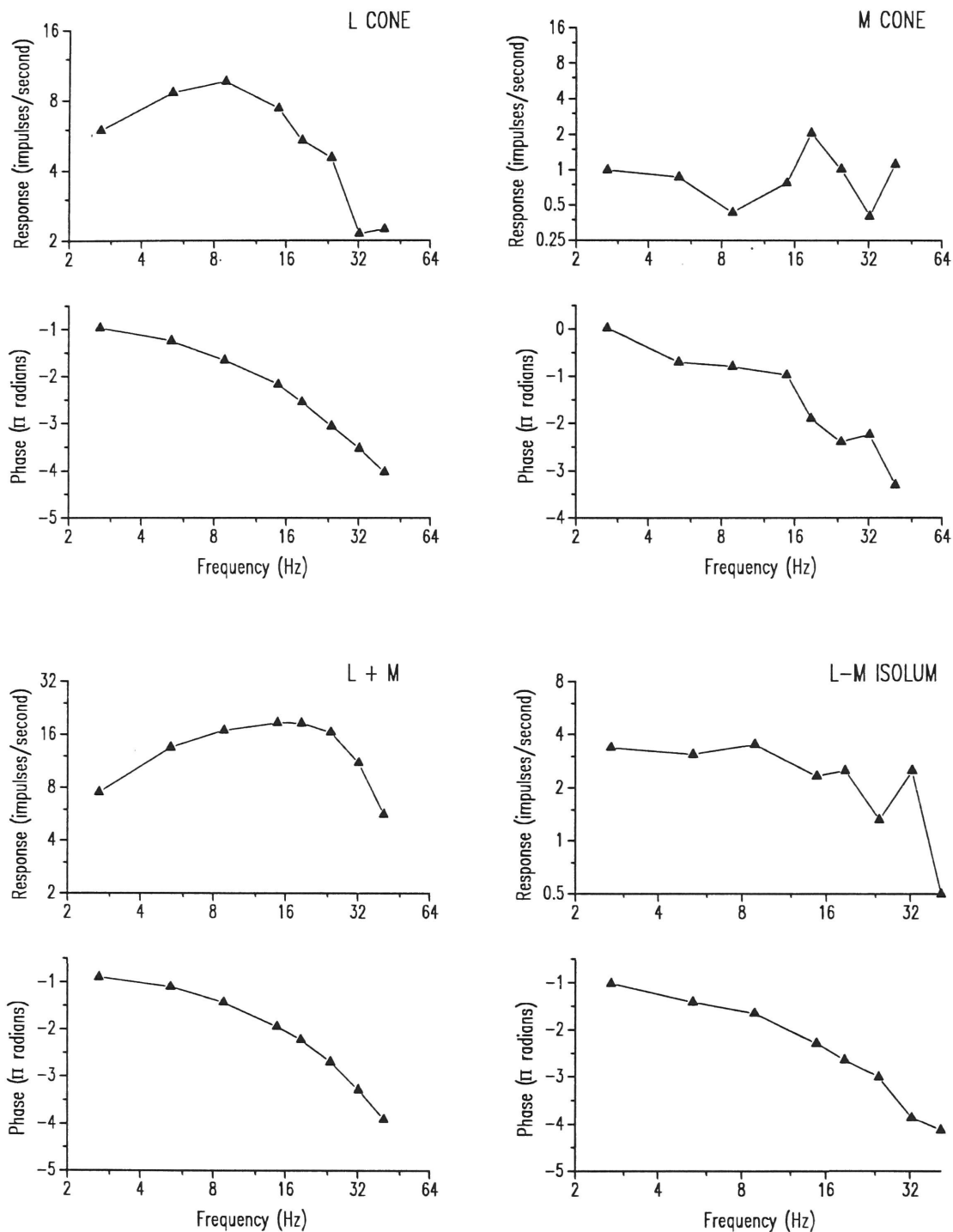


Figure 6-17. Temporal frequency responses of an M OFF (X) cell (unit 28/52). The stimulus conditions were the same as described in Fig. 6-16. This cell shows strong responses to the L cone-isolating grating but weak responses to the M cone-isolating grating. For this cell, the isoluminant grating does not null out the response.

Finally, a third type of cell, one of which was analyzed in detail (although a few others were encountered) had both L and M cone input but the response to the L cone-isolating gratings were opponent to the response to the M cone-isolating gratings (Fig. 6-18). Furthermore, the L cone input seemed to be a surround contribution since the response was eliminated with a high spatial frequency grating although the M cone response was still strong. In addition, the response to the M cone-isolating grating had the same signature as the overall response. For this cell notice that the isoluminant grating does not null out the response. This cell type is probably what Wiesel and Hubel (1966) called the type IV cell.

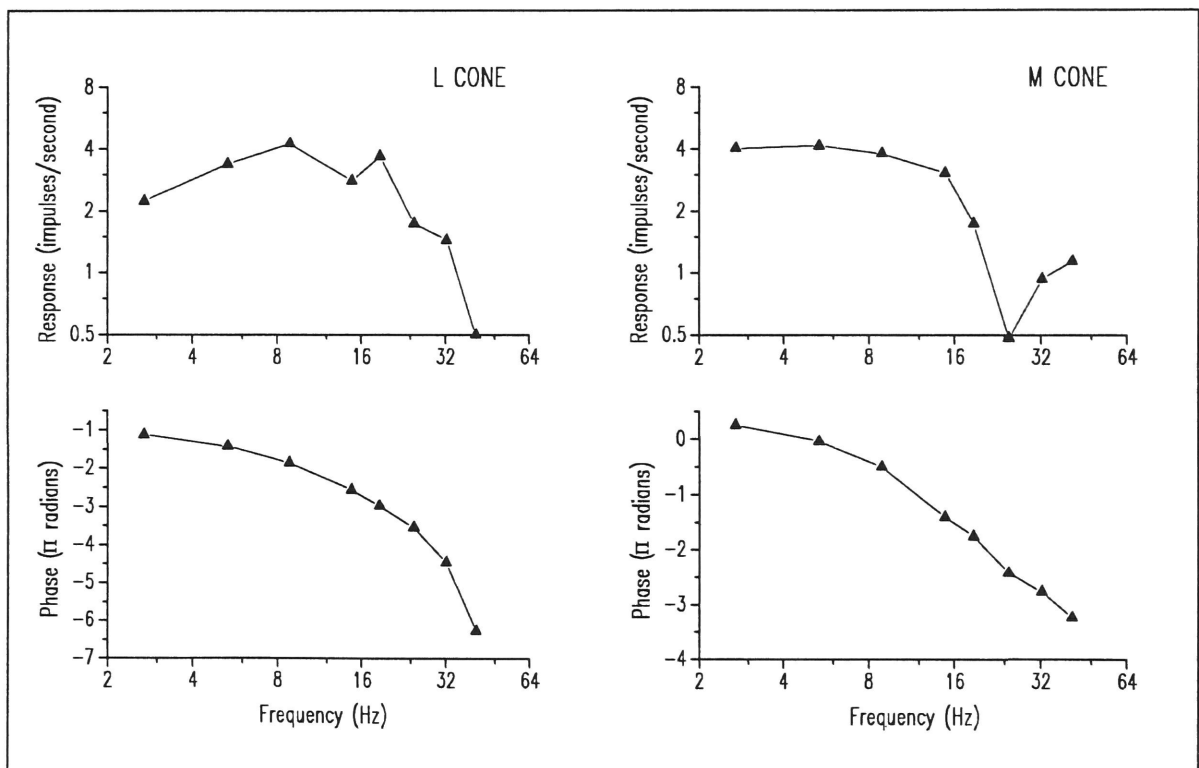


Figure 6-18. Continued (with caption) on following page.

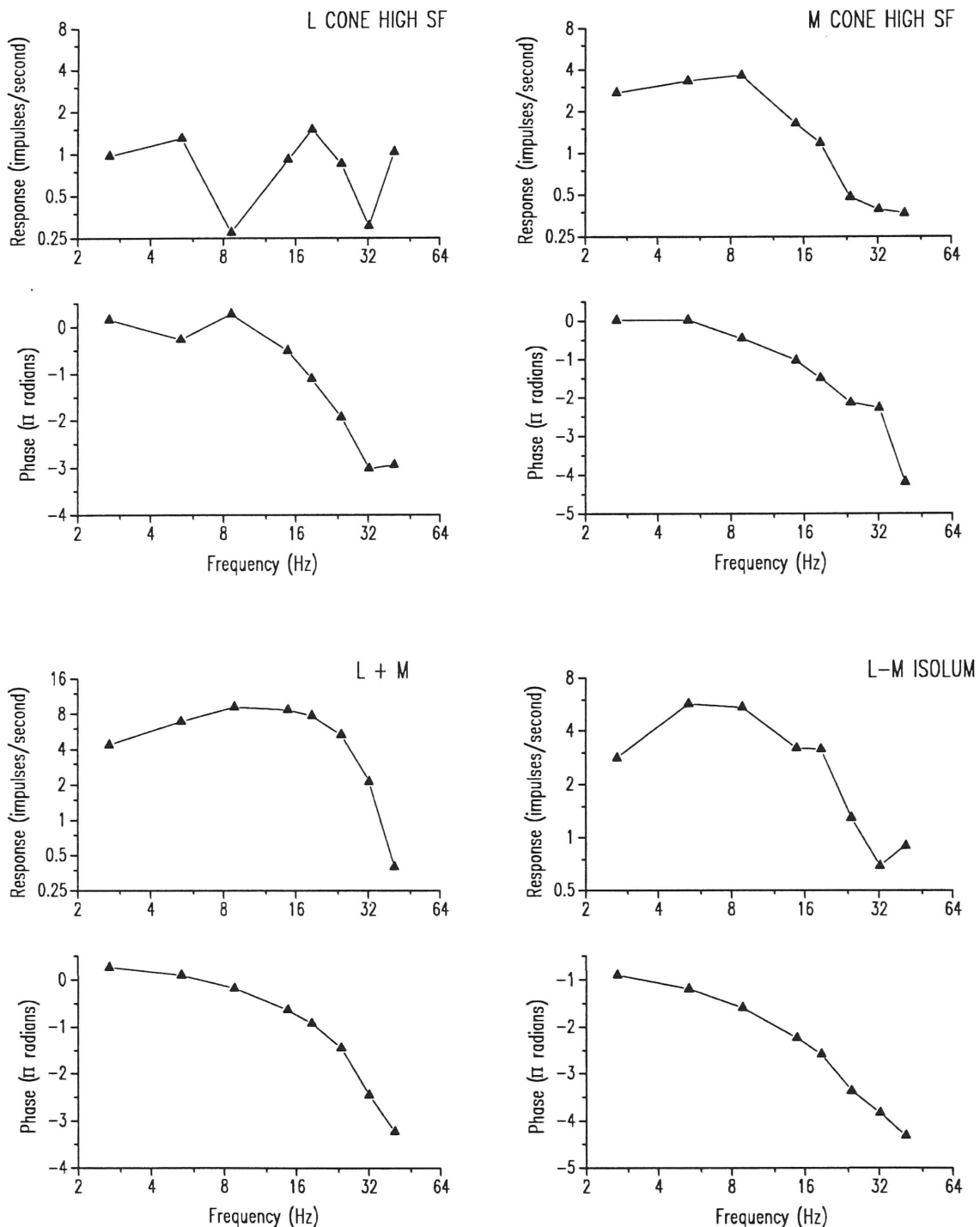


Figure 6-18. The temporal frequency responses of an M ON cell (unit 41/33) that shows opponent responses from an L cone-driven surround. The stimulus conditions are the same as described in Fig. 6-16 except that a high spatial frequency (2.181 c/d) set of L cone-isolating and M cone-isolating gratings is included. Notice that this cell shows opponent responses to the low spatial frequency L cone-isolating and M cone-isolating gratings (previous page).

The same two major types of M cells were encountered with the multiple m-sequence method. One cell showed first-order responses to both an L cone-isolating grating and an M cone-isolating grating and a null to the isoluminant grating (Fig. 6-19, top). The second cell showed responses only to an L cone-isolating grating (Fig. 6-19, bottom).

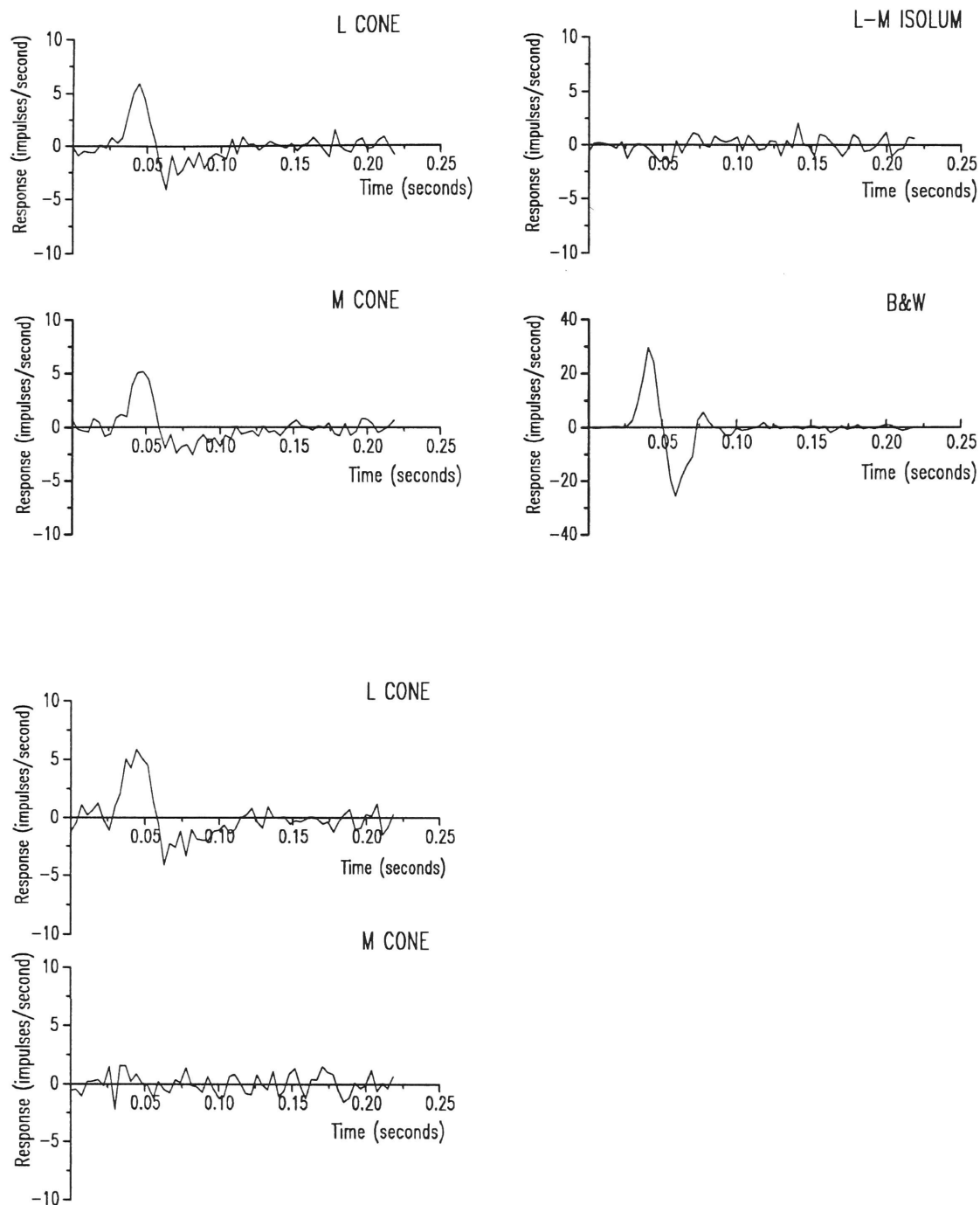


Figure 6-19. First-order responses of two M cells obtained in the time domain with the multiple m-sequence method. The chromatic and achromatic gratings were modulated by the sum of two m-sequences at a contrast of 0.25. The spatial frequency of these gratings was 0.145 c/d. Top two rows) an M ON cell (unit 28/54) with L and M cone-driven responses and nulled out by the isoluminant grating. Bottom rows) an M ON cell (unit 43/18) that is primarily driven by L cones.

From these data, it is clear that the peak of the temporal frequency response to cone-isolating gratings is generally lower than the peak to achromatic gratings. However, if the luminance energy in the chromatic and achromatic stimuli is equated, the shape of the two responses is the same (Fig. 6-20). On the left, the frequency response to an L cone-isolating stimulus is shown. On the right is the family of curves showing the response to black-white gratings of increasing contrast. The typical progression of phase advance and peak temporal frequency is shown. The L cone stimulus has approximately the same luminance as the black-white grating that produced the lowest response curve on the right. These data suggest that the luminance contrast provides the signal for the contrast gain control.

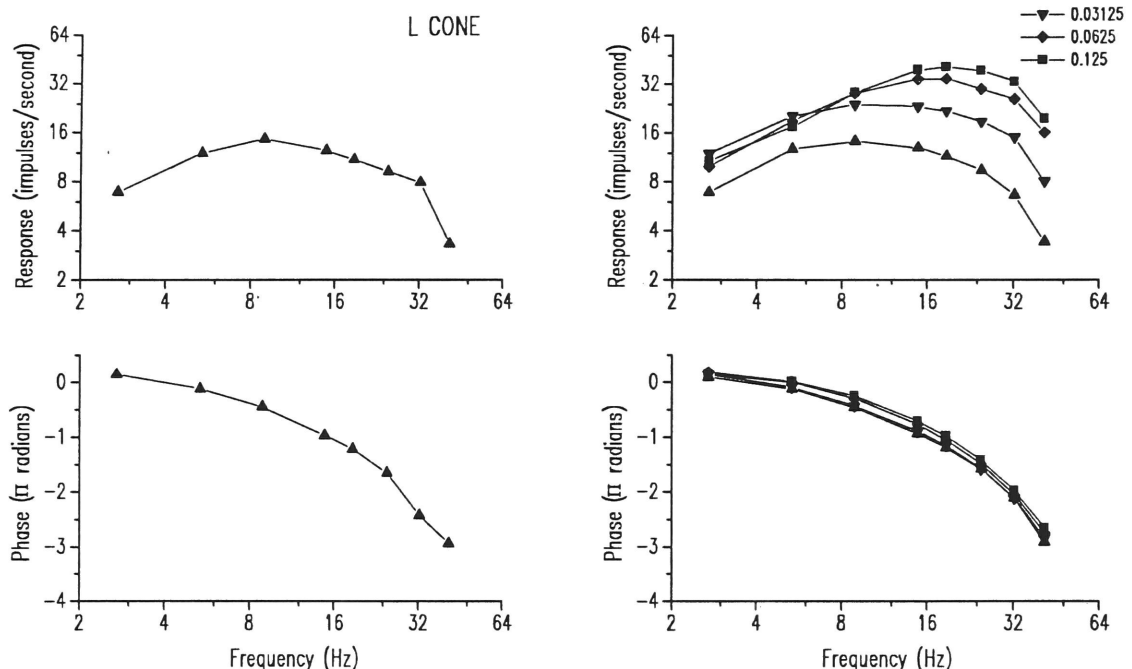
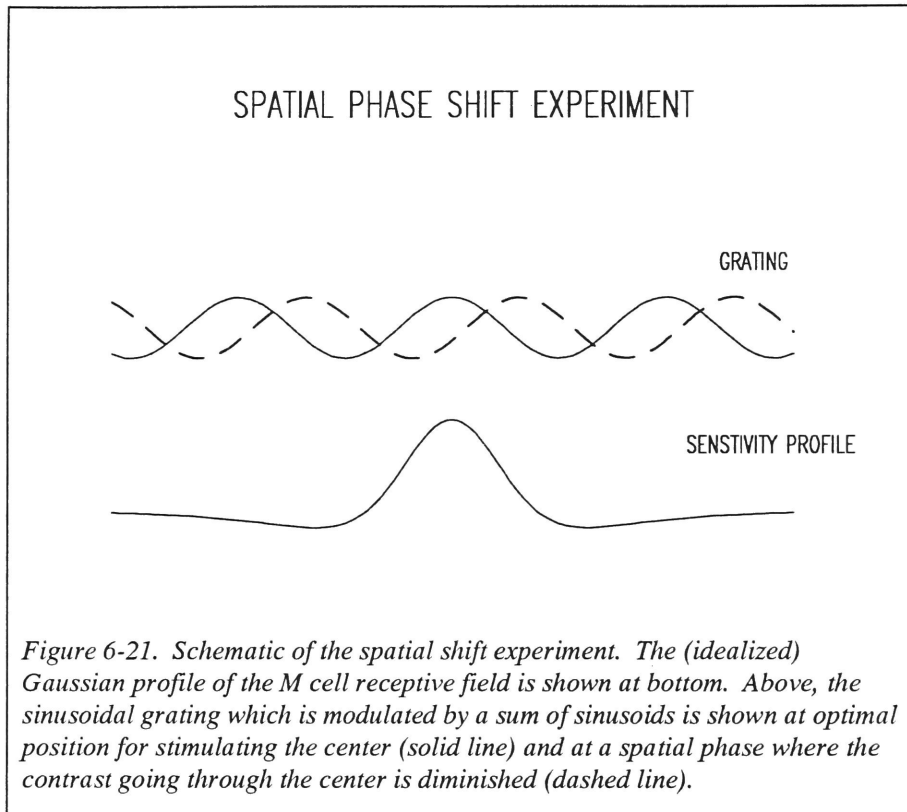


Figure 6-20. Comparison of the response of an M cell to chromatic and achromatic stimuli. On the left, the temporal frequency responses of an M ON (X) cell (unit 43/15) to an L cone-isolating grating (0.727 c/d) modulated with a sum of sinusoids. On the right are the responses of the same cell to black-white gratings (0.727 c/d) of increasing contrast. The amplitude and phase of the response to the L cone-isolating grating approximately matches that of the response to the lowest contrast black-white grating. These two stimuli are closely matched for luminance contrast.

6.7 The Spatial Profile of the Contrast Gain Control

Work on cat retinal ganglion cells showed that the contrast gain control signal most likely was produced by a spatially distributed network of small subunits that adjusts the response of the receptive field center (Shapley and Victor, 1979b, 1981). It was important to test this idea in the monkey since it was possible that a similar dynamical phenomenon could be produced by a different spatial organization. To test this notion, the spatial phase shift experiment used by Shapley and Victor was tried on M cells (Benardete *et al.*, 1992b).

Shifting the spatial phase of the sum-of-sinusoids-modulated grating reduces the contrast on the receptive field center and the reduces the overall size of the response (Fig. 6-21).



If the characteristics of the temporal frequency response are controlled by the size of the contrast signal going through the center mechanism of the M cell, then shifting the phase of the grating would reduce the peak temporal frequency of the response. However, if the measure of contrast comes from a distributed network of small subunits, shifting the phase will reduce the amplitude of the response, but in addition, the overall shape of the amplitude curve will reflect the high contrast signal over that part of the retina. The M cell does indeed use a spatially distributed measure of contrast to feed the contrast gain control (Fig. 6-22). On the left, notice that shifting the phase of the grating

greatly reduces the overall size but does not change the shape of the temporal frequency response. On the right, the shift experiment demonstrates that although the shifted grating may give rise to a smaller center response, it is the amount of ambient contrast that sets the gain control.

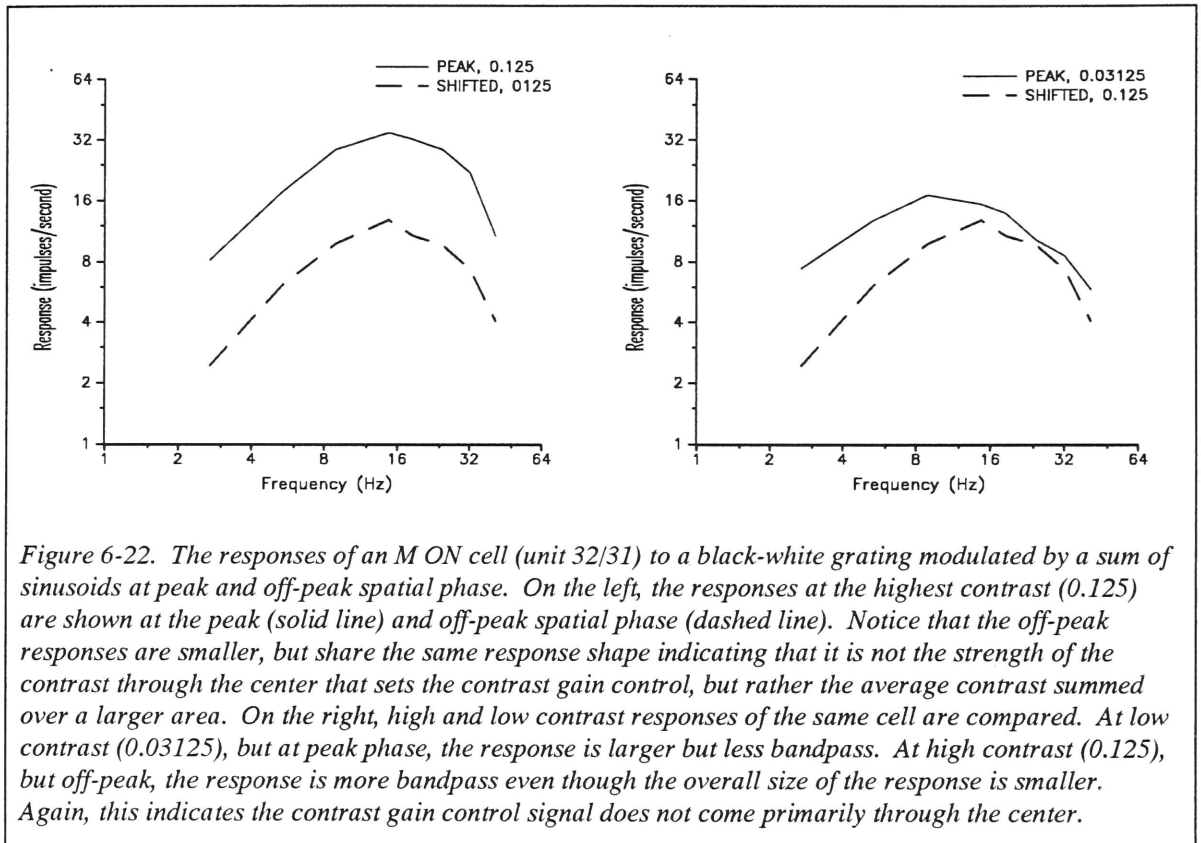


Figure 6-22. The responses of an M ON cell (unit 32/31) to a black-white grating modulated by a sum of sinusoids at peak and off-peak spatial phase. On the left, the responses at the highest contrast (0.125) are shown at the peak (solid line) and off-peak spatial phase (dashed line). Notice that the off-peak responses are smaller, but share the same response shape indicating that it is not the strength of the contrast through the center that sets the contrast gain control, but rather the average contrast summed over a larger area. On the right, high and low contrast responses of the same cell are compared. At low contrast (0.03125), but at peak phase, the response is larger but less bandpass. At high contrast (0.125), but off-peak, the response is more bandpass even though the overall size of the response is smaller. Again, this indicates the contrast gain control signal does not come primarily through the center.

A further clue to the spatial organization of the contrast gain control is the fact that a small central spot does not invoke the contrast gain control as a center-isolating grating does (Fig. 6-23).

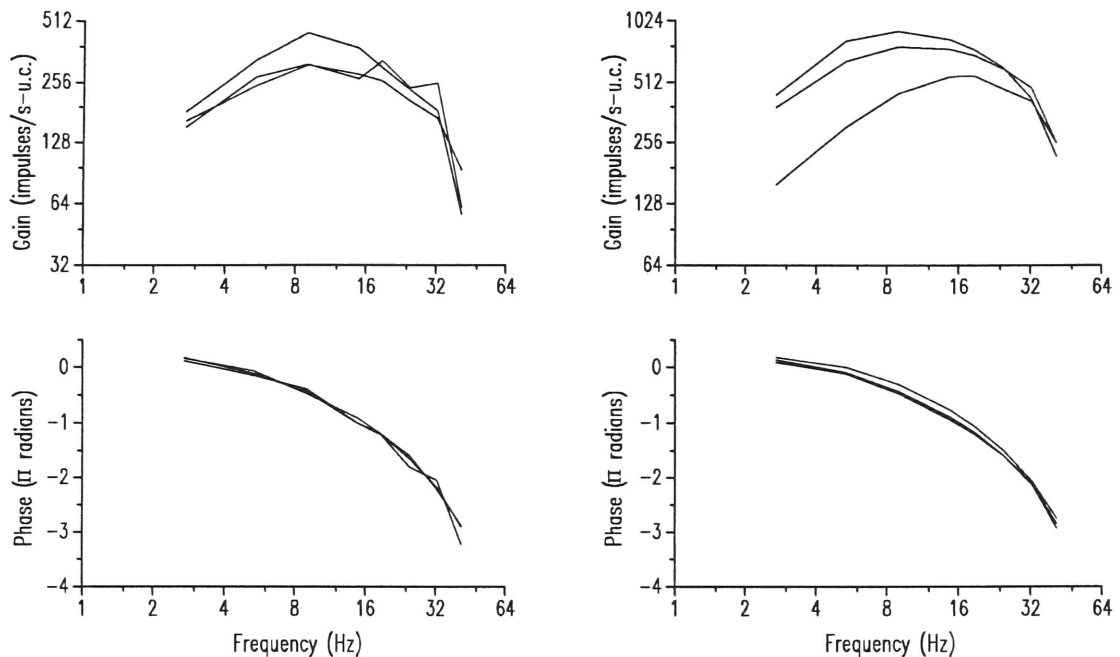


Figure 6-23. Gain and phase of the response of an M ON cell (unit 43/15) to a spot (left) and a grating (0.727 c/d) (right) of increasing contrast. The curves on the right show the contrast gain control effect with increasing contrast (0.015625, 0.03125, 0.0625) while the response to the small spot (0.5 deg radius) does not show the contrast gain control effect. The largest gain curve for the spot for the lowest contrast and is at the top, while the other curves nearly overlap. The phase curves are overlapping for all three conditions. On the right, the gain curve for the lowest contrast grating is at the top while the gain curve for the highest contrast grating is at the bottom. The phase of the response advances with increasing contrast as shown below.

When a surrounding annulus is modulated, it changes the dynamics of the response to a central spot even when the annulus contains high spatial frequencies (Fig. 6-24). In successive episodes, the annulus was modulated with either a positive or a negative contrast of the same magnitude while the spot was also modulated by a sum-of-sinusoids signal. The response of the unit on these two trials was averaged to eliminate the first-order response to the annulus. The remaining response indicates the response to the spot in the presence of surround modulation. An earlier observation called the “shift effect” in which light in far outside the classical receptive field modulates the response of cells in the

magnocellular layers of the LGN (McIlwain, 1966; Krüger *et al.*, 1975; Krüger, 1977) is probably a reflection of the contrast gain control mechanism.

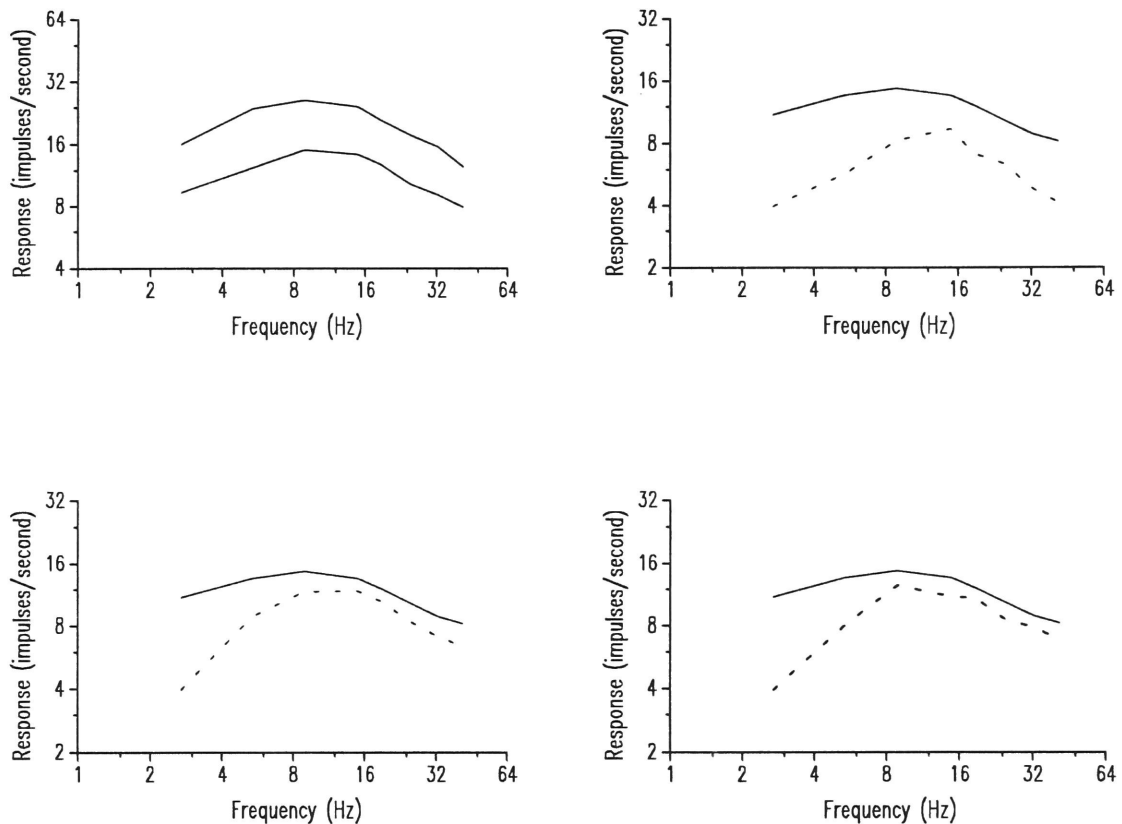
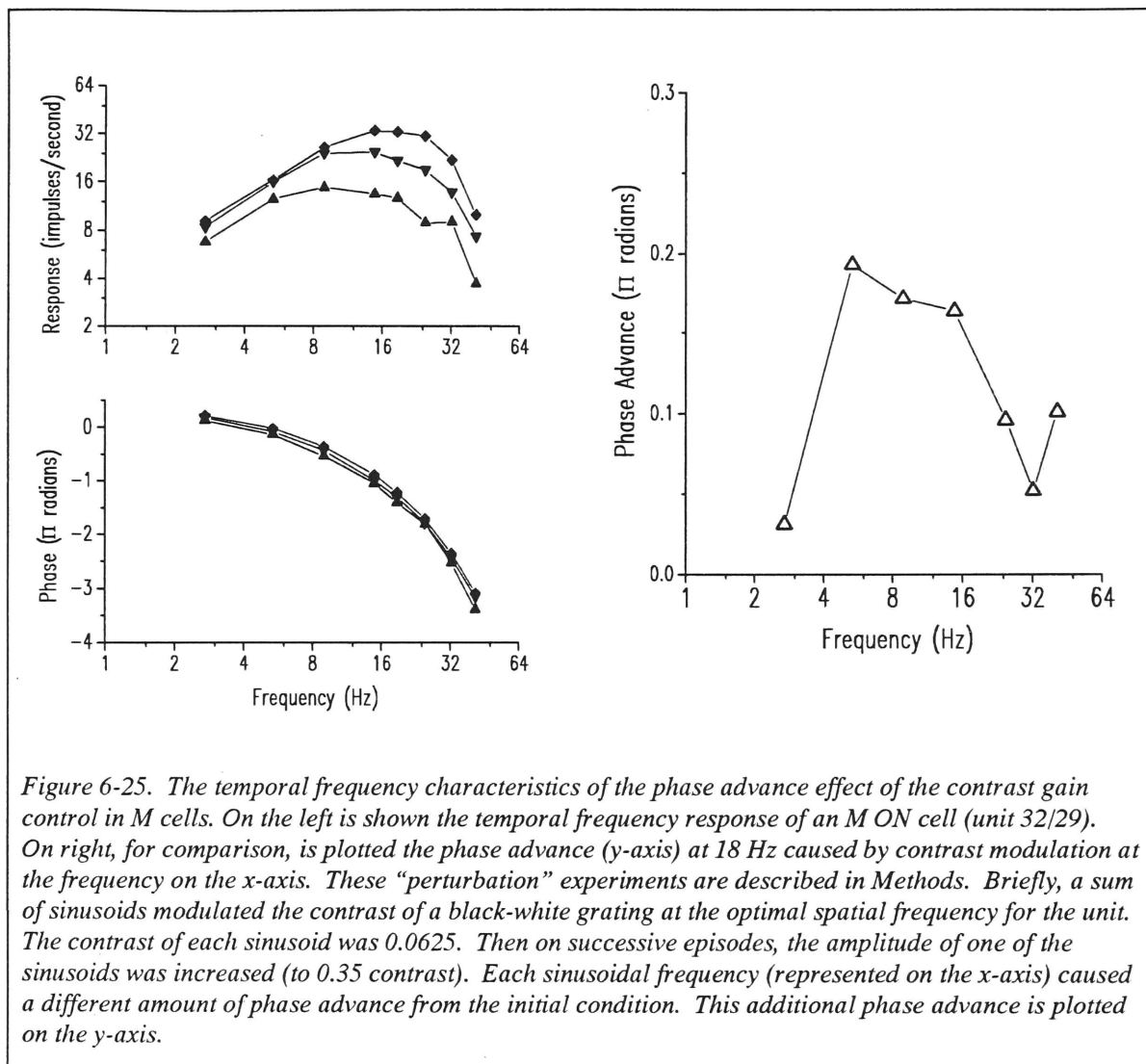


Figure 6-24. Temporal frequency responses of an M ON (Y) cell (unit 47/45) to a small spot (0.5 deg) with increasing amount of contrast in a surrounding annulus (0.5 deg ID, 3.5 deg OD). Upper left shows the amplitude of the response to the spot at two contrasts (0.03125 and 0.0625). Upper right, the surrounding annulus is modulated at 0.125 contrast and the spatial frequency 0 (dashed curve). Bottom left) annulus is modulated at 0.125 contrast at 0.727 c/d. Bottom right) the annulus is modulated at 0.125 contrast and 2.181 c/d.

6.8 The Temporal Characteristics of the Contrast Gain Control

An additional set of pilot studies, also suggested by work on cat retinal ganglion cells (Shapley and Victor, 1978), examined which frequencies were most effective in

advancing the phase of the M cell response. The perturbation experiments are described in Methods. From these studies, the frequencies for phase advancement basically follow a transfer function similar to the first-order temporal frequency response (Fig. 6-25).



6.9 Nonlinear Responses

Although many of the M cells studied seemed X-like (i.e. with linear spatial summation), they demonstrated reproducible second-order kernels. These second-order

responses were not due to truncation as can be seen from the asymmetrical shape of the frequency kernel. In addition, in most cases, the mean rate was such that the amount of truncation would be minimal. Typical second-order response from an M ON and an M OFF cell were fit to the LNL model (Figs. 6-26 -6-27). Measurements of these second-order responses with increasing contrast showed that the size of the second-order response increases proportionally with contrast suggesting that the source of this nonlinearity may be the same kind of rectifying subunit as found in the cat (Victor and Shapley, 1979a,b). Table 6-2 summarizes the parameters of LNL model fits to the second-order responses. The LNL model was fit only to data from complete or nearly complete phase sets (see Methods) in order to avoid higher-order contamination of the second-order kernel as much as possible.

The average pre- and post-nonlinearity filters in the LNL model fit are shown in Fig. 6-28. The pre-nonlinearity filter, U , has similar characteristics to the first-order frequency kernel of M cells (*cf.* Fig. 6-9). The post-nonlinearity filter, W , has very sharp bandpass characteristics and very little phase roll-off. The values of the LNL fits did not differ significantly between the ON and OFF populations.

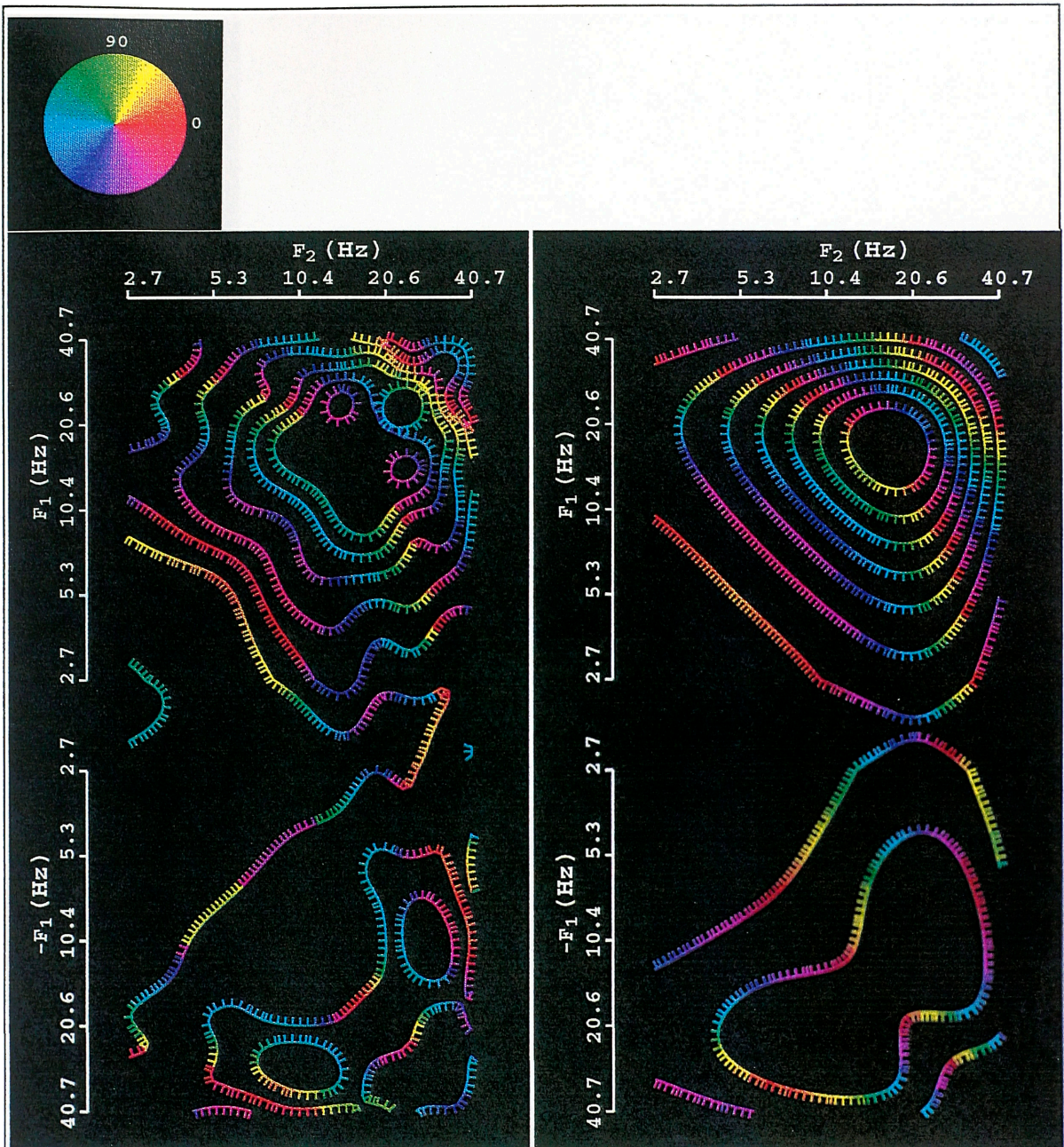


Figure 6-26. The second-order responses of an M ON (X) cell (unit 20/3) on the left and the fit of the LNL model on the right. The contours are separated by 1.4 impulses/second (0.727 c/d) and the tick marks point in the downhill direction. The contrast of the grating was 0.12. The color of the contours represents the phase of the response as indicated by the color circle above. The parameters of the LNL fit are: A: 121121 impulses/second-unit contrast²; $H_{S,U}$: 0.99; $\tau_{S,U}$: 2.53 ms; $N_{L,U}$: 16; $\tau_{L,U}$: 2.53 ms; $H_{S,W}$: 0.93; $\tau_{S,W}$: 1.64; $N_{L,W}$: 3; $\tau_{L,W}$: 1.64 ms; D: 2.0 ms.

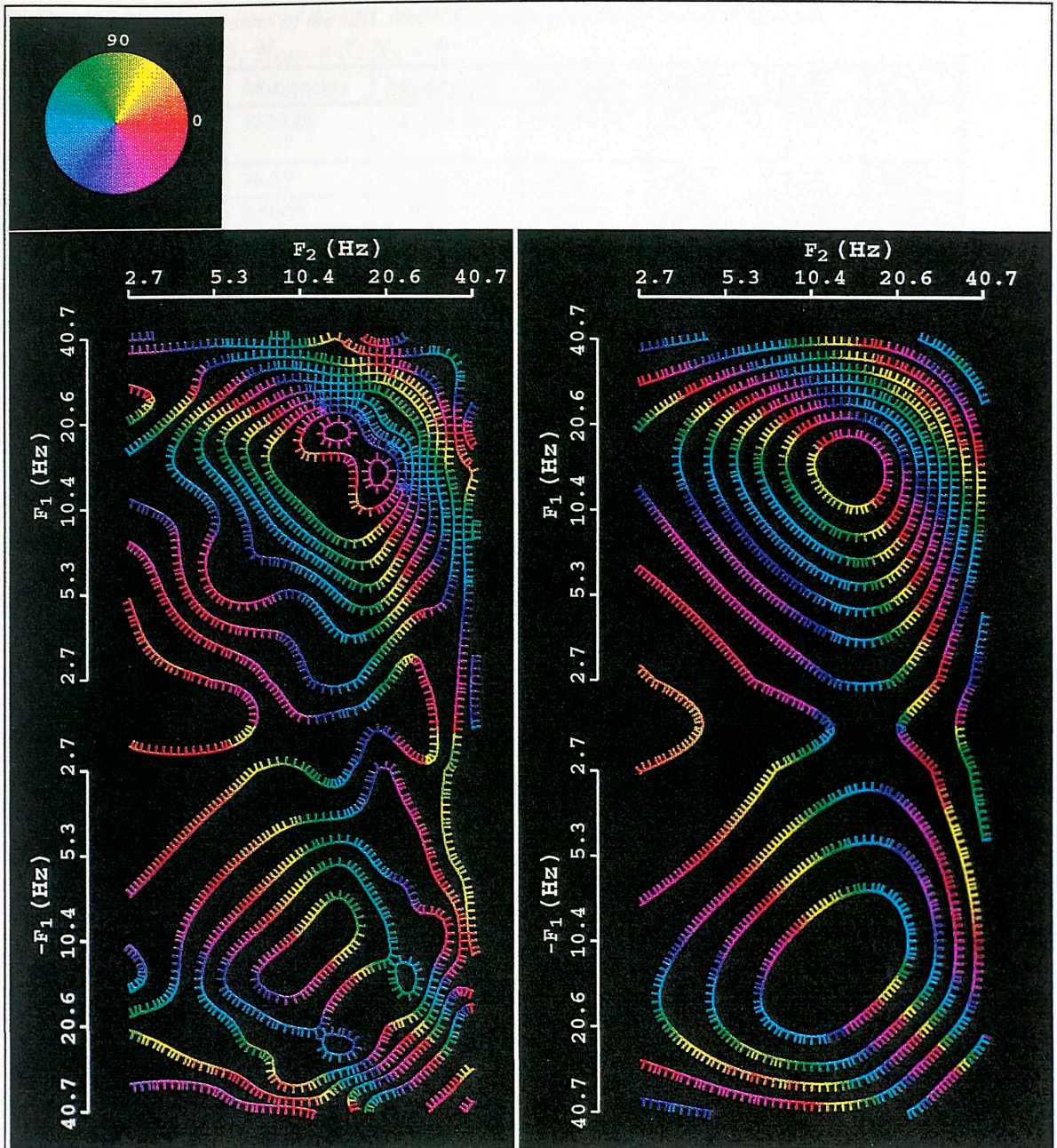
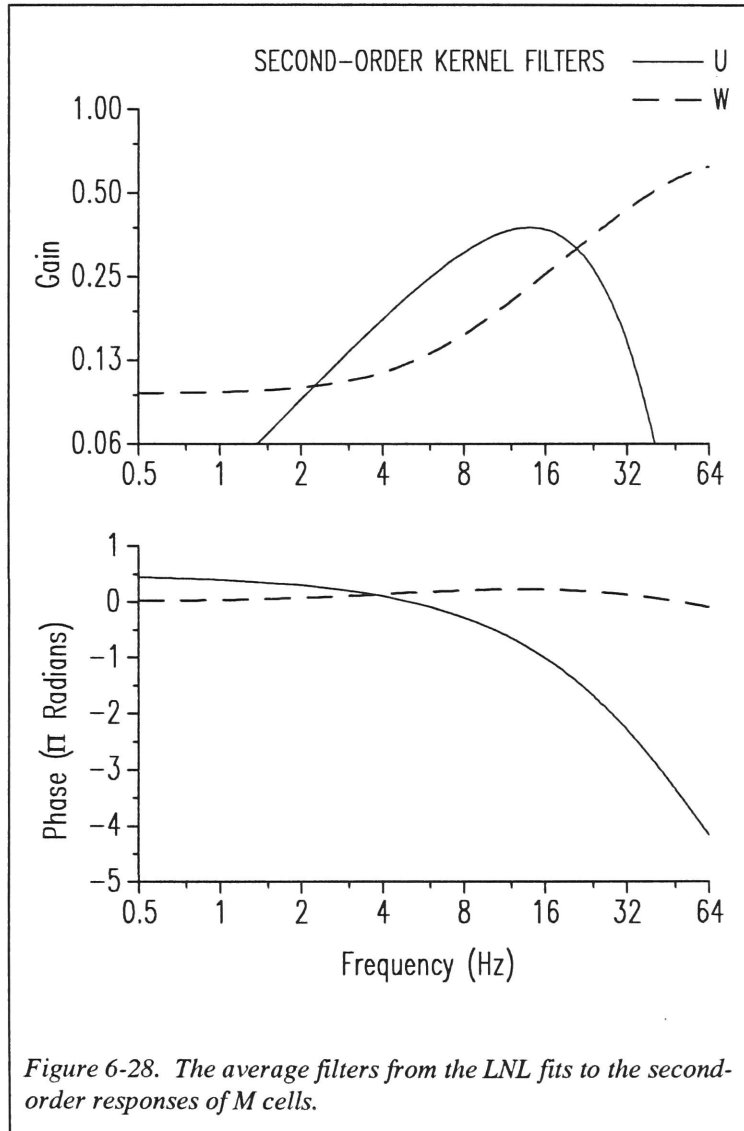


Figure 6-27. The second-order responses of an M OFF (X) cell (unit 14/15) and the model fit on the right. The contours are separated by 1.4 impulses/second. The contrast of the stimulus was 0.1125 and the spatial frequency of the grating was 2.181 c/d. The color of the contours represents the phase of the response as indicated by the color circle above. . The parameters of the LNL fit are: A : 33466 impulses/second-unit contrast²; $H_{S,U}$: 0.99; $\tau_{S,U}$: 6.43 ms; $N_{L,U}$: 14; $\tau_{L,U}$: 3.31 ms; $H_{S,W}$: 0.91; $\tau_{S,W}$: 2.94; $\tau_{L,W}$: 0 ms; D : 2.0 ms.

Table 6-2. The Parameters of the LNL model Fit to Second-Order *M* cell Responses.

$N_{TOTAL} = 8$; $N_{ON} = 5$; $N_{OFF} = 3$; $N_X = 8$

Parameter	Minimum	Maximum	Median	Mean	S.D.	C.V.
A (impulses/s-u.c. ²)	5529.68	121121.40	19051.64	37517.63	43008.57	1.15
$N_L\tau_L$ (msec)	36.59	51.75	39.76	41.45	5.11	0.12
$H_{S,U}$	0.9068	1.0646	0.9953	1.0004	0.0503	0.05
$\tau_{S,U}$ (msec)	2.15	11.82	7.97	7.33	3.65	0.50
$N_{L,W}\tau_{L,W}$ (msec)	0	7.06	1.07	2.50	2.97	1.19
$H_{S,W}$	0.8181	0.9644	0.9183	0.9051	0.0520	0.06
$\tau_{S,W}$ (msec)	1.64	4.19	2.25	2.48	0.82	0.33



6.10 Summary

This chapter investigated the responses of M cells to temporal contrast. The major results can be summarized as follows:

1. The temporal frequency responses of M cells show a contrast gain control, similar to that found in cat retinal ganglion cells.
2. The temporal frequency response of M cells can be used to predict the response of M cells to steps of contrast. These experiments demonstrate how the contrast gain control makes the M cell response more phasic to high contrast steps. It also demonstrates the dynamic resetting of the temporal frequency response of the M cell by the contrast signal.
3. Chromatic gratings identify three types of M cells: one class driven by both L and M cones; a second class driven primarily by L cones, and a third type that has a L cone driven surround. The amount of luminance contrast in a chromatic signal provides the signal for setting the contrast gain control.
4. The contrast gain control arises from a broad spatially distributed area of the retina. The response to small spots shows greatly diminished contrast gain control effects while shifted gratings show that the spatial resolution of the contrast gain control is on the order the M cell center or smaller.
5. The nonlinear responses of M cells show characteristics similar to those of cat Y cells, although some of the M cells are nominally X-like because of the linearity of their spatial summation.

DISCUSSION

Summary

The Multiple M-sequence Technique

P cell Results

- Linearity of the P cell Center and Surround

- Nonlinear Responses of P cells

- P Cell Chromatic Responses

- M and P Differences

- P Cell Anatomy

M cell results

- The Contrast Gain Control

- M Cell Relationship to Cat Retinal Ganglion Cells

- M Cell Responses to Chromatic Stimuli

Conclusion

7. Discussion

This thesis has explored a number of facets of primate retinal ganglion cell behavior. This section will summarize these results and then relate them to previous experimental and theoretical work. It will also discuss the possible functional roles of these effects.

7.1 *Summary*

The work presented in this thesis has focused on the detailed dynamics and functional organization of M and P cell receptive fields. The major experimental results can be organized into four areas: the linear analysis of the P cell center and surround, the nonlinear analysis of the same, the spatiochromatic analysis of P cell receptive fields, and finally, the detailed analysis of M cell dynamics focusing on the contrast gain control mechanism. A new method, the multiple m-sequence technique, was developed for these investigations.

The experimental work in this thesis extends the analysis of the M and P cell pathways begun by Hubel and Wiesel (1966), DeMonasterio and Gouras (1975), Derrington and Lennie (1984), and Kaplan and Shapley (1986) and will lead to a fuller understanding of the roles of these pathways in visual information-processing.

7.2 *The Multiple M-sequence Technique*

To better understand the functional roles of M and P cells, an extension of the m-sequence technique (Sutter, 1992) was designed to facilitate analysis of the receptive fields of these neurons. The major advantages of this multiple m-sequence method are three-fold: access to higher-order, multi-input kernels (e.g. the center-surround cross-kernel of

P cells), improved separation of kernel responses in less time than with the traditional m-sequence method, and a fast method for data processing (FMT) that is easily carried over from the basic m-sequence technique.

The multiple m-sequence technique enabled the calculation of second-order kernels from P cells and parvocellular LGN cells. The multiple m-sequence technique also took full advantage of the spatial patterns generated on the CRT because different lags of the same m-sequence were assigned to modulate different spatial regions. Second-order interaction kernels were then be estimated.

7.3 P cell Results

7.3.1 Linearity of the P cell Center and Surround

As made clear by Kaplan and Shapley (1986), the responses of P cells to sinusoidal gratings increase nearly linearly with contrast (see Fig. 2-8; also Derrington and Lennie, 1984). Experiments in this thesis showed that by using spots and annuli modulated by a sum of two m-sequences, the first-order kernels of the P cell center and surround regions could be calculated. The first-order response of both the center and the surround were nearly linear with increasing contrast under these conditions. The linearity of the response may largely reflect the linear responses of cones which provide the major input to midget ganglion cells through midget bipolar cells. Direct recordings from cones demonstrate this linearity over a broad range of steps in illumination around a fixed operating point (Schnapf *et al.*, 1990). The impulse response of the cone, however, has a much longer time course (approximately 300 ms) than the P cell response. Thus, part of the function of

the retinal machinery that follows the cone must be to filter the low frequencies out of the cone signal.

In the preceding analysis, it was useful to develop a quantitative approach to the dynamics of the P cell center and surround. By fitting the linear filter model (Eq. (2-23)), a set of parameters was found that characterized the major features of the response. These parameters were used to compare neuronal subpopulations.

7.3.2 Nonlinear Responses of P cells

Several efforts were made by earlier investigators to find an effect of surround illumination on the responses of cat X and Y cell centers (Enroth-Cugell *et al.*, 1974; Shapley and Enroth-Cugell, 1984); however, no significant effect was found in the cat.

Earlier intracellular work on the mudpuppy retina demonstrated a variety of effects of surround illumination on center sensitivity (Werblin and Dowling, 1969; Werblin, 1974). Illumination by a surrounding annulus shifts the operating curve of a bipolar's response to a test flash. In this way, the annular surround can increase or decrease the central bipolar's sensitivity. Other investigators (Burkhardt, 1974) found that mudpuppy retinal ganglion cells were progressively sensitized by annular backgrounds as these were increased in diameter. These experiments were directly influenced by psychophysical experiments that demonstrated a similar effect (Westheimer, 1965). The intracellular studies suggested that an interaction in the outer plexiform layer between cones, horizontal cells, and bipolars regulates sensitivity.

In the primate, preliminary results by Kaplan and Shapley (1989) suggested that the gain of P cells was also regulated by surround illumination. Interestingly, M cells, like cat retinal ganglion cells, lack this effect. By using steady annuli and sinusoidally

modulated spots, they found that increasing the size of an annular surround steadily reduced the gain of a P ON cell to a flickering spot.

The multiple m-sequence technique has provided an opportunity for a more complete dynamical characterization of this effect, since, rather than measuring the response at a single temporal frequency, an entire first-order kernel (and higher-order kernels) can be obtained. The results in this thesis show that for P ON cells, increased surround illumination decreases the gain and reduces the time course of the center's response. For P OFF cells, the gain is increased by surround illumination while the time course speeds up. The nature of these effects suggested a biophysical model, described in Chapter 4, that explains the results.

Such membrane models have interesting features and have previously been used to describe other kinds of retinal processing. One successful implementation of this type of model has been to explain directional selectivity in the fly (Torre and Poggio, 1978) and mammalian retinae (Borg-Graham and Grzywacz, 1992). Several computational models based on the same circuit have been investigated (Pinter, 1983a,b, 1984, Nabet and Pinter, 1991). Networks that employ this basic design exhibit dynamic sensitivity adjustment similar to that found in the P cell.

Grossberg (1983) has suggested that a similar model explains several features of precortical visual processing. As he points out, such dynamic regulation of sensitivity allows the neuron to broaden its dynamic range, while avoiding both saturation and excessive insensitivity (the “noise-saturation” dilemma).

The dynamic regulation of center gain by the surround shares some similarities to adaptation since it affects the gain of the cell; however, the two phenomena also have important differences. Work on adaptation in retinal ganglion cells (Purpura *et al.*, 1990) showed that as the level of mean illumination in the P cell's receptive field increases the temporal frequency response becomes more transient, similar to what was found in *Limulus* photoreceptors (Dodge *et al.*, 1968) and in human psychophysics (DeLange, 1958; Kelly, 1972). However, the nonlinear effect of the surround on the dynamics of the P cell center affects only the gain and the time course, not the degree of transience. Other work by Purpura *et al.* (1988) showed that decreasing the background light decreases the contrast gain of P cells, but for P ON cells, decreasing the surround illumination increases the gain.

7.3.3 P Cell Chromatic Responses

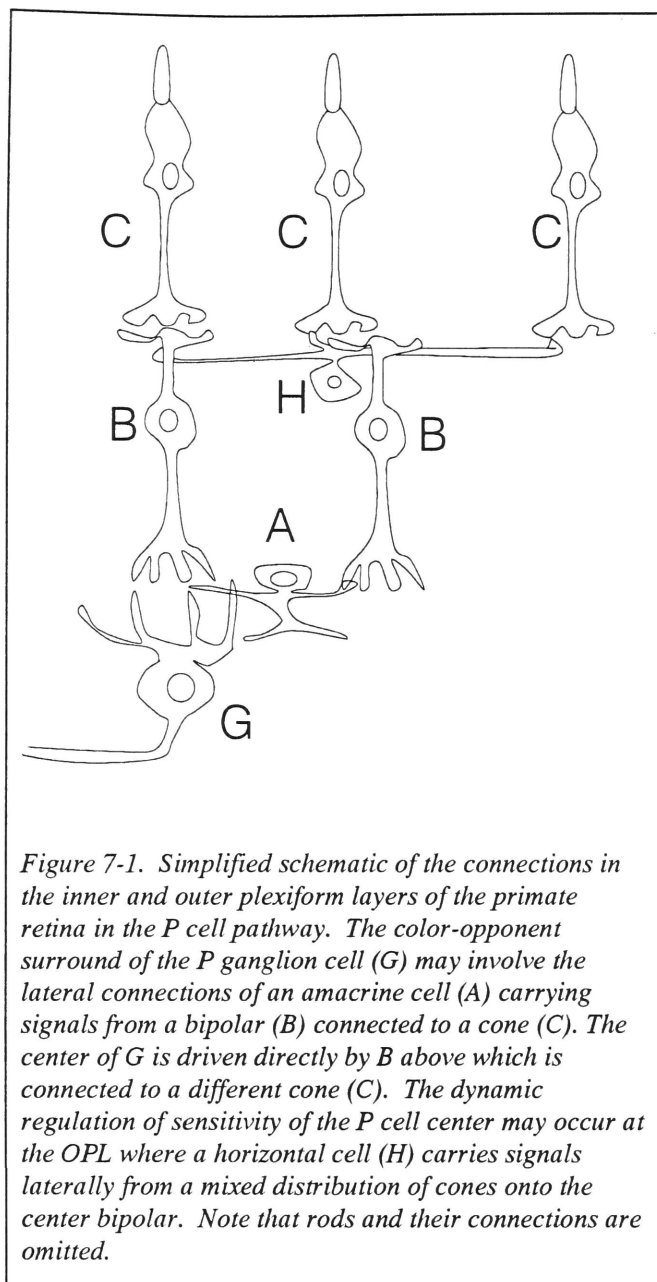
Previous work on the LGN showed that the parvocellular cells are spatially and chromatically opponent (Wiesel and Hubel, 1966; DeValois *et al.*, 1966, Derrington *et al.*, 1984). However, this work provided little dynamical information about the responses of P cells to chromatic stimuli. Gielen *et al.* (1982) using white-noise methods were able to calculate the first-order kernels of parvocellular units in the LGN at different spectral wavelengths. They also used the silent substitution method and calculated the time courses for the L, M and S cone input to parvocellular neurons. However, these experiments were done only using full field stimuli. Reid and Shapley (1992) used an m-sequence modulated checkerboard to more fully examine the spatial extent of the cone driven inputs to P cells. Their results suggested that the center and surround of P cells are each driven by a single, different cone type. However, their data lack fine temporal detail.

The work shown in Chapter 5 strikes a balance between fine temporal and spatial detail, and provides a more complete spatiotemporal characterization of P cell responses to chromatic stimuli. The spatial and chromatic opponency of the P cell receptive field is demonstrated.

Several groups have tried to determine the cone inputs to P cells. Derrington *et al.* (1984) used an elegant technique to quantify the chromatic opponency of P cells and concluded that the cone inputs are linearly summed by the P cell. For instance, they concluded that (RG) P cells get input almost exclusively from a linear summation of L and M cone input. A similar approach by Lee *et al.* (1989a) yielded similar results. Gielen *et al.* (1982) used a different approach to examine the same question. These authors measured the first-order responses of parvocellular neurons to full-field monochromatic stimuli, and then from known psychophysical spectral sensitivities of human receptors, a linear regression model was used to predict the response to other monochromatic stimuli. The results of these studies showed that the responses to relatively weak chromatic stimuli can be predicted by a simple linear models of the P cell. A certain amount of emphasis has been placed on linearity because of the historical background in human psychophysics on color perception (Ingling and Martinez-Uriegas, 1983; Mullen and Kingdom, 1991). However, the data in this thesis, while consistent with the previous experimental work, also indicate that responses to larger luminance stimuli with or without a chromatic component are not well predicted by linear models. The actual responses are smaller than the linear predictions, and this suggests that the surround gain control mechanism (discussed above) may be involved.

7.3.4 M and P Differences

Much evidence has accumulated that the M and P pathways form the substrate for separate luminance and chromatic channels in psychophysics, respectively (Livingstone and Hubel, 1988; reviewed in Kaplan *et al.*, 1990). Although it is clearly an oversimplification, the comparisons are strong. M cell centers are less delayed, more transient, and more sensitive than P cell centers, an observation that agrees with the higher sensitivity of the visual system to luminance flicker. The chromatic system is relatively slower and more spatially lowpass, like the responses of P cells to chromatic stimuli. However, it should be noted that in the data shown here, P cells can be quite responsive under luminance conditions and probably contribute to luminance detection and discrimination under most conditions.



7.3.5 P Cell Anatomy

It is interesting to speculate about the possible anatomical organization of the P cell receptive field. Horizontal cells in the OPL get inputs from a mixed group of cones in their dendritic fields (Boycott *et al.*, 1987; Dacheux and Raviola, 1990). Therefore, the chromatically opponent surround may be generated by amacrine cells impinging on ganglion cells at the level of the IPL (Fig. 7-1). Recent electronmicroscopic examination of the synaptic input to midtemporal ganglion cells shows that they receive as much synaptic input from amacrine cells as they do from bipolars (Kolb

and DeKorver, 1991). At the level of the OPL, the cone-horizontal-bipolar circuit may be involved in generating the dynamic regulation of P cell center sensitivity seen in the data in this thesis. The broadband sensitivity of the H1 horizontal cell might serve this role (Fig. 7-1).

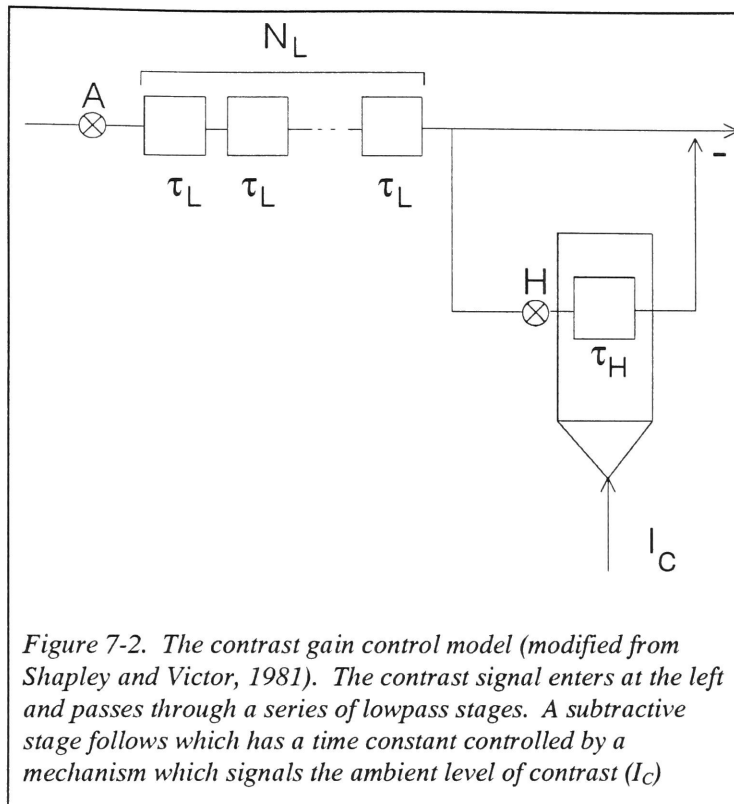
7.4 M cell results

7.4.1 The Contrast Gain Control

The most dramatic feature of the temporal frequency response of M cells is the contrast gain control. Once this effect was recognized (Benardete *et al.*, 1992a), the work of Shapley and Victor (1981) lent insight into M cell behavior.

The contrast gain control mechanism provides a means for the M cell to behave as an adaptive luminance filter. As contrast increases, the cell responds to higher and higher temporal frequencies with a corresponding phase advance. There are theoretical reasons to expect this relationship. Information theory suggests that as the signal becomes larger more of the essentially redundant information, i.e. the low temporal frequencies, can be trimmed away (Goldman, 1953). Theoretical studies by Srinivasan *et al.* (1982) and Attick, and Redlich (1992) applied these ideas to the retina and found that other features of retinal receptive fields could be explained on the basis of such information-processing principles.

The data on the spatial and temporal properties of the contrast gain control mechanism suggest that it must be supported by a network of retinal processing elements. Work on the cat suggested that a rectified signal from amacrine cells might control the time constant of a feedback stage (Shapley and Victor, 1981). The dynamics in the M cell were investigated by fitting the linear model and letting the time constant of the subtractive stage, τ_s , vary with contrast. This model gives a concise explanation of M cell responses (Fig. 7-2).



Recent anatomical evidence from the primate retina suggests that a network of amacrine cells and M cells exists in the IPL and that they are tightly coupled (Dacey and Brace, 1992). This may explain how the contrast signal from a large region of retina affects the dynamics of single M cell. The older

results on the “shift effect” in M cells (Krüger, 1977) are probably manifestations of the contrast gain control mechanism.

7.4.2 M Cell Relationship to Cat Retinal Ganglion Cells

The similarity between the functional dynamics of M cells and that of cat retinal ganglion cells suggests a certain evolutionary relationship between the structure of the primate retina and that of lower mammals. It would appear that the M cell pathway is similar to the retina of animals specialized for luminance and scotopic vision, while the P cell pathway is a new specialization for photopic, color vision. Various other studies support this idea, including current source density analysis of Mitzdorf and Singer (1977) as well as the anatomical data of Rakic (1977) and Shatz (1981). This hypothesis is reviewed in Kaplan and Shapley (1982).

It also appears that the functional dualism of the X and Y types, based on nonlinear spatial summation, is less prominent in the primate, where the vast majority of M cells seem to be X-like. Under close inspection, most X-like M cells, however, have consistent second-order responses like those of Y cells in the cat although these second-order responses do not dominate. Other investigators have found similar results using less sophisticated techniques (Irvin *et al.*, 1993; Sherman *et al.*, 1984). Lee *et al.* (1989c) only found significant second-order responses in M cells under conditions of heterochromatic flicker near the first-order response null. With single sinusoidal stimuli, this paradigm may be an effective way to uncover the underlying second-order response which is being dominated by first-order responses under strong luminance conditions.

7.4.3 M Cell Responses to Chromatic Stimuli

The data shown here segregated M cells into 3 classes based on their responses to cone-isolating gratings. These data agree with studies that show that M cells vary in their amounts of L and M cone input (Lee *et al.*, 1989a,b; Derrington *et al.*, 1984). In addition, the data suggest that the contrast gain control signal comes from a distributed network of retinal interneurons and therefore may represent a less biased measure of L and M cone excitation than does the signal at the M cell center. Indeed, when equated for luminance energy, the responses to chromatic gratings and black-white gratings for an M cell are nearly identical. These results may help explain why heterochromatic flicker photometry is so effective. At high temporal frequencies, an isoluminant stimulus might activate some M cells with uneven L and M cone input; however, since the contrast gain control is a distributed mechanism, it is effectively nulled out by isoluminance, leaving a

strongly filtered (lowpass) M cell frequency response that is relatively insensitive to high frequency flicker.

7.5 Conclusion

M and P cells subserve different roles that are brought into sharp relief by their diverse dynamical and spatial properties. The nonlinear properties described here are the newest clues to their functional roles. As shown here, P cells have a nonlinear gain control that strongly depends on lateral multiplicative interactions to regulate sensitivity. On the other hand, the contrast gain control of M cells forms an adaptive stage of temporal frequency filtering for luminance stimuli. Both P and M cells, therefore, have significant nonlinear components to their responses. Linear models (e.g. Ingling and Martinez-Uriegas, 1983) are not adequate to fully describe the responses of M and P cells. An understanding of the nonlinearities in these two pathways is important for understanding the human visual system.

8. References

- Atick, J.J. & Redlich, A.N. (1992). What does the retina know about natural scenes? *Neural Comput.* **4**:196-210.
- Barrett, J.F. (1963). The use of functionals in the analysis of non-linear physical systems. *J.Electron.Control* **15**:567-615.
- Baylor, D.A. (1987). Photoreceptor signals and vision. *Invest.Ophthalmol.Visual Sci.* **28**:34-49.
- Beauchamp, K.G. (1984). *Applications of Walsh and Related functions. With an Introduction to Sequency Theory*. London: Academic Press.
- Benardete, E.A., Kaplan, E. & Knight, B.W. (1991). Contrast gain control in the primate retina. *Soc.Neurosci.Abstr.* **17**(1):345(#143.13).
- Benardete, E.A., Kaplan, E. & Knight, B.W. (1992). Contrast gain control in the primate retina: P cells are not X-like, some M cells are. *Visual Neurosci.* **8**:483-486.
- Benardete, E.A., Kaplan, E. & Victor, J.D. (1992). The contrast gain control of primate M ganglion cells: spatial organization and temporal properties. *Soc.Neurosci.Abstr.* **18**(1):394(#171.12).
- Benardete, E.A., Victor, J.D. & Kaplan, E. (1992a). Temporal properties of primate P retinal ganglion cells investigated with a new discrete multi-level stimulus. *Invest.Ophthalmol.Visual Sci. (suppl)* **33**(4):1410(#3591).
- Benardete, E.A. & Kaplan, E. (1993). Spatiotemporal dynamics of P cells and their cone inputs. *Soc.NeurosciAbstr.* **19**(1):15(#13.8).
- Benardete, E.A. & Victor, J.D. (1994). An extension of the m-sequence technique for the analysis of multiple-input nonlinear systems. In: *Advanced Methods of Physiological Systems Modelling. Vol. 3.* (Marmarelis, V.Z., ed) New York: Plenum Press (in press).
- Borg-Graham, L.J. & Grzywacz, N.M. (1992). A model of the directional selectivity circuit in retina: transformations by neurons singly and in concert. In: *Single Neuron Computation* (McKenna, T., Davis, J. & Zornetzer, S.F., eds) pp347-375. London: Academic Press, Inc.
- Boycott, B.B. & Wässle, H. (1991). Morphological classification of bipolar cells of the primate retina. *Eur.J.Neurosci.* **3**:1069-1088 .
- Boycott, B.B., Hopkins, J.M. & Sperling, H.G. (1987). Cone connections of the horizontal cells of the rhesus monkey's retina. *Proc.R.Soc.Lond. B.* **229**:345-379.
- Boynton, R.M. (1992). *Human Color Vision*. Second Edition. Optical Society of America.

- Brodie, S.E., Knight, B.W. & Ratliff, F. (1978a). The response of the *Limulus* retina to moving stimuli: a prediction by Fourier synthesis. *J.Gen.Physiol.* **72**:129-166.
- Brodie, S.E., Knight, B.W. & Ratliff, F. (1978b). The spatiotemporal transfer function of the *Limulus* lateral eye. *J.Gen.Physiol.* **72**:167-202.
- Burkhardt, D.A. (1974). Sensitization and centre-surround antagonism in *Necturus* retina. *J.Physiol.(Lond)* **236**:593-610.
- Chaparro, A., Stromeyer, C.F., Huang, E.P., Kronauer, R.E. & Eskew, R.T. (1993). Colour is what the eye sees best. *Nature* **361**:348-350.
- Dacey, D.M. & Brace, S. (1992). A coupled network for parasol but not midget ganglion cells in the primate retina. *Visual Neurosci.* **9**:279-290.
- Dacey, D.M. (1993). The mosaic of midget ganglion cells in the human retina. *J.Neurosci.* **13**:5334-5355.
- Dacheux, R.F. & Raviola, E. (1988). Intracellular recordings from HI horizontal cells in the monkey retina. *Invest.Ophthalmol.Visual Sci. (Suppl.)* **29**:224.
- Dacheux, R.F. & Raviola, E. (1990). Physiology of H.I horizontal cells in the primate retina. *Proc.R.Soc.Lond. B* **239**:213-230.
- Dawis, S., Shapley, R., Kaplan, E. & Tranchina, D. (1984). The receptive field organization of X-cells in the cat: spatiotemporal coupling and asymmetry. *Vision Res.* **24**:549-564.
- De Lange, H. (1958). Research into the dynamic nature of the human fovea-cortex systems with intermittent and modulated light. II. Phase shift in brightness and delay in color perception. *J.Opt.Soc.Am.* **48**:784-789.
- De Monasterio, F.M. & Gouras, P. (1975). Functional properties of ganglion cells of the rhesus monkey retina. *J.Physiol.(Lond)* **251**:167-195.
- De Valois, R.L., Abramov, I. & Jacobs, G.H. (1966). Analysis of response patterns of LGN cells. *J.Opt.Soc.Am.* **56**:966-977.
- De Valois, R.L., Morgan, H.C. Polson, M.C., Mead, W.R. & Hull, E.M. (1974a). Psychophysical studies of monkey vision—I. Macaque luminosity and color vision tests. *Vision Res.* **14**:53-67.
- De Valois, R.L. & Morgan, H.C. (1974). Psychophysical studies of monkey vision. II. Squirrel monkey wavelength and saturation discrimination. *Vision Res.* **14**:69-73.
- De Valois, R.L., Morgan, H. & Snodderly, D.M. (1974b). Psychophysical studies of monkey vision - III. Spatial luminance contrast sensitivity tests of macaque and human observers. *Vision Res.* **14**:75-81.
- De Valois, R.L. & De Valois, K.K. (1993). A multi-stage color model. *Vision Res.* **33**:1053-1065.
- Derrington, A.M. & Lennie, P. (1984). Spatial and temporal contrast sensitivities of neurones in lateral geniculate nucleus of macaque. *J.Physiol.(Lond)* **357**:219-240.

- Derrington, A.M., Krauskopf, J. & Lennie, P. (1984). Chromatic mechanisms in lateral geniculate nucleus of macaque. *J.Physiol.(Lond)* **357**:241-265.
- Dodge, F.A., Knight, B.W. & Toyoda, J. (1968): Voltage noise in *Limulus* visual cells. *Science* **160**:88-90.
- Enroth-Cugell, C. & Robson, J.G. (1966). The contrast sensitivity of retinal ganglion cells of the cat. *J.Physiol.(Lond)* **187**:517-552.
- Enroth-Cugell, C., Hertz, B.G. & Lennie, P. (1974). Convergence of rod and cone signals on retinal ganglion cells of the cat. *J.Physiol.(Lond)* **242**:126P-127P.
- Enroth-Cugell, C., Robson, J.G., Schweitzer-Tong, D.E. & Watson, A.B. (1983). Spatio-temporal interactions in cat retinal ganglion cells showing linear spatial summation. *J.Physiol.(Lond)* **341**:279-307.
- Estévez, O. & Spekreijse, H. (1974). Relationship between pattern appearance-disappearance and pattern reversal responses. *Exp.Brain Res.* **19**:233-238.
- Estévez, O. & Spekreijse, H. (1982). The "silent substitution" method in visual research. *Vision Res.* **22**:681-691.
- Feller, W. (1968). *An Introduction to Probability Theory and its Applications. Volumes 1 & 2*. New York: JohnWiley & Sons, Inc.
- Field, D.J. (1987). Relations between the statistics of natural images and the response properties of cortical cells. *J.Opt.Soc.Am.A* **4**:2379-2394.
- Gielen, C.C.A.M., van Gisbergen, J.A.M. & Vendrik, A.J.H. (1982). Reconstruction of cone-system contributions to responses of colour-opponent neurones in monkey lateral geniculate. *Biol.Cybern.* **44**:211-221.
- Goldman, S. (1953). *Information Theory*. New York: Prentice-Hall, Inc.
- Golomb, S.W. (1968). *Shift Register Sequences*. San Francisco: Holden-Day, Inc.
- Gouras, P. (1967). Visual adaptation: its mechanism. *Science* **157**:583-584.
- Gouras, P. (1967). The effects of light-adaptation on rod and cone receptive field organization of monkey ganglion cells. *J.Physiol.(Lond)* **192**:747-760.
- Gouras, P. (1968). Identification of cone mechanisms in monkey ganglion cells. *J. Physiol.(Lond)* **199**:533-547.
- Gouras, P. & Zrenner, E. (1979). Enhancement of luminance flicker by color-opponent mechanisms. *Science* **205**:587-589.
- Grossberg, S. (1983). The quantized geometry of visual space: the coherent computation of depth, form, and lightness. *Behav.Brain Sci.* **6**:625-692.
- Hamer, R.D. & Tyler, C.W. (1992). Analysis of visual modulation sensitivity. V. Faster visual response for G- than for R-cone pathway? *J.Opt.Soc.Am.A.* **9**:1889-1904.
- Hartline, H.K. (1942). The neural mechanisms of vision. *Harvey Lectures* **37**:39-68.

- Hirsch, M.W. & Smale, S. (1974). *Differential Equations, Dynamical Systems, and Linear Algebra*. New York: Academic Press, Inc.
- Hochstein, S. & Shapley, R.M. (1976). Quantitative analysis of retinal ganglion cell classifications. *J.Physiol.(Lond)* **262**:237-264.
- Hochstein, S. & Shapley, R.M. (1976). Linear and nonlinear spatial subunits in Y cat retinal ganglion cells. *J.Physiol.(Lond)* **262**:265-284.
- Ingling, C.R. & Martinez-Uriegas, E. (1983). The relationship between spectral sensitivity and spatial sensitivity for the primate r-g X channel. *Vision Res.* **23**:1495-1500.
- Irvin, G.E., Casagrande, V.A. & Norton, T.T. (1993). Center/surround relationships of magnocellular, parvocellular, and koniocellular relay cells in primate lateral geniculate nucleus. *Visual Neurosci.* **10**:363-373.
- Kandel, E.R. & Schwartz, J.H. (1985). *Principles of Neural Science. Second Edition*. New York: Elsevier.
- Kaplan, E. & Shapley, R.M. (1982). X and Y cells in the lateral geniculate nucleus of macaque monkeys. *J.Physiol.(Lond)* **330**:125-143.
- Kaplan, E. & Shapley, R. (1984). The origin of the S (slow) potential in the mammalian lateral geniculate nucleus. *Exp.Brain Res.* **55**:111-116.
- Kaplan, E. & Shapley, R.M. (1986) The primate retina contains two types of ganglion cells, with high and low contrast sensitivity *Proc.Natl.Acad.Sci.USA* **83**:2755-2757.
- Kaplan, E. & Shapley, R.M. (1989). Illumination of the receptive field surround controls the contrast gain of macaque P retinal ganglion cells. *Soc.Neurosci.Abst.* **15**(1):174(#75.1).
- Kaplan, E., Lee, B.B. & Shapley, R.M. (1990). New views of primate retinal function. In: *Progress in Retinal Research* Vol. **9** (Osborne, N.N. & Chader, G.J., eds) pp273-336. New York:Pergamon Press.
- Klein, S. (1987). Relationships between kernels measured with different stimuli. In: *Advanced Methods of Physiological System Modeling*. Vol. 1. (Marmarelis, V.Z., ed). University of Southern California, Los Angeles.
- Klein, S.A. (1992). Optimizing the estimation of nonlinear kernels. In: *Nonlinear Vision: Determination of Neural Receptive Fields, Function, and Networks*. (Pinter, R.B. & Nabet, B., eds) pp109-170. Boca Raton: CRC Press.
- Koch, C. & Poggio, T. (1992). Multiplying with synapses and neurons. In: *Single Neuron Computation* (Mc. Kenna, T., Davis, J. & Zornetzer, S.F., eds). London: Academic Press.
- Kolb, H. & Dekorver, L. (1991) Midget ganglion cells of the parafovea of the human retina: A study by electron microscopy and serial section reconstructions. *J.Comp.Neurol.* **303**:617-636.

- Krüger, J., Fischer, B. & Barth, R. (1975). The shift-effect in retinal ganglion cells of the rhesus monkey. *Exp.Brain Res.* **23**:443-446.
- Krüger, J. (1977). The shift-effect in the lateral geniculate body of the rhesus monkey. *Exp.Brain Res.* **29**:387-392.
- Kuffler, S.W. (1953). Discharge patterns and functional organization of mammalian retina. *J.Neurophysiol.* **16**:37-68.
- Kunt, M. (1975). On computation of the Hadamard transform and the *R* transform in ordered form. *IEEE Trans.Comput.* **C-24**:1120-1121.
- Lee, B.B., Valberg, A., Tigwell, D.A. & Tryti, J. (1987). An account of responses of spectrally opponent neurons in macaque lateral geniculate nucleus to successive contrast. *Proc.R.Soc.Lond.B* **230**:293-314.
- Lee, B.B., Martin, P.R. & Valberg, A. (1988). The physiological basis of heterochromatic flicker photometry demonstrated in the ganglion cells of the macaque retina. *J.Physiol.(Lond)* **404**:323-347.
- Lee, B.B., Martin, P.R. & Valberg, A. (1989a). Sensitivity of macaque retinal ganglion cells to chromatic and luminance flicker. *J.Physiol.(Lond)* **414**:223-243.
- Lee, B.B., Martin, P.R. & Valberg, A. (1989b). Amplitude and phase of responses of macaque retinal ganglion cells to flickering stimuli. *J.Physiol.(Lond)*. **414**:245-263.
- Lee, B.B., Martin, P.R. & Valberg, A. (1989c). Nonlinear summation of M- and L-cone inputs to phasic retinal ganglion cells of the macaque. *J.Neurosci.* **9**:1433-1442.
- Lee, Y.N. & Schetzen, M. (1965). Measurement of the kernels of a nonlinear system by cross-correlation. *Int.J.Control* **2**:237-254.
- Levick, W.R., Cleland, B.G. & Dubin, M.W. (1972). Lateral geniculate neurons of cat: retinal inputs and physiology. *Invest.Ophthalmol.* **11**:302-311.
- Linsenmeier, R.A., Frishman, L.J., Jakiela, H.G. & Enroth-Cugell, C. (1982). Receptive field properties of X and Y cells in the cat retina derived from contrast sensitivity measurements. *Vision Res.* **22**:1173-1183.
- Marmarelis, P.Z. & Naka, K.-I. (1972). White-noise analysis of a neuron chain: an application of the Wiener theory. *Science* **175**:1276-1278.
- Marmarelis, P.Z. & Marmarelis, V.Z. (1978). *Analysis of Physiological Systems: The White Noise Approach*. New York: Plenum Press.
- McIlwain, J.T. (1966). Some evidence concerning the physiological basis of the periphery effect in the cat's retina. *Exp.Brain Res.* **1**:265-271.
- Merigan, W.H., Byrne, C.E., & Maunsell, J.H.R. (1991). Does primate motion perception depend on the magnocellular pathway? *J.Neurosci.* **11**:3422-3429.
- Merrill, E.G. & Ainsworth, A. (1972). Glass-coated platinum-plated tungsten microelectrodes. *Med.Biol.Eng.* **10**:662-672.

- Milkman, N., Schick, G., Rossetto, M., Ratliff, F., Shapley, R. & Victor, J. (1980). A two-dimensional computer-controlled visual stimulator. *Behav.Res.Meth.Instrum.* **12**:283-292.
- Mitzdorf, U. & Singer, W. (1977). Laminar segregation of afferents to lateral geniculate nucleus of the cat: an analysis of current source density. *J.Neurophysiol.* **40**:1227-1244.
- Mullen, K.T. (1985). The contrast sensitivity of human colour vision to red-green and blue-yellow chromatic gratings. *J.Physiol.(Lond)* **359**:381-400.
- Mullen, K.T. & Kingdom, F.A.A. (1991). Colour contrast in form perception. In: *Vision and Visual Dysfunction, (The Perception of Colour)*. (Gouras, P.,ed) Vol. **6**. pp198-217, Macmillan Press.
- Nabet, B. & Pinter, R.B. (1991). *Sensory Neural Networks: Lateral Inhibition*. Boca Raton: CRC Press.
- Nathans, J., Thomas, D. & Hogness, D.S. (1986). Molecular genetics of human color vision: the genes encoding blue, green, and red pigments. *Science* **232**:193-202.
- Nathans, J., Piantanida, T.P., Eddy, R.L., Shows, T.B. & Hogness, D.S. (1986). Molecular genetics of inherited variation in human color vision. *Science* **232**:203-210.
- Nelson, R., Famiglietti, E.V. & Kolb, H. (1978). Intracellular staining reveals different levels of stratification for on- and off-center ganglion cells in cat retina. *J.Neurophysiol.* **41**:472-483.
- Oppenheim, A.V. & Willsky, A.S., with Young, I.T. (1983). *Signals and Systems*. Englewood Cliffs, NJ: Prentice-Hall, Inc.
- Pinter, C.C. (1990). *A Book of Abstract Algebra. Second Edition*. New York: McGraw-Hill.
- Pinter, R.B. (1983a). Product term nonlinear lateral inhibition enhances visual selectivity for small objects or edges. *J.Theor.Biol.* **100**:525-531.
- Pinter, R.B. (1983b). The electrophysiological bases for linear and for nonlinear product term lateral inhibition and the consequences for wide field textured stimuli. *J.Theor.Biol.* **105**:233-243.
- Pinter, R.B. (1984). Adaptation of receptive field spatial organization via multiplicative lateral inhibition. *J.Theor.Biol.* **110**:435-444.
- Press, W.H., Flannery, B.P., Teukolsky, S.A. & Vetterling, W.T. (1989). *Numerical Recipes in Pascal: The Art of Scientific Computing*. Cambridge: Cambridge University Press.
- Purpura, K., Kaplan, E. & Shapley, R.M. (1988). Background light and the contrast gain of primate P and M retinal ganglion cells. *Proc.Natl.Acad.Sci.USA* **85**:4534-4537.

- Purpura, K. Tranchina, D., Kaplan, E. & Shapley, R.M. (1990). Light adaptation in the primate retina: analysis of changes in gain and dynamics of monkey retinal ganglion cells. *Visual Neurosci.* **4**:75-93.
- Rakic, P. (1977). Genesis of the dorsal lateral geniculate nucleus in the rhesus monkey: site and time of origin, kinetics of proliferation, routes of migration and pattern of distribution of neurons. *J.Comp.Neurol.* **176**:23-52.
- Ratliff, F. (1965). *Mach Bands: Quantitative Studies on Neural Networks in the Retina*. San Francisco: Holden-Day, Inc.
- Reid, R.C. & Shapley, R.M. (1992). Spatial structure of cone inputs to receptive fields in primate lateral geniculate nucleus. *Nature* **356**:716-718.
- Riggs, L.A., Ratliff, F., Cornsweet, J.C. & Cornsweet, T.N. (1953). The disappearance of steadily fixated visual test objects. *J.Opt.Soc.Am.* **43**:495-501.
- Rodieck, R.W. (1965). Quantitative analysis of cat retinal ganglion cell response to visual stimuli. *Vision Res.* **5**:583-601.
- Rodieck, R.W., Binmoeller, K.F. & Dineen, J. (1985). Parasol and midget ganglion cells of the human retina. *J.Comp.Neurol.* **233**:115-132.
- Rodieck, R.W. (1988). The primate retina. In: *Comparative Primate Biology*, **4**: Neurosciences, pp203-278, New York: Alan R. Liss.
- Rugh, W.J. (1981). *Nonlinear Systems Theory: The Volterra/Wiener Approach*. Baltimore: The Johns Hopkins University Press.
- Rushton, W.A.H., Powell, D.S. & White, K.D. (1973). Pigments in anomalous trichromats. *Vision Res.* **13**:2017-2031.
- Purpura, K. Tranchina, D., Kaplan, E. & Shapley, R.M. (1990). Light adaptation in the primate retina: analysis of changes in gain and dynamics of monkey retinal ganglion cells. *Visual Neurosci.* **4**:75-93.
- Sakai, H.M. & Naka, K.-I. (1988a). Neuron network in catfish retina: 1968-1987. In: *Progress in Retinal Research* Vol. **7** (Osborne, N. & Chader, J., eds) pp149-208. New York: Pergamon Press.
- Sakai, H.M. & Naka, K.-I. (1988b). Dissection of the neuron network in the catfish inner retina. I. Transmission to ganglion cells. *J.Neurophysiol.* **60**:1549-1567.
- Sakai, H.M. & Naka, K.-I. (1988c). Dissection of the neuron network in the catfish inner retina. II. Interactions between ganglion cells. *J.Neurophysiol.* **60**:1568-1583.
- Sakai, H.M., Naka, K.-I. & Korenberg, M.J. (1988). White-noise analysis in visual neuroscience. *Visual Neurosci.* **1**:287-296.
- Schetzen, M. (1980). *The Volterra and Wiener Theories of Nonlinear Systems*. New York: John Wiley & Sons.
- Schiller, P.H. & Logothetis, N.K. (1990). The color-opponent and broad-band channels of the primate visual system. *Trends Neurosci.* **13**:392-398.

- Schiller, P.H., Logothetis, N.K. & Charles, E.R. (1990a). Functions of the colour-opponent and broad-band channels of the visual system. *Nature* **343**:68-70.
- Schiller, P.H., Logothetis, N.K. & Charles, E.R. (1990b). Role of the color-opponent and broad-band channels in vision. *Visual Neurosci.* **5**:321-346.
- Schnapf, J.L., Kraft, T.W. & Baylor, D.A. (1987). Spectral sensitivity of human cone photoreceptors. *Nature* **325**:439-441.
- Schnapf, J.L., Nunn, B.J., Meister, M. & Baylor, D.A. (1990). Visual transduction in cones of the monkey *Macaca fascicularis*. *J.Physiol.(Lond)* **427**:681-713.
- Shapley, R.M. & Victor, J.D. (1978). The effect of contrast on the transfer properties of cat retinal ganglion cells. *J.Physiol.(Lond)* **285**:275-298.
- Shapley, R. & Victor, J.D. (1979). The contrast gain control of the cat retina. *Vision Res.* **19**:431-434.
- Shapley, R.M. & Victor, J.D. (1979). Nonlinear spatial summation and the contrast gain control of cat retinal ganglion cells. *J.Physiol.(Lond)* **290**:141-161.
- Shapley, R.M. & Victor, J.D. (1981). How the contrast gain control modifies the frequency responses of cat retinal ganglion cells. *J.Physiol.(Lond)* **318**:161-179.
- Shapley, R. & Enroth-Cugell, C. (1984). Visual adaptation and retinal gain controls. In: *Progress in Retinal Research* (Osborne, N.N. & Chader, G.J., eds) Vol. **3**, pp263-346. New York: Pergamon Press.
- Shapley, R. & Kaplan, E. (1990). Tonic suppressive interactions between center and surround in P ganglion cells and parvocellular neurons. *Invest.Ophthalmol.Visual Sci.(suppl)*. **31(4)**:88 (#434).
- Shatz, C.J. (1981). Inside-out pattern of neurogenesis of the cat's lateral geniculate nucleus. *Soc.Neurosci.Abstr.* **7**:140(#47.4).
- Sherman, S.M., Schumer, R.A. & Movshon, J.A. (1984). Functional cell classes in the macaque's LGN. *Soc.Neurosci.Abstr.* **10**:296.
- Smith, V.C. & Pokorny, J. (1972). Spectral sensitivity of color-blind observers and the cone photopigments. *Vision Res.* **12**:2059-2071.
- Smith, V.C., Pokorny, J. & Lee, B.B. (1991). The contrast gain of P- and M-pathway cells expressed in cone contrast units. *Invest.Ophthalmol.Visual Sci.(Suppl)* **32(4)**:1034(#1799).
- Srinivasan, M.V., Laughlin, S.B. & Dubs, A. (1982). Predictive coding: a fresh view of inhibition in the retina. *Proc.R.Soc.Lond. B.* **216**:427-459.
- Sutter, E.E. (1987). A practical nonstochastic approach to nonlinear time-domain analysis. In: *Advanced Methods of Physiological Systems Modelling. Vol. 1* (Marmarelis, V.Z., ed) Los Angeles: University of Southern California.
- Sutter, E.E. (1991). The fast m-transform: a fast computation of cross-correlations with binary m-sequences. *SIAM J.Comput.* **20**:686-694.

- Sutter, E.E. (1992). A deterministic approach to nonlinear systems analysis. In: *Nonlinear Vision: Determination of Neural Receptive Fields, Function, and Networks*. (Pinter, R.B. & Nabet, B., eds) pp171-220. Boca Raton: CRC Press.
- Torre, V. & Poggio, T. (1978). A synaptic mechanism possibly underlying directional selectivity to motion. *Proc.R.Soc.Lond. B* **202**:409-416.
- Vaney, D.I. (1990). The mosaic of amacrine cells in the mammalian retina. In: *Progress in Retinal Research*, (Osborne, N.N. & Chader, G.J., eds), Vol. **9**, pp49-100, New York: Pergamon Press.
- Victor, J.D. (1979). The functional organization of the receptive fields of cat X and Y retinal ganglion cells. Ph.D. Thesis. The Rockefeller University, New York City.
- Victor, J.D. (1987). The dynamics of the cat retinal X cell centre. *J.Physiol.(Lond)* **386**:219-246.
- Victor, J.D. (1988). The dynamics of the cat retinal Y cell subunit. *J.Physiol.(Lond)* **405**:289-320.
- Victor, J.D. (1991). Asymptotic approach of generalized orthogonal functional expansions to Wiener kernels. *Ann.Biomed.Eng.* **19**:383-399.
- Victor, J.D. (1992). Nonlinear systems analysis in vision: overview of kernel methods. In: *Nonlinear Vision: Determination of Neural Receptive Fields, Function, and Networks* (Pinter, R.B. & Nabet, B., eds). Boca Raton: CRC Press.
- Victor, J.D. & Knight, B.W. (1979). Nonlinear analysis with an arbitrary stimulus ensemble. *Q.Appl.Math.* **37**:113-136.
- Victor, J.D. & Shapley, R.M. (1979a). Receptive field mechanisms of cat X and Y retinal ganglion cells. *J.Gen.Physiol.* **74**:275-298.
- Victor, J.D. & Shapley, R.M. (1979b). The nonlinear pathway of Y ganglion cells in the cat retina. *J.Gen.Physiol.* **74**:671-689.
- Victor, J.D. & Shapley, R. (1980). A method of nonlinear analysis in the frequency domain. *Biophys.J.* **29**:459-484.
- Victor, J.D. & Mast, J. (1991). A new statistic for steady-state evoked potentials. *Electroenceph.Clin.Neurophysiol.* **78**:378-388.
- Volterra, V. (1932). *The Theory of Functionals and of Integrals and Integro-Differential Equations*. London: Blackie.
- Wässle, H. & Boycott, B.B. (1991). Functional architecture of the mammalian retina. *Physiol.Rev.* **71**:447-480.
- Watson, A.B., Barlow, H.B. & Robson, J.G. (1983). What does the eye see best? *Nature* **302**:419-422.
- Werblin, F.S. (1974). Control of retinal sensitivity. II. Lateral interactions at the outer plexiform layer. *J.Gen.Physiol.* **63**:62-87.

- Werblin, F.S. & Dowling, J.E. (1969). Organization of the retina of the mudpuppy, *Necturus maculosus*. II. Intracellular recording. *J.Neurophysiol.* **32**:339-355.
- Westheimer, G. (1965). Spatial interaction in the human retina during scotopic vision. *J.Physiol.(Lond)*. **181**:881-894.
- Wiener, N. (1958). *Nonlinear Problems in Random Theory*. New York: John Wiley & Sons, Inc.
- Wyszecki, G. & Stiles, W.S. (1982). *Color Science: Concepts and Methods, Quantitative Data and Formulae*. Second edition. New York: John Wiley & Sons.

End